Structure/Function Studies of Manganese Peroxidase

Heather L. Youngs
B.S., Michigan Technological University, 1996

A dissertation submitted to the faculty of the
OGI School of Science & Engineering
at Oregon Health & Science University
in partial fulfillment of the
requirements for the degree

Doctor of Philosophy
in
Biochemistry and Molecular Biology

May 2003

The dissertation "Structure/Function Studies of Manganese Peroxidase" by Heather L. Youngs has been examined and approved by the following Examination Committee:

Thomas M. Loehr, Advisor
Professor

Pierre Moënne-Loccoz
Assistant Professor

Matthew S. Sachs
Associate Professor

A. Grant Mauk
Professor
University of British Columbia

ACKNOWLEDGMENTS

I'd like to dedicate this dissertation to the people who kindled my interest in science and fostered that interest to make this day possible.

To my parents for having infinite patience with a daughter who entered the "why phase" at age four and has never gotten over it.

To Dr. Karen Strickler for showing me that asking why is paramount to good science, but it is only the beginning.

To Virginia Scott for introducing me to the world of insects and plants and showing me that expertise outranks credentials any day of the week and that love of science does not mean giving up your life to it.

To Dr. Michael Gretz for being kind, encouraging, and crazy enough to let an undergraduate take the wheel at his "benchtop Ferrari." Most especially, I'd like to thank Dr. Gretz for being the only voice shouting "go for it" above the chorus of "wait until you're in graduate school."

To Dr. Thomas Loehr for his quiet support, good humor, and lust for science, sailing and living well. Most of all I will miss his merciless attention to detail. I can honestly say that his superb editing skills produced my finest writing.

To Nancy Christie and Terrie Hadfield, the heart and soul of our department, for providing invaluable advice, innumerable favors, and life-saving laughter (not to mention life-saving seminar cookies). I owe what tiny bit of sanity I retain to these two extraordinary women.

Finally, to all my friends for sharing triumphs and tragedies, for coffee, Thai food, stomps around the duck pond, home-brewed beer, political rants, lunchtime small talk, and for magically finding a way to make me feel a bit better. I remain forever in your debt.

TABLE OF CONTENTS

LIST OF TABLES

LIST OF FIGURES

LIST OF ABBREVIATIONS

Ca^{2+}	calcium cation
Cd^{2+}	cadmium cation
EPR	electron paramagnetic resonance
IR-MCD	infrared magnetic circular dichroism
LiP	lignin peroxidase
LMCT	ligand to metal charge transfer
MCD	magnetic circular dichroism
Mn^{2+}	manganous ion
Mn^{3+}	manganic ion
MnP	manganese peroxidase
MnPI	oxidized manganese peroxidase compound I oxyferryl porphyrin pi cation radical
MnPII	oxidized manganese peroxidase compound II oxyferryl
RR	resonance Raman
UV	ultra-violet

Abstract

Structure/Function Studies of Manganese Peroxidase

Heather L. Youngs

Ph.D., OGI School of Science and Engineering

at Oregon Health & Science University

May 2003

Thesis Advisors: Drs. Thomas M. Loehr and Michael H. Gold

Lignin is a cell wall polymer that provides rigidity, cell adhesion, and microbial resistance to vascular plants. A sort of natural plastic, lignin contains more than 13 different randomly arranged chemical linkages and is responsible for sequestering roughly 25% of the world's terrestrial biomass. The resulting heterogeneous three-dimensional matrix is resistant to enzymatic hydrolysis and is chemically stable under most environmental conditions. White-rot fungi are the only organisms capable of completely degrading the lignin polymer, and manganese peroxidase is a key enzyme in this process. It is the only enzyme known that selectively binds Mn^{2+}, oxidizes it and releases Mn^{3+}. In this work, the unique Mn-binding site of the enzyme was probed by site-directed mutagenesis. The results indicate that the ability of the enzyme to bind and oxidize Mn^{2+} is highly dependent on the specific ligation geometry of the site. Kinetic and structural analyses indicate that occupation of the Mn^{2+}-binding site by foreign metal ions prolongs inactivation of the enzyme by heating and exposure to high pH. Finally, Cd^{2+} was identified as a reversible, competitive inhibitor of Mn^{2+} oxidation. Kinetic constants for inhibition were derived in the steady and transient states. Physical studies indicate a possible

secondary metal binding site at the C-terminus that may play a role in thermal stabilization of the protein and/or selective occupation of the Mn-binding site by metal ions.

CHAPTER 1
INTRODUCTION

1.1 LIGNIN IN WOOD

1.1.1 The Biochemistry of Wood

Wood is arguably the most used biomaterial in all of human history. A conglomerate of "modified" plant cell walls, wood contains four main types of biopolymers. Three of these wood polymers are polysaccharides: cellulose, glucan, and hemicellulose (consisting of xylans and mannans). Polysaccharides comprise $\sim 75\%$ of the total carbon in wood. The remainder is sequestered in the fourth biopolymer, lignin.

Primary cell walls, formed first by plant cells, consist almost exclusively of cellulose, hemicellulose, and pectin. Cellulose micro- and macrofibrils form the major oriented skeleton of the wall. Hemicelluloses are thought to reinforce and cross-link the fibrils while pectins fill in the matrix and provide adhesion between walls [207]. Secondary cell walls are produced during (and may very well be the cause of) the cessation of cell growth and expansion. These structures contain lignin, an aromatic polymer highly associated with the hemicellulose matrix (Figure 1.1) [97, 207]. The exact chemicostructural variations, weight percentages, and crosslinking of polymers differ greatly among woody plants. Furthermore, these properties have tremendous effects on the recycling of 10^4 tons of biomass by saprophytic organisms each year [33, 54, 178, 318].

Generally, wood is divided into two types: hardwood, produced by angiosperms, and softwood, produced by gymnosperms. Hardwoods contain slightly less lignin than softwoods and the chemical composition of the lignin differs [117]. Angiosperm lignin contains nearly equal mixtures of syringyl and guaiacyl units (the

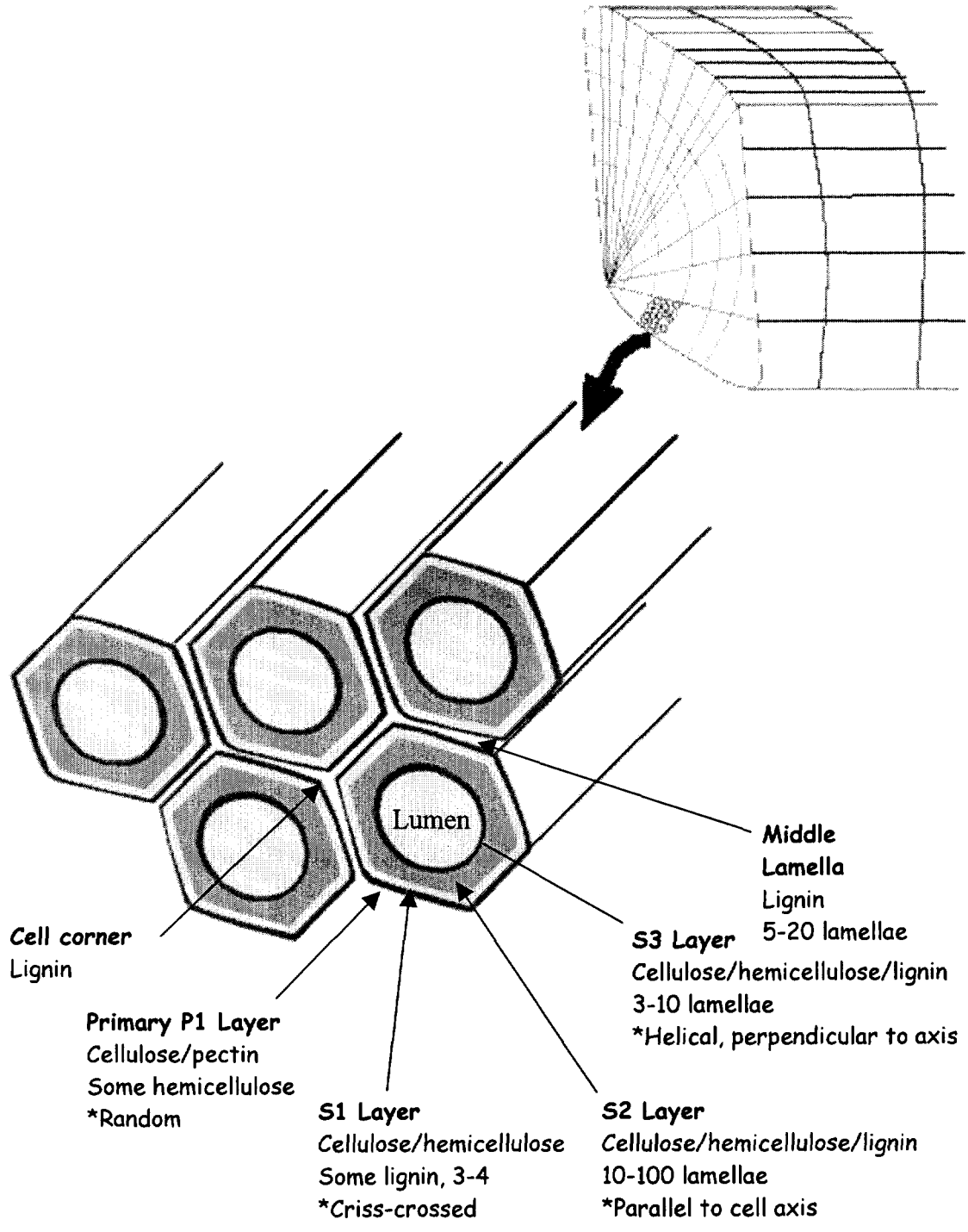

Figure 1.1 The structure of wood. Tracheary elements are simply arranged in a block of gymnosperm wood. Deposition of cell wall material begins with primary wall, followed by the S layers moving in towards the lumen of the cell. Lignification occurs as cell growth and expansion ceases, beginning at the cell corners and spreading through the middle lamella. The S layers become increasingly lignified as the vessels mature and the cells perish, leaving the ater conducting lumen. *Indicates the orientation of cellulose fibrils [201].

lignin from grasses also containing p-coumaryl units), whereas gymnosperm lignin contains predominantly guaiacyl moieties (Figure 1.2) [243]. Composition of lignin within various tissues is also variable and greatly affects the physical properties and degradation of the wood substrate [331].

The hemicellulose composition of the two groups is also quite different. Hardwoods typically contain 3-fold higher percentages of xylans and are almost devoid of mannans compared to softwoods, which may contain up to 15% mannans [117]. Finally, the distribution of polymers differs in various layers of the cell wall. For example, the secondary cell walls of tracheary vessels in white birch (*Betula papyrifera*), an angiosperm, contain mostly guaiacyl lignin. In contrast, fiber and ray cells in this tree contain mostly syringyl lignin, and the middle lamellae of fiber cells contain syringyl-guaiacyl lignin (Figure 1.1) [278].

1.1.2 Nutrients in Wood

Wood is a nutrient-poor substrate. Although containing abundant organic carbon, it is sequestered in polymeric form, the majority of which is either crystalline cellulose or non-hydrolyzable lignin. The woody matrix has low nitrogen levels resulting in an extraordinarily high carbon to nitrogen ratio. The C:N ratio in wood averages around 400:1 and ratios as high as 1250:1 have been found in Sitka spruce. In contrast the C:N ratios of fungal mycelia averages 35:1 [77, 383, 441]. These component ratios offer important environmental cues to invading microorganisms. For example, low levels of nutrient nitrogen and/or available organic carbon are among several inducers of lignin-degrading enzyme production in white-rot fungi [31, 140, 212, 244].

Wood contains a variety of trace metal nutrients [441]. Magnesium and potassium are the most abundant. Manganese ranks third at 2–10 times the levels of iron and sodium [441]. Wood-degrading organisms are essential for the re-entry of these nutrients into the biosphere. During degradation, many of the nutrients are absorbed by fungi or concentrated as precipitates and later resolubilized by bacteria [317]. For example, calcium oxalate deposits are often observed along fungal hyphae [81] and, although evenly distributed in sound wood, large dark deposits of oxidized

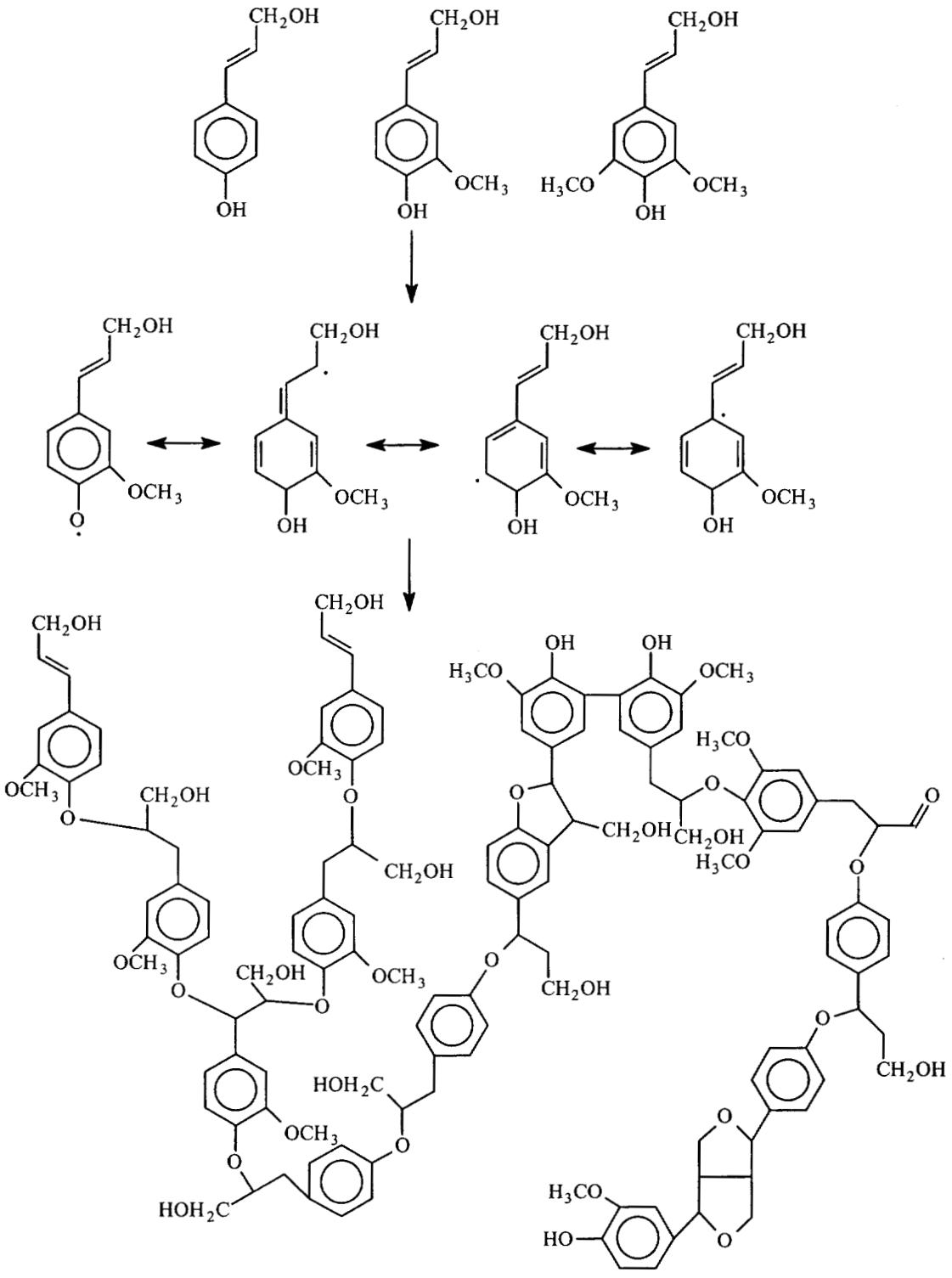

Figure 1.2 Lignin structure and biosynthesis. Aromatic precursors, p-coumaryl, guaiacyl, and syringyl alcohols (top left to right), are oxidized to form radicals (shown for guaiacyl alcohol), which undergo radical isomerization and condensation to form the various linkages in lignin (bottom) [339].

manganese (MnO_2) are often visible at sites of white rot by basidiomycetes [35]. This latter phenomenon and the role of manganese in lignin degradation are discussed in more detail in Section 1.10.

1.1.3 The Structure of Lignin

Lignin is a phenylpropanoid polymer formed by the extracellular, free radical condensation of phenolic precursors (Figure 1.2) [243]. The cinnamyl alcohol precursors, *p*-coumaryl, sinapyl, and coniferyl alcohols, are formed as secondary metabolites from amino acids via the phenylalanine-cinnamic acid pathway [152, 279]. The free phenols and their dimers (lignans) are cytotoxic [303], therefore, the precursors are stored in the vacuole and/or excreted into the plant apoplast as phenyl-glycosyl conjugates [307, 390]. The sugar blocks the reactive phenol moiety and may provide a checkpoint in lignin formation. Extracellular glycosidases are believed to release the phenolic precursors, which may then undergo oxidation by plant cell wall peroxidases and laccases to produce free radical phenylpropane derivatives [163, 257]. Condensation reactions then occur, resulting in a heterogeneous, optically inactive, amorphous, highly branched polymer containing more than 13 different internuclear linkages (Figure 1.2) [79, 273]. The majority of internuclear linkages in lignin are ether bonds, however, the polymer also contains many different non-phenolic carbon–carbon bonds. In addition, the lignin is often covalently linked to carbohydrate and/or to cell wall proteins such as extensin via hydroxyproline residues [122].

Often described as a random, three-dimensional polymer, lignin may actually be a fractal crystal [314, 315]. The fractal dimension of *in vitro* synthesized lignin, determined by scanning tunneling electron microscopy, indicates that the polymer chains are arranged as regular objects [315]. Similar results have been reported from hydrodynamic studies of isolated lignin. The underlying geometry of the polymer is consistent with calculations for both endwise and bulkwise polymerization mechanisms [289], indicating that both types of polymerization may occur within the cell wall. Most of the aromatic rings in lignin are found oriented parallel to the cell wall surface and involvement of the underlying cellulose matrix in directing lignin polymerization

has been suggested [16, 388]. In addition, there is evidence for directed polymerization via "dirigent" or guiding proteins within the cell wall matrix [55, 92, 127]. These proteins, heterologously expressed in the baculovirus system, contain no discernable enzymatic activity yet can direct stereospecific coupling of chemically generated free radical lignin precursors (Figure 1.2) [127].

1.1.4 The Function of Lignin

The chemical complexity of lignin underlies many of its most useful features. The polymer is highly branched and hydrophobic, allowing complete intercalation and encrustation of the polysaccharide extracellular matrix. The type and variation of bond linkages in the polymer make it virtually invulnerable to hydrolytic attack. Thus, lignin imparts structural integrity and microbial resistance to woody tissues, forming a water-impermeable cement that is crucial to the development of water conducting vasculature in higher plants.

All modern plants, except true mosses and algae, manufacture lignin [79]. Lignin formation is believed to have evolved as a waste disposal method, the oxidative polymerization and subsequent precipitation of excreted phenolic byproducts and secondary metabolites [279]. Following lignification, the newly encrusted cell wall can no longer expand under increasing turgor pressure. Thus, although cell growth is limited, the decreased elasticity of the wall allows sufficient hydrodynamic potentials to allow extended vertical growth on land. The adaptation of height and resulting competition for light resources are thought to be responsible, in part, for the explosion of land tracheophyte speciation in the early Paleozoic era [17]. The evolution of lignin also created new niches for organisms capable of its utilization. Fossil evidence for white-rot decay by basidiomycetes also dates to this era [374]. It is perhaps not surprising that lignin formation and degradation may have evolved simultaneously. The enzymes involved appear to be highly related (see Section 1.4).

The resistance of lignin to enzymatic degradation has profound ecological significance. In addition to affording microbial resistance to intact plants, lignocellulosic material serves as a carbon sink, constituting roughly 25% of the world's terrestrial biomass [47]. Partially degraded lignin products (humus) bind and

control release of cationic nutrients in forest soils [186, 265]. It is clear that research on lignin-degrading organisms and their extracellular enzyme systems is important, not only for understanding important arboreal ecosystems, but for developing technology to efficiently produce food, fuel, and manufacturing materials from terrestrial biomass.

1.2 LIGNIN-DEGRADING MICROORGANISMS

There are four basic classes of wood-degrading microorganisms: bacteria and the soft-rot, brown-rot, and white-rot fungi. White-rot fungi appear to be the only organisms that can fully mineralize lignin, however, they rarely exist alone in nature. Rather, a consortium of lignin-degrading and lignin-modifying microorganisms is present in, on, and surrounding the rotting wood matrix in nature. More than 30 different species of fungi have been identified on a single fallen tree and there is evidence that the population changes as the substrate composition is altered through decay [317].

Consortium composition profoundly affects the rate and extent of lignin degradation. For example, wood in wet environments is preferentially attacked and degraded by soft-rot fungi and bacteria, which are more tolerant to high moisture and reduced oxygen conditions than basidiomycetes. Since basidiomycetous fungi are normally more aggressive and can degrade wood faster than soft-rot fungi and bacteria, wood in wet, especially anaerobic environments may survive for millions of years [353, 363]. Morphological evidence exists for both antagonistic inhibition and synergistic associations within wood-rotting consortia [37, 317].

1.2.1 Bacteria

Wood-degrading bacteria often function as primary colonizers by removing antimicrobial free phenols and degrading tyloses, structures that occlude the pit connections between xylem cells [150]. The increased permeability of the woody matrix [151] following colonization allows diffusion of oxidative enzymes, small molecule mediators, and breakdown products. Bacteria cannot completely degrade

lignin; however, several Actinomycetes (*Streptomyces* spp.) and Gram-negative Eubacteria (Pseudomonadaceae and *Xanthomonas* sp.) are capable of modifying lignin substructures [78, 234]. These organisms can also metabolize a variety of lignin-related aromatic compounds [80, 247]. For example, *Sphingomonas paucimobilis* SYK-6 can grow on various lignans, which are converted to vanillate and syringate and further metabolized [180].

1.2.2 Soft-Rot Fungi

Soft rot is characterized by specific degradation of the S2, or middle layer of the secondary cell wall (Figure 1.1) by fungi in the Ascomycotina and Deuteromycotina [111]. This type of rot is named for the "soft" appearance of the decayed surface layer when moist. Although when dry, soft-rotted wood appears much like brown rot, the two groups of fungi are quite easily distinguished morphologically. Soft-rot fungi can modify and slowly degrade some lignins. They preferentially degrade hardwoods over softwoods, primarily because the high guaiacyl content in softwood lignin is particularly difficult for these fungi to degrade [59, 444]. Overall, the rates of lignin decay by soft-rot fungi are quite slow, compared to the white-rot basidiomycetes (Table 1.1). As a result, this group of fungi is less studied than either the brown- or white-rot fungi.

1.2.3 Brown-Rot Fungi

Brown rot appears to be the product of fungal species only in the Basidiomycotina [133, 134]. During brown rot, a single hypha in the cell lumen can accomplish extensive cell wall destruction [111], characterized by substantial loss (80–95%) of carbohydrate but minimal lignin degradation ($\sim$10%) (Table 1.1). Extensive removal of carbohydrate from the wood matrix by hydrolytic enzymes leaves the brown lignin framework, which becomes loose and brittle [111]. Brown-rot fungi are poor lignin degraders but can efficiently demethylate both phenolic and non-phenolic lignin components [219, 220].

Although brown-rot fungi account for less than 6% of all wood-rotting fungi in North America [133], the powdered lignin byproduct of brown rot may constitute up

Table 1.1

Comparison of the Extent of Hardwood Birch (*Betula papyrifera*) or Poplar (*Populus basamifera*) and Softwood Pine (*Pinus stroba* or *P. monticola*) Degradation by Various Wood-Rotting Fungi after 12 Weeks

	Percentage loss				
	Weight	Lignin	Glucose	Xylose	Mannose
HARDWOOD					
Soft-rot					
Papulaspora sp.	21	4	27	29	25
Paecilomyces sp.	28	11	41	37	30
Thielavia terrestris	23	13	25	27	43
Brown-rot					
Poria placenta	57.9	4.7	81.2	81.8	95.0
Gloeophyllum trabeum	43.7	13.1	48.6	71.1	95.0
Lentinus lepidius	59.2	7.9	78.6	79.8	95.0
White-rot					
Phanerochaete chrysosporium	39.1	72.9	15.1	55.1	0
Coriolus versicolor	65.3	64.6	65.4	68.8	71.7
Dichomitus squalens	44.4	71.2	43.8	43.5	40.4
Ustilina vulgaris	22.9	6.3	25.0	14.9	25.5
SOFTWOOD					
Soft-rot					
Papulaspora sp.	15	12	18	18	13
Paecilomyces sp.	10	14	7	8	6
Thielavia terrestris	7	14	3	9	0

Table 1.1 (continued)

	Percentage loss				
	Weight	Lignin	Glucose	Xylose	Mannose
Brown-rot					
Poria placenta	55.1	12.5	78.7	81.1	92.1
Gloeophyllum trabeum	57.2	27.3	73.9	90.7	91.8
Lentinus lepidius	59.7	11.4	83.8	98.2	94.1
White-rot					
Phanerochaete chrysosporium	19.5	30.5	3.9	44.1	0
Coriolus versicolor	25.3	35.4	22.1	46.7	11.6
Dichomitus squalens	43.1	53.0	48.3	56.9	64.9
Ustilina vulgaris	3.3	–	–	–	–

Compiled from data in ref. 111.

to 30% of humic soils and supports high levels of microbial activity [265]. Functioning to retain and slowly release moisture and micronutrients, brown-rot residues serve an important role in the arboreal ecosystem [241].

1.2.4 White-Rot Fungi

White-rot basidiomycetes may be the oldest class of wood-degrading fungi and are the only organisms capable of completely mineralizing lignin [222, 374]. Although, "white" rot by actinomycetous fungi such as *Ustilina vulgaris* has been observed, lignin degradation by these organisms occurs at a significantly lower rate than for most basidiomycetes (Table 1.1) [36, 38]. Therefore, the inclusion of Actinomycetes as white-rot fungi is dubious, in spite of the prevalence of this classification in the literature.

White-rot basidiomycetes display multiple modes of attack on the wood substrate. The two most commonly observed types of decay are: (1) sequential decay, characterized by the preferential degradation of lignin followed by cellulose and carbohydrate metabolism and (2) simultaneous decay of all cell wall components [34, 110]. Both types of attack are displayed by individual species and there is some evidence that cell type and lignin composition influence the mode of attack and progress of degradation [54, 236]. Sequential decay by white-rot fungi has been particularly well studied. Complete delignification of the xylem is typically noted, along with partial removal of hemicellulose, leaving the white cellulose matrix. Because the middle lamella is mostly lignin, removal of this layer during sequential decay often eliminates cohesion of the tracheids giving a stringy appearance to the wood [111]. The enzymes involved in lignin degradation by these organisms are discussed in Sections 1.3 and 1.8.

1.2.5 Litter-Decomposing Fungi

Wood is not the only lignified plant tissue. Significant quantities of lignin are also deposited in other plant tissues such as leaves and herbaceous stems. Annually, an average two tons of plant debris per hectare are deposited on forest floors [175]. Leaf litter comprises 60–70% of the material; branches (12–15%), bark (1–14%) and

fruits (1–17%) make up the remainder [185]. 80–90% of the tissues contain some lignin. Recently several species of plant litter decomposing basidiomycetes have been shown to possess lignin-degrading enzymes [369]. Closely related to wood-rotting basidiomycetes, these organisms do not grow directly on wood but are widespread in forest and grassland soils [95]. Analysis of different plant litter decaying species indicates the presence of laccase in 25 of 27 species tested [369]. Manganese peroxidase production was detected in 10 species and aryl oxidase in one species. Apparently, lignin peroxidase has not yet been detected in this group of fungi [369].

1.3 THE EXTRACELLULAR LIGNIN DEGRADING SYSTEM OF *PHANEROCHAETE CHRYSOSPORIUM*

The white-rot fungus *Phanerochaete chrysosporium*, formerly known as *Chrysosporium lignorum* and *Sporotrichum pulverulentum* [52, 53], is the best-studied lignin-degrading microorganism. This fungus has several advantages for scientific study including ease of culture, relatively fast growth, tolerance to higher incubation temperatures, and relatively high lignin degradation rates in nature and in culture [224]. Finally, the fungus is a prolific sporulator in culture. Both sexual and asexual reproductive cycles can be manipulated by culture conditions, allowing genetic studies [6, 8, 53, 140, 141].

Lignin degradation is an extracellular, oxidative process [29, 114, 222] while concomitant reduction of byproducts occurs intracellularly [48, 58, 325]. Production of the extracellular lignin degradation system by *P. chrysosporium* is triggered by the onset of idiophase, the switch to secondary metabolic pathways, following cessation of primary growth (trophophase) due to nutrient limitation [212, 224, 404]. Under these conditions, *P. chrysosporium* secretes two peroxidases, lignin peroxidase and manganese peroxidase, a hydrogen peroxide generating system and several small molecule mediators that act in concert to depolymerize and fragment the lignin matrix [140].

1.3.1 Peroxidases

The first lignin-degrading peroxidases were discovered in *Phanerochaete chrysosporium* [137, 142, 395, 396]. Under ligninolytic conditions, *P. chrysosporium* produces manganese peroxidase (MnP, EC 1.11.1.13) [136] and lignin peroxidase (LiP, EC 1.11.1.14) [143]. Both are heme proteins, sharing very similar overall structures and reaction cycles, as discussed in Sections 1.5.1 and 1.6.3. The two enzymes, produced as a series of isozymes, are encoded by families of genes sharing ~60% nucleotide identity [140]. Both enzymes use diffusible mediators and are capable of oxidizing phenolic linkages in lignin model compounds [26, 41, 403, 424]. In addition, LiP is capable of oxidizing non-phenolic linkages using its normal mediator, veratryl (3,4-dimethoxybenzyl) alcohol [251]. The Mn^{3+}-chelates generated by MnP cannot oxidize nonphenolic linkages directly, however, other mediators, such as lipids, may perform this reaction [366, 427] (see Section 1.6). Relevant comparisons of the two enzymes are made throughout this text; however, LiP is not discussed at length in this work [see 100, 140, 144, 177, 222, 343, 344].

1.3.2 Hydrogen Peroxide Generating Enzymes

Under ligninolytic conditions, *P. chrysosporium* secretes two hydrogen peroxide generating enzymes. The first discovered was the copper-containing enzyme, glyoxal oxidase (EC 1.2.3.5) [92, 210, 434]. This enzyme, encoded by at least two allelic variants [211], can oxidize a variety of substrates including glyoxal, methyl glyoxal and other α-hydroxy- and dicarbonyl compounds to produce H_2O_2 from O_2 [208, 210]. There is also evidence that the enzyme works in concert with LiP, using glycoaldehyde, produced by certain C_α-C_β cleavages, as a substrate [161]. The second enzyme isolated from *P. chrysosporium*, pyranose oxidase (also called glucose-2-oxidase, EC 1.1.3.10), is widely found in other white-rot fungi [86, 417]. This enzyme has broad substrate specificity for pyranoses such as D-glucose and D-xylose [131]. Pyranose oxidase is a homotetrameric flavoprotein, localized in the hyphal periplasm [87]. The enzyme from *P. chrysosporium* is nonglycosylated, whereas the homologues produced by other white-rot fungi are highly glycosylated

[13, 131]. Other sources of H_2O_2 may include the hydrolysis of the fungal glucan sheath and/or reactions between MnP-generated Mn^{3+} and glyoxalate [232, 332].

1.3.3 Other Enzymes and Small Molecules/Mediators

Under ligninolytic conditions, *P. chrysosporium* also secretes at least two acidic proteases [89, 90], a galactosidase [51], and complex xylanolytic [74, 75, 91] and cellulolytic systems [108, 174, 350]. In addition to enzyme systems, several low molecular weight metabolites are produced. *P. chrysosporium* secretes several organic acids such as oxalate, malonate, citrate, and glyoxalate during idiophasic metabolism [30, 103, 233, 426]. The pH optima for most of the extracellular lignin degrading enzymes range from pH 3 to 5 [90, 135, 143, 397]. In addition, these acids serve as chelators for calcium and manganese in the wood substrate. Oxalate performs a critical functional role in removing oxidized manganese from the MnP active site, allowing turnover of the enzyme [214, 227, 445]. The role of chelators in the MnP reaction and of Mn-chelates as diffusible mediators is discussed in detail in Section 1.6. Finally, *P. chrysosporium* secretes veratryl (3,4-dimethoxybenzyl) alcohol, which is a substrate and mediator for lignin peroxidase [83, 166, 216, 399, 445].

1.4 HEME PEROXIDASES

1.4.1 The Heme Peroxidase/Catalase Superfamily

Most heme-containing peroxidases and catalases are considered members of an evolutionarily related protein superfamily divided into three classifications: plant/fungal peroxidases, animal peroxidases, and catalases. The plant/fungal peroxidase family is further separated into three classes: intracellular/bacterial peroxidases (class I), extracellular fungal peroxidases (class II) and extracellular plant peroxidases (class III). Only features of the plant/fungal peroxidase family are presented in this work. For an excellent comprehensive review of the entire superfamily, see *Heme Peroxidases* by H. B. Dunford [100].

1.4.2 Plant Peroxidases

1.4.2.1 Shared structural and catalytic features. Classification of the plant peroxidases is largely based on sequence homologies and available crystal structure data. A prototypical peroxidase fold was identified from the intracellular yeast cytochrome *c* peroxidase (CcP) [430]. The basic structure contains ten major α-helices, lettered A–J, arranged in two similar domains. A pentacoordinate ferric heme is sandwiched between the domains, near helices B and F (Figure 1.3).

Based on the conserved positions of catalytic residues, introns, and calcium ligands, it is believed that this arrangement evolved by a gene duplication and subsequent fusion of the sequence encoding the first five helices [432]. Surface loops connecting the helices vary considerably and many peroxidases contain additional smaller alpha helices [432]. The extracellular class II and III enzymes typically, though not always, contain structural modifications including calcium binding sites, cystine bridges, and/or glycosylation [430].

Plant and fungal peroxidases contain nine completely conserved residues: Arg48, His52, and Asn82 in the distal domain, and Val169, His175, Asp235, Asp106, Gly129, and Arg130 in the proximal domain, using the yeast CcP amino acid sequence numbering (Figure 1.4) [384, 433]. His175 is the fifth heme ligand and is H-bonded to Asp235 [119]. Asp106, Gly129 and Arg130 form a buried salt bridge in the proximal domain. Asn82 forms an H-bond with His52, the catalytic histidine [119]. In conjunction with Arg48, His52 assists peroxide binding to the open coordination site of the heme iron and promotes peroxide cleavage [416]. In addition, there are approximately twenty "nearly invariant" residues, which include several aromatic residues in the heme pocket.

All the plant/fungal peroxidases also share a common catalytic cycle (Figure 1.5). Hydrogen peroxide is heterolytically cleaved through interaction with the native, ferric heme to produce a ferryl-oxoheme. An additional reducing equivalent is required to complete the reaction and affect release of a water molecule. In some members of the family, this equivalent is supplied by oxidation of a tryptophan in the proximal heme pocket to form a Trp radical [261, 352]. In other members, the

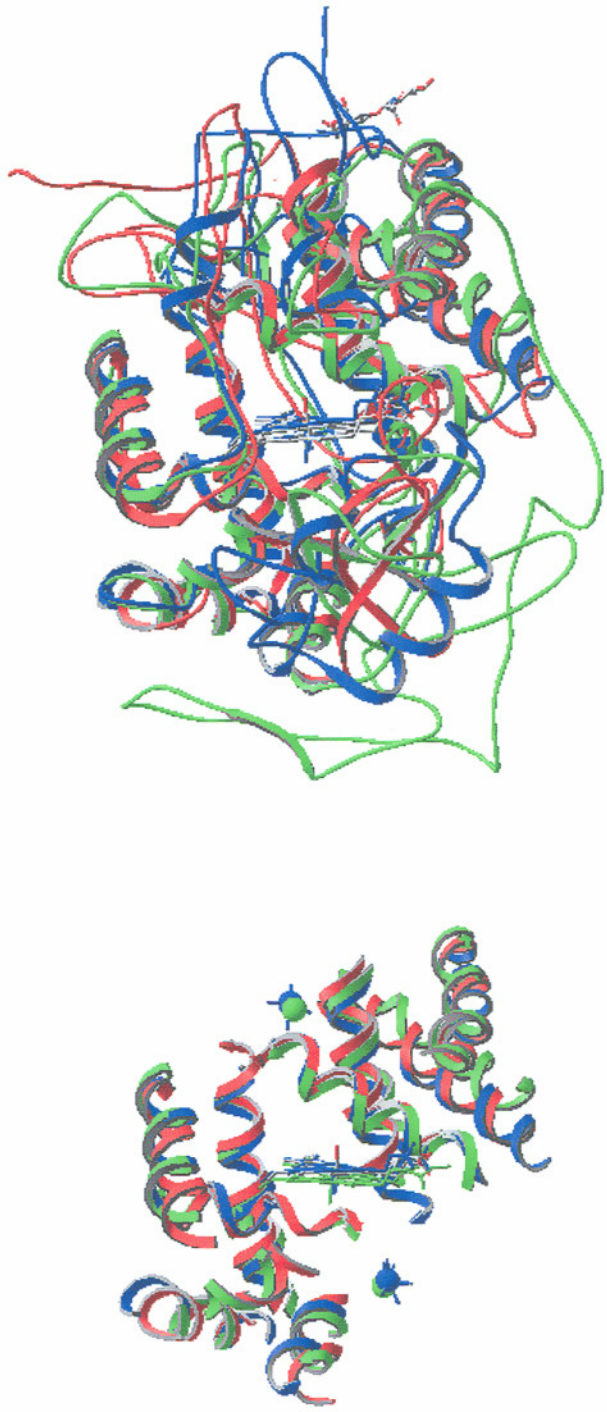

Figure 1.3 Comparison of plant peroxidase crystal structures. Type I, cytochrome *c* peroxidase (red) [421]. Type II, manganese peroxidase (green) [376]. Type III, horseradish peroxidase (blue) [125]. Total structure overlay (**top**) and conserved helices, hemes and calcium atons (type II and III only) (**bottom**). Overlays were done using the Swiss PDB Viewer from Glaxo-Wellcome.

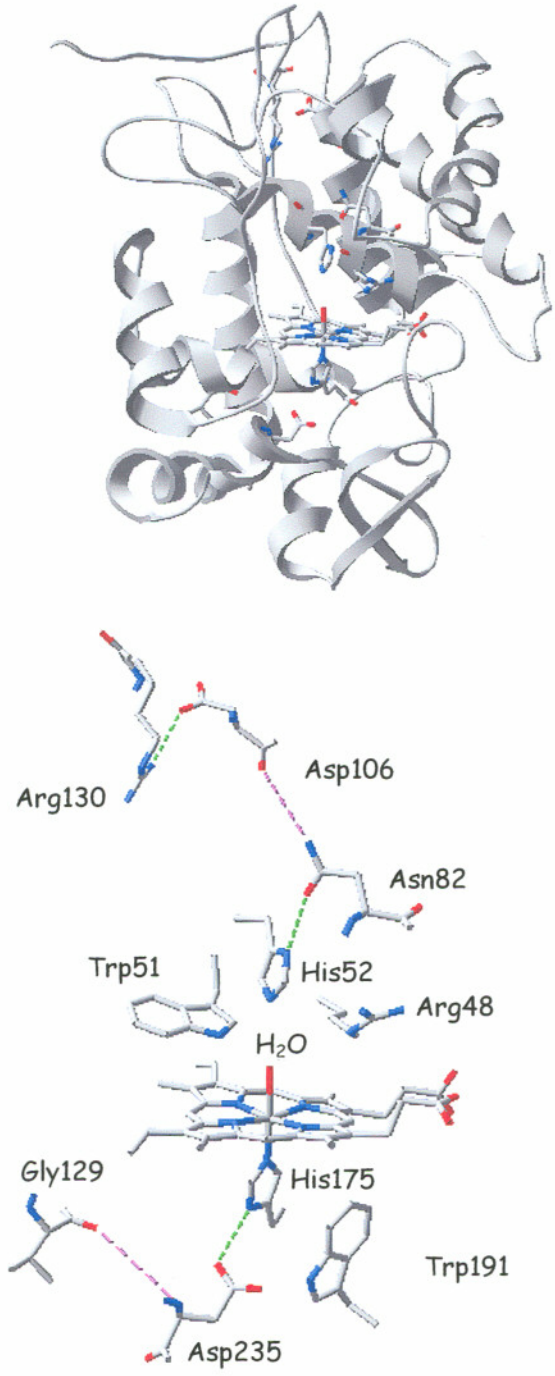

Figure 1.4 The crystal structure of cytochrome *c* peroxidase. The overall structure (**top**) and heme environment (**bottom**) [421].

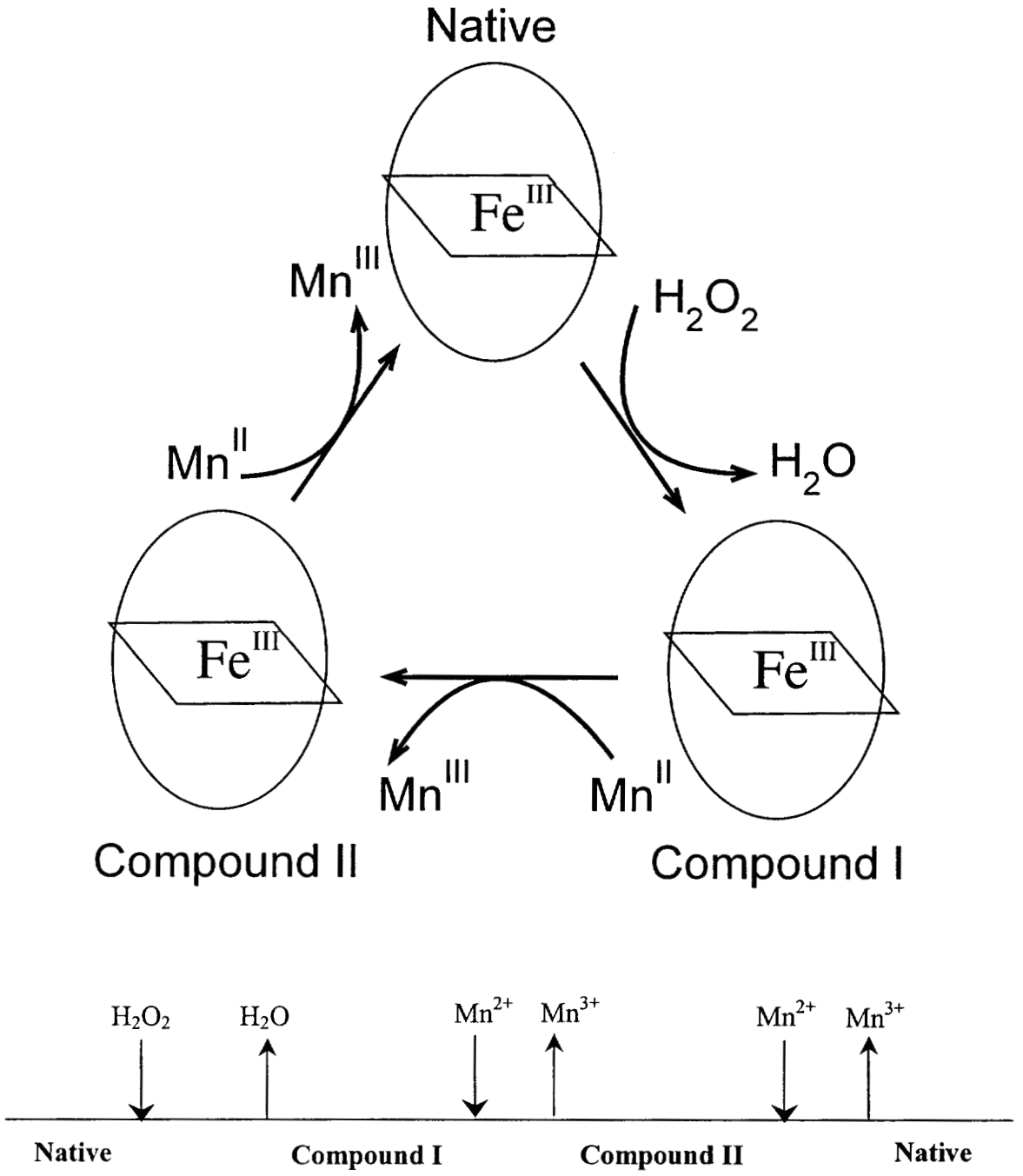

Figure 1.5 The catalytic cycle and kinetic mechanism of manganese peroxidase. The native ferric heme is oxidized by hydrogen peroxide to produce a water molecule and compound I, which contains a ferryl-oxo heme and porphyrin pi cation radical. The porphyrin radical is reduced by Mn^{2+} to yield Mn^{3+} and compound II. A second molecule of Mn^{2+} reduces compound II back to the native ferric state, with the release of a second water molecule Compound II can also react with excess hydrogen peroxide to form an inactive Fe^{II}-O_2 species, compound III (not shown) [422]. The kinetic model is a modified bi-bi ping pong mechanism with sequential substrate binding and product release [100].

electron comes directly from the heme, resulting in a porphyrin π cation radical [287, 327].

All plant/fungal peroxidases oxidize a range of small aromatic compounds, depending on the redox potential of the enzyme. However, MnP is the only enzyme in this group with a non-aromatic preferred substrate, the manganous ion (Mn^{2+}) [413, 422]. In the absence of manganese, MnP is a uniquely poor oxidizer of aromatic compounds, though it has a relatively high redox potential compared to other heme peroxidases [3, 226, 237, 398, 423, 436].

1.4.2.2 Class I extracellular fungal peroxidases. The class I plant/fungal peroxidases, considered to be of prokaryotic origin, include the cytosolic and chloroplastic ascorbate peroxidases (APX), yeast cytochrome *c* peroxidase (CcP) and the bacterial catalase-peroxidases. The enzymes do not contain calcium, carbohydrate or disulfide bridges [430]. Most of the enzymes in this class contain a heme pocket tryptophan. In CcP, this residue (Trp191) is oxidized to a radical during the reaction cycle. Protonation state of the Trp, mediated by the proximal hydrogen bonding triad, His175, Asp235, and Trp191 (Figure 1.4), appears to modulate the site of radical formation. If the H-bond shifts the proton from Trp to Asp, a Trp cation radical is formed, whereas, if the Trp remains protonated, the electron is taken from the porphyrin [266]. Uniquely, APX appears to have a potassium-binding site near the proximal Trp and does not form a Trp cation radical following oxidation by peroxide. Rather, this enzyme forms a porphyrin π-cation radical, as observed in type II and III enzymes that do not contain a proximal Trp residue [292]. In APX, the potassium-binding site may important in preventing radical formation at the proximal Trp [44, 67, 312].

Although yeast cytochrome *c* peroxidase has been chosen as the prototypical member of this class, it appears that many of the bacterial cytochrome *c* peroxidases belong to a group of diheme peroxidases that do not fit any of the current classifications. Examples include cytochrome *c* peroxidases from several *Pseudomonas* sp. and *Nitrosomonas europea* [100 and references therein]. The dimeric enzymes contain two interacting hemes, one ferrous and one ferric, in each monomer. Only one of the hemes is pentacoordinate and functions in peroxide

binding. The second, hexacoordinate heme provides additional reducing equivalents such that, unlike the plant peroxidases, no radical enzyme intermediate is ever formed during the reaction cycle [100 and references therein].

1.4.2.3 Class II extracellular fungal peroxidases. Members of this class include lignin and manganese peroxidases (LiP and MnP), several "versatile" peroxidases (see Section 1.8), and a peroxidase from *Coprinus cinereus* (also known as *Arthromyces ramosus*) (CiP/ArP). In all class II enzymes, the proximal Trp in CcP is replaced by either Phe [309, 376] or Leu [235, 302]. Thus, reaction with H_2O_2 produces a porphyrin π-cation radical. Lignin peroxidase was the first enzyme in this class to yield an X-ray structure [105, 304, 309]. These enzymes share several structural features with the class III enzymes, including two structural calcium ions, glycosylation, leader peptides for secretion, and disulfide linkages [248]. The structural features of this class, and specifically MnP, are discussed in detail in Section 1.5.

1.4.2.4 Class III extracellular plant peroxidases. Examples of class III include turnip peroxidases, several dozen enzymes generically classified as "acidic" or "basic" peroxidases from various plants, barley peroxidase, and the most well-studied peroxidase, horseradish peroxidase (HRP). The first peroxidase intermediates were isolated from HRP in the late 1930's [206, 393]. HRP was also the first peroxidase to be sequenced [428]. Although peanut peroxidase was the first class III enzyme to yield reliable crystallographic information [345], the structure for HRP was eventually determined [125]. Interestingly, the structural and catalytic similarities between CiP/ArP and HRP further indicate the ancestral ties between these two classes of enzymes [100 and references therein].

Overall, the class III enzymes appear to be more glycosylated than the class II enzymes, containing up to 25% sugar [100]. Many contain N-terminal leader peptides for secretion, although some, such as HRP, contain C-terminal sequences and are directed to the vacuole [432]. Like the class II enzymes, class III peroxidases contain structural calcium and disulfide linkages [329]. Class III peroxidases also often contain additional α-helices [100, 345]. Peanut peroxidase, an extremely thermostable enzyme, also contains an extra disulfide linkage near the distal calcium

(see Section 1.6.2) [345]. Finally, as in class II enzymes, the proximal Trp191 in CcP is replaced by Phe in most class III enzymes, such as HRP; however, several peroxidases from *Arabidopsis thaliana* contain Met at this position [297].

1.5 THE CRYSTAL STRUCTURE OF MANGANESE PEROXIDASE FROM *P. CHRYSOSPORIUM*

1.5.1 Overall Crystal Structure

Initial biophysical studies indicated that MnP, like other class II and class III plant and fungal peroxidases, is glycosylated and contains one ferric, high-spin, pentacoordinate iron protoporphyrin IX ligated to the protein via a histidyl ligand to the iron [24, 136, 144, 270, 291, 313, 422]. The crystal structure, published in 1994, confirms these observations [376]. MnP contains 10 major α-helices and 1 minor α-helix arranged in two approximately equal sized domains, proximal and distal to the heme, each containing one calcium atom (Figure 1.6) [376]. The overall polypeptide fold is similar to that of other plant and fungal peroxidases [105, 235, 302, 345, 376].

The positions of the calcium sites in MnP are homologous to those in LiP, and CiP/ArP, although the exact ligands are not conserved [235, 309, 376]. In MnP, each calcium is heptacoordinate (Figure 1.7). The distal calcium is bound by the side-chains of Asp47, Ser66, and Asp64, the backbone carbonyls of Gly62 and Asp47, as well as two water molecules (Figure 1.7). As in other peroxidases, the distal calcium provides thermal stability to the enzyme [329, 379, 381, 387].

One of the water ligands to the distal calcium is hydrogen-bonded to Glu74, which forms an H-bond network through Asn80 with the distal His46 [376]. In both MnP and LiP, the distal calcium is coordinated to Asp47, which forms part of the active site and is conserved in many peroxidases [309, 376, 430] (Figure 1.7). The proximal calcium is ligated to the backbone carbonyls of Thr196, Ser174, and Thr193 and the side-chains of Asp191, Thr193, Asp198, and Ser174, adjacent to the proximal His173 [376].

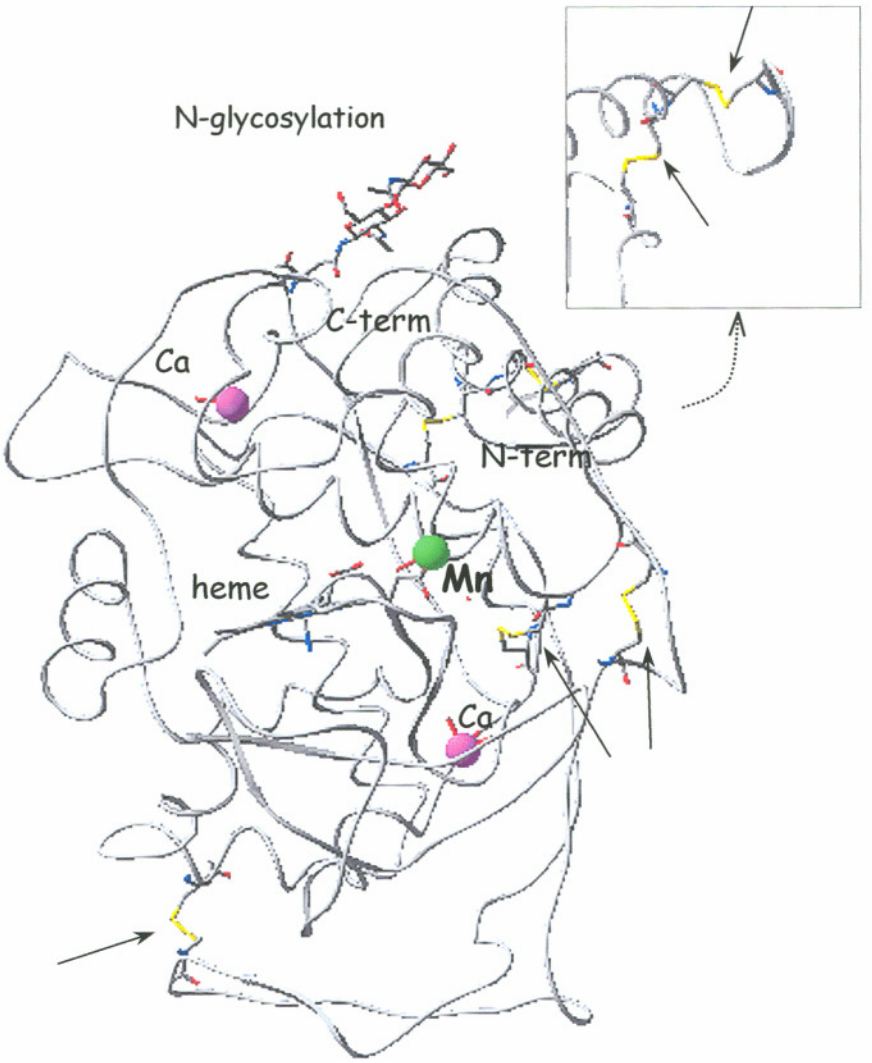

Figure 1.6 The crystal structure of manganese peroxidase from *Phanerochaete chrysosporium* [376]. (**Inset**) Expanded view of the N-terminus depicting the first two disulfide bonds not visible in the main structure.

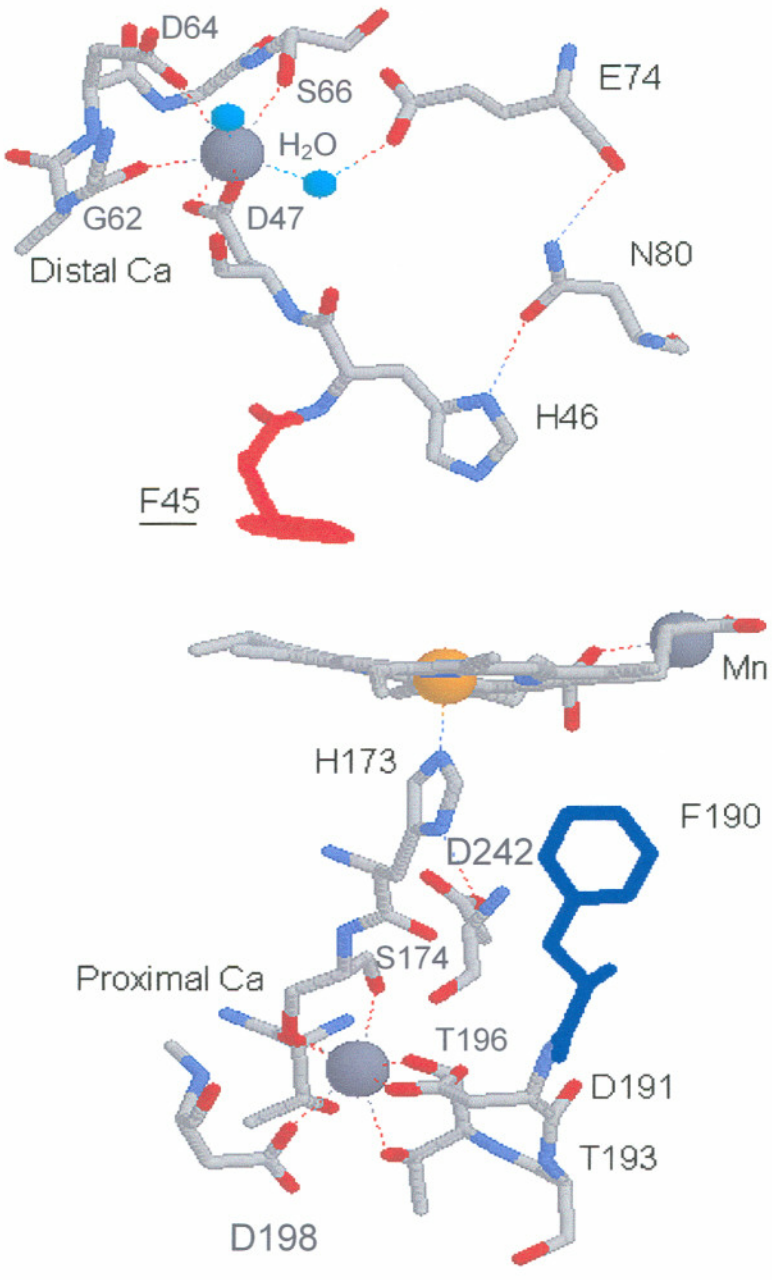

Figure 1.7 Structure of the heme environment and calcium binding sites of manganese peroxidase from *Phanerochaete chrysosporium* [376]. The two catalytic histidines distal (H46) and proximal (H173), conserved aromatic residues F45 and F190, and important H-bonded residues are indicated.

MnP contains five disulfide linkages, four of which are identical to those in both LiP and ArP/CiP [105, 235, 302, 304, 309, 376]. The disulfide linkage pattern of these first four bridges in MnP, 1–3, 2–7, 4–5, 6–8, is identical to that found in other fungal peroxidases and differs from the linkage pattern of homologous plant peroxidases [248, 345]. It has been proposed that the fifth linkage unique to MnP, Cys341-Cys348, not only stabilizes the carboxy-terminal "tail", which is longer than those of LiP and CiP/ArP, but may also participate in stabilization of the manganese-binding site [376]. Several so-called "versatile" peroxidases, exhibiting characteristics of both MnP and LiP, have been identified in other white-rot fungi (see Section 1.8) [15, 189, 194, 197, 204, 333]. The deduced amino acid sequences for these enzymes show shortened carboxy-terminal regions that lack the fifth disulfide, similar to that of LiP. These enzymes oxidize Mn^{II}, but with much slower rates than MnP from *P. chrysosporium* [62, 268].

The MnP crystal structure indicates N-glycosylation at Asn131 (Figure 1.6) [376], one of the putative glycosylation sites predicted by the cDNA sequence [313]. MnP contains several putative sites for O-glycosylation [313] and O-mannosylation has been observed at Ser336 [378] (Figure 1.6). This observation is consistent with glycosylation patterns observed in other extracellular fungal peroxidases [248].

1.5.2 The Heme Environment and Peroxide Binding Site

The heme environment of MnP contains several conserved amino acid residues in the distal domain, including His46, Arg 42, Asn80, Glu74, and Phe45 (Figure 1.7), which are involved in the heterolytic cleavage of peroxide and in heme stabilization. In all heme peroxidases, the distal histidine is believed to act as an acid-base catalyst, accepting a proton from peroxide and facilitating O–O bond cleavage [183, 310]. Arg42, the distal arginine, appears to facilitate the heterolytic cleavage of the peroxide anion as well as to stabilize compound I [311]. Mutation studies of the homologous residue in CiP suggest that this distal arginine may also influence the solvent accessibility to the H_2O_2-binding pocket [281]. The distal Arg in many other peroxidases interacts directly, or through a bridging water molecule, with one of the heme propionates, whereas in MnP, this propionate is rotated such that it

cannot interact with Arg42 [376]. Asn80, Glu74, and His46 form a hydrogen-bonding network believed to participate in modulation of the acid-base character and optimal positioning of the distal histidine for peroxide cleavage (Figure 1.7). These residues and the H-bond distance between Asn80 and His46 are conserved among MnP and other plant and fungal peroxidases [376]. Finally, extracellular plant and fungal peroxidases contain a Phe residue adjacent to the heme in the position of Phe45 [429, 430]. This residue in other peroxidases appears to be involved in stabilizing compound I [354]. Interestingly, MnP contains only one tryptophan, buried in the distal domain, and absolutely no tyrosine residues [313, 376]. Presumably these functional groups have been eliminated by evolution to prevent inter- and intra-protein oxidations, radical formation, and dimerization events.

In the proximal domain, His173, Asp242, and Phe190 are important conserved residues (Figure 1.7). His173, the proximal histidine, forms the fifth ligand to the heme iron thereby tethering the heme to the protein [376]. Asp242 forms a hydrogen bond with His173, which is believed to render more acidic character to His173 [310, 376]. This interaction lowers the redox potential of the heme iron and may stabilize the ferryl-heme intermediates [310, 338, 356, 421]. Additionally, Asp242, along with Phe190, participate in maintaining the high-spin, pentacoordinate heme iron (see Section 1.6.2). Phe190 is conserved in LiP [309], peanut peroxidase (PNP) [345], and HRP [125] but is replaced by Trp in CcP and ascorbate peroxidase (APX) [430] and Leu in ArP/CiP [235, 302]. The orientations of Phe190 in MnP and LiP differ considerably [309, 376]. This difference in orientation may influence the redox potential of the two enzymes [23, 24, 338]. The role of Phe190 in MnP has been investigated in mutant studies (see Section 1.7.3 and Chapter 2) [21, 225, 338, 438].

1.5.3 The Manganese Binding Site

MnP contains a single catalytic manganese-binding site (Figures 1.6 and 1.8). Prior to the elucidation of the crystal structure of MnP, several sites for manganese binding were proposed on the basis of heme modification experiments and homology-based molecular modeling [164, 196].

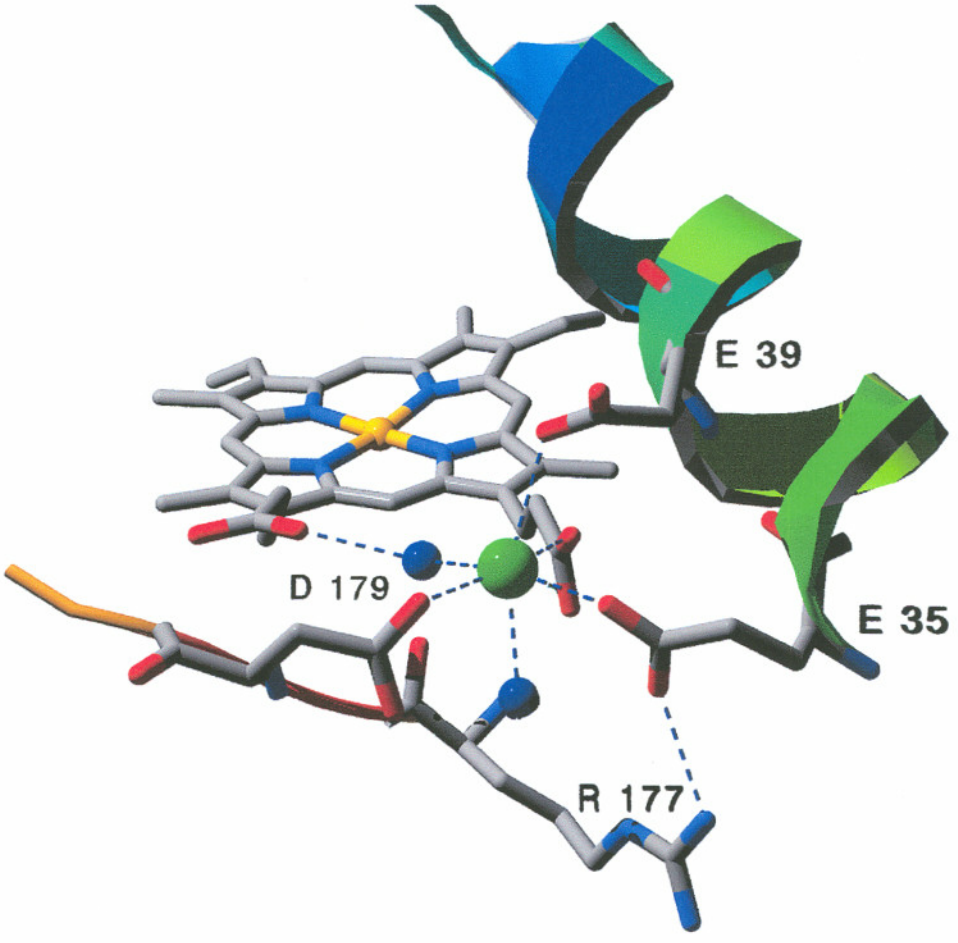

Figure 1.8 The Mn-binding site of manganese peroxidase. The Mn is hexacoordinate with oxygen ligands from two water molecules, heme propionate 6, and amino acids Glu35, Glu39, and Asp179. From the crystal structure [376].

The accessibility of the heme to substrates was studied by addition of azides to the δ-meso-carbon of the heme in MnP and LiP [94, 164]. While Co^{2+} competitively inhibits Mn^{2+} oxidation by the enzyme, it does not inhibit inactivation by azides, suggesting that Mn^{2+} binds at some distance from the δ-meso-carbon [164]. NMR studies indicated an upper limit for this distance at around 11 Å [20]. Three different manganese-binding sites were proposed by homology model comparisons of two MnP isozymes [196]. The most favorable binding site proposed in that study is the only apparent Mn^{2+} binding site in the crystal structure [376]. pH titration studies suggest that there may be a second, low-affinity, manganese-binding site not apparent in the crystal structure [260]. The possible location of this second site near the C-terminus is discussed in Chapters 3 and 5.

The enzyme-bound manganese at the functional site (Figure 1.8) is hexacoordinate, with two water ligands and four carboxylate ligands contributed by heme propionate 6 and three acidic amino acids, Glu35, Glu39, and Asp179 [376]. One water ligand is hydrogen bonded to heme propionate 7 (Figure 1.8) and all Mn–O bond distances range from 2.34 to 2.82 Å $\pm$ 0.5 Å [376], typical of coordinated Mn^{2+} [93]. Electron transfer presumably occurs via a direct pathway through the heme propionate 6 ligand. Of the amino acids forming the manganese-binding site, only Glu39 is present in LiP and none of these residues are present in ArP/CiP [235, 302, 376]. The role of Glu39 in the manganese-binding site is further discussed in Sections 1.7.3 and in Chapter 4.

One additional residue, Arg177, appears to be important in manganese binding. Arg177 forms a salt bridge with Glu35 (Figure 1.8) thereby orienting this ligand, which is at the surface of the protein [376]. This residue is not conserved in LiP nor, it has been argued, can the LiP structure accommodate Arg177 [376]. The amino acid residues forming the manganese-binding site have been examined in detail by site-directed mutagenesis (see Section 1.7.2).

1.6 BIOPHYSICAL AND KINETIC STUDIES OF MANGANESE PEROXIDASE FROM *P. CHRYSOSPORIUM*

1.6.1 Spectroscopic Studies

Electronic absorption maxima for native, oxidized, and various ligated forms of MnP are similar to those of both horseradish peroxidase (HRP) and LiP [39, 101, 136, 324, 386, 422] indicating that the heme iron is high-spin, ferric, and pentacoordinate, with a histidine acting as the fifth ligand (Figure 1.7). Detailed EPR and resonance Raman studies of various forms of MnP confirm that the heme in the native enzyme exists in a high-spin ferric state [270]. Resonance Raman and NMR studies show that the native enzyme forms low-spin complexes with CN^- and N_3^- [23, 24, 270] and a high-spin complex with F^- [270] and that the heme environment of MnP is similar to those of HRP and LiP [23, 24, 270]. NMR studies of native, ferric MnP confirm that the fifth ligand to the heme iron is a histidine imidazole [23, 24].

Spectra of the reduced enzyme are typical of high-spin, pentacoordinate, ferrous heme with the heme iron ligated to the protein though a proximal His [270]. The ferrous enzyme forms a complex with CO, which has a spectrum typical of other peroxidases [101, 136]. Finally, EPR of the ferrous heme-^{14}NO and -^{15}NO adducts of MnP confirms that the fifth ligand is the N-imidazole of a histidine residue as in LiP and HRP [270 and references therein].

The heme propionates form part of the Mn-binding site (see Section 1.5.3). Upon binding of Mn to native, ferric MnP, the electronic state of the heme is slightly altered. An increase in the heme Soret is observed, from which a 1:1 stoichiometry and a binding constant of $\sim 60\ \mu M$ have been determined [426]. Replacement of the normal heme with modified hemes alters spectral and kinetic properties of the enzyme. Substitutions on the α- and β-meso edges change the spectral characteristics, whereas substitution of γ-meso edge groups affects Mn binding and oxidation [318]. NMR studies show line broadening of some heme methyl groups and single proton signals upon addition of Mn^{2+} to the ferric enzyme [20]. These data indicate an association constant of $\sim 100\ \mu M$ with slow exchange of bound and free Mn^{2+} [20]. Lanthanides also bind to the Mn-binding site and have been proposed to mimic Mn^{3+}

[22]. The binding of lanthanides and association of chelator complexes with the enzyme are further discussed in Section 1.6.4.

1.6.2 The Enzyme at High Temperature and pH

MnP is inactivated at high temperature and high pH. The first step in inactivation under both conditions appears to be a high-spin to low-spin conversion of the heme iron, indicating coordination of a sixth ligand. The UV-visible spectra of the enzyme at pH 9.0 and following thermal inactivation at pH 4.5 are identical, indicating similar phenomena [225, 379] (Figure 1.9). The transition is apparently accompanied by a loss of calcium from the enzyme. Addition of exogenous calcium protects the enzyme from thermal inactivation and can partially restore activity [379–381]. Loss of the distal calcium has been proposed, accompanied by coordination of the distal histidine to the heme and inactivation (Figure 1.7) [225, 381]. This hypothesis is further explored in Chapter 2. Engineering of a disulfide bond near the distal calcium site, similar to that found in some plant peroxidases, increases thermal stability in MnP (see Section 1.7.3.3) [319].

Addition of manganese to the enzyme also increases thermal stability and it was hypothesized that Mn^{2+} may bind at the distal calcium site [379]. Evidence presented in Chapter 2 indicates that this is not the case. Rather, possible roles for the Mn-binding site in thermal stability are explored in Chapter 5.

Proximal residues are also important in enzyme stability, particularly in maintaining the heme environment. Replacement of the proximal Asp242 or Phe190 residues in MnP lowers the pH of inactivation [21, 225, 338]. MnP variants in either of these positions undergo alkaline inactivation at $\sim$2 pH units lower than the wild-type enzymes (see Sections 1.7.3.1 and 1.7.3.2). The nature of the alkaline transition in wild-type MnP and a Phe190 variant are discussed in Chapter 2.

Glycosylation also appears to be important in stabilization of peroxidase structures. All class II and class III peroxidases contain highly branched sugar residues linked to the protein via Asn (N-linked) or Ser/Thr (O-linked) residues [410, 432]. The carbohydrate additions are best characterized in the plant peroxidases [410]. Removal of carbohydrate from HRP, which contains 8 N-linked glycans, and

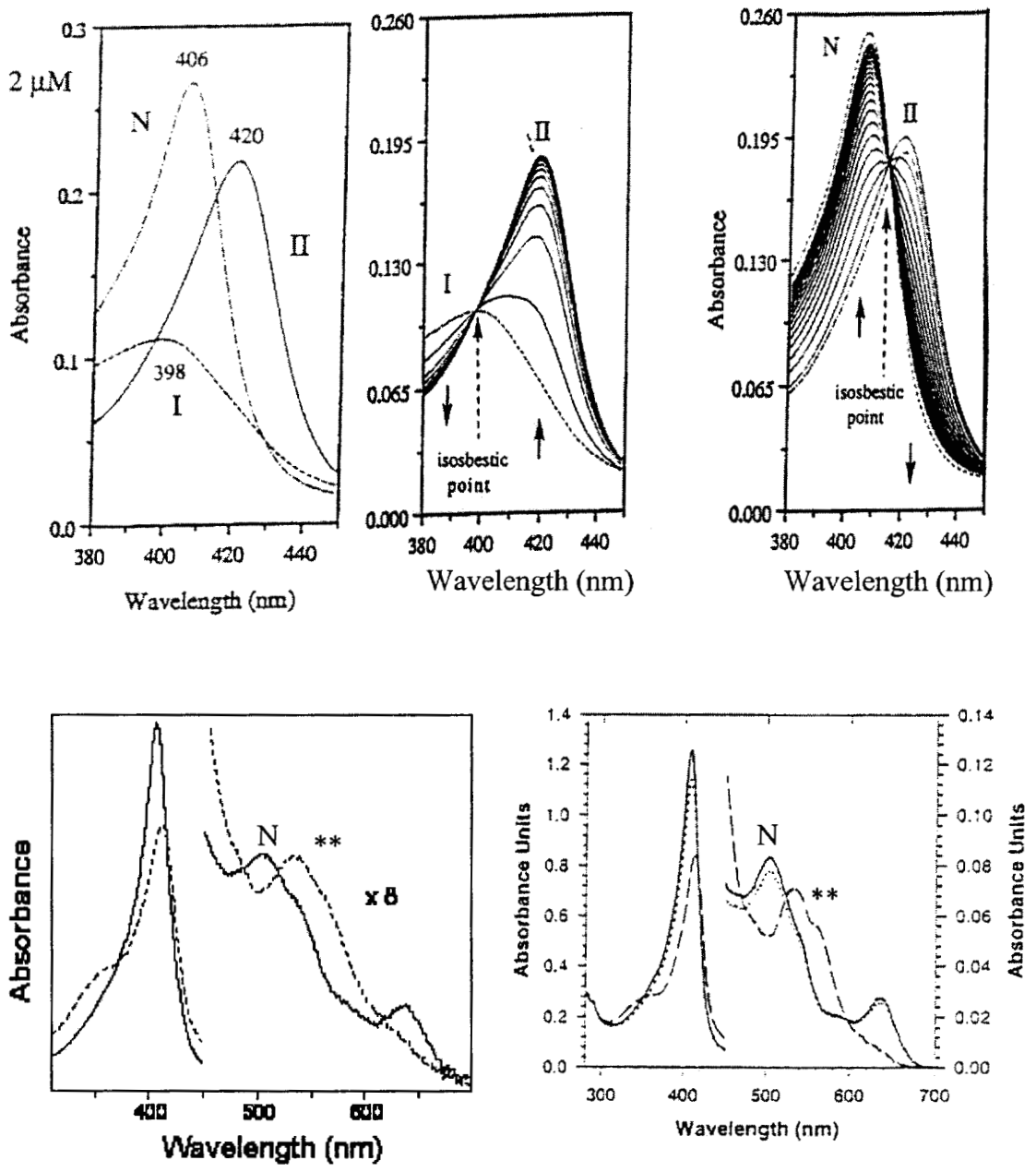

Figure 1.9 UV-visible spectra of manganese peroxidase. (**Top**) The native ferric enzyme (N) and oxidized intermediates, compounds I and II (**top left**). The isosbestic points for reduction of compound I to II and II to N are also shown (**top middle** and **top right**, respectively). (**Bottom**) Inactivation of manganese peroxidase by alkaline pH (**bottom left**) and heat (**bottom right***) alters the visible spectrum.

*Originally published as Figure 1B in: Sutherland, G., Zapanta, L., Tien, M., and Aust, S. (1997) Role of calcium in maintaining the heme environment of manganese peroxidase. *Biochemistry* **36,** 3654-3662. Used with permission of the American Chemical Society.

peanut peroxidase affects the structural integrity of the enzymes significantly [385, 410]. MnP from *P. chrysosporium* contains both N- and O-linked carbohydrates; however, they have not been characterized [136, 139, 376]. Studies of MnP heterologously expressed in *E. coli*, which is not glycosylated, and selective removal of carbohydrate from the wild-type protein indicate that loss of O-linked carbohydrates decreases the thermal stability of the enzyme [284].

1.6.3 The Catalytic Cycle and Kinetic Mechanism

The catalytic cycle of MnP is shown in Figure 1.5. Optical absorption maxima for the oxidized intermediates of MnP are similar to those of LiP and HRP [101, 324, 422]. Ferric MnP undergoes a two-electron oxidation by H_2O_2 to yield compound I, a ferryl-heme species with a porphyrin π-cation radical [422]. Reaction with Mn^{2+}, or another reducing substrate, preferentially reduces the porphyrin, resulting in the ferryl-oxo intermediate, compound II [422]. Compound II then undergoes a second single-electron reduction by Mn^{2+} to yield the native ferric enzyme, with the release of a water molecule [422]. The addition of excess H_2O_2 to the native enzyme results in formation of the inactive intermediate, compound III [422]. The various intermediates are easily distinguished by their spectral characteristics (Figure 1.9), allowing transient-state kinetic analysis of each step in the reaction cycle. Although MnP can slowly oxidize a variety of phenols or aromatic amines, Mn^{2+} is clearly the preferred substrate [135, 422, 423].

Steady-state kinetic analysis of Mn^{2+} oxidation in the presence of fixed concentrations of H_2O_2 suggests a typical peroxidase mechanism [426]. Classified as a bi-bi ping-pong mechanism, the individual reaction steps are considered ordered and irreversible (Figure 1.5) [101].

Transient-state kinetic results support the mechanism described above. Formation of compound I occurs at a rate of $k_1 \sim 3 \times 10^6\ M^{-1} \cdot s^{-1}$, independent of pH [227, 423, 436]. The reduction of compound I by Mn^{2+} in malonate buffer is too fast to measure ($k_2 > 10^7\ M^{-1}s^{-1}$) at the pH optimum of 4.5. In contrast, the second-order rate constant for reduction of compound I by 2,6-dimethoxyphenol (DMP) is $\sim 10^4$-fold slower at this pH ($k_2 \sim 5.0 \times 10^3\ M^{-1}s^{-1}$) [360, 423, 436]. Reduction of

compound II is the rate-limiting step in the reaction cycle. The first-order rate constant for Mn^{2+} is $k_3 \sim 5.48 \times 10^2\ s^{-1}$, whereas, the rate constant for reduction of compound II by DMP is >650-fold lower [227, 423, 436]. Indeed, the rate constant for reduction of compound II by DMP is too slow to support efficient enzyme turnover. Similarly, while the dissociation constant for Mn^{2+} is $K_D \sim 1.66\ x10^{-4}$ M, that of DMP is 100-fold lower [360].

1.6.4 The Role of Chelators

To date, MnP and the related hybrid MnP-LiP or "versatile" peroxidases appear to be the only enzymes that use manganese as a diffusible substrate rather than a permanent enzyme-bound cofactor. The unique binding site in these enzymes preferentially binds Mn^{2+} and releases Mn^{3+}. The presence of dicarboxylic acid or α-hydroxyacid chelators is required for complete turnover of the enzyme by Mn^{2+} [135, 227, 231, 426]. *P. chrysosporium* secretes several organic acids such as oxalate, malonate, citrate and glyoxalate during idiophasic metabolism [30, 102, 233, 426]. However, only oxalate is produced at concentrations sufficient to stimulate MnP activity [227, 233].

The actual role of chelators in the MnP mechanism has been debated for years. Two major mechanisms have been proposed. The first involves binding of free Mn^{2+} to the enzyme, with chelator facilitating release of Mn^{3+} [426]. The second involves binding, oxidation and release of a Mn-chelator complex (Figure 1.10) [231]. The formation and reduction of compound I are reportedly not affected by the presence or type of chelator in reaction mixtures [231]. In contrast, the reduction of compound II is greatly affected by both the concentration and type of chelator present [227, 231]. Maximum rates for the reduction of compound II are reportedly observed when the Mn^{2+} in solution is stoichiometrically chelated by oxalate [227, 231].

The formation of an enzyme-Mn^{2+}-oxalate ternary complex during the reaction cycle has been postulated based on the observed kinetic activation [231]. However, recent NMR [22] and crystal structure [376] studies clearly indicated that free (aquo-) Mn^{2+}, rather than a Mn^{2+}-chelator complex, binds to the native ferric enzyme, as proposed by Wariishi et al. [426]. Examination of Mn^{3+} binding to MnP is hampered

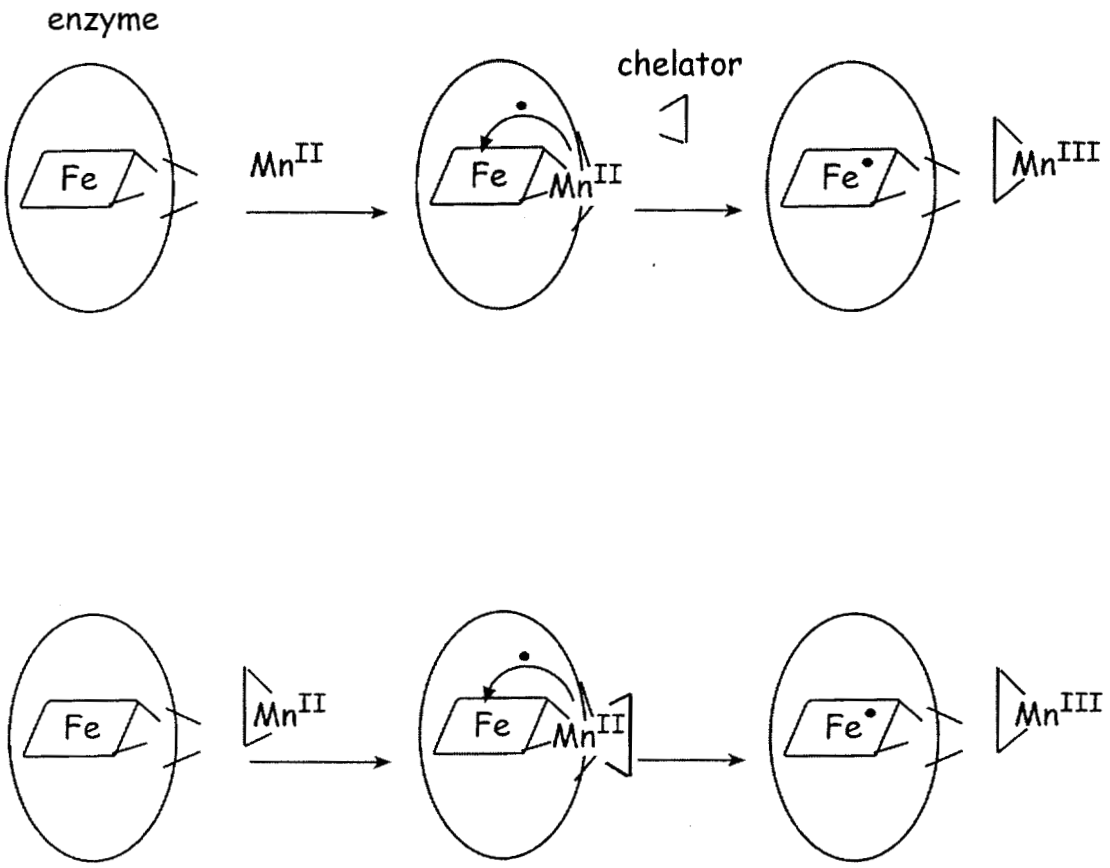

Figure 1.10 Two theories on the role of chelators in the reaction cycle of manganese peroxidase. (**Top**) Free (aquo) Mn^{2+} binds to the enzyme, with chelator effecting release of Mn^{3+} [22, 245]. (**Bottom**) A 1:1 chelator:Mn^{2+} complex binds to the enzyme, is oxidized and released [227, 231].

because Mn^{3+} disproportionates in the time period required for most studies [426]; however, trivalent lanthanides, such as Sm^{3+}, Ce^{3+} and Gd^{3+}, also bind at the manganese-binding site [22, 378] and have been proposed to mimic the behavior of Mn^{3+} [22]. Although the Mn-binding site is on the surface of the enzyme [376], bound Mn^{2+} is difficult to remove completely from the native, ferric enzyme, even with strong chelators [22, 377]. In contrast, the lanthanide ions are removed quite easily by oxalate [22, 378]. NMR investigation of lanthanide bound MnP suggests the transient existence of an enzyme-Ln^{3+}-chelator complex [22], although no such complex has been observed by X-ray crystallography [376, 378]. Mn complexes are further discussed in Section 1.9 and the role of chelators in the MnP reaction is further explored in Chapter 6.

1.7 STRUCTURE/FUNCTION STUDIES OF MANGANESE PEROXIDASE FROM *P. CHRYSOSPORIUM*

1.7.1 Homologous and Heterologous Expression of Manganese Peroxidase

MnP from *P. chrysosporium* has been expressed in a number of organisms including *Escherichia coli* [435], baculovirus [294], and *Aspergillus oryzae* [372]. MnP expressed in *E. coli* is not glycosylated and is produced as inclusion bodies [435]. The recombinant enzyme requires reconstitution with heme and calcium under anaerobic conditions. While many kinetic features appear similar to the wild-type enzyme [435, 436], the enzyme is apparently less thermotolerant [284]. No detailed spectroscopic or crystallographic studies of this enzyme have been reported. Expression of recombinant MnP in *A. oryzae* produces active, glycosylated protein, however, addition of hemin to cultures is required [372]. Unfortunately, the only recombinant MnP produced in this system to date has Mn^{2+} oxidation kinetics significantly lower than the wild-type enzyme [372].

Recombinant MnP has also been homologously expressed in *P. chrysosporium* [263]. The recombinant enzyme displays kinetic and spectroscopic properties similar to those of the wild type [263]. The wild-type enzyme is only expressed during secondary (idiophasic) metabolism, triggered by nutrient nitrogen depletion [140,

222]. Placement of the *mnp* gene under control of a glycolytic promoter, such as that of glyceraldehyde-phosphate dehydrogenase, allows expression of the recombinant protein during primary metabolic growth, when wild-type enzymes are not produced [263].

1.7.2 Site-Directed Mutations of the Manganese-Binding Ligands

As described in Section 1.5.3, in addition to the heme propionate, the Mn^{2+} binding site of MnP contains three amino acid ligands, E35, E39, and D179, as well as the residue R177 (Figure 1.8) [376]. Each of these residues has been altered by site-directed mutagenesis.

1.7.2.1 Mutations of the Manganese Ligands: Glu39, Glu35, and Asp179. The first site-directed mutagenesis studies on MnP focused on the three amino acid ligands. Each proposed ligand was changed to its respective amide to obtain D179N, E35Q, and E39Q. In addition, one double mutant, D179N-E35Q was constructed [226, 237]. The altered genes were constructed and homologously expressed in *P. chrysosporium* [226, 237]. The variant proteins displayed chromatographic properties, molecular weights and spectral characteristics similar to those of the wild type [226, 237]. X-ray crystallographic analysis confirmed that the overall structure of the mutants was unchanged, as were the kinetic constants for binding and reactivity towards peroxide, ferrocyanide, and small phenolic compounds such as *p*-cresol [226, 237, 377]. However, steady-state kinetic analyses of all the mutants showed significant increases in K_m and decreases in k_{cat} for Mn^{2+} [226, 237]. The catalytic efficiency of the enzyme for Mn^{2+}, k_{cat}/K_m, was $\sim 10^4$-fold lower for the single mutants and $\sim 10^5$-fold lower for the double mutant [226, 237].

Transient-state kinetic analysis of compound II reduction of the variants by Mn^{2+} showed K_D values $\sim$100-fold and $\sim$200-fold higher than wild type for the single mutants and double mutant, respectively, indicating poor binding of Mn^{2+}. The first-order rate constants were also altered. Rates were $\sim$200-fold and $\sim$4000-fold less than that of wild type for the single and double mutants, respectively [226, 237]. X-ray crystallographic analysis indicated decreased electron density in the Mn-

binding sites of the variants compared to wild-type MnP, indicating much weaker Mn^{2+} binding at the altered sites [376, 377]. The mutations resulted in increased exposure of the Mn-binding site to solvent, primarily through rotation of residues 35 and 39, at the surface of the enzyme, to a more open configuration than observed in the wild-type enzyme [377].

A second set of Mn^{2+} binding-site mutations, D179A, E35D, and E39D, was constructed and heterologously expressed in *E. coli* [436]. Although no detailed spectroscopic analysis of these variants was published, binding and reactivity towards ferrocyanide and small phenols was not altered [226, 237]. Steady-state kinetic analyses of D179A and E35D showed decreases in k_{cat} and increases in K_m, resulting in a $\sim 10^4$-fold decrease in catalytic efficiency (k_{cat}/K_m) for Mn^{2+}, compared to the unaltered recombinant enzyme [436]. Compound I reduction by Mn^{2+} was reduced 63- and 220-fold for E35D and D179A, respectively. The dissociation constants for Mn^{2+} binding to compound II increased 42- and 240-fold for E35D and D179A, respectively and the first-order rate constants decreased ~ 110-fold compared to unaltered recombinant enzyme [436]. In contrast, the kinetic analysis of E39D suggested that this mutation had little effect on the catalytic properties of the enzyme [436], unlike previous results for the amide substitution [226, 377]. The role of E39 in Mn binding is discussed further in Chapter 4.

1.7.2.2 Mutations of Arg177. Arg177 is conserved in all MnPs but is not present in LiPs or the hybrid versatile peroxidases [62, 144, 181, 218, 326, 333, 335, 419]. The crystal structure of MnP from *P. chrysosporium* indicates that Arg177 forms a salt bridge with the Mn-binding ligand, Glu35 (Figure 1.8) [376]. Site-directed mutagenesis was used to replace Arg177 with Ala, Lys, Glu, Asp, Gln, and Asn. All of the variants displayed increased K_m values for Mn^{2+} compared to wild type, confirming involvement of this residue in Mn^{2+} binding [360, 362]. Interestingly, the k_{cat} values were decreased in the R177E, R177D, R177N, and R177Q mutants but no decrease in k_{cat} values was observed in the R177A and R177K mutants [360].

Transient-state kinetic analyses indicated decreases in the second-order rate constant for the reduction of compound I in all the variants. Similarly, all the variants showed increased dissociation constants, K_D, for Mn^{2+} reduction of compound II, indicating a decrease in the binding affinity for Mn^{2+}. However, consistent with the steady-state data, the first-order rate constants were only affected in the R177D, R177E, R177Q, and R177N variants. Therefore, although Mn^{2+} binding was decreased in all the variants, the electron transfer rate for the oxidation of Mn^{2+} was not affected in the R177A and R177K variants [360].

Molecular modeling indicated that electron transfer was disrupted only when the substituting residue interfered with the Mn coordination geometry, as in the R177D, R177E, R177Q, and R177N variants [362]. In both the R177A and R177K variants, the substituted sidechains did not interfere with the Mn-binding site, instead they occupied positions similar to the original Arg residue [362]. These results clearly demonstrate that Mn^{2+} oxidation by MnP can be separated into two events, binding of Mn^{2+}, which is facilitated by Arg177, and electron transfer from Mn^{2+} to the enzyme, where Arg177 is apparently not directly involved [360, 362]. The absence of Arg177 in the versatile peroxidases may, in part, explain the lower rates of Mn^{2+} oxidation observed in these enzymes. The importance of ligand geometry in Mn^{2+} binding and oxidation by MnP is further explored in Chapter 4.

1.7.3 Mutations in the Proximal Domain and the Distal Calcium Binding Site

1.7.3.1 Mutation of the Proximal Residue, F190. Phe190 is located on the proximal side of the heme cavity in MnP (Figure 1.7) and is equivalent to Trp191 in yeast CcP [261]. In most plant and fungal peroxidases, Trp191 is replaced by either Phe [304, 309, 376, 430] or Leu [235, 302]. This residue has been studied by site-directed mutagenesis by two independent groups.

The first variants of this residue, F190Y, F190L, F190I, and F190A, were created as a series of homologously expressed site-directed mutants [225]. The variants exhibited spectral and steady-state characteristics similar to those of wtMnP for both Mn^{2+} and peroxide [225]. An F190W substitution was also constructed but an insufficient amount of protein was recovered for analysis. Replacement of Phe190

with either Ile or Ala significantly enhanced the thermal denaturation rate of the protein and decreased the pH of alkaline inactivation by ~2 pH units, from pH 9 to pH 7 [225]. Moreover, the rates of spontaneous reduction of the oxidized intermediates were dramatically increased for the F190A mutant [225]. These results indicated a role for F190 in maintenance of the heme environment.

A second set of F190 mutations, F190V, F190L and F190W, was later constructed by another group and heterologously expressed in *E. coli* [438]. The F190W variant was highly unstable, but no evidence for Trp radical formation was found [438]. Peroxide kinetics remained unchanged in the variants, as previously reported for the other F190 mutations [225]. Interestingly, the F190W variant exhibited an apparent 10-fold decrease in k_{cat} and a 30-fold increase in the K_m for Mn^{2+}, resulting in an overall 300-fold decrease in the catalytic efficiency for Mn^{2+} oxidation in the steady state. However, this result was not supported by the transient-state analysis, which indicated that only the rate of compound II reduction was affected while the K_D for Mn^{2+} remained unchanged [438]. No thermal stability studies were conducted with this set of variants; however, spectroscopic studies indicated that the F190V mutant underwent the alkaline inactivation at lower pH, as reported for the F190A and F190I variants [225, 438]. Also consistent with the earlier reports, the alkaline transition in the F190L variant was only slightly affected [225, 438]. The nature of the alkaline transition in MnP and the role of F190 is further explored in Chapter 2.

1.7.3.2 Mutation of the Proximal Asp242. Asp242 is conserved in all heme peroxidases. This residue forms an important hydrogen bond with the proximal His173 (Figure 1.7), thereby modulating its electrostatic potential [119, 147, 431]. Additionally, in peroxidases such as CcP, which contain a proximal Trp, Asp242 forms an H-bond triad with the proximal His and Trp residues. The protonation state of the Trp, modulated by this interaction with Asp242, is believed to determine whether the radical in compound I forms on the indole ring or the porphyrin [147, 266].

Two heterologously expressed MnP variants, D242E and D242S, were generated. Both variant proteins contained high-spin and pentacoordinate hemes,

however, the redox potential of the enzymes were slightly lower than observed in the wild type [338, 438], similar to those of the D235E variant of CcP and a D245N variant of CiP. All have high-spin and pentacoordinate hemes at normal pH, however, these variants undergo alkaline inactivation ~2 pH units lower than in the wild-type enzymes [147, 358, 438]. In contrast, the D235N and D235A variants of CcP have low-spin, hexacoordinate hemes, even at normal pH [118, 340, 415]. MnP does not have a proximal Trp, thus Asp242 interacts only with the proximal His, perhaps lending MnP more flexibility to mutation at this site [147, 376]. The results indicate that weakening of the Asp-His H-bond reduces the imidazolate character of the proximal His and lowers the redox potential of the heme in MnP [147]. Accordingly, the kinetic properties of the enzyme were slightly affected. The catalytic efficiency for peroxide was lowered 2-fold in the D242E variant and the efficiencies for Mn^{2+} oxidation were lowered 2- and 4-fold in the D242S and D242E variant, respectively. Binding of Mn^{2+} to the enzyme was not affected by either mutation, however, both variants exhibited lower alkaline transitions similar to those of the proximal Phe190 mutations [21, 338, 438].

*1.7.3.3 **Mutation of Proximal Residues Ser172 and Leu169.*** Two additional proximal residue variants of MnP from *P. chrysosporium*, S172A and L169F, were heterologously expressed in *E. coli* [10]. Kinetic analyses indicated no significant differences between these variants and wild-type MnP. Some small decrease in the ability of their compound II to oxidize Mn^{2+} were noted, however, the values reported are within the variation for the wild-type enzyme in various literature reports [10, 263, 435].

*1.7.3.4 **Mutation of the Calcium Binding Ligand Asp47.*** Only one variant of a calcium-binding site ligand in MnP has been reported [381]. A D47A variant was heterologously expressed in *E. coli*. The protein contained only one equivalent of calcium, suggesting complete functional loss of the distal calcium-binding site. The enzyme was inactive, exhibiting altered UV-visible spectra with maxima at 412, 553, and 561 nm, similar to thermally inactivated MnP. These data support the hypothesis that loss of structural calcium may be involved in thermal inactivation [379, 381] (see Section 1.6.2).

1.8 LIGNINOLYTIC ENZYMES FROM OTHER WHITE-ROT FUNGI

White-rot fungi can be divided into three main groups: those that produce MnP and LiP, those that produce MnP and laccase, and those that produce all three enzymes [168, 411]. *P. chrysosporium* is a member of the first group. Most of other lignin-degrading fungi produce or contain genes encoding the copper-containing oxidase, laccase (EC 1.10.3.2) [98, 323]. Additionally, several fungi, particularly *Pleurotus* spp., produce "versatile" peroxidases, which appear to have features of both MnP and LiP [40, 62, 66, 258, 418]. There are also scattered reports of extracellular Mn-independent peroxidases in *Junghuhnia separabilima* [412] and *Pleurotus ostreatus* [412] but these enzymes remain uncharacterized.

1.8.1 Laccases

Laccases from fungi including *Trametes (Coriolus) versicolor* [112], *Coprinus cinereus* [99], *Pycnoporus cinnabarinus* [107], *Ceriporiopsis subvermispora*, *Pleurotus ostreatus* [130], *Letinus edodes* [230], *Dichomitus squalens* [298] and *Phlebia radiata* [336, 337], have been studied and appear to be related to the plant enzyme ascorbate oxidase [267, 394] and the mammalian enzyme ceruloplasmin [267]. Laccases oxidize phenols at the hydroxyl position, effecting both depolymerization and/or further polymerization of the substrate [252]. There is only one, as yet unsubstantiated, report of this enzyme being produced by a strain of *P. chrysosporium* under fermentation conditions [328]. Sequencing of the *P. chrysosporium* genome is currently underway and will reveal whether, in fact, this organism contains laccase genes that are not expressed in laboratory culture [168, 411]. Several reviews on laccases are available [323, 394, 440].

1.8.2 Manganese and Lignin Peroxidases

The MnP and LiP enzymes characterized from other fungi appear to be very similar to the enzymes from *P. chrysosporium*, although far more gene sequences have been obtained than actual enzymes isolated. Whereas all known white-rot fungi

produce MnP [46, 57, 107, 126, 136, 145, 149, 168, 195, 204, 242, 254, 259, 271, 282, 285, 299, 305, 316, 341, 342, 346, 369, 389, 405, 411, 448], there are efficient lignin-degraders, such as *D. squalens* and *Phanerochaete laevis*, that do not appear to produce LiP [42, 240, 282, 299]. This is puzzling since LiP can directly oxidize non-phenolic lignin substructures, a reaction required for mineralization of lignin [179, 251]. While MnP and laccase can oxidize phenolic linkages, neither enzyme is able to directly oxidize non-phenolic linkages [192, 202, 203, 229, 366, 403, 424]. Therefore, how these fungi degrade non-phenolic lignin substructures is of considerable interest. Additional mediators, such as lipids, may allow the MnP and laccase systems to perform this function, however, the physiological relevance of these reactions has yet to be demonstrated [27, 106, 200, 427]. It is also possible that enzymes from this group of fungi possess additional capabilities. However, this does not appear to be the case for MnP from *D. squalens*, which is discussed in Chapter 5.

A new class of hybrid enzymes or "versatile" peroxidases, combining properties of MnP and LiP, has been identified in several species of *Pleurotus* [15, 62, 63, 66, 153, 155, 171, 258], *Bjerkandera adusta* [170, 171, 268], and *Lentinula edodes* [88]. Structural alignments and sequence comparison indicate that these enzymes are more closely related to LiP than MnP [333, 334]. The enzymes contain the conserved Mn-binding site residues, except Arg177, as well as certain LiP features, including a catalytic surface Trp, analogous to Trp171 in *P. chrysosporium*, and shortened C-terminal tail [62, 333]. These proteins appear to be able to oxidize veratryl alcohol and Mn^{2+}; however, the affinity for both substrates is lower than in other MnPs and LiPs. Although possessing structural features and k_{cat} values for veratryl alcohol oxidation that are similar to wild-type LiP, the K_m for veratryl alcohol is in the millimolar range in the enzymes examined kinetically, suggesting that these enzymes may still act primarily as Mn peroxidases [104, 258, 268]. The physiological role of these enzymes and substrate interactions require a more systematic and focused evaluation. The enzyme from *P. eryngii* has been heterologously expressed in hemin-supplemented cultures of *Aspergillus nidulans* [334], while the enzyme from *P. ostreatus* has been expressed homologously [190].

However, the expressed enzymes have not been thoroughly examined kinetically or structurally.

1.8.3 Hydrogen Peroxide Producing Enzymes

In addition to glucose oxidase [242], many white-rot fungi, including *Trametes (Polystictus) versicolor, Pleurotus eryngii* and *Bjerkandera adusta*, produce extracellular H_2O_2 via an extracellular FAD-containing aryl-alcohol oxidase [115, 153, 277]. As yet, the H_2O_2 producing systems of other fungi, such as *Dichomitus squalens* remain unelucidated.

1.9 THE ROLE OF MANGANESE IN LIGNIN DEGRADATION

1.9.1 Manganese Speciation and Availability

Manganese is the eleventh-most common element, the third-most available transition metal in the Earth's crust ($\sim$900 mg/kg) [121, 275], and the most abundant transition metal in wood [441]. The three oxidation states common in biological systems are Mn^{2+}, Mn^{3+} and Mn^{4+}. Mn^{4+} forms insoluble oxides (MnO_2), whereas the less oxidized forms exist primarily as soluble complexes [76, 275]. Some biotic processes mediate reduction and resolubilization of Mn^{4+} complexes [317, 330], although these reactions are most commonly performed by anaerobic bacteria [275].

1.9.2 Manganese Complexes

Mn^{2+}, Mn^{3+}, and Mn^{4+} are strong Lewis acids and bind well to oxygen ligands such as hydroxide and carboxylate [76, 121]. Nitrogen may also serve as a less preferred ligand and both ligand types are observed in the Mn-binding sites of various enzymes [82, 121]. Mn in most complexes, including the aquo-ion, is hexacoordinate. Exceptions included heptacoordination by ethylenediaminetetraacetic acid (EDTA) and tetra- or penta-coordinate Mn^{3+} and Mn^{4+} sites in some enzymes [82, 121].

Mn^{2+} has five unpaired electrons, one each of the five d orbitals and is thus neither a good oxidant nor reductant. As such, Mn^{2+} does not exhibit ligand field

stabilization, forming hexacoordinate complexes with octahedral geometry, although some tetrahedral complexes are observed [76]. In contrast Mn^{3+} (d^4) is both a good oxidant and reductant. Reduction produces stable Mn^{2+}, half-filling the d orbitals; whereas oxidation removes an electron from an antibonding orbital, yielding Mn^{4+} with a d^3 configuration with maximal ligand field stabilization energy (LFSE). As a result, Mn^{3+} complexes tend to be more stable than Mn^{2+} complexes. For example, the water exchange rate is 100-fold lower for Mn^{3+} than Mn^{2+} [76]. Mn^{3+} can be either penta- or hexacoordinate, normally with a tetragonally distorted octahedral geometry. At neutral and acidic pH, Mn^{3+} complexes undergo spontaneous disproportionation to Mn^{2+} and Mn^{4+} [275].

The nature (donor capacity) and geometry of ligands strongly mediate the redox potential of the various oxidation states of manganese. For example, the reduction potential of aquated Mn^{3+}/Mn^{2+} (~ 1.5 V) drops to ~ 1.0 V upon ligation [275]. Similarly, the charge, size and electronic configurations of the different oxidations states influence their preferred coordination geometries [72, 275]. As a consequence, redox reactions of Mn centers may involve rearrangement of ligands in the first coordination sphere. Tempering these rearrangements, as often occurs in metal binding sites of proteins, may influence the redox potential of the metal.

1.9.3 Manganese as an Enzyme Cofactor

Manganese is the most soluble transition metal. Although it will form complexes with sulfur species, it does so to a far lesser extent than other transition metals [121]. It is therefore likely, that manganese was the redox-active transition element most available when life was first evolving [121]. Manganese is a cofactor in more than 160 proteins and enzymes, slightly less than half of which are involved in carbohydrate metabolism [82]. Interestingly, many tissue-specific protein isoforms in mammals can use a variety of metals, whereas the brain isoforms use manganese exclusively [29, 82]. In fact, madness (hallucinations and paranoia) and Parkinson's type behavior are the first symptoms of manganese overdose in humans [29]. Plants efficiently take up and transport Mn^{2+}. Concentrations can range from 1 μM to 2 mM in the xylem and are typically higher in the phloem [275]. Manganese has a few

specialized roles in plants, forming the catalytic center of the oxygen evolving complex in photosystem II and mediating H_2O_2 generation in the apoplast during lignification [177, 306]. The absolute requirement for manganese in some proteins is difficult to determine, as Mn^{2+} will often substitute for Mg^{2+} and even Zn^{2+} in many systems [322].

1.9.4 Manganese in Lignin Degradation

The involvement of manganese in wood degradation has been long noted. The concomitant appearance of black or brown deposits with white-rot in wood had been observed in the 1800s [35, 110, 134, 223, 317]. Although the role of copper-containing laccases in lignin degradation was being investigated as early as the 1960s [113, 116, 191, 223], the involvement of manganese in this process would not be elucidated for another 25 years [35, 136, 238]. The identification Mn peroxidase [238], the most-prevalent lignin degrading enzyme [168], and elucidation of its mechanism changed thinking about the seemingly nonspecific, oxidative process of lignin degradation. Mn was identified as the sole substrate for MnP [135]. Moreover, production of small, stable, oxidized Mn-chelates was documented [135]. These complexes could easily diffuse into a sound wood matrix capable of excluding fungal hyphae and even most proteins [86, 87, 367, 368], spawning the concept of mediator molecules as the agents of lignin degradation.

Mn peroxidases are unique in their ability to selectively bind Mn^{2+}, and efficiently oxidize and release Mn^{3+}. All other enzymes capable of efficient oxidation of Mn have binding sites buried within the protein matrix and hold the metal as permanently bound cofactor(s) [82]. Claims of Mn^{2+} oxidation by the related enzyme LiP [213] have been disproven [361]. Mn^{3+}-chelate formation by catalase-peroxidase of the mycobacterium *Mycobacterium smegmatis* has been claimed [255]. However, although displaying sufficient Mn^{2+}-binding ($K_m \sim 5\ \mu M$), the enzyme oxidizes Mn^{2+} at a rate $\sim$2000-fold slower than Mn peroxidase [255, 425]. The crystal structure of chloroperoxidase also revealed an Mn-binding site near the heme propionates (377a); however there is no evidence for Mn oxidation by this enzyme and the role of metal binding remains unclear. Heme independent Mn peroxidase activity has also been

reported for the C-terminal domain of catalase-peroxidase CpeB from *Streptomyces reticuli*; however the phenomenon has not been extensively studied [448].

It is widely observed and accepted that Mn^{3+}-chelators can oxidize phenolic linkages [26, 41, 403, 426]. However, direct oxidation of non-phenolic linkages by MnP is not observed without additional mediators such as lipids [26, 27, 120, 200, 366]. A series of methoxybenzenes, $E_{1/2} \sim 1.76–0.81$ V was used to investigate the oxidizing ability of both chemically and enzymatically generated Mn^{3+}-chelates [308]. The results showed that manganese peroxidase, or physiological concentrations of Mn^{3+}, oxidize only the lower potential congeners. Unfortunately, the oxidation of these compounds occurs only via electron abstraction. Hydrogen abstraction mediated by Mn-complexes may also occur. For example, HRP was found to oxidize veratryl alcohol only in the presence of chelated Mn and glutathione [264]. It was hypothesized that either a Mn^{3+}-glutathione or a Mn^{2+}-glutathionyl radical complex abstracted a hydrogen from the benzylic carbon of veratryl alcohol, followed by a disproportionation reaction to produce the veratryl aldehyde [264]. Similar reactions are presumed to occur during the MnP-mediated oxidtion of non-phenolic linkages in the presence of thiols and lipids [26, 27, 120, 200, 366, 427].

Finally, in addition to action as a substrate mediator in the oxidation of lignin substructures, Mn^{2+} stimulates MnP activity in cultures of many white-rot fungi [45, 57, 123, 389]. The metal functions as a genetic regulator, increasing transcription of the *mnp* genes in *P. chrysosporium* [49, 50, 129, 138, 140, 253].

1.10 SUMMARY OF RESEARCH

1.10.1 Relevance

The resistance of lignin to hydrolytic degradation has profound ecological significance. In addition to affording microbial resistance to intact plants, lignocellulosic material serves as a carbon sink, constituting roughly 25% of the world's terrestrial biomass [47]. Partially degraded lignin products (humus) bind and control release of cationic nutrients in forest soils [186]. It is clear that research on lignin-degrading organisms and their extracellular enzyme systems is important, not

only for understanding important arboreal ecosystems, but for developing technology to efficiently produce food, fuel and manufacturing materials from terrestrial biomass. In addition, the lignin-degrading machinery of white-rot fungi can also be utilized to degrade aromatic pollutants and other xenobiotics. Table 1.2 lists some of the toxic substances degraded by this organism, most under ligninolytic conditions [64]. The unique enzyme, manganese peroxidase, has been identified in the cultures or genomes of all white-rot fungi studied to date, indicating its importance in the lignin-degradation systems of these organisms. The present work focuses on biophysical, mutagenic, and kinetic studies of this interesting enzyme.

1.10.2 Biophysical Studies of Manganese Peroxidase: Heat and pH Inactivation

Upon inactivation by heat or high pH, manganese peroxidase (MnP) exhibits changes in the electronic absorption spectrum (Figure 1.9). Although the role of calcium in this transition in the heat-inactivated protein has been studied extensively, the alkaline transition had been only partially characterized. This high- to low-spin alkaline transition occurs at $\sim$ 2 pH units lower in an F190I mutant MnP when compared to the wild-type enzyme. In Chapter 2, evidence from resonance Raman and UV-visible spectra from the oxidized and reduced proteins are presented, which indicate the formation of a bis-histidyl heme iron complex. No shifts in the low frequency RR bands are observed in 75% ^{18}O-labeled water. Therefore, the low-spin species is most likely not a hydroxo-heme derivative. Electronic and RR spectra also indicate that addition of Ca^{2+} to either the ferric or ferrous enzymes at high pH completely restores the high-spin pentacoordinate species, whereas addition of Ca^{2+} after returning the enzyme to low pH only partially restores the native species, indicating limited availability of the site under these conditions. Other divalent metals such as Mn^{2+}, Mg^{2+}, Zn^{2+} or Cd^{2+} do not restore the enzyme.

In Chapter 5, studies on the thermal inactivation of wild-type MnP and several binding-site variants from *P. chrysosporium* and a MnP from *Dichomitus squalens*, heterologously expressed in *P. chrysosporium* are discussed. Although similar in amino acid sequence [245], the enzyme from *D. squalens* is 20-fold more thermostable than the enzyme from *P. chrysosporium*. The addition of Mn^{2+} and

Table 1.2

A Partial Listing of Pollutants Degraded by *Phanerochaete chrysosporium* [64]

Chemical classification	Compound
Biopolymers	Cellulose Lignin
Synthetic polymers	Polyacrylate Polyacrylamide Nylon
Chlorinated aromatic compounds	2,4-Dichloroaniline 2,4-Dichlorophenol Pentachlorophenol 2,4,6- and 2,4,5-Trichlorophenols 2,4,5-Trichlorophenoxyacetic acid Aroclor 1242 and 1254 2,3,7,8-tetrachloro-*p*-dioxin
Dyes	Azo-dyes Azure blue Bomphenol blue Crystal violet Cresol red
Munitions	TNT (2,4,6-Trinitrotoluene) DNT (2,4-Dinitrotoluene) Nitroglycerin RDX (Hexahydro-1,3,5-trinitro-1,3,5-triazine)
Pesticides	DDT (1,1,1-Trichloro-2,2-bis-(4-chlorophenyl)ethane) Chlordane (Octachlorohexahydromethanoindane) Lindane (Hexachlorohexane) Toxaphene (chlorinated camphenes)
Polycyclic compounds	Anthracene Benzopyrene Chrysene Naphthalene Pyrene

Cd^{2+} increases stability to heat in both the wild-type enzymes, while addition of both Mn^{2+} and Cd^{2+} causes synergistic stabilization. Zn^{2+} also stabilized MnP from *D. squalens*, whereas it does not influence stability of MnP from *P. chrysosporium*. The ability of Mn^{2+} to protect the enzyme from heat is decreased in the binding-site variants. Also, as observed by decrease in the UV-visible heme absorption and measurement of secondary structure at A_{280} by circular dichroism (CD), the melting temperature of the variant enzymes is decreased compared to the wild type. The melting temperature of MnP from *D. squalens* was too high to be determined by CD using a water bath, indicating that although activity is lost, significant secondary structure remains in the heated enzyme. These combined results indicate a role for Mn^{2+} in stabilization of the heme and overall structure of Mn peroxidase.

1.10.3 Mutational Studies of Manganese Peroxidase: The Role of Glu39

Mn peroxidase is unique among Mn containing enzymes in that it selectively binds Mn^{2+} and releases Mn^{3+}, rather than sequestering the Mn ions as permanent redox cofactors in a buried active site. The exact selective mechanism of binding and release in MnP is not yet understood. Previous mutational analyses and crystal structure determinations indicated that three amino acids, Glu35, Glu39, and Asp179, form the only functional binding site in Mn peroxidase [226, 237, 376, 377]. The X-ray crystal stucture indicates a hexacoordinate Mn atom with nearly octahedral geometry and moderately long Mn-ligand bond distances. The Glu39-Mn bond appears to be the weakest. It deviates from the octahedral geometry and has the longest bond distance at $\sim 2.8 \pm 0.5$ Å. Data presented in Chapter 4 indicates that Glu39 does, in fact, function as a Mn-ligand. Both steady-state and transient-state kinetic analyses of three variants, E39D, E39A, and E35D-E39D-D179E, indicate that Mn^{2+} binding and oxidation is impaired when Glu39 is replaced. The kinetic data, combined with molecular modeling of the variants also indicates the importance of the coordination geometry in the selective mechanism of this unique enzyme.

1.10.4 Kinetic Studies of Manganese Peroxidase: The Role of Chelators

Activity of Mn peroxidase has been widely reported to depend on the presence of chelators in the reaction media [135, 146, 215, 227, 231, 233, 398, 425]. However, their exact role in the reaction mechanism has remained controversial. Two main theories persist, that free (aqua) Mn^{2+} binds to the enzyme and that chelator functions to effect release of Mn^{3+} [22, 425], and that a 1:1 Mn^{2+}-chelator complex is the true substrate for MnP [227, 233]. The data and suppositions supporting these two mechanisms are re-examined in Chapter 6, along with kinetic analyses of the wild-type enzyme from *P. chrysosporium* with various concentrations of chelator. Past and present evidence clearly support the theory of Wariishi et al. [425] that free Mn^{2+} is, in fact the substrate for MnP and chelator facilitates release of Mn^{3+}.

1.10.5 Research Impact

This work has contributed to our understanding of manganese peroxidase and to peroxidase kinetics. The first constants for the transient-state inhibition of a peroxidase are derived. Also, for the first time, a role for Mn-binding site in the stability of MnP is presented. The formation of a bis-histidyl heme structure, proposed to occur upon alkaline inactivation, is supported. The role of calcium in the process is examined and found to be similar to that for thermally inactivated MnP, providing evidence that these phenomena are related structural events. Finally, the role of Glu39 as a catalytically important Mn-binding ligand is shown and the importance of ligation geometry within the binding site is explored. This work provides important information regarding Mn chemistry useful for protein engineering, especially in the application and engineering of MnP for biomaterial transformation and synthesis, bioremediation, and other important industrial processes.

CHAPTER 2

FORMATION OF A BIS(HISTIDYL) HEME IRON COMPLEX IN MANGANESE PEROXIDASE AT HIGH pH AND RESTORATION OF THE NATIVE ENZYME STRUCTURE BY CALCIUM*

2.1 INTRODUCTION

Manganese peroxidase (MnP) is an extracellular heme protein produced by virtually all lignin-degrading white-rot fungi [140, 144, 168]. Sequences have been determined for *mnp* cDNA (293, 313) and genomic clones [4, 139, 262] encoding three MnP isozymes from *Phanerochaete chrysosporium*, the best-studied lignin-degrading fungus. These sequences and spectroscopic studies of the native and oxidized enzyme intermediates indicate that the heme environment in MnP is similar to that of other plant and fungal peroxidases [24, 101, 135, 164, 270, 313, 422]. Kinetic and spectroscopic studies of the purified enzyme indicate a typical peroxidase reaction catalytic cycle:

$$MnP + H_2O_2 \rightarrow MnPI + H_2O \quad (1)$$

$$MnPI + Mn^{2+} \rightarrow MnPII + Mn^{3+} \quad (2)$$

$$MnPII + Mn^{2+} \rightarrow MnP + Mn^{3+} + H_2O \quad (3)$$

However, MnP is unique in its ability to efficiently oxidize Mn^{2+} to Mn^{3+} [135, 136, 426]. The released Mn^{3+} is stabilized by organic acid chelators, such as oxalate and malonate, which are secreted by the fungus [233, 425]. The Mn^{3+}-chelator complex is capable of diffusing from the enzyme to oxidize terminal substrates including lignin

---

* Originally published in this or similar form in *Biochemistry* and used with permission of the American Chemical Society.

Youngs, H. L., Moënne-Loccoz, P., Loehr, T. M., and Gold, M. H. (2000) Formation of a bis(histidyl) heme iron complex in manganese peroxidase at high pH and restoration of the native enzyme structure by calcium. *Biochemistry* **39,** 9994–10000.

substructures, phenolic compounds, and pollutants [27, 140, 144 and references therein].

The three amino acid residues believed to bind Mn^{2+}, D179, E35, and E39, were investigated by site-directed mutagenesis of recombinant MnP homologouslyt expressed in *P. chrysosporium* [226, 237, 263, 436]. These studies, combined with X-ray crystal structure analyses of the proteins [376, 377], confirmed that the side-chain carboxylates of D179, E35, and E39 form the only apparent Mn^{2+}-binding site in MnP from *P. chrysosporium*. In addition to the three amino acid ligands, the hexacoordinate enzyme-bound Mn^{2+} is ligated to the carboxylate of heme propionate 6 and two water molecules, one of which is H-bonded to heme proprionate 7 [376]. An additional residue, R177, which forms a salt bridge with E35, was also recently shown to affect Mn^{2+} binding [360]. The enzyme contains two heptacoordinate structural Ca^{2+} ions, one distal and one proximal to the heme, which are believed to provide thermal stability to the enzyme (Figure 2.1) [380, 381].

Other than the unique Mn^{2+}-binding site, the heme environment in MnP appears to be similar to those in other plant and fungal peroxidases [105, 235, 301, 345, 376]. All of the important catalytic residues, including the distal His and Arg and proximal His and Asp, are conserved in MnP, LiP, cytochrome *c* peroxidase, horseradish peroxidase (HRP), and *Coprinus cinereus* peroxidase (CiP)/*Arthomyces ramosus* peroxides (ArP) [105, 119, 140, 172, 235, 301, 304, 309]. In addition, MnP has two Phe residues in the heme pocket, F45 and F190, which are conserved in HRP and LiP [105, 172, 304, 309, 376] but are replaced by Trp in cytochrome *c* perioxidase (CcP) and ascorbate peroxidase [119, 292] and Leu in CiP/ArP [235, 301]. Site-directed mutagenesis of F190 (Figure 2.1) in MnP from *P. chrysosporium* indicates a role for this residue in enzyme stabilization [21, 225].

In mutants where the F190 residue had been changed to Ala, Leu, Ile [225], or Val [21], a high-spin (HS) to low-spin (LS) conversion of the heme iron was noted when the solution pH was raised above 6.5. A similar spin change occurred in wild-type MnP but only when the pH was raised above 8.4 (225). Preliminary magnetic circular dichroism (MCD) evidence suggested the formation of a bis(histidyl)-coordinated heme iron at high pH in both the wild-type and F190I mutant MnP [225].

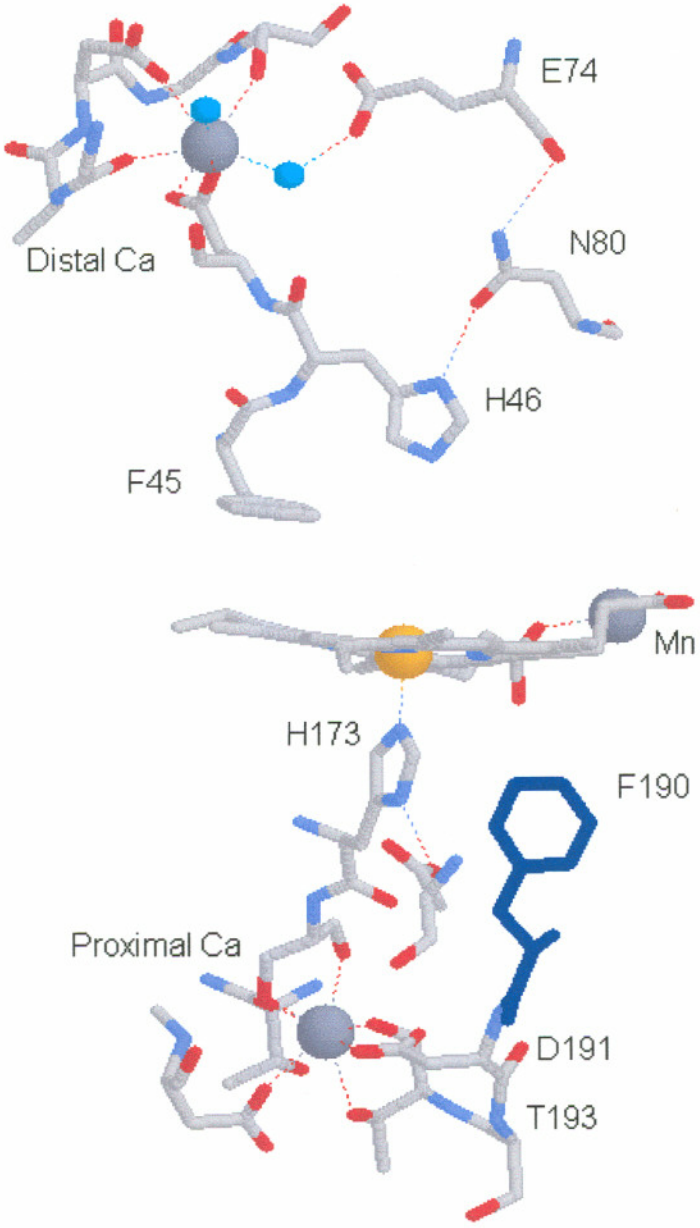

Figure 2.1 Distal and proximal Ca^{2+} binding sites in wild-type MnP from *P. chrysosporium* [376]. The distal Ca^{2+} is connected to the catalytic distal H46 via the D47 ligand and a hydrogen-bonding network through a water ligand, E74, and N80. The proximal Ca^{2+} is ligated to S174, adjacent to the proximal H173, and D191 and T193, adjacent to F190.

In this chapter, we provide additional evidence that, in both the F190I mutant MnP and wild-type MnP, this HS → LS transition is due to formation of a low-spin hexacoordinate (6cLS) bis(histidyl) heme iron complex, rather than a hydroxo-heme species, and that the native high-spin pentacoordinate (5cHS) heme iron is fully restored by the addition of excess calcium to the bis-His protein at high pH.

2.2 MATERIALS AND METHODS

2.2.1 Enzyme Purification

Wild-type MnP was purified from nitrogen-limited shaking cultures of *P. chrysosporium* strain OGC101 as previously described [136, 442]. The purified protein had an R_z (A_{406}/A_{280}) > 5. F190I mutant MnP was purified from a transformed strain of *P. chrysosporium*, pAGM5 [225], during primary metabolic growth, when endogenous wild-type MnP was not expressed [225, 360]. Enzyme concentrations were determined from the Soret absorbance (ϵ_{406} = 129 mM^{-1} cm^{-1}) [136].

2.2.2 UV-Visible Spectroscopy

Electronic absorption spectra of samples containing 100 μM enzyme used in resonance Raman (RR) experiments (Figures 2.1 and 2.4) were recorded directly from capillary tubes using a Perkin-Elmer Lambda 9 spectrophotometer. Spectra were obtained before and after laser illumination to monitor sample integrity. Low-pH samples were incubated in water, pH 5.0. High-pH samples were incubated in 50 mM sodium bicine, pH 9.0 (wild type), or 40 mM phosphate, pH 7.5 (F190I). All other electronic absorption spectra were recorded on a Shimadzu UV-260 spectrophotometer with a 1-mL quartz cuvette. Enzymes were reduced by addition of excess dithionite. Solutions were allowed to equilibrate until no further spectral changes occurred (at least 1 min) following addition of components such as dithionite, $CaCl_2$, or buffers to change pH before spectra were recorded. All recorded spectra were stable over the entire time course of experiments (up to 30 min).

2.2.3 RR Spectroscopy

RR spectra were obtained on a custom spectrograph consisting of a McPherson (Chelmsford, MA) model 2061/207 monochromator operated at a focal length of 0.67 m and a Princeton Instruments (Trenton, NJ) LN1100 CCD detector with a Model ST-130 controller. Laser excitation was from a Coherent (Santa Clara, CA) Innova 302 krypton (413.1 nm) laser. The laser line was filtered through an Applied Photophysics (Leatherhead, U.K.) prism monochromator to remove plasma emissions. Incident laser power at the sample was $\sim$15 mW. Spectra were collected in a 90° scattering geometry from solution samples contained in glass capillary tubes at room temperature. Rayleigh scattering was attenuated by the use of a Kaiser Optical (Ann Arbor, MI) super-notch filter. Spectral resolution was set to 4 cm^{-1}. Indene and CCl_4 were used as frequency and polarization standards, respectively.

2.2.4 Chemicals

All chemicals were of reagent grade, obtained from Sigma or Aldrich, and used without further purification.

2.3 RESULTS

2.3.1 UV-Vis and RR Spectroscopy of the Oxidized Proteins

Wild-type MnP exhibits a HS ferric heme absorption spectrum with a Soret maximum at 407 nm and visible band maxima at 502 and 632 nm [136]. When the pH is raised above 8.4, the spectrum changes to that of a LS ferric heme, as indicated in Figure 2.2 and Table 2.1. The Soret peak is red-shifted to 412 nm, becomes less intense, and gains a shoulder at 350 nm; the visible bands at 502 and 632 nm disappear and a new peak is formed at 535 nm. Similar spectral changes also occur in the F190I mutant MnP, though at lower pH (>6.5) [data not shown]. The spectra observed are similar to those previously reported for both the F190I mutant and wild-type MnP [225] and are provided here as a reference. The alkaline spectra of both proteins resemble the ferric form of the known bis-His protein, cytochrome b_5 (Table 2.1) [373]. However, the spectra are markedly different than that of alkaline HRP

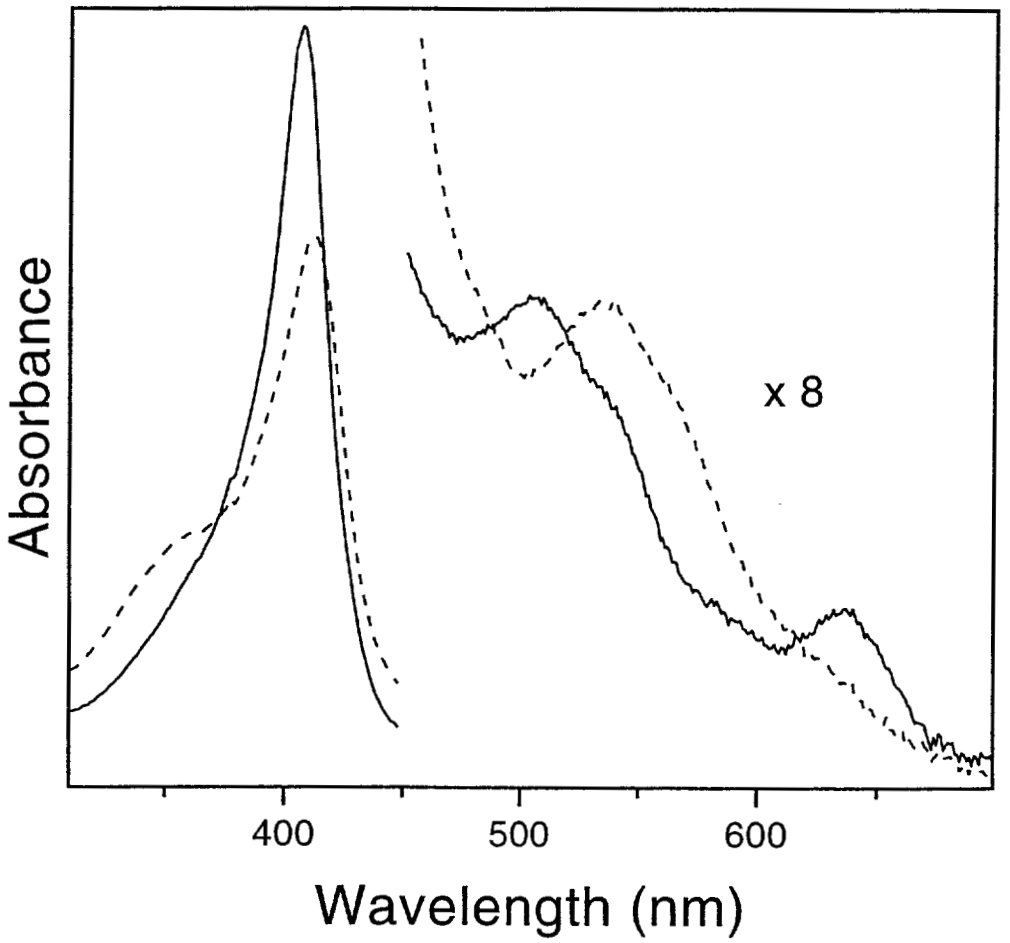

Figure 2.2 Electronic absorption spectra of oxidized (native, ferric) wild-type MnP in distilled water, pH 5.0 (—) and 50 mM sodium bicine, pH 9.0 (---). Spectra are of capillary samples that were used in resonance Raman experiments.

Table 2.1

Optical Spectral Features of Several Oxidized and Reduced Heme Proteins at Various pH Values

Enzyme	pH	Electronic Absorption Maxima (nm)			
Ferric wild-type MnP[a,b]	5.0	407	502	530	632
	9.0	412	535	559 (sh)	
Ferric cytochrome b_5[c]	5.5	413	532	560	
Ferric HRP-OH[d]	11.0	416	545	572	
Ferrous reduced wild-type MnP[a]	5.0	435	515 (sh)	557	586 (sh)
	9.0	425	529	559	
Ferrous F190I MnP[a]	5.0	435	513 (sh)	557	585 (sh)
	9.0	425	529	558	
Ferrous cytochrome b_{558}[e]	7.4	426	529	558	

[a] This work.
[b] From ref 225.
[c] From ref 373.
[d] From ref 205.
[e] From ref 296.

(Table 2.1) [373], strongly suggesting that the alkaline structure is a bis(histidyl) heme complex rather than a hydroxo-heme complex.

To further investigate the nature of the pH-induced HS → LS transition, RR and additional optical spectroscopy were performed. The high-frequency RR spectra for Soret excitation (413.1 nm) characteristic of heme coordination and spin state are shown in Figure 2.3 and listed in Table 2.2. The RR spectrum of the wild-type protein at room temperature in distilled water, pH 5.0, is identical to those previously reported in 20 mM succinate, pH 4.5 [270], and 20 mM phosphate, pH 6.0 [226]. The frequencies of the ν_3 modes at 1484 and 1492 cm^{-1} indicate HS species arising from mixed hexa- and pentacoordination in native MnP [270, 360]. The F190I mutant MnP displays a similar spectrum in water, pH 5.0 (Figure 2.3), indicating that the porphyrin core is not affected by the F190I mutation in the proximal domain. At pH 9.0, in 50 mM bicine, HS ν_3 modes for the wild-type MnP disappear with the appearance of a 6cLS ν_3 mode at 1505 cm^{-1} (Figure 2.3). A concomitant shift of ν_2 from $\sim$1565 to 1580 cm^{-1} and the appearance of a shoulder at $\sim$1638 cm^{-1} from ν_{10} are additional indicators of the pH-induced HS → LS conversion. A similar spectrum is observed in the F190I mutant MnP in 40 mM phosphate, pH 7.5 (Figure 2.3), indicating that similar LS species are formed in the two proteins, although the transition occurs at lower pH in the mutant enzyme. Both spectra resemble RR spectra of ferric bis(imidazole) heme and ferric cytochrome b_{558} (Table 2.2) [70, 187]. These data strongly suggest that the 6cLS species is formed by a rearrangement at the heme, which allows coordination of the distal imidazole, H46, resulting in a bis(histidyl) heme iron structure. Low-frequency RR spectra of the wild-type MnP at pH 9.0 in bicine buffer were also recorded [data not shown]. No shifts in any bands occurred following incubation of the sample in 75% $H_2{}^{18}O$, consistent with assignment of the LS species as a bis-His coordinated heme iron rather than an hydroxo-iron heme derivative.

2.3.2 Restoration of the Native Structure by Calcium

The ability of calcium to restore the native electronic absorption spectrum in wild-type MnP is demonstrated in Figure 2.4. The first two spectra are the same in

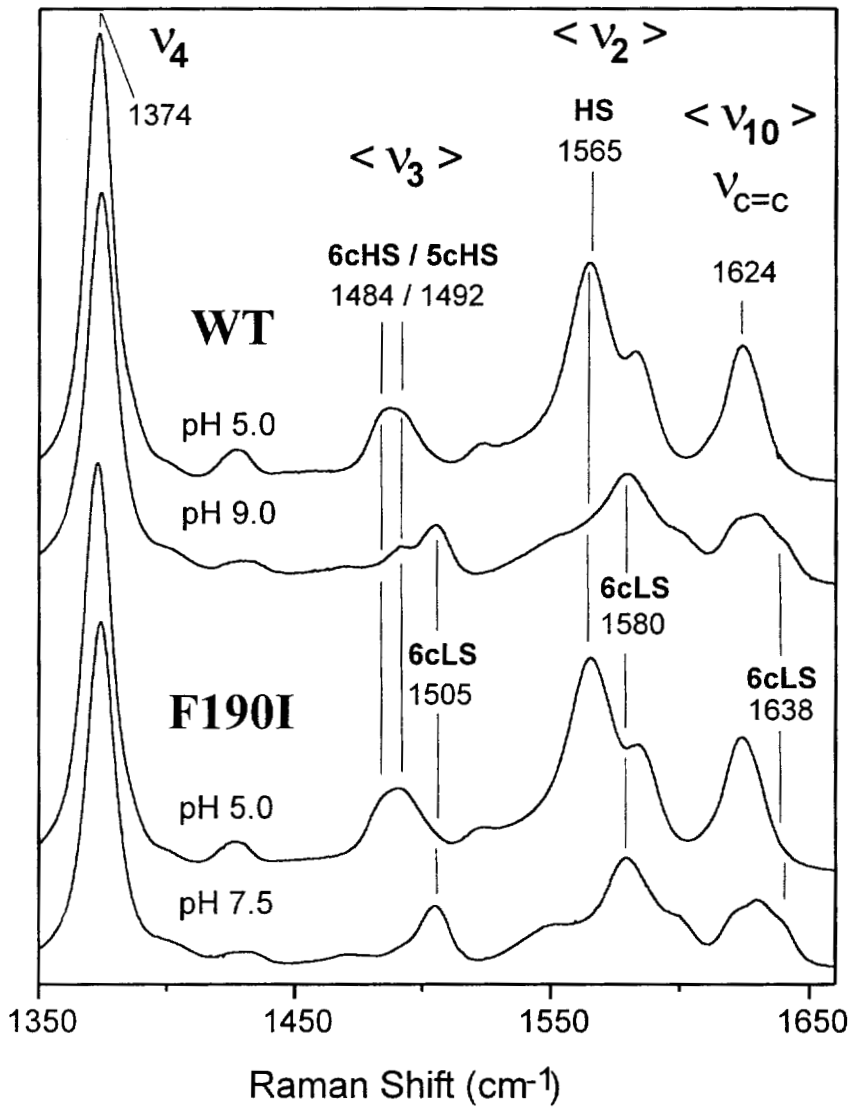

Figure 2.3 High-frequency region of resonance Raman spectra of MnP ($\sim$100 μM) at low and high pH obtained with Soret excitation (413 nm) as described. From top to bottom: wild type in distilled water, pH 5.0; wild type in 50 mM sodium bicine, pH 9.0; F190I in distilled water, pH 5.0; and F190I in 40 mM potassium phosphate, pH 7.5. HS, high-spin; LS, low-spin; 5c, pentacoordinate; 6c, hexacoordinate.

Table 2.2

High-Frequency Resonance Raman Spectral Modes[a]

Enzyme	pH	ν_4	ν_3	ν_2	ν_{10}
Ferric wild-type MnP[b]	5.0	1374	1484/1492	1565	1624
	9.0	1374	1505	1580	1638
Ferric F190I MnP[b]	5.0	1374	1484/1492	1565	1624
	9.0	1374	1505	1580	1638
Ferric cytochrome b_{558}[c]		1376	1510	1583	1642
Ferric bis(imidazole) heme[d]		1373	1502	1579	1640
Ferrous wild-type MnP[b]	5.0	1360	1475	1563	1610
	9.0	1360	1493	1582	1620
Ferrous F190I MnP[b]	5.0	1355	1470	1563	1606
	9.0	1359	1493	1582	1626
Ferrous cytochrome b_{558}[c]		1360	1490	1585	1610
Ferrous bis(imidazole) heme[d]		1359	1493	1584	1617

[a] Freqencies are given in reciprocal centimeters; excittion was at 413.1 nm within the Soret band.
[b] This work.
[c] From ref 187.
[d] From ref 70.

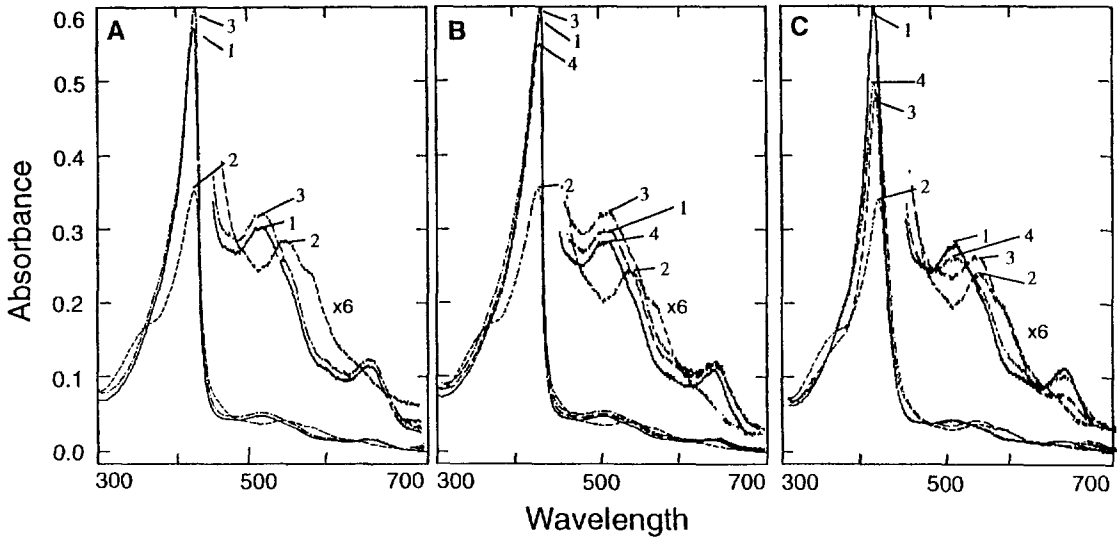

Figure 2.4 Electronic absorption spectra of oxidized (native, ferric) wild-type MnP in distilled water, pH 5.0 (spectrum 1 in all panels) and in 50 mM bicine, pH 8.45 (spectrum 2 in all panels). Addition of 100 mM $CaCl_2$ to the enzyme in water, pH 5.0, does not perturb the spectrum of native MnP (spectrum A3). Addition of 100 mM $CaCl_2$ to the enzyme at pH 8.45 restores the native spectrum at high pH (spectrum B3). Subsequently lowering the solution pH to 5.5 by the addition of 100 mM sodium succinate does not alter the Ca^{2+}-restored spectrum (spectrum B4). First lowering the pH from 8.45 to 5.5 with the addition of 100 mM succinate only partially restores the enzyme (spectrum C3). Subsequent addition of $CaCl_2$ (100 mM) at pH 5.5 (spectrum C4) restores the optical spectrum but does not fully restore the Soret absorption, unlike the addition of $CaCl_2$ at high pH (spectrum B3).

all three panels. Spectrum 1 is of the 5cHS native enzyme in distilled water at pH 5.0, while spectrum 2 is of the 6cLS enzyme formed at pH 8.45 in 50 mM bicine. The same change was also seen upon comparing spectra of the enzyme in 20 mM phosphate at pH 5.0 and 9.0 [data not shown], excluding a buffer effect. Addition of 100 mM $CaCl_2$ to the native enzyme at pH 5.0 (Figure 2.4A, spectrum 1) has no effect on the native 5cHS optical spectrum (Figure 2.4A, spectrum 3). However, addition of calcium to the 6cLS enzyme at pH 8.45 (Figure 2.4B, spectrum 2) completely restores the native 5cHS spectrum (Figure 2.4B, spectrum 3). Subsequently lowering the pH of the calcium-restored enzyme by the addition of 100 mM succinate, pH 5.5, does not further alter the HS spectrum (Figure 2.4B, spectrum 4). In contrast, first lowering the pH from 8.45 (Figure 2.4C, spectrum 2) to 5.5 without the addition of $CaCl_2$ only partially restores the enzyme (Figure 2.4C, spectrum 3). The Soret peak is blue-shifted, though less intense, but the visible portion of the spectrum is not restored. Subsequent addition of $CaCl_2$ (Figure 2.4C, spectrum 4) restores the ligand-to-metal charge transfer (LMCT) bands at 502 and 632 nm but does not completely restore the Soret absorption. Other divalent cations, such as Mn^{2+}, Mg^{2+}, Zn^{2+}, and Cd^{2+}, were incapable of restoring the native spectrum at high-pH [data not shown].

2.3.3 UV-Vis and RR Spectroscopy of the Reduced Enzymes

Reduction of the native ferric enzyme with dithionite causes noticeable changes in the electronic absorption spectrum (Figure 2.5). In distilled water, pH 5.0, the spectrum exhibits maxima at 435, 557, and 586 nm (Table 2.1), similar to that previously observed in 20 mM succinate, pH 4.5 [136]. The reduced F190I mutant protein at low pH displays a spectrum nearly identical to that of wild-type MnP (Figure 2.5, Table 2.1). At high pH, the spectra of both the reduced wild-type and F190I mutant proteins change (Figure 2.5). The Soret band at 435 nm is blue-shifted by 10 nm and loses intensity. The peak at 557 nm is slightly red-shifted, shoulders at 515 and 585 nm disappear, and a new β band appears at 529 nm. Importantly, the alkaline spectra are very similar to that of ferrous cytochrome b_{558} (Table 2.1), which is a known 6cLS bis-His heme iron protein (187, 296).

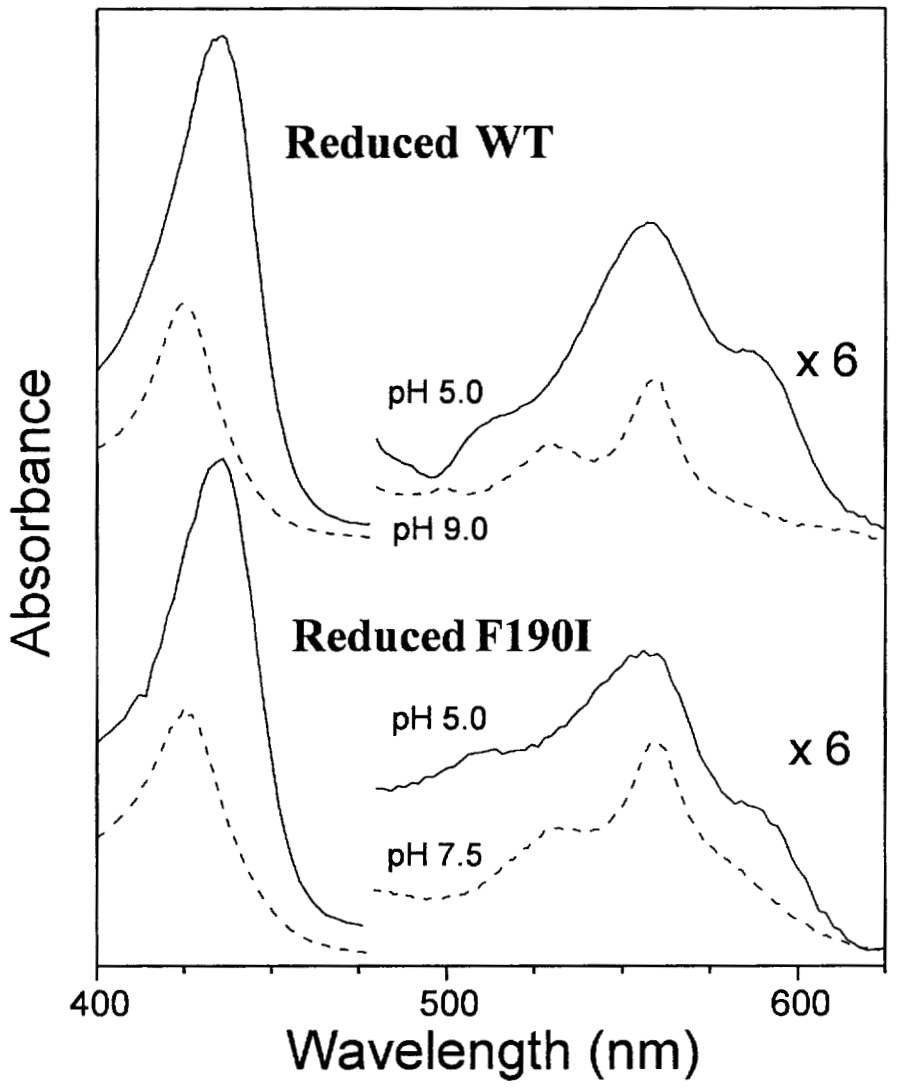

Figure 2.5 Electronic absorption spectra of reduced (ferrous) wild-type MnP and F190I MnP at low pH (—) with both proteins in distilled water, pH 5.0, and at higher pH (---) with the wild-type in 50 mM bicine, pH 9.0, and the F190I in 40 mM potassium phosphate, pH 7.5.

RR spectra of the reduced wild-type and F190I mutant MnP proteins at low and high pH are shown in Figure 2.6. The spectra of both the reduced wild-type MnP and the F190I mutant exhibit ν_3, ν_2, and ν_{10} modes at 1475, 1563, and 1610 cm^{-1}, respectively, indicating a ferrous HS species in water at pH 5.0, similar to that previously reported for the wild type in 20 mM succinate, pH 4.5 [270] (Table 2.2). At higher pH, the reduced wild-type (pH 9.0) and F190I (pH 7.5) enzymes exhibit similar changes in their RR spectra. The HS modes disappear with appearance of LS modes at 1493, 1582, and 1626 cm^{-1}, resulting in spectra similar to those of bis(imidazole) heme and cytochrome b_{558} (Table 2.2) [70, 187].

2.3.4. Restoration of the Reduced Proteins by Calcium

Addition of exogenous Ca^{2+} restored the HS pentacoordinate reduced wild-type structure (Figure 2.7), similar to results with the oxidized proteins. The 5cHS spectrum of reduced wild-type MnP at pH 5.0 is shown in spectrum 1 of Figure 2.7. The 6cLS species is formed after the pH is raised to 9.0 by addition of 50 mM bicine (spectrum 2), while subsequent addition of 100 mM $CaCl_2$ at pH 9.0 restores the 5cHS species (spectrum 3).

2.4 DISCUSSION

Electronic absorption spectra of heme proteins are indicators of the HS and LS states of the ferric heme iron. In most plant and fungal peroxidases, the heme iron is coordinated to the protein through the imidazole group of the proximal His residue [100, 256, 287). Primary spectroscopic differences among the various heme proteins result from variations in coordination on the distal side of the iron [100]. Whereas pentacoordinate heme iron is typically HS, coordination of a sixth ligand results in HS or LS ferric heme species, depending on the ligand field strength of the donor [290, 355]. In addition to the Soret band near 405 nm, ferric heme proteins typically exhibit four absorption bands in the visible region of the electronic spectrum. Two LMCT bands near 500 and 630 nm are apparent in spectra of HS derivatives, such as in native MnP, whereas spectra of LS derivatives exhibit the two bands designated α

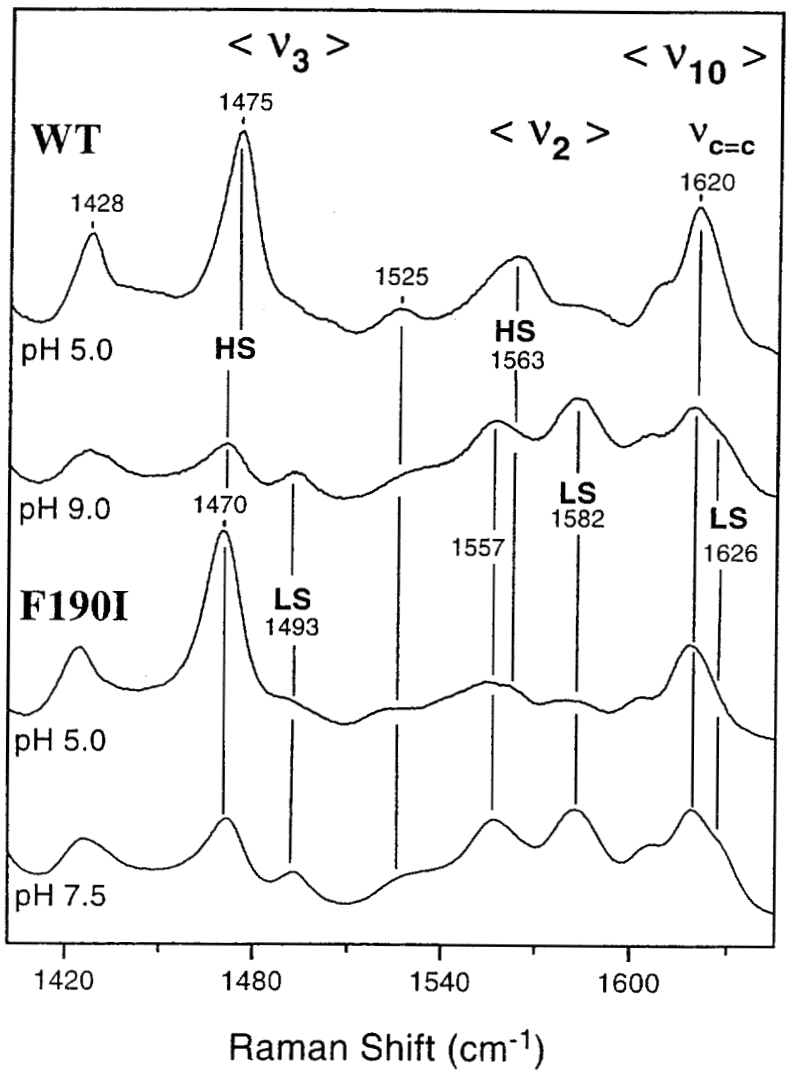

Figure 2.6 High-frequency region of the resonance Raman spectra of reduced MnP under conditions used in Figure 2.3. From top to bottom: reduced wild type in distilled water, pH 5.0; reduced wild type in 50 mM bicine, pH 9.0; reduced F190I in distilled water, pH 5.0; and reduced F190I in 40 mM phosphate, pH 7.5. HS, high-spin; LS, low-spin.

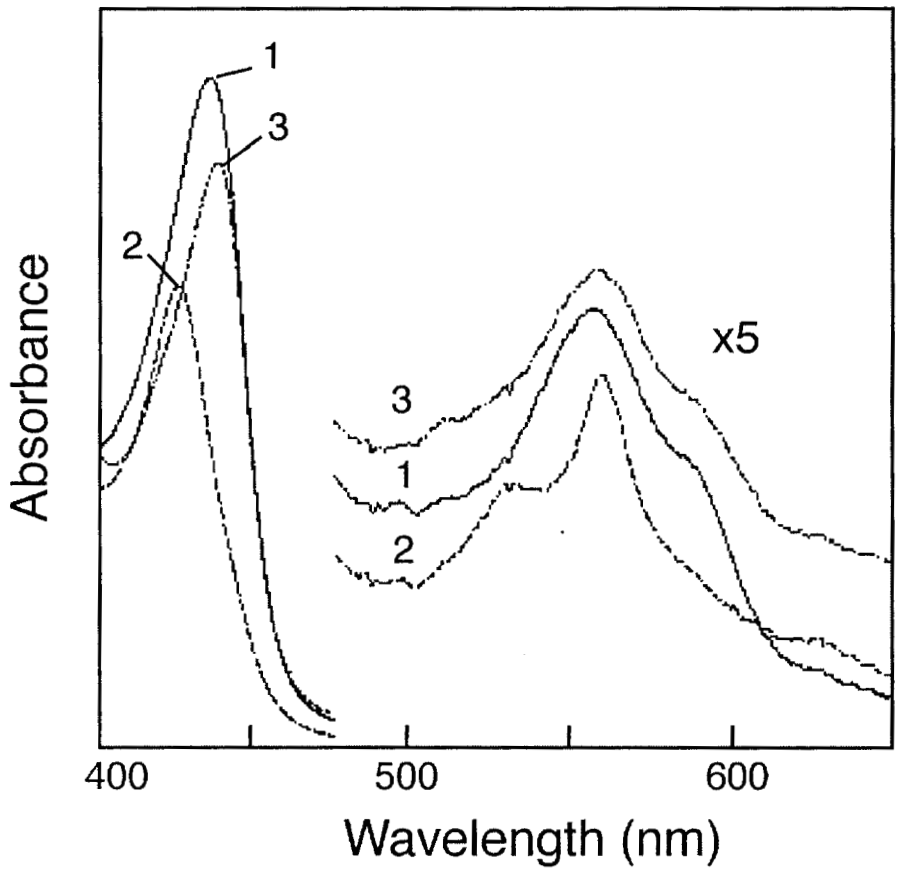

Figure 2.7 Electronic absorption spectra of reduced wild-type MnP in water, pH 5.0 (spectrum 1), or in 50 mM bicine, pH 8.45 (spectrum 2). Addition of 100 mM $CaCl_2$ to the enzyme in spectrum 2, pH 8.45, restores the native spectrum (spectrum 3).

and β near 570 and 540 nm, respectively [290]. HS → LS transitions frequently occur in peroxidases as the pH is raised. Such "alkaline transitions" appear to involve the ligation of a sixth axial ligand to the pentacoordinate heme iron by either a hydroxyl group, as in HRP [205, 351], or the imidazole of a distal His, as in CcP [357].

As previously reported, the electronic absorption spectrum of wild-type MnP indicates an alkaline transition from HS to LS, evidenced by the disappearance of the LMCT bands at 505 and 636 nm and appearance of α and β bands at 559 and 535 nm, respectively, when the pH is raised above 8.4 (Figure 2.2) [225]. The resulting spectrum is similar to that of ferric cytochrome b_5 [373] (Table 2.1), a heme protein with bis-His axial coordination of the heme iron. The optical spectrum of the alkaline LS MnP is very different from that of hydroxo-HRP [205] (Table 2.1), supporting the assignment of the LS species in MnP to the formation of a bis-His, rather than a hydroxo-His, coordinated iron. A similar transition occurs in a mutant of MnP where F190 has been replaced by Ile (F190I), Ala (F190A) [225], or Val (F190V) [21], though at ~ 2 pH units lower than for the wild-type MnP. Previous visible MCD spectroscopy of the wild-type and F190I MnP at high pH indicated spectral features similar to those of the imidazole complexes of cytochrome *c* and myoglobin, as well as cytochrome b_5 [225, 414].

Replacement of the proximal residue F190, with Ile, Leu, Tyr, or Ala, does not affect the binding or oxidation of Mn^{2+} [225]. However, the thermal stability of the protein and the stability of oxidized enzyme intermediates are decreased in the mutant proteins [225]. The bulky Phe residue may provide a steric barrier that restricts mobility within the heme pocket [225]. Replacement of the large aromatic ring with smaller hydrophobic residues, such as Ile, may remove these restrictions, resulting in increased movement in the heme pocket. This may allow coordination of the distal H46 to the heme iron, thus accounting for the sensitivity of these mutants to external conditions, such as pH.

Upon reduction with dithionite, the electronic spectra of the wild-type and F190I mutant proteins at pH 5.0 display a prominent absorption band at 557 nm with shoulders near 515 and 585 nm (Figure 2.5), characteristic of pentacoordinate ferrous

heme proteins [386]. When the pH is raised to 7.5 for F190I and pH 9.0 for wild-type MnP, the spectra display two prominent absorption bands at 558 and 529 nm, similar to the optical spectrum of ferrous cytochrome b_{558} (Table 2.1) [296], a known bis-His coordinated iron heme protein [124, 187], strongly suggesting the formation of a bis-His heme iron at high pH.

RR spectroscopy is sensitive to the oxidation and spin state of iron porphyrins in proteins. Excitation within the Soret region enhances symmetric modes of vibration within the porphyrin [365]. The modes ν_3, ν_{10}, and ν_2 are primary RR markers bands that characterize spin state, a measure of the pyrrole nitrogen–carbon stretching frequencies within the porphyrin core that respond to changes in the iron spin [364]. The RR spectra of the ferric wild-type and F190I mutant MnP are very similar (Figure 2.3, Table 2.1), indicating that the F190I mutation alone does not disturb the porphyrin core. The location of the oxidation state marker band, ν_4, at 1374 cm^{-1} exhibited by both proteins is typical of ferric hemes [365]. Raising the pH has no effect on the oxidation state of either the wild-type or the F190I MnP (Figure 2.3). However, shifts in the ν_3, ν_2, and ν_{10} bands at high pH evidence a transition from a predominantly 5cHS species, with a small 6cHS component consistent with an aquo-heme, to a fully 6cLS heme iron species (Figure 2.3). The RR spectra of the alkaline ferric MnPs closely resemble those of ferric cytochrome b_{558} and ferric bis(imidazole) heme (Tables 2.2) [70, 124, 187], further supporting the assignment of the 6cLS species to a bis-His axial ligated heme iron.

Incubation of the protein in ^{18}O-labeled water did not result in any changes in the low-frequency spectrum, as would be expected for a hydroxo-ligated heme iron. Other peroxidases, such as HRP and turnip peroxidase, also exhibit HS → LS transitions at high pH that had been previously attributed to coordination of a distal His to the heme iron [276, 391]. However, more recent studies have shown that incubation of several HRP isozymes in ^{18}O-labeled water at high pH results in shifts in the low-frequency RR spectra [351]. Bands in the spectra of LS alkaline HRP and turnip peroxidase have since been assigned to Fe–OH stretching at 500–520 cm^{-1}. These peaks are shifted by -9 to -24 cm^{-1} in $H_2{}^{18}O$ [351]. No corresponding change was detected in the alkaline ferric wild-type MnP, consistent with the assignment of

the 6cLS species to a bis-His iron heme rather than a hydroxo-His iron heme complex.

RR spectra of the reduced proteins at high pH (Figure 2.6, Table 2.2) also show changes for the ν_3, ν_2, and ν_{10} spin-state modes at high pH for both the wild-type and F190I mutant MnP indicating a HS → LS transition. The RR spectra of the reduced alkaline proteins resemble those of ferrous cytochrome b_{558} and ferrous bis(imidazole) heme [69, 187], further supporting the formation of a bis-His species in MnP at high pH.

Together these results provide strong evidence that the 6cLS species formed in both the oxidized and reduced proteins is a bis-His heme iron. It has been proposed that this alkaline 6cLS complex is formed by ligation of the distal His46 to the heme iron as shown for alkaline cytochrome *c* peroxidase [357]. The identical RR spectra exhibited by the wild-type and F190I mutant proteins indicate that the same heme species is formed by both proteins; however, the F190I mutation allows coordination of the distal His to the heme iron at a lower pH than is observed in the wild-type protein.

The electronic absorption spectrum of the 6cLS MnP formed at high pH is similar to that previously observed in thermally inactivated MnP [379]. Near IR-MCD spectroscopic analysis suggested the formation of a highly symmetric heme iron in the heat-treated enzyme [381]. The addition of excess calcium to the thermally inactivated MnP restored the HS native optical spectrum [379, 381]. Our present results indicate that excess calcium also restores the HS optical (Figure 2.4) and RR [data not shown] spectra of both wild-type and F190I MnP at high pH. Together, these results indicate that Ca^{2+} mediates the transition from a 6cLS bis-His heme iron back to 5cHS heme iron.

Sutherland and co-workers proposed that loss of the distal Ca^{2+} is responsible for the HS → LS transition upon thermal inactivation [379, 381]. However, the loss of either or both of the distal or proximal Ca^{2+} ions (Figure 2.1) could conceivably result in the observed changes. The distal Ca^{2+}-binding site comprises the side chains of D47, S66, and D64, the backbone carbonyls of G62 and D47, as well as two water molecules (Figure 2.1) [376]. D47 is on helix B adjacent to the catalytic distal H46,

and one of the water ligands to the calcium is bound to E74, which forms part of the H-bond network through Q80 which terminates at the catalytic distal H46 (Figure 2.1) [ref 376 and references therein]. Loss of the distal calcium could result in changes in helix B and/or the E74–N80–H46 H-bond network, which could permit the ligation of the distal H46 to the heme iron.

However, loss of the proximal Ca^{2+} could conceivably result in changes in the conformation of the proximal domain or in the position of the proximal His173, resulting in movement of the heme iron, thus also enabling ligation to the distal H46. The proximal calcium is bound by the backbone carbonyls of T196, S174, and T193 and the side chains of D191, T193, D198, and S174, which is adjacent to the proximal H173 (Figure 2.1B) [376]. Indeed, F190 is adjacent to D191 and replacement of F190 may affect stability of the proximal Ca^{2+} binding site. It is therefore conceivable that both Ca^{2+} ions may be involved in preventing/reversing the formation of the bis-His heme complex.

The accessibility of the Ca^{2+} binding site(s) appears to be diminished at low pH. In thermal stability experiments, the addition of exogenous Ca^{2+} was less effective in preventing inactivation of the enzyme at low pH [379]. Protonation of the carboxyl ligands at the sites may alleviate repulsion in the empty site, resulting in a "collapse" of the site(s) preventing access by Ca^{2+}. The resulting limited access may explain the inability of the cation to completely restore the HS species after the pH was lowered to 5.5 (Figure 2.4C, spectrum 3). Other cations, such as Mn^{2+} [379, 442], also have been observed to confer thermal stability to MnP. Sutherland and coworkers hypothesized that Mn^{2+} stabilized the enzyme by binding at the distal calcium binding site. However, since Mn^{2+} is unable to restore the native HS enzyme at high pH when the site is most exposed, it probably does not bind efficiently at the Ca^{2+} binding site(s). Rather, Mn^{2+} probably confers stability to the enzyme by binding at the Mn^{2+}-binding site. Coordination of a metal at this site, which includes three amino acids and the two heme propionates, may provide additional anchoring of the heme to the protein [442].

In conclusion, optical absorption and resonance Raman spectroscopy indicate that, at high pH, MnP undergoes a transition from a 5cHS to a 6cLS bis-His iron

heme species. No evidence for a hydroxo-heme species was found. Similar LS bis-His heme species are formed in both the wild-type and F190I mutant MnP proteins, although the pH at which this transition occurs is significantly lower in the F190I variant. The optical spectra of the reduced proteins at high pH closely resemble those of cytochrome b_{558} [296], a known bis-His-ligated protein [124, 187]. Moreover, the RR spectra of the oxidized and reduced MnP proteins are also similar to those of cytochrome b_{558} and bis(imidazole) heme [69, 70, 187]. Finally, the 5cHS species is restored upon addition of excess calcium at high pH. This suggests that loss of one or both of the structural Ca^{2+} ions may result in conformational changes that permit coordination of the distal H46 to the heme iron. Other metal cations, including Mg^{2+}, Mn^{2+}, and Cd^{2+}, were unable to restore the HS pentacoordinate species at high pH.

CHAPTER 3
EFFECTS OF CADMIUM ON MANGANESE PEROXIDASE: COMPETITIVE INHIBITION OF Mn^{2+} AND THERMAL STABILIZATION OF THE ENZYME*

3.1. INTRODUCTION

White-rot basidiomycetous fungi are primarily responsible for the degradation of lignin, a heterogeneous phenylpropanoid polymer constituting 20–30% of woody plant cell walls [58a, 143, 222, 339]. Major components of the extracellular lignin-degrading system of the white-rot fungus, *Phanerochaete chrysosporium*, include two heme peroxidases, lignin peroxidase and manganese peroxidase (MnP), as well as enzymes involved in peroxide generation [140, 143, 222, 238]. Unlike other enzymes involved in lignin degradation by *P. chrysosporium*, MnPs are produced by essentially all lignin-degrading fungi [168, 299]. Investigation of this enzyme is therefore important to our understanding of this important degradative pathway.

Manganese peroxidase isozyme I from *P. chrysosporium* has been purified and extensively characterized by a variety of biochemical and biophysical techniques [135, 140, 226, 426]. Spectroscopic, DNA sequence, and crystallographic studies suggest that the heme environment of MnP is similar to that of other plant and fungal peroxidases [24, 164, 313, 376, 426]. However, MnP is the only such peroxidase

---

* Originally published in this or similar form in the European Journal of Biochemistry and used here with permission of Blackwell Publishing Ltd. on behalf of the Federation of European Bioch4emical Societies.

Youngs, H. L., Sundaramoorthy, M., and Gold, M. H. (2000) Effects of cadmium on manganese peroxidase: competitive inhibition of Mn^{II} oxidation and thermal stabilization of the enzyme. *Eur. J. Biochem.* **267**, 1761–1769.

that catalyzes the one-electron oxidation of Mn^{2+}, a component of woody plant tissues [441], to Mn^{3+} [135, 426] in a typical peroxidase cycle:

$$MnP + H_2O_2 \rightarrow MnPI + H_2O \quad \text{(reaction 3.1)}$$

$$MnPI + Mn^{2+} \rightarrow MnPII + Mn^{3+} \quad \text{(reaction 3.2)}$$

$$MnPII + Mn^{2+} \rightarrow MnP + Mn^{3+} + H_2O \quad \text{(reaction 3.3)}$$

where MnPI and MnPII are the oxidized intermediate compounds I and II of MnP.

Oxalate, which is secreted by the fungus, and other organic acid chelators, such as malonate, stabilize the enzyme-generated Mn^{3+} [227, 233, 426]. These Mn^{3+}–chelate complexes diffuse away from the enzyme to oxidize phenolic substrates, including lignin, lignin model compounds [308, 403, 425], and aromatic pollutants [321, 406, 407]. In addition to oxidizing Mn^{2+}, MnPI and MnPII can directly oxidize small phenolic compounds, such as guaiacol and dimethoxyphenol, although the rates are greatly reduced compared with the Mn-mediated reaction [26, 227, 422, 436].

Crystal structure [376, 377] and site-directed mutagenesis studies [226, 237, 436] indicate that the Mn^{2+} in the MnP binding site is hexacoordinate with four carboxylate ligands from the side chains of three amino acids, Asp179, Glu35, Glu39, and heme propionate 6, as well as two water ligands, one of which is hydrogen-bonded to heme propionate 7. Competition for these ligands by other metal ions has not been studied extensively. Sm^{3+}, Eu^{3+} [H. L. Youngs and M. H. Gold, unpublished results], and Co^{2+} ($K_i \approx 1$ mM) [164] are competitive inhibitors for Mn^{2+}, whereas, Ca^{2+} and Mg^{2+} do not inhibit Mn^{2+} oxidation by MnP [H. L. Youngs and M. H. Gold, unpublished results].

Recently, Cd^{2+} has been reported to inhibit the oxidation of 3-dimethylaminobenzoic acid, poly R, and polycylic aromatic hydrocarbons [18, 19] by the unpurified extracellular fluids of the white-rot fungi *P. chrysosporium* and *Pleurotus ostreatus*. However, Cd^{2+} also inhibits fungal growth [19, 392] and may affect extracellular enzyme levels. Herein, we report the results of steady-state and transient-state kinetic experiments on the inhibition of purified MnP by Cd^{2+}. We also investigate thermal stabilization of MnP by Cd^{2+} alone and by Cd^{2+} and Mn^{2+} together.

3.2 MATERIALS AND METHODS

3.2.1 Enzyme Preparation

MnP isozyme I was purified from the concentrated extracellular medium of acetate-buffered, high-carbon/low-nitrogen liquid agitated cultures [136] of *P. chrysosporium* wild-type strain OGC101 [8]. The concentrated medium was pH-adjusted to 6.5 and loaded on a DEAE-Sepharose column equilibrated with 20 mM potassium phosphate, pH 6.5. The column was washed with 20 mM potassium phosphate, pH 6.0, and MnP was eluted as a single band with 20 mM sodium succinate, pH 5.5. The eluate was washed, concentrated, and further purified by Cibacron Blue 3GA dye affinity chromatography and FPLC using a Mono Q column as previously described [237, 263]. To remove bound Mn^{2+}, the enzyme was gel-filtered on a G-25 Sephadex column in sodium succinate, pH 4.5. Metal (Mn, Fe, Cd) content was determined by atomic absorption spectroscopy using a Varian SpectraAA 20B spectrometer fitted with a graphite furnace. Enzyme was incubated with a 100-fold excess of either Cd^{2+}, Mn^{2+}, or a mixture of half Mn^{2+} and Cd^{2+} in 50 mM malonate, pH 4.5, for 1 h at 4°C. The enzyme solutions were then concentrated and washed extensively using Centricon membranes (Amicon). Atomic absorption measurements for each metal were quantified by comparison with standard solutions. Purified enzyme had an $Rz_{406/280} \geq 5$. The enzyme concentration was determined using $\epsilon_{406} = 129\ mM^{-1} \cdot cm^{-1}$ [136].

3.1.2 Kinetic and Spectrophotometric Analyses

Steady-state kinetics of Mn^{2+} oxidation were measured as Mn^{3+}–malonate formation at 270 nm as previously described [426], using a Shimadzu UV-260 spectrophotometer. Binding of Cd^{2+} to MnP in 50 mM sodium malonate, pH 4.5, was determined using difference spectroscopy, as previously described for Mn^{2+} binding [426]. Transient-state kinetic experiments were performed on an Applied PhotoPhysics SX.18 MV sequential stopped-flow reaction analyzer at 25.0 ± 0.2°C, as recently described [359]. Complete formation of enzyme intermediates was confirmed by rapid scanning. Substrates oxidations were analyzed in the presence or

absence of various amounts of $CdSO_4$ in 50 mM potassium malonate, pH 4.5, as indicated. The ionic strength (I) of all solutions was adjusted to 0.1 M with K_2SO_4. A minimum 10-fold excess of substrate over enzyme was used in all reactions to ensure pseudo-first-order reaction kinetics. Reduction of MnPI was followed at 416 nm, the isosbestic point between MnPII and native enzyme. Formation of MnPI and reduction of MnPII were followed at 397 nm, the isosbestic point between MnPI and MnPII. All kinetic traces displayed single-exponential character, from which pseudo-first-order rate constants were calculated.

3.2.3 Thermal Inactivation of Enzyme

Dilute, metal-free enzyme (10 $\mu g \cdot mL^{-1}$) in 50 mM malonate, pH 4.5, was incubated at 55°C for up to 15 min, alone, or in the presence of the metals indicated. Aliquots (50 μL) of the heat-treated enzyme were removed at various time intervals and diluted to 1 mL with a room-temperature solution containing 500 μM $MnSO_4$ in 50 mM potassium malonate, pH 4.5. The ionic strength was adjusted to 0.1 M with K_2SO_4. The rate of Mn^{3+}–malonate formation was recorded at 270 nm on addition of H_2O_2 to 100 μM. The initial activity was considered to be 100% for each run.

3.2.4 Chemicals

DEAE Sepharose CL-6B, Cibacron Blue 3GA, Sephadex G-50, potassium ferrocyanide, 2-methoxyphenol (guaiacol), 2,6-dimethoxyphenol (DMP), and H_2O_2 (30% solution) were obtained from Sigma-Aldrich. $CdSO_4$ was obtained from Mallinckrodt. The concentration of H_2O_2 was determined using $\epsilon_{240nm} = 39.6$ $M^{-1} \cdot cm^{-1}$ [280]. Solutions used for kinetic assays were prepared with HPLC-grade water from Sigma-Aldrich. Atomic absorption standards for Mn, Fe, and Cd were obtained from Sigma-Aldrich. Other solutions were prepared using distilled water further purified by the MilliQ 50 (Millipore) filtration system. DMP was purified by silica gel chromatography in hexane/ethyl acetate before use.

3.3 RESULTS

3.3.1 Steady-State Kinetics of Inhibition by Cd^{2+}

Under steady-state conditions, the effect of Cd^{2+} on the oxidation of Mn^{2+} by MnP was determined by following the formation of Mn^{3+}-malonate at 270 nm. Table 3.1 lists the K_i values determined. With Mn^{2+} as the varied substrate, inverse plots at varying concentrations of $CdSO_4$ were linear with a common ordinate-intercept (Figure 3.1A), indicating that Cd^{2+} is a competitive inhibitor of MnP-catalyzed Mn^{3+}–malonate formation. A $K_i \approx 10$ μM was calculated from the replot of the slope ($K_{m,app}/V_{max}$) vs. [Cd] (Figure 3.1A, inset).

The inverse plots of the steady-state kinetic analysis of Mn^{3+}–malonate formation with H_2O_2 as the varied substrate are shown in Figure 3.1B. The inverse plots at various Cd^{2+} concentrations were linear and parallel, indicating that Cd^{2+} is an uncompetitive inhibitor of H_2O_2. A $K_i \approx 8$ μM was calculated from the replot of intercepts ($1/V_{max}$) vs. [Cd] (Figure 3.1B, inset).

The effect of Cd^{2+} on the oxidation of 2,6-DMP by MnP in the presence of Mn^{2+} was also investigated. The inverse plot shows competitive inhibition with a calculated $K_i \approx 4$ μM [data not shown]. Under steady-state conditions, the direct oxidation of 2,6-DMP or guaiacol by MnP in the absence of Mn^{2+} was not inhibited by Cd^{2+} [data not shown].

3.3.2 Binding of Cd^{2+} to MnP

Cd^{2+} binding to MnP in malonate, pH 4.5, produces characteristic difference spectra similar to those observed for Mn^{2+}–MnP binding [426]. The spectra display a maximum at $\approx$403 nm and minimum at $\approx$424 nm (Figure 3.2). The apparent dissociation constant, $K_d \approx 8$ μM, was calculated from the plot of $1/\Delta A$ vs. 1/[S] (Figure 3.2, inset) according to Eqn (3.4), where ΔA_∞ is the absorbance change for the complete formation of the complex.

$$1/\Delta A = K_d/\Delta A_\infty 1/[Cd^{2+}] + 1/\Delta A_\infty \qquad (3.1)$$

Table 3.1

Inhibition Constants for Cd^{2+} [a]

Steady-state inhibition		Transient-state inhibition		Binding	
$K_{i\text{-}Mn}$	10 μM	$K_{i\text{-}MnPI}$ [b]	ND	$K_{d,Mn}$	10 μM
$K_{i\text{-}Mn/2,6\text{-}DMP}$	4 μM	$K_{i\text{-}MnPI\ (pH\ 4.5)}$ [c]	3 μM	$K_{d,Cd}$	8 μM
$K_{i\text{-}2,6\text{-}DMP}$	ND	$K_{i\text{-}MnPI\ (pH\ 3.0)}$ [c]	1 mM		
$K_{i\text{-}guiaicol}$	ND	$K_{i\text{-}MnPII}$ [d]	5 μM		

[a] Reactions were conducted in 50 mM malonate, pH 4.5, except where indicated. The ionic strength of all solutions was adjusted to 0.1 M with K_2SO_4. Inhibition of 2,6-DMP oxidation was evaluated in the presence ($K_{i,Mn/2,6\text{-}DMP}$) and absence ($K_{i,2,6\text{-}DMP}$) of Mn^{2+}. Inhibition of guaiacol oxidation was evaluated in the absence of Mn^{2+}. ND indicates no inhibition detected. Constants of inhibition in the transient-state were calculated using assumptions described in the text.

[b] MnPI formation.

[c] MnPI reduction.

[d] MnPII reduction.

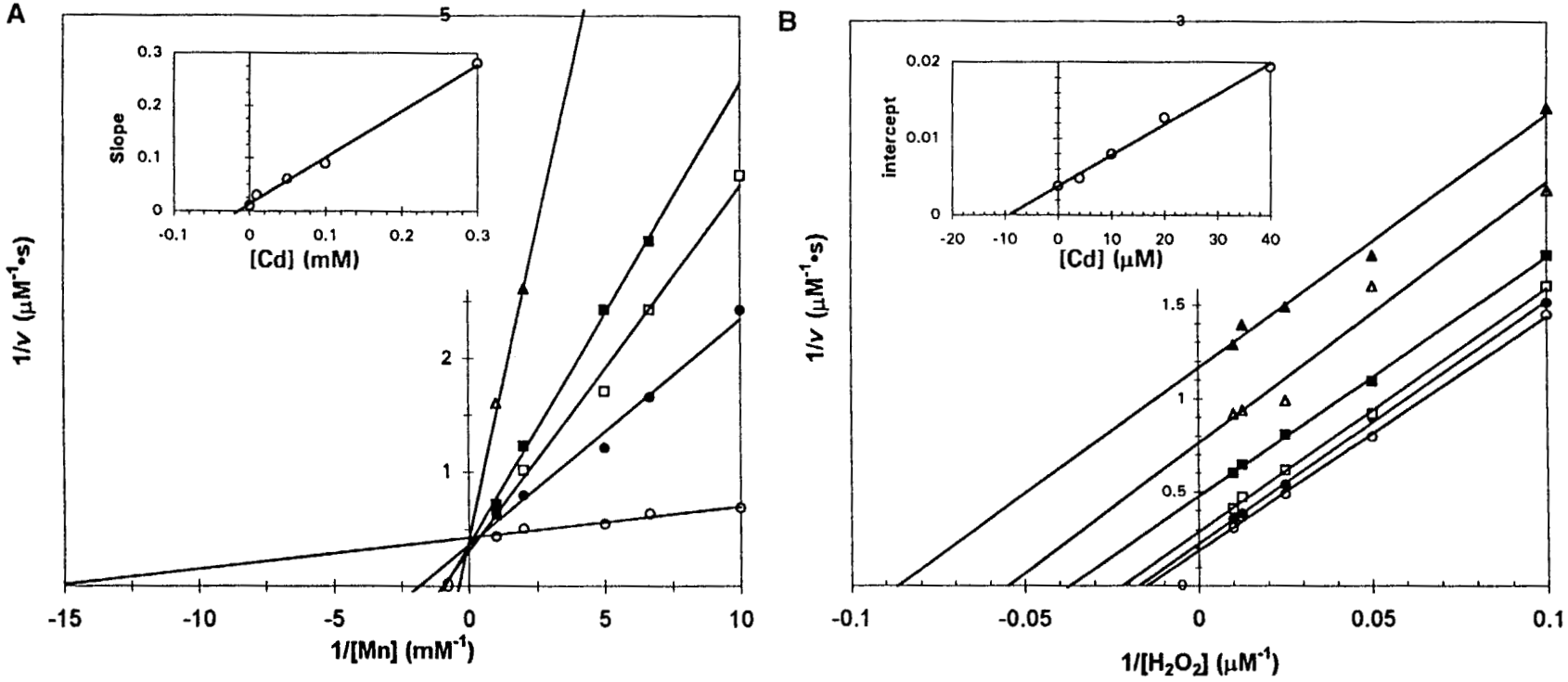

Figure 3.1 Inverse plot of (A) 1/rate vs. 1/[Mn] and (B) 1/rate vs. $1/[H_2O_2]$. (A) Reaction mixture contained 0.5 $\mu g \cdot mL^{-1}$ MnP (10 nM), 100 μM H_2O_2, in 50 mM malonate, pH 4.5, with $MnSO_4$ concentrations from 0.1 to 1 mM. $CdSO_4$ concentrations of 0 (○), 0.01 (•), 0.05 (□), 0.1 (■) and 0.3 (△) mM were used. The rate of Mn^{3+}–malonate fotrmation was calculated using $\epsilon = 9.7\ mM^{-1} \cdot cm^{-1}$. Inset: Replot of the slope of the inverse plot vs. [Cd]. (B) Reaction mixtures contained 1 $\mu g \cdot mL^{-1}$ MnP (20 nM), 100 μM $MnSO_4$, 50 mM malonate at pH 4.5, and H_2O_2 concentrations of 10–100 μM. $CdSO_4$ concentrations of 0 (○), 2.0 (•), 4.0 (□), 10 (■), 20 (△) and 40 (▲) mM were used. Inset: Replot of $1/V_{max}$ vs. $[Cd^{2+}]$.

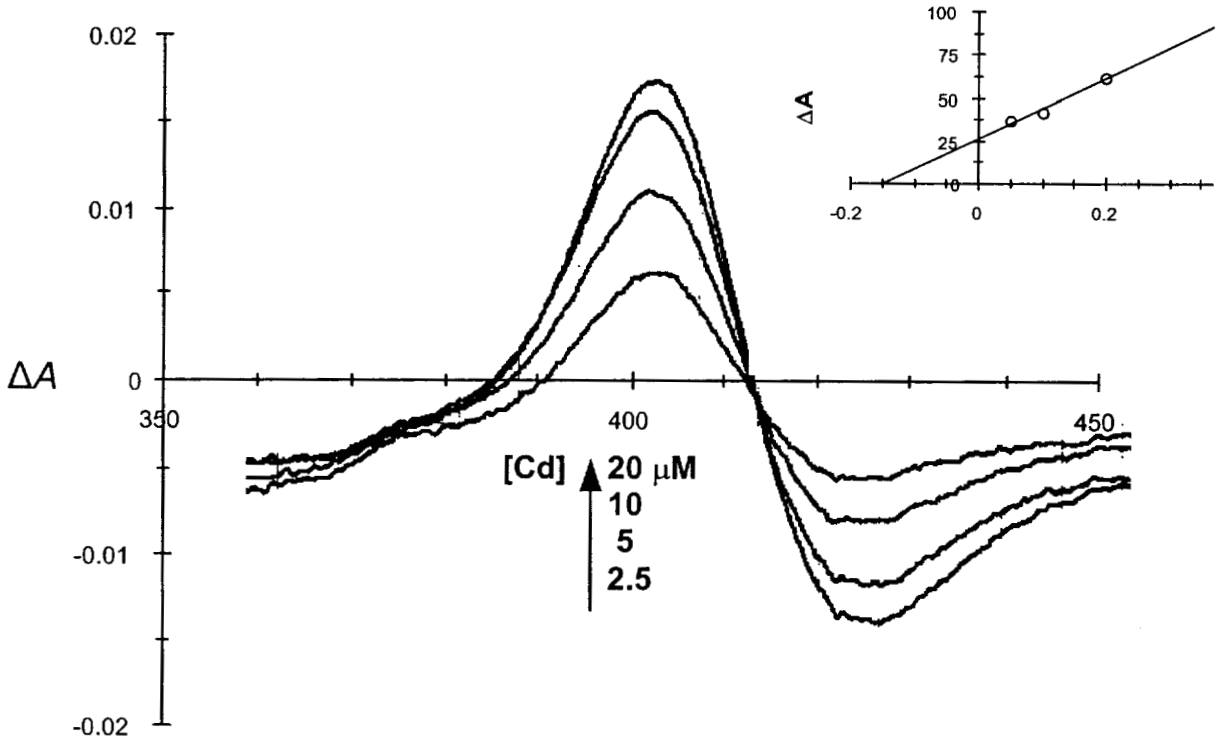

Figure 3.2 Binding of Cd^{2+} to manganese peroxidase. Difference spectra were recorded after addition of $CdSO_4$ to the sample cuvette. The change in absorbance increased with increasing $CdSO_4$ concentrations as shown. Sample and reference cuvettes both contained 3 μM MnP in 50 mM malonate at pH 4.5. Inset: The inverse plot, $1/\Delta A$ vs. $1/[Cd^{2+}]$.

Binding of Cd^{2+} to MnP in 50 mM malonate, pH 4.5, was also measured by atomic absorption spectroscopy. The enzyme was incubated with buffer containing either no metal, 100-fold excess of Mn^{2+} or Cd^{2+}, or a mixture of half Mn^{2+} and Cd^{2+}, then repeatedly concentrated and washed with water. In all solutions, 0.9 equiv. Fe were observed per protein molecule. No Cd^{2+} or Mn^{2+} was detected in the control sample. The enzyme incubated with only Mn^{2+} contained 0.9 equiv. Mn per protein molecule. The enzyme incubated with only Cd^{2+} contained 0.7 equiv. Cd per protein molecule. The sample incubated with half Cd^{2+} and Mn^{2+} contained 1.3 equiv. Mn and 1.0 equiv. Cd per protein molecule.

3.3.3 Transient-State Kinetics of Cd^{2+} Inhibition

3.3.3.1 Effect of Cd^{2+} on MnPI formation. MnPI formation (reaction 3.1) was monitored as a decrease in A_{397}, the isosbestic point between MnPI and MnPII. The plots of k_{obs} vs. $[H_2O_2]$ were linear (Figure 3.3A) with calculated apparent second-order rate constants for MnPI formation, $k_{1,app} \approx 3 \times 10^6\ M^{-1} \cdot s^{-1}$, for all concentrations of Cd^{2+} (Table 3.2), similar to previous reports of wild-type and various mutant MnPs [226, 237, 423, 436]. Cd^{2+} does not appear to affect MnPI formation (Figure 3.3A), in accordance with the steady-state kinetic results which indicate that Cd^{2+} is uncompetitive for H_2O_2.

3.3.3.2 Effect of Cd^{2+} MnPI reduction. As predicted by the steady-state kinetics, reduction of MnPI by Mn^{2+} (see reaction 3.2) was inhibited by Cd^{2+} (Figure 3.3B). The plots of the observed rate constants (k_{2obs}) vs. [Mn] were linear, indicating a second-order reaction as presented in Scheme 3.1.

$$\begin{array}{lc} & \overset{k_2}{} \\ & \text{MnPI} + \text{Mn}^{2+} \rightarrow \text{MnPII} + \text{Mn}^{3+} \\ & + \\ & \text{Cd}^{2+} \\ K_{\text{iMnPI}} & \downarrow\uparrow \\ & \text{MnPI} - \text{Cd}^{2+} \end{array}$$

Scheme 3.1

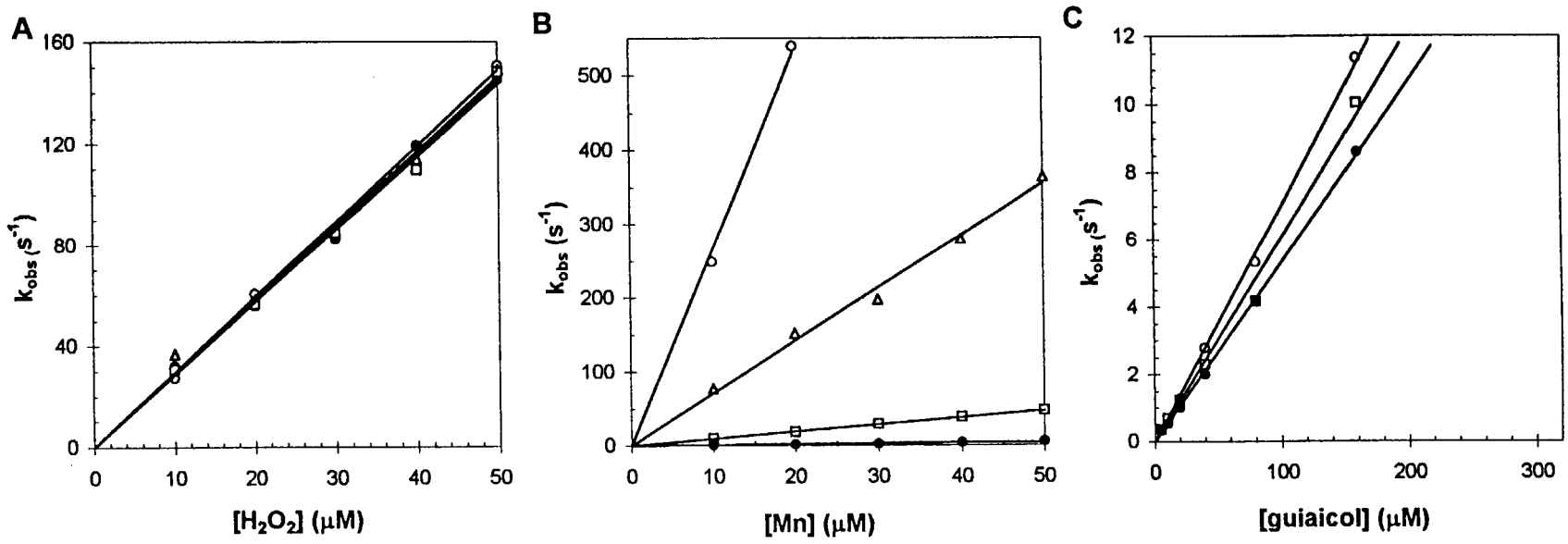

Figure 3.3 MnPI formation (A) and inhibition of MnPI reduction by Mn^{2+} (B) and guaiacol (C) in the presence of Cd^{2+}. (A) Reaction mixtures contained 2 μM MnP in 20 mM malonate. The ionic strength was adjusted to 0.1 M with K_2SO_4. The H_2O_2 concentrations varied from 10 to 50 μM. $CdSO_4$ concentrations of 0 (○), 5 (•), 50 (□), and 500 (Δ) μM were used. (B,C) Reaction mixtures contained 1 μM MnP and 1 mM H_2O_2 in 20 mM malonate. Ionic strength as adjusted to 0.1 M with K_2SO_4. The $MnSO_4$ concentration was varied from 10 to 50 μM. The guaiacol concentration was varied rrom 10 to 60 μM. $CdSO_4$ concentrations of 0 (○), 5.0 (Δ), 50 (□), and 500 (•) μM were used.

Table 3.2

Kinetic Parameters of Compound I Formation and Reduction of Compounds I and II in the Presence of Cd^{2+} [a]

$[Cd^{II}]$ (μM)	Apparent second-order rate constants ($M^{-1} \cdot s^{-1}$)				
	MnPI formation H_2O_2	MnPI reduction			MnPII reduction *p*-Cresol
		Mn	Guaiacol	*p*-Cresol	
0	2.97×10^6	2.7×10^7	7.0×10^4	6.3×10^3	1.2×10^3
5	2.89×10^6	7.1×10^6	6.6×10^4	4.7×10^3	9.0×10^2
50	2.87×10^6	9.5×10^5	6.1×10^4	4.2×10^3	8.3×10^2
500	2.92×10^6	1.0×10^5	5.3×10^4	3.0×10^3	7.2×10^2

The second-order rate constants for several concentrations of Cd^{2+} are shown in Table 3.2. As Cd^{2+} is a competitive inhibitor of Mn^{2+}, presumably only Cd^{2+}-free enzyme is able to react with Mn^{2+}.

In this case, k_{obs} is described by Eqn (3.2), where [MnPI] is the concentration of cadmium-free MnPI.

$$k_{2,obs} = k_2[Mn^{2+}][MnPI] \quad (3.2)$$

The reactions are carried out under pseudo-first order conditions such that:

$$-d[MnPI]_{total}/dt = k_{2,obs}[MnPI]_{total} \quad (3.3)$$

Assuming a rapid pre-equilibrium reaction between MnPI and Cd^{2+}, the $K_{i,MnPI}$ representing the equilibrium dissociation constant for the MnPI–Cd^{2+} complex can be used to obtain the following expression for $k_{2,obs}$:

$$k_{2,obs} = k_2[Mn^{2+}]\{1 - [[Cd^{2+}]/([Cd^{2+}] + K_{i,MnPI})]\} \quad (3.4)$$

The apparent second-order rate constant ($k_{2,app}$) is calculated for the enzyme in the absence of inhibitor when $k_{obs} = k_{2,app}[Mn^{2+}]$. The apparent second-order rate constants for various concentrations of Cd^{2+} are listed in Table 3.2. An average $K_{i,MnPI} \approx 3$ μM (Table 3.1) was calculated for Cd^{2+} inhibition of MnPI reduction by Mn^{2+}. At pH 3.0, inhibition by Cd^{2+} was much weaker than a $K_{i,MnPI} \cong 1$ mM (Table 3.1). Reduction of MnPI by guaiacol and *p*-cresol in the absence of Mn^{2+} showed only slight inhibition in the presence of Cd^{2+} (Figure 3.3C, Table 3.2). K_i values could not be calculated for these substrates because of the unknown nature of the inhibition (i.e., competitive or mixed), as no inhibition was observable for these substrates in the steady-state analysis.

3.3.3.2 Effect of Cd^{2+} on MnPII reduction. Cd^{2+} also inhibited the reduction of MnPII to native enzyme (MnP) by Mn^{2+} (reaction 3.3). The plots of the observed rate constants (Figure 3.4) showed saturation at higher levels of Mn^{2+}, indicating the formation of a MnPII–Mn^{2+} complex according to Scheme 3.2. At higher concentrations of Cd^{2+} (> 10 μM) the plots became linear, suggesting that exchange of Mn^{2+} for Cd^{2+} became the limiting step in the reaction. The first-order and second-order rate constants, the calculated apparent second-order rate constants ($k_{3,app}$), and apparent dissociation constants (K_d) are listed in Table 3.3.

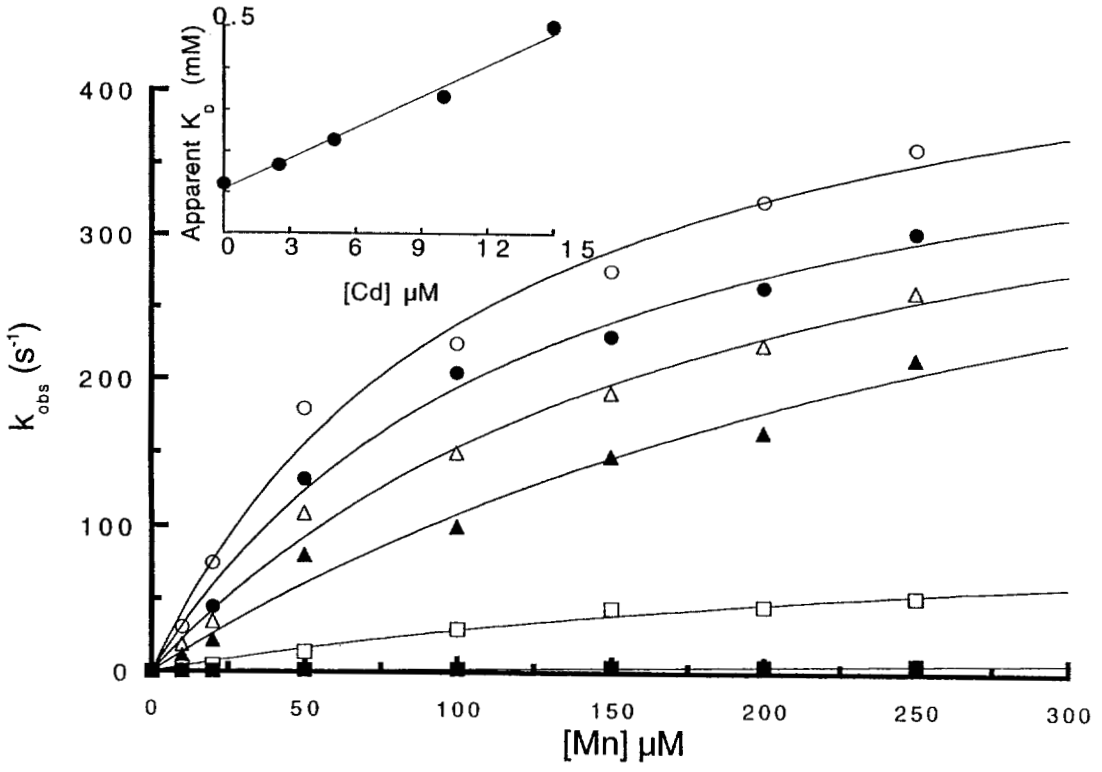

Figure 3.4 Inhibition of MnPII reduction by Mn^{2+} in the presence of Cd^{2+}. Reaction mixtures contained 1 μM MnP, 1 μM H_2O_2, and 1 μM $K_4Fe(CN)_6$ in 20 mM malonate (I = 0.1 M, K_2SO_4). The $MnSO_4$ concentration was varied from 10 to 150 μM. $CdSO_4$ concentrations of 0 (○), 2.5 (●), 5 (△), 10 (▲), 50 (□), and 500 (■) μM were used. Each k_{obs} was obtained from the exponential change in A_{397}. Inset: Replot of apparent K_d vs. [Cd].

Table 3.3

Kinetic Parameters for the Reduction of MnP Compound II by Mn^{2+} in the Presence of Cd^{2+} [a]

$[Cd^{II}]$ (μM)	Apparent binding constant K_d (μM)	Apparent first order rate constant (s^{-1})	Apparent and calculated second order rate constants ($M^{-1} \cdot s^{-1}$)
0	120	552	4.6×10^{6} [b]
2.5	167	503	3.0×10^{6} [b]
5	228	498	2.1×10^{6} [b]
10	333	498	1.5×10^{6} [b]
50	-	-	3.0×10^{5} [c]
500	-	-	2.6×10^{4} [c]

[a] Reactions were conducted and kinetic values were determined in 50 mM malonate, pH 4.5, as described in the text.

[b] Calculated second-order rate constants.

[c] Apparent second-order rate constants.

$$\begin{array}{ccccc} & & \xrightarrow{K_d} & & \xrightarrow{k_3} \\ \text{MnPII} & + \text{Mn}^{2+} & \leftrightarrow & [\text{MnPII–Mn}^{2+}] & \rightarrow \text{MnP} + \text{Mn}^{3+} \\ & + & & & \\ & \text{Cd}^{2+} & & & \\ K_{\text{iMnPII}} & \downarrow\uparrow & & & \\ & \text{MnPII} - \text{Cd}^{2+} & & & \end{array}$$

Scheme 3.2

An expression for k_{obs} (Eqn 3.5) can be derived from Scheme 3.2 (see Appendix 1), assuming competitive inhibition and rapid pre-equilibria between MnPII and both metals, which appears to hold for lower Cd^{2+} concentrations (< 10 μM):

$$k_{obs} = k_{3app}[Mn^{2+}]K_{i,MnPII}/(K_dK_{i,MnPII} + [Mn^{2+}]K_{i,MnPII} + K_d[Cd^{2+}]) \quad (3.5)$$

This expression reduces to Eqn (3.6) when the Cd^{2+} concentration is zero:

$$k_{obs} = k_{3,app}[Mn^{2+}]/([Mn^{2+}] + K_d) \quad (3.6)$$

The K_d and $k_{3,app}$ values were calculated by fitting the k_{obs} vs. $[Mn^{2+}]$ plot to Eqn (3.6). Using this technique, values of $K_d \approx 120$ μM and $k_{3,app} \approx 550$ s^{-1} were obtained, in the absence of Cd^{2+}, similar to values previously reported [360]. These values were then used to calculate inhibition constants for all $[Mn^{2+}]$ and $[Cd^{2+}]$ studied, yielding an average $K_{i,MnPII} \approx 5$ μM for Cd^{2+} inhibition of MnPII reduction by Mn^{2+} in 50 mM malonate, pH 4.5. MnPII reduction by guaiacol [data not shown] and *p*-cresol (Table 3.2) in the absence of Mn^{2+} showed negligible inhibition by Cd^{2+}, similar to that observed for MnPI reduction.

3.3.3.4 Effect of Cd^{2+} on thermal inactivation of MnP. The effect of Cd^{2+} on the thermal inactivation of MnP was investigated by monitoring the activity remaining after the enzyme was incubated alone and in the presence of metal at 55°C, as described above. The fraction of activity remaining vs. time is plotted in Figure 3.5, and the half-lives for each combination are reported in Table 3.4. Cd^{2+} and Mn^{2+}, and to a lesser extent Ca^{2+}, protected the enzyme from thermal inactivation. Both Mn^{2+} and Cd^{2+} at 1 mM extended the half-life of the enzyme by 2.7-fold and 2.2-fold, respectively, whereas 1 mM Ca^{2+} only extended the half-life by 1.28-fold. Combinations of Cd^{2+} and Mn^{2+} protected the enzyme far more efficiently than either metal alone or either metal with Ca^{2+}. The combination of 0.5 mM Mn^{2+} and 0.5 mM Cd^{2+} extended the enzyme half-life by over 10-fold. In contrast, half-lives of

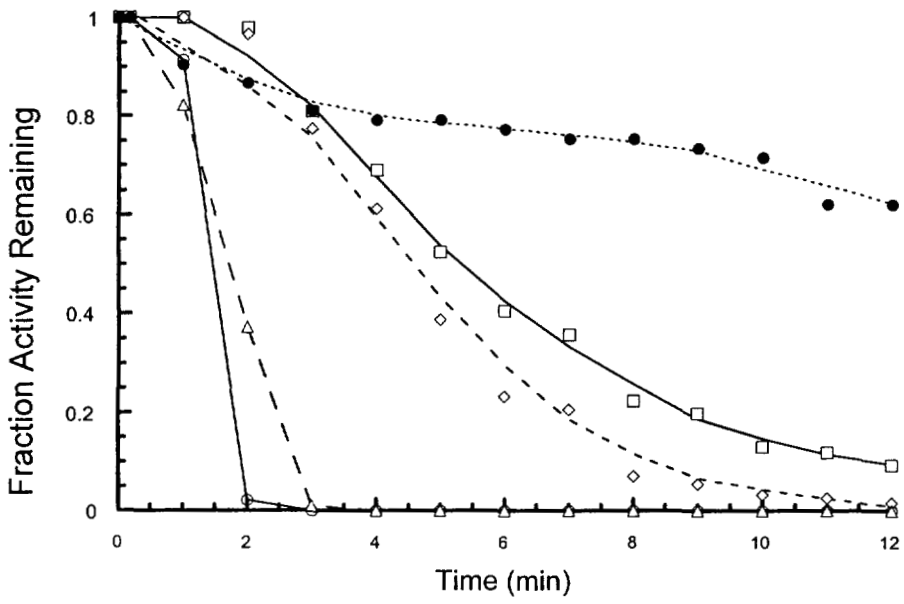

Figure 3.5 Effect of Cd^{2+} on the thermal inactivation of MnP. MnP (10 $\mu g \cdot mL^{-1}$) in 50 mM malonate, pH 4.5, was incubated alone (○) or in the presence of 1 mM $CaCl_2$ (Δ), 1 mM $MnSO_4$ (□) or 1 mM $CdSO_4$ (◇), or 0.5 mM $MnSO_4$ + 0.5 mM $CdSO_4$ (●) at 55°C for up to 15 min. The ionic strength of all incubations was adjusted to 0.1 M with K_2SO_4. Aliquots of 50 μL were diluted to 1 mL (0.5 $\mu g \cdot mL^{-1}$ MnP) and assays for Mn^{3+}–malonate formation was conducted at 270 nm as described with 100 μM H_2O_2 and 500 μM $MnSO_4$ in 50 mM malonate, pH 4.5, I = 0.1 M K_2SO_4.

Table 3.4

Half-Lives of MnP Incubated at 55°C with Various Metals in 50 mM Potassium Malonate, pH 4.5

Metals added	$t_{1/2}$ (min)
None	1.4
1 mM Ca	1.8
1 mM Cd	4.5
1 mM Mn	5.2
0.5 mM Mn + 0.5 mM Cd	16.0
1 mM Ca	2.1
2 mM Cd	7.3
2 mM Mn	8.4
1 mM Mn + 1 mM Ca	6.4
1 mM Cd + 1 mM Ca	5.2
1 mM Mn + 1 mM Cd	26.4

enzyme incubated with Mn^{2+} and Ca^{2+} or Cd^{2+} with Ca^{2+} were extended only slightly over those of enzyme incubated with Mn^{2+} or Cd^{2+} alone.

3.4 DISCUSSION

The binding of Cd^{2+} to MnP results in a perturbation the heme Soret which is similar to that observed on binding of Mn^{2+} to the enzyme. This suggests that Cd^{2+} is binding at a site close enough to the heme to affect the electronic absorption spectrum of the prosthetic group. X-ray crystallographic analysis indicates that the Mn^{2+}-binding site comprises the carboxylate of three amino acids, Asp179, Glu35, and Glu39, as well as the carboxylate of heme propionate 6 and, through a bridging water, heme propionate 7 [376]. The binding of Mn^{2+} to the heme propionates is probably responsible for the change in the Soret observed when this metal binds to MnP. Consistent with kinetic data indicating competition of Cd^{2+} and Mn^{2+}, binding of Cd^{2+} to MnP produces a similar perturbation in the Soret. These results suggest that the Mn^{2+}-binding site is the most likely site for Cd^{2+}-binding.

Our preliminary spectroscopic results do not, however, exclude alternative or additional sites for Cd^{2+} binding. The preference of group 12 metals such as Cd^{2+} and Hg^{2+} for "soft" ligands such as thiols or imidazole is well known [249]. The Mn^{2+}-binding site in MnP is composed of relatively "hard" carboxylate ligands. However, our steady-state kinetic analyses indicate that Cd^{2+} is an effective, reversible, competitive inhibitor of Mn^{2+} oxidation by MnP. Transient-state kinetics confirm Cd^{2+} inhibition of both MnPI and MnPII reduction by Mn^{2+}. However, Cd^{2+} does not interfere with MnPI formation as shown by both steady-state and transient-state kinetics, suggesting that Cd^{2+} does not bind to other important catalytic residues involved in MnPI formation, such as the distal His.

There is evidence that Cd^{2+} can substitute for Mn^{2+} in other enzymes, such as photosystem II [400] and Mn-dependent protein serine phosphatase [288]. Furthermore, Mn^{2+} and Cd^{2+} can replace other hard metals, such as Mg^{2+}, in the binuclear metal-binding site of D-xylose isomerase [43] and Ca^{2+} in peanut peroxidase [256], phospholipase A [402, 443], and Ca^{2+}-dependent endonuclease [250]. Finally,

there is evidence that Cd^{2+} can effectively compete with Mn^{2+} in Mn^{2+}-specific transport systems [239, 300, 401].

Previous kinetic analyses of binding site mutants show that reduction of enzyme intermediates by phenols are not affected by mutations at the Mn^{2+}-binding site, which drastically reduce Mn^{2+} binding and oxidation [226, 237, 436]. This indicates that phenols bind at sites other than to the Mn^{2+}-binding site. Accordingly, Cd^{2+} does not appear to significantly inhibit the direct oxidation of phenols by MnP in the steady state in the absence of Mn^{2+}, while Cd^{2+} does inhibit the Mn^{3+}-mediated steady-state oxidation of phenols by MnP, indicating specific inhibition of Mn^{3+}-chelate formation.

Cd^{2+} can compete with Mn^{2+} for its binding site on the enzyme, but additional competition between the two metals for chelator presumably also occurs. The contribution of this competition to the observed inhibition cannot be determined from the data presented here. However, considering the excess chelator concentrations used in our experiments, we believe the inhibition observed is primarily due to competition at the Mn^{2+}-binding site. In support of this, the recently solved crystal structure of Cd^{2+}-bound MnP indicates Cd^{2+} binding at the Mn^{2+}-binding site [M. Sundaramoorthy, H. L. Youngs, M. H. Gold & T. L. Poulos, unpublished work]. Cd^{2+} is the only metal studied to date that binds to MnP with an equilibrium dissociation constant similar to that of Mn^{2+}. The K_d for Cd^{2+} is $\approx$10-fold less than those recently determined for MnP–Gd^{3+} and MnP–Ce^{3+} [22]. These trivalent lanthanides have been proposed to mimic Mn^{3+} [22]. We propose that Cd^{2+} is an effective nonoxidizable mimic of Mn^{2+} in MnP.

The results of the transient-state kinetic analyses suggest the inhibition by Cd^{2+} of Mn^{2+} binding to the enzyme intermediates, MnPI and MnPII. Because reduction of MnPI by Mn^{2+} is a second-order process, information on binding and catalysis are combined in the rate constant and cannot be distinguished (Scheme 3.1). In contrast, the reduction of MnPII displays "saturation kinetics," indicating that at high concentrations the formation of the productive ES complex consisting of Mn^{2+}-bound MnPII (Scheme 3.2) can be observed. In this case, binding is so much faster than catalysis that the ES accumulates and the kinetics of binding and catalysis can be

separated into an apparent binding constant, K_d, and apparent first-order catalytic rate constant, k_{3app}. The addition of Cd^{2+} to the reaction (Scheme 3.2) most likely results in a depletion of the functional ES complex via formation of a competing EI complex, resulting in an increase in the apparent K_d for Mn^{2+}, as shown in the Figure 3.4 inset. At Cd^{2+} concentrations exceeding the apparent equilibrium $K_{i,MnPII}$ for Cd^{2+} (≈ 5 μM), the formation of EI may dominate. In this case, the rate of formation of ES probably becomes limiting; thus, ES forms at the same rate or more slowly than it is subsequently converted into product. Such an effect would presumably result in apparent second-order kinetics, where binding and catalysis are again combined into a single rate constant. The linear plots of k_{obs} vs. [S] for reactions containing > 10 μM Cd^{2+} support this probable transition (Figure 3.4).

Kinetic studies also indicate that Cd^{2+} is not a dead-end inhibitor of MnP. The enzyme can presumbably oxidize substrates such as phenols at sites alternative to the Mn^{2+}-binding site while Cd^{2+} is bound at the Mn-binding site. Very slight inhibition reduction of MnPI and MnPII by phenols was observed in the transient state; however, no inhibition of phenol oxidation was apparent under steady-state conditions in the absence of Mn^{2+}. It is possible that interactions of Cd^{2+} with the phenolic substrates occur under transient-state conditions, in which the solutions are much more concentrated. Other substrates previously used in transient-state studies of MnP-intermediate reduction [360] such as halides and ferrocyanide could not be examined because of their precipitation in the presence of Cd^{2+}. Alternatively, changes in protein conformation and/or redox potential on binding of Cd^{2+} were considered. However, we expect that a Cd^{2+}-induced change in the protein redox potential would affect the rate of MnPI formation and should be observable in the steady state. No such effects were observed.

In addition to inhibition of Mn^{2+}-oxidation, Cd^{2+} appears to afford thermal stability to MnP. Almost all of the thermal stability studies of MnP have focused on the role of structural Ca^{2+} ions, particularly the distal Ca^{2+} [379–381]. The addition of exogenous Ca^{2+} to thermally inactivated MnP restores enzyme activity and helps protect the enzyme from thermal denaturation [260, 379, 381]. Mn^{2+} also protected MnP from thermal inactivation. Under the conditions of the previous study, notably

high pH (6.5) and low temperature (37°C), Ca^{2+} and Mn^{2+} afforded the same degree of protection to MnP. It was hypothesized that Mn^{2+} could bind at the Ca^{2+}-binding site, protecting the enzyme in a fashion similar to Ca^{2+} [381]. Howevwe, our results indicate that, when MnP is incubated at high temperature (55°C) and the optimal pH (4.5), Ca^{2+} and Mn^{2+} differ markedly in their ability to stabilize the enzyme (Table 3.4). It is likely that, under these conditions, Ca^{2+} and Mn^{2+} protect the enzyme by different mechanisms. Rather than binding to the Ca^{2+}-binding site, Mn^{2+} and Cd^{2+} may stabilize the heme through its propionate ligands at the Mn^{2+}-binding site and may therefore stabilize the enzyme by anchoring the heme to the protein.

The combination of Mn^{2+} and Cd^{2+} dramatically increased the half-life of the enzyme by 10-fold over that of the enzyme in the absence of Mn^{2+} and Cd^{2+} and 3–4-fold over an equivalent concentration of either metal alone, suggesting a possible additional interaction. The preliminary X-ray crystal structure of Cd-MnP indicates that, in addition to binding of Cd^{2+} at the Mn^{2+}-binding site, MnP apparently binds Cd^{2+} at the C-terminus in the crystal [M. Sundaramoorthy, H. L. Youngs, M. H. Gold & T. L. Poulos, unpublished work]. However, the site itself appears to be quite weak, affording only two amino acid ligands to the metal. The existence of a second low-affinity metal-binding site on MnP is supported by previous potentiometric studies [260]. Metal ligation at the C-terminus could offer additional stabilization of the enzyme by tethering the C-terminal tail to the body of the protein. However, no metal has been observed at this site in previous crystal structure of Mn–MnP [376, 377], and it is unclear whether this apparent binding site in the crystal structure occurs in solution. Crystals used for X-ray analysis were formed in cacodylate buffer at pH 6.5 [376, 377] rather than under conditions optimal for activity (oxalate or malonate buffer at pH 4.5).

Metal binding in solution under conditions optimal for activity was studied by atomic absorption analysis. When MnP was incubated with Mn^{2+} alone, 1 equiv. of the metal was bound to the enzyme, in accordance with our original X-ray-crystallography study [376]. Unlike the crystal structure of Cd–MnP, incubation of MnP in malonate solution at pH 4.5 with Cd^{2+} alone resulted in only 1 equiv. Cd^{2+} bound to the enzyme. It is probable that the crystal structure is not indicative of the

solution state of the enzyme and that Cd^{2+} preferentially binds to the Mn^{2+}-binding site in solution under conditions optimal for activity. However, we cannot rule out partial occupation of both sites with our current data.

In contrast, when MnP was incubated with a mixture of half Mn^{2+} and half Cd^{2+}, atomic absorption results suggest that the enzyme binds 1 equiv. of each metal. Binding of this second metal equivalent is most likely responsible for the additional thermal stabiity of enzyme incubated with the Mn^{2+}/Cd^{2+} mixture vs. either metal alone. Differences in the occupancy of each site under different conditions may indicate subtle changes in geometry and binding preferences of the different sites for each metal. For example, binding of Mn^{2+} to the Mn^{2+}-binding site may facilitate binding of Cd^{2+} to the C-terminal site, whereas binding of Cd^{2+} to the Mn^{2+}-binding site does not. Further experiments will be necessary to interpret the apparent additional interaction when MnP is incubated with both metals.

In conclusion, Cd^{2+} is a reversible competitive inhibitor of Mn^{2+} in MnP. It does not inhibit substrates other than Mn^{2+}, such as H_2O_2 and phenols, indicating specific interaction at the Mn-binding site. We also find that binding of Mn^{2+} or Cd^{2+} to the Mn-binding site affords considerable thermal stability to MnP. At low pH, this stabilization exceeds that offered by the binding of exogenous Ca^{2+} to the Ca^{2+}-binding sites. Finally, binding and kinetic studies indicate that Cd^{2+} is the only metal studied to date that binds to MnP with an affinity similar to Mn^{2+} and may therefore be a nonoxidizable mimic of Mn^{2+} which could be useful for further probing this unique Mn^{2+}-binding site.

CHAPTER 4

THERMAL STABILIZATION OF MANGANESE PEROXIDASES FROM *PHANEROCHAETE CHRYSOSPORIUM* AND *DICHOMITUS SQUALENS*: ROLE OF THE MANGANESE BINDING SITE AND A PUTATIVE C-TERMINAL METAL BINDING SITE

4.1 INTRODUCTION

Over the last thirty years, heme peroxidases have been applied to a wide range of basic research and industrial problems. Recent applications range from the release of caged molecules by peroxidases [348] to use of the enzymes in innovative sensitive diagnostic and biosensing assays [154, 193, 201]. Horseradish peroxidase isozymes (HRP) are the most extensively used peroxidases because they exhibit broad substrate specificity, are easy to isolate, and somewhat resistant to alkaline inactivation [101, 385].

Extracellular fungal peroxidases such as lignin peroxidase (LiP) and manganese peroxidase (MnP) offer potential in biomaterial manufacture and detoxification of recalcitrant pollutants. These enzymes are of particular interest for several reasons: (1) they have higher redox potentials than HRP [25, 209, 269]; (2) they are more active and stable in acidic environments ($\sim$pH 3–4) than other peroxidases [1, 60, 68, 276]; (3) they contain no tyrosine residues which are prone to oxidation and intra- and intermolecular crosslinking in other peroxidases [4, 11, 14, 97, 139, 169, 293, 313, 445]; and (4) although they can directly oxidize a wide variety of phenols, they can also nonspecifically oxidize substrates via oxidative intermediates [26, 109, 160, 165, 166, 178, 424]. The veratryl alcohol cation radical is produced by LiP [132, 156, 214, 216, 217]. Chelated Mn^{3+} is generated by MnP [2, 135, 425]. Both are powerful oxidants, small and stable enough to diffuse away

from the protein to oxidize terminal substrates, including large polymers such as lignin [32, 65, 73, 83, 120, 148, 162, 167, 228].

In spite of these advantages, the use of MnP and LiP in biotechnological applications is somewhat limited by their sensitivity to thermal and alkaline inactivation [283, 380]. Although LiP has a higher redox potential than MnP, it is also less stable [24, 60]. An overlay of the two enzymes (Figure 4.1) shows that they share very similar structures [71, 105, 376], although MnP has a longer C-terminal tail than LiP and a Mn-binding site at the γ-edge of the heme [71, 105, 376].

The biophysical properties of an enzyme constrain the environmental conditions in which it may be applied. Therefore, rational approaches to extending enzyme serviceability require a thorough understanding of the enzyme active site(s) and the structural components necessary to maintaining active site integrity.

Heme peroxidases are excellent subjects for structure/function analysis. The enzyme activity is easily determined by use of a variety of chromogenic substrates, usually dyes or phenolic compounds, and the spectral properties of the heme provide a sensitive probe of the proteins inner core. In the present study, residual activity, the heme absorption, and the circular dichroism spectra are used to monitor the effect of exogenous metals on the thermal stability of MnP.

Since the publication of the X-ray crystal structure of manganese peroxidase isozyme 1 from *Phanerochaete chrysosporium* (PcMnP1) in 1994 [376], several components have been shown to increase the thermal stability of the enzyme. These include: N-linked and O-linked sugar moieties [144, 284], the conserved heme pocket residue, Phe190 [21, 225], and the two structural calcium atoms [376, 380, 381].

The effects of Ca^{2+} on thermal stability in MnP and LiP have been studied extensively. Loss of Ca^{2+} upon thermal inactivation and the ability of calcium to prevent thermal inactivation in MnP and LiP have been demonstrated [128, 283, 319, 379–381]. Mutation of the distal Ca-binding ligand, Asp47, causes loss of the distal Ca^{2+} and inactivation of the enzyme, presumably through ligation of the distal histidine to the heme iron. A similar event is believed to occur during alkaline inactivation [see Chapter 2].

A

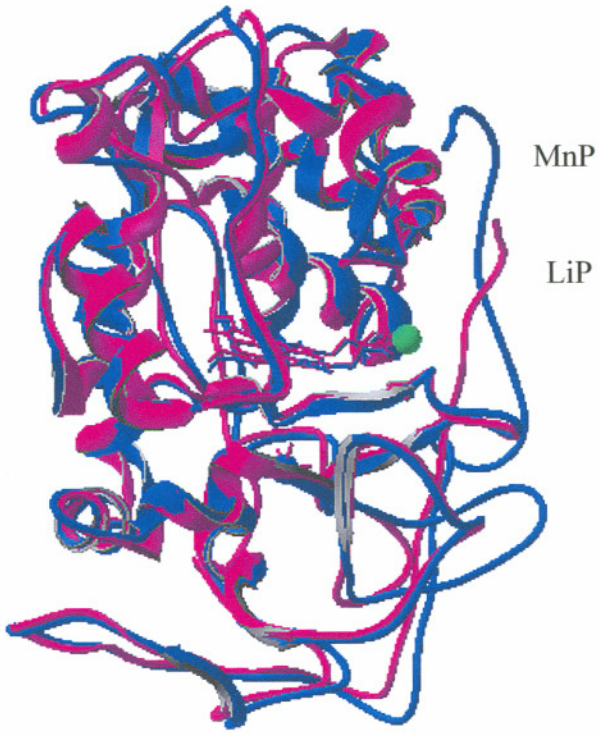

B

Enzyme	C-terminal amino acid sequence
PcLiPH8	S V A R I P P H K A-COOH
PcMnP1	S L I A H C P D G S M S C P G V Q F N G P A-COOH
DsMnP2	T L I P H C S N G S M N C T T V Q F D G P A T N F D G D D S-COOH

Figure 4.1 (**A**) Overlay of the X-ray crystal structures of Mn peroxidase [376] and lignin peroxidase isozyme H8 [309] from *P. chrysosporium* generated from coordinates in the Brookhaven data bank in Swiss PDB Viewer. The C-termini and Mn binding site are indicated. (**B**) Amino acid sequence alignment of the C-termini of these enzymes and Mn peroxidase from *D. squalens* [245].

Emphasis on the role of Ca^{2+} in thermal stabilization of Mn peroxidase is logical. The Ca-binding sites are directly connected via H-bonding networks and through the backbone to the catalytic residues His46 and His173, distal and proximal to the heme [376]. Thus, loss of one or both calciums has significant impact on the heme environment, coordination, and activity [see Chapter 2]. Such effects following alkaline inactivation are explored in Chapter 2. The structural calcium sites do, therefore, provide protection from thermal and alkaline inactivation.

Certainly, studies on the addition of *exogenous* Ca^{2+} to the enzyme are of importance for *in vitro* application; however, they are of little physiological importance. First, the concentration of manganese in wood is in the mM range, 10- to 100-fold higher than that of calcium [441]. Second, all the studies to date have been conducted at pH 6.5, rather than at the enzyme's optimal pH of 4.5 [136, 380, 381]. This is significant as the enzyme exhibits comparatively little activity at pH 6.5. At neutral pH, reduction of compound II is significantly impaired and turnover is disrupted [227]. Also, as shown in Chapter 2, the Ca-binding sites are partially unavailable for binding exogenous metal at neutral pH. Thus, although Ca^{2+} does stabilize the enzyme, the work in Chapter 2 clearly shows that the addition of Mn^{2+} at pH 4.5 stabilizes the enzyme to a far greater extent. Furthermore, the only exception is in the specialized case of the Mn-binding site variants, indicating that stabilization occurs at the Mn-binding site, rather than the Ca-binding sites.

In a previous study, Mn^{2+} was also shown to protect the enzyme from thermal inactivation but this effect was dismissed as binding of Mn^{2+} to the structural calcium binding sites [379]. This assertion is disproved by studies of the alkaline transition in MnP [Chapter 2] that indicate Mn^{2+} does not bind to the Ca-binding sites in MnP under normal physiological conditions (acidic pH). Thus, a physiologically important role for occupation of the Mn-binding site by manganese in thermal stabilization of the enzyme is indicated.

Cd^{2+} also binds at the Mn-binding site and protects MnP from thermal inactivation to a degree similar to that of Mn^{2+} [Chapter 3]. In addition, Cd^{2+} apparently also binds to a site at the C-terminus of the protein in the X-ray crystal structure at pH 6.0 [Chapter 3]. The effect of Cd^{2+} on thermal stability may indicate

a role for the C-terminus in protein stability. MnP sequences have longer C-terminal peptides than other class II peroxidases [144]. Recently, two *mnp* genes from *Dichomitus squalens* (DsMnP) were cloned and sequenced that have extended C-terminal regions. The predicted proteins share 69% overall sequence identity with MnP isozyme 1 from *P. chrysosporium* (PcMnP). The C-terminal regions in the DsMnPs are eight to twelve amino acids longer, compared to PcMnP sequences, and contain several polar and acidic amino acid residues [245] (Figure 4.1).

Although the role of the calcium in thermal inactivation of MnP has been studied extensively, the roles of the Mn-binding site and C-terminus in the thermal stability of MnP remain unexplored. In this chapter, the effects of exogenous metals on the residual activities, heme Soret absorptions, and secondary structures of various MnP proteins are examined. Analysis of the wild-type PcMnP indicates that, at low pH, addition of exogenous Mn^{2+} stabilizes the protein to a greater extent than Ca^{2+}. Analyses of the Mn-binding site variants, D179N and E39D, indicate that the stabilization is due to interactions at the Mn-binding site. A putative C-terminal binding site variant, D84N, is also examined. The data indicate that this secondary site also contributes to thermal stability, although to a lesser extent than either the Mn-binding or Ca-binding sites. Finally, a recombinant MnP from *D. squalens* (rDsMnP) is examined. This protein, containing an extended C-terminus, exhibits kinetics similar to PcMnP, but is much more stable to thermal inactivation. The melting temperature of rDsMnP is almost 50°C higher than that of the PcMnP and the protein is 20 times more stable at 55°C.

4.2 MATERIALS AND METHODS

4.2.1 Organisms

P. chrysosporium wild-type strain, OGC101, and prototrophic transformants expressing the D179N PcMnP construct pAGM6 [237], the D179N-E35Q PcMnP construct pAGM9 [226], the D84N PcMnP construct [D. Li, unpublished], the E39D PcMnP construct [Chapter 5], and the rDsMnP construct pUDGM2 [246] were maintained as described previously [5].

4.2.2 Purification of Proteins

Wild-type MnP from *P. chrysosporium* was purified as previously described from shaking cultures grown in HCLN medium [136, Chapter 3]. The D179N, D179N-E35Q, E39D, and D84N PcMnP variants were purified from shaking cultures grown in HCHN medium as previously described [237, 360]. The rDsMnP protein was expressed and isolated by Dongmei Li, as described previously [246].

4.2.3 Spectroscopic Procedures and Enzyme Assays

Enzyme absorption spectra were determined using a Shimadzu UV-260 spectrophotometer equipped with a jacketed cell and circulating water bath using a quartz cuvette with a 1-cm light path. Temperatures in the cell were measured directly using a Fluke 51 K/J temperature probe. Thermal stability analyses were conducted as previously described [Chapter 3]. Steady-state kinetic analyses were conducted as described [425] in 50 mM malonate (pH 4.5). MnP activity was determined at room temperature by monitoring the formation of Mn^{3+}-malonate at 270 nm (ϵ_{270} = 11.6 $mM^{-1} \cdot cm^{-1}$) as described previously [136, 425]. Reaction mixtures (1 mL) contained 0.5 μg MnP, 2.5 to 200 μM $MnSO_4$, 5 to 100 μM H_2O_2 in 50 mM sodium malonate (pH 4.5). Purified enzyme had an $R_z > 5$ for the wild-type PcMnP, $R_z > 4.5$ for the D179N PcMnP and $R_z > 4.3$ for the rDsMnP. The enzyme concentration was determined using ϵ_{406} = 129 $mM^{-1} \cdot cm^{-1}$ [423].

4.2.4 Binding and Atomic Absorption Analyses

Enzymes were passed over a Chelex-100 column (25 mL) pre-equilibrated with potassium phosphate (pH 6.0). Solutions used in binding experiments, including 50 mM malonate (pH 4.5) and HPLC-grade water, were also treated with chelex, pH 6.0, to remove metals. Metal (Mn, Fe, Cd) content was determined by atomic absorption spectroscopy using a Varian SpectraAA 20B spectrometer fitted with a graphite furnace as previously described [Chapter 3].

4.2.5 Circular Dichroism

Protein samples (10 μM in 4 mM sodium succinate, pH 4.5) were incubated in a cylindrical, water-jacketed quartz cell (l = 0.1 cm) connected to a Neslab RS-2 circulating water bath with remote sensor. Spectra were recorded using a Jasco J-720 spectropolarimeter. Spectra ranging from 180 to 300 nm were recorded prior to and following temperature changes. Melting curves were determined by following the ellipticity at 230 nm as the cell was heated from 35 to 65°C for the PcMnPs and 35 to 95°C for the DsMnP, at a rate of 30°C $\cdot$ h^{-1}. Plots were smoothed using the Jasco software and T_m determined by a first derivative plot of the smoothed curve. (Values did not differ more than 0.3°C from derivatives of raw data.)

4.2.6 Chemicals

Phenyl sepharose CL-4B, DEAE sepharose CL-6B, sephadex G-100, potassium ferrocyanide, H_2O_2 (30% w/w), and HPLC-grade water were obtained from Sigma-Aldrich. All solutions used in kinetic analyses were prepared using HPLC-grade water. Otherwise, solutions were prepared using water purified by the MilliQ-50 ultrafiltration system (Millipore). Urea solutions were prepared fresh daily. The concentration of H_2O_2 was determined using ϵ_{240} = 43.6 M^{-1} cm^{-1} [280]. Atomic absorption standards for Mn, Fe, and Cd were obtained from Sigma-Aldrich.

4.3 RESULTS AND DISCUSSION

4.3.1 Analysis of Wild-Type Mn Peroxidase

4.3.1.1 Kinetics and metal binding. The steady-state kinetic parameters for the enzymes used in this study are indicated in Table 4.1A. The transient-state kinetic parameters of the wild-type PcMnP and recombinant DsMnP are compared in Table 4.1B. Binding of metal ions to the enzymes was determined by atomic absorption spectroscopy following incubation with 1 mM Mn^{2+}, 1 mM Cd^{2+}, or 0.5 mM of both metals in the presence of malonate at pH 4.5 and subsequent washing with chelex-treated HPLC water (Table 4.2). Wild type PcMnP binds 1.0 equivalent Mn^{2+} and 1.0 equivalent Cd^{2+} per mole protein, when incubated with an excess of

Table 4.1

(A) Steady-State Kinetic Parameters of rDsMnP and PcMnP
(B) Transient-State Kinetic Parameters of rDsMnP and PcMnP

A

Enzyme	k_{cat} (s^{-1})	K_m (μM)		k_{cat}/K_m ($M^{-1}s^{-1}$)	
		Mn^{2+}	H_2O_2	Mn^{2+}	H_2O_2
wtPcMnP[a]	3.0×10^2	6.0×10^1	4.0×10^1	5.0×10^6	7.5×10^6
rDsMnP	1.9×10^2	6.3×10^1	5.6×10^1	2.9×10^6	3.3×10^6
D179N[b]	2.87×10^0	2.0×10^3	1.6×10^0	1.4×10^3	2.9×10^5
E39D[c]	6.5×10^0	1.3×10^3	6.0×10^0	5.0×10^3	1.8×10^6
D84N	3.1×10^2	1.6×10^2	4.0×10^1	5.2×10^6	7.8×10^6

Values for Mn^{2+} were determined using 100 μM H_2O_2. Values for H_2O_2 were determined using 500 μM $MnSO_4$. All reactions contained 50 mM malonate, pH 4.5, and 0.1 $\mu g \cdot mL^{-1}$ enzyme. Mn^{3+}-malonate formation was followed at 270 nm. [a]From ref. 425. [b]From ref. 237. [c]See Chapter 4.

B

Enzyme	Compound I Formation (H_2O_2)	Compound I Reduction (Mn^{2+})	Compound II Reduction (Mn^{2+})		
	k_{1app} (M^{-1} s^{-1})	k_{2app} (M^{-1} s^{-1})	K_D (μM)	k_3 (s^{-1})	k_{3app} (M^{-1} s^{-1})
rDsMnP	3.0×10^6	4.8×10^5	2.4×10^1	2.4×10^2	1.0×10^6
PcMnP	4.3×10^6	1.4×10^5	1.1×10^2	5.6×10^2	5.1×10^6

Kinetic values were determined as described in the text. Solutions contained final concentrations of 1 μM enzyme in 50 mM malonate (ionic strength = 0.1 M K_2SO_4). Compound I formation and compound II reduction were performed at the pH optimum of 4.5, whereas compound I reduction was followed at pH 3.0, due to the extremely fast rate of reduction at pH 4.5.

Table 4.2

Equivalents (per mole protein) of Metal Binding to Various Mn Peroxidases Determined by Atomic Absorption Spectroscopy

	Equivalents of metal per protein					
	wtPcMnP			rDsMnP		
Metal added[a]	Fe	Mn	Cd	Fe	Mn	Cd
None	1.0	0	0	1.0	0	0
Mn^{2+}	1.0	1.0	0	0.9	1.5	0
Cd^{2+}	0.9	0	0.9	1.0	0	0.7
$Mn^{2+}+Cd^{2+}$	1.0	1.0	0.9	1.0	1.0	0.9

	Equivalents of metal per protein					
	D179N			D84N		
Metal added[a]	Fe	Mn	Cd	Fe	Mn	Cd
None	1.0	0	0	1.0	0	0
Mn^{2+}	1.0	0	0	1.0	1.0	0
Cd^{2+}	0.9	0	0	1.0	0	1.0
$Mn^{2+}+Cd^{2+}$	1.0	0	0	1.0	0.3	1.0

Solutions contained 1 μM enzyme in 50 mM malonate, pH 4.5. Exogenous metal was added to a final concentration of 1 mM $MnSO_4$, 1 mM $CdSO_4$, or 0.5 mM $MnSO_4$ + 0.5 mM $CdSO_4$ and incubated for >20 min on ice. The enzyme was then concentrated in a centricon (Amicon) and washed with Chelex-treated, MilliQ-purified deionized H_2O.

either metal ion alone. Surprisingly, the enzyme binds one equivalent each Mn^{2+} and Cd^{2+} when incubated with both metals. The amount of iron, 1.0 equivalent per mole protein is unchanged by incubation with exogenous metals.

4.3.1.2 Residual activity kinetics and heme absorption. The purified enzyme was evaluated for thermal stability in the presence of exogenous metal. Half-lives were calculated from semi-log plots of the fraction activity remaining (residual activity) over time (Table 4.3). Denaturation of the protein, upon heating (49°C) or upon incubation in 4 M urea (37°C), was followed by measuring the decrease in the heme Soret absorbance at 406 nm. Denaturation constants (k_{den}) and half-lives ($t_{1/2}$) (Table 4.4) were determined from the slope of first-order plots (Figure 4.2) according to the relationship:

$$\ln|A_t - A_\infty| = -k_{den}t + \ln|A_0 - A_\infty| \qquad \text{(Equation 4.1)}$$

where A_0, A_∞, and A_t are the initial and final absorptions and the absorption at time t, respectively.

The kinetics of inactivation measured by residual activity at pH 4.5 and 55°C are biphasic with an initial slow phase and secondary fast phase; whereas the loss of Soret absorption (pH 4.5, 49°C) is monophasic. This is in contrast to previous studies conducted at pH 6.5 and 37°C and higher where residual activity studies showed biphasic inactivation kinetics with a rapid initial phase and a slow secondary phase [380]. In that study, the authors also measured the Soret and tenuously correlated the change in absorbance to the second, slow phase of inactivation. Because the inactivation was largely reversible under the conditions of that study and upon the addition of calcium, the authors attributed the change in Soret to formation of a bis-histidyl heme complex with a lower extinction coefficient. However, under the conditions of this study, only the initial inactivation (slow phase) is reversible by lowering temperature. The initial phase was accompanied by an increase in the A_{360}, indicative of a bis-histidyl heme, a complex whose formation was shown to be reversible in Chapter 2. The enzyme appears to be irreversibly inactivated during the secondary phase [data not shown]. A likely mechanism for this is loss of the heme from the protein. The decrease in the Soret absorption A_{406} is consistent with this hypothesis.

Table 4.3

Half-Lives (in minutes) of rDsMnP and PcMnP
in the Presence of Various Metals Determined from Semi-Log Plots
of the Fraction Activity Remaining Versus Time

	Half-lives (in minutes)				
	55°C				65°C
Metal Added	wtPcMnP	E39D	D84N	rDsMnP	rDsMnP
none	1.4	1.4	1.8	22	2.0
1 mM Mn^{2+}	5.2	1.8	4.0	210	3.1
1 mM Zn^{2+}	1.4	n.m.	n.m.	100	2.5
1 mM Cd^{2+}	4.5	2.8	4.5	100	6.0
0.5 mM Mn^{2+} + 0.5 mM Cd^{2+}	16	2.8	6.0	205	12

Activity was measured as the formation of Mn^{3+}-malonate at 270 nm. Incubation mixtures contained 10 $\mu g \cdot mL^{-1}$ enzyme in 50 mM malonate, pH 4.5, plus the various metals. Reaction mixtures contained a final concentration of 0.5 $\mu g \cdot mL^{-1}$ enzyme in 50 mM malonate with 1 mM $MnSO_4$ and 0.1 mM H_2O_2. The ionic strength of solutions was adjusted to 0.1 M with K_2SO_4. n.m. indicates not measured.

Table 4.4

Kinetics of Heme Soret (A_{406}) Absorbance Loss during Denaturation of MnP by Heat and Urea

		Heat (49°C)		4M Urea (37°C)	
Enzyme	Metal added[a]	$t_{1/2}$ (min)	k_{den} (s^{-1})	$t_{1/2}$ (min)	k_{den} (s^{-1})
wtPcMnP	none	2.0	5.4×10^{-3}	15.5	7.3×10^{-4}
	Ca	6.6	1.0×10^{-3}	22.8	5.8×10^{-4}
	Mn	13	0.9×10^{-3}	28.6	4.3×10^{-4}
rPcMnP	none	2.6	4.3×10^{-3}	11.9	9.7×10^{-4}
	Ca	6.8	1.6×10^{-3}	12.7	9.1×10^{-4}
	Mn	10	1.1×10^{-3}	14.8	7.8×10^{-4}
D179N	none	1.9	5.7×10^{-3}	15.8	7.3×10^{-4}
	Ca	6.1	1.9×10^{-3}	29.2	9.1×10^{-4}
	Mn	1.8	6.3×10^{-3}	21.1	7.8×10^{-4}
D84N	none	2.0	5.9×10^{-3}	15.0	7.7×10^{-4}
	Ca	6.3	1.8×10^{-3}	25.2	4.6×10^{-4}
	Mn	9.2	1.3×10^{-3}	28.5	4.1×10^{-4}

Solutions contained 1.5 μM protein in 20 mM malonate, pH 4.5. Exogenous $CaCl_2$ or $MnSO_4$ was added to a final concentration of 1 mM. The ionic strength of all solutions was adjusted to 0.1 M with K_2SO_4.

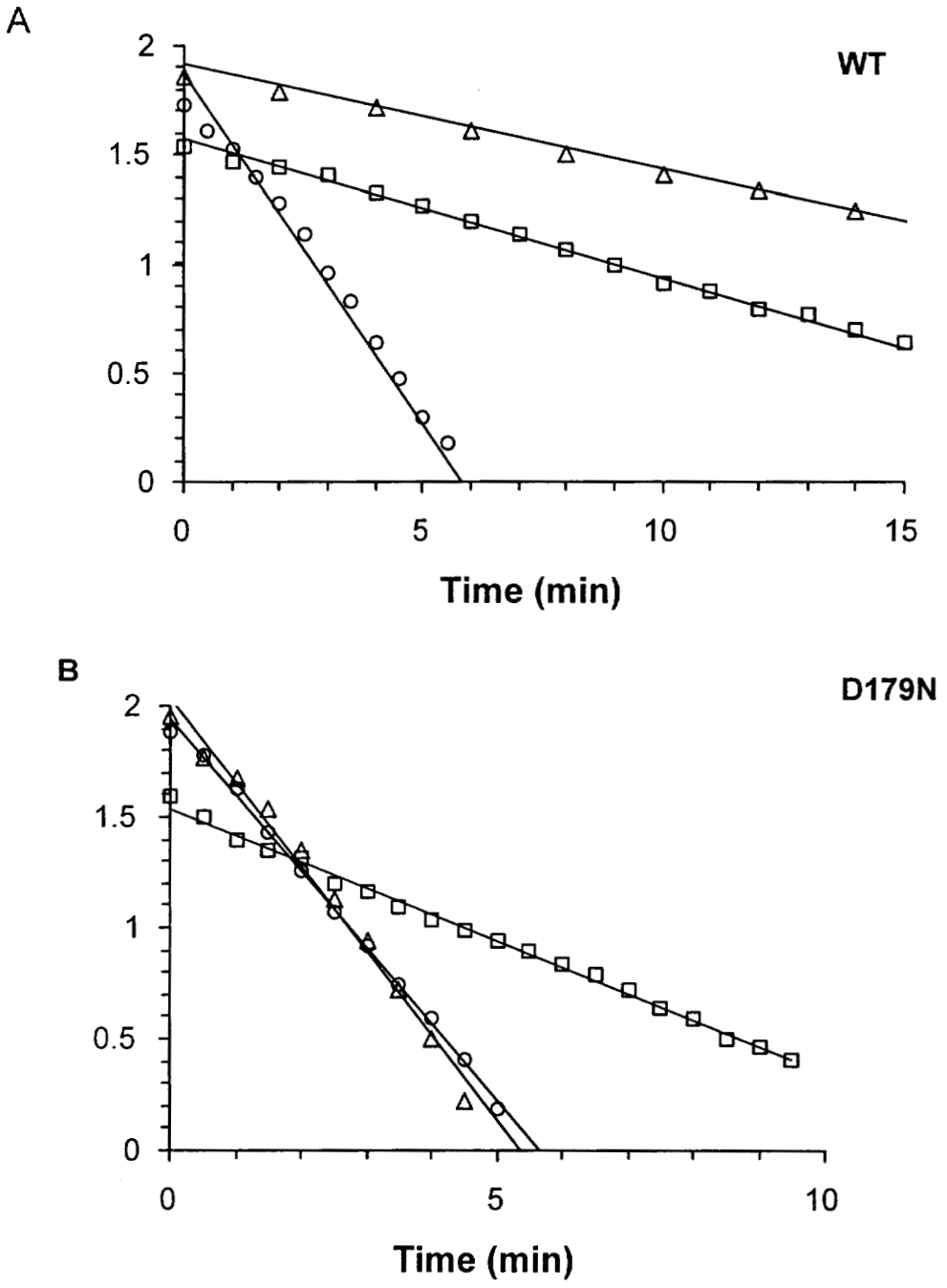

Figure 4.2 Decrease in the heme Soret absorbance (A_{406}) upon heating the wild-type Mn peroxidase (**A**) and D179N variant MnP (**B**) in the absence of exogenous metal (○), 1 mM $CaCl_2$ (□), or 1 mM $MnSO_4$ (Δ). Solutions contained 1.5 μM enzyme in 20 mM malonate, pH 4.5. The ionic strength of all solutions was adjusted to 0.1 M with K_2SO_4.

The presence of Mn^{2+} prolongs the initial reversible phase during thermal inactivation, possibly by preventing the secondary phase loss of heme. Since Mn^{2+} is not effective at recovering the enzyme from the bis-histidyl form [see Chapter 2] and provides no protection from alkaline inactivation, it is unlikely to be affecting heme anchoring via histidyl coordination the heme. However, Mn^{2+} binds to the two heme propionates at the Mn-binding site and could provide additional anchoring by occupying the site [376].

The Arrhenius energy of activation (E_a) for denaturation in the absence of metal ions is $\sim 328\ kJ \cdot mol^{-1}$. The E_a increases to $\sim 331\ kJ \cdot mol^{-1}$ in the presence of 1 mM $CaCl_2$ and $\sim 333\ kJ \cdot mol^{-1}$ in the presence of 1 mM $MnSO_4$, corresponding to 2-fold and 8-fold increases in the rate constant for inactivation (Table 4.4). These values are in close correlation with the previously reported E_a of $335\ kJ \cdot mol^{-1}$ for wild-type MnP most likely containing bound Mn^{2+} [225]. The change in the heme Soret in the presence of $CdSO_4$ could not be measured due to an increase in absorbance upon denaturation. The stability of the enzymes in the presence of 4 M urea at 37°C is improved only marginally by the addition of exogenous metal ions (Figure 4.3). Whether this is due to a difference in the stabilization by the metals to thermal versus chemical denaturation or simply due to an interaction between the metals and urea is not discernable from the data. Experiments with other chemical denaturants such as SDS or guanidinium chloride might be useful in exploring this phenomenon.

4.3.1.3 Circular dichroism measurements. Half-lives of thermal denaturation were determined by circular dichroism measurements. Melting curves were generated by slowly heating the proteins ($0.5°C \cdot min^{-1}$) and following changes in circular dichroism at 230 nm. Melting temperatures (T_m) were determined from the first derivative replots. In most cases, the first-derivative plots indicate two transitions, an initial minor transition, indicating a small perturbation in the secondary structure, and a second major transition, indicating melting of the protein. The minor transition is small or unmeasurable in many of the samples, but more pronounced in samples containing cadmium and, to a lesser degree, calcium. The temperatures for the transitions are listed in Table 4.5 and overlays of the first-derivative plots indicating

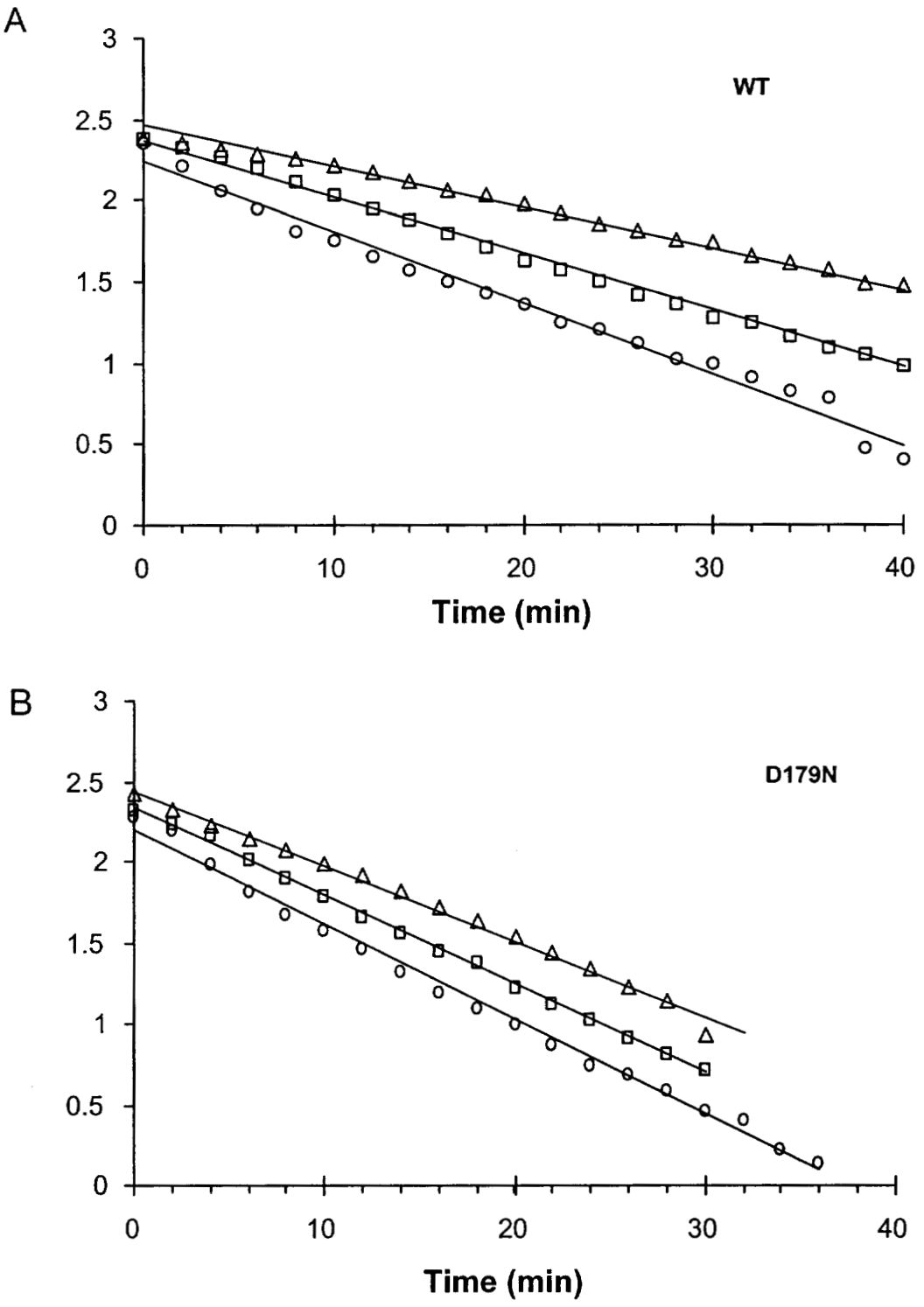

Figure 4.3 Decrease in the heme Soret absorbance (A_{406}) of the wild-type Mn peroxidase (**A**) and D179N variant MnP (**B**) in 4 M urea at 37°C. Solutions contained 1.5 μM enzyme in 20 mM malonate, pH 4.5, and the absence of exogenous metal (○), 1 mM $CaCl_2$ (□), or 1 mM $MnSO_4$ (Δ). The ionic strength of all solutions was adjusted to 0.1 M with K_2SO_4.

Table 4.5

Melting Temperatures Determined by Circular Dichroism Spectroscopy

Primary Transitions [Melting Temperatures (°C)]

Enzyme	none	Ca	Δ	Mn	Δ	Cd	Δ	Mn+Cd	Δ
wild-type	54.0	57.4	3.4	58.1	4.1	58.5	4.5	59.0	5.0
D179N	51.3	54.0	2.7	53.4	2.1	55.8	4.5	54.3	3.0
D179N-E35Q	52.2	55.0	2.8	54.1	1.9	56.1	3.9	54.1	1.9
D84N	52.7	54.1	1.4	55.0	2.3	53.9	1.2	55.6	2.9

Secondary Transitions (°C)

Enzyme	none	Ca	Mn	Cd	Mn + Cd
wild-type	44.6	46.7	47.2	47.6	48.0
D179N	45.8	48.7	48.5	49.4	47.7
D179N-E35Q	45.7	50.0	49.3	49.2	49.7
D84N	n.d.[b]	41.1	n.d.	43.9	47.5

Δ indicates the difference between the protein T_m with metal added minus the T_m without exogenous metal added. Solutions contained 10 μM enzyme in 4 mM sodium succinate, pH 4.5. 500 μM (final concentration) of $CaCl_2$, $MnSO_4$, $CdSO_4$, or 250 μM each $MnSO_4$ + $CdSO_4$ were added to samples as indicated. The ionic strength of all solutions was adjusted to 0.1 M with K_2SO_4. n.d. indicates not discernable.

the melting points are shown in Figure 4.4. The T_m values increased upon incubation with metal. Addition of Ca^{2+} increased the T_m by 3.4°C, Mn^{2+} and Cd^{2+} individually increased the T_m by 4.1 and 4.5°C, respectively, and Mn + Cd increased the T_m by 5°C. Typically, though slightly less in degree, the minor transitions follow the trend of the major transitions. Melting of all samples was irreversible. Samples containing Mn^{2+} showed some residual spectrum (< 10 % intensity) following melting [data not shown]; whereas in the absence of Mn, samples precipitated.

The results of the CD measurements correlate with those of the residual activity and heme Soret measurements. In all the analyses, exogenous Mn^{2+} stabilized the protein to a greater extent than Ca^{2+} at pH 4.5, indicating an important role in the Mn-binding site in stabilization of the enzyme in addition to catalysis. That is not to say the Mn-binding site offers more stability to the protein structure than the Ca sites, simple that the availability of these sites to exogenous metal at pH 4.5 is different. Whereas, the Mn-binding site is on the surface of the protein and freely accessible to solvent, the Ca-binding sites are buried within the distal and proximal domains, with somewhat limited solvent accessibility. The data presented in this chapter support the pH studies presented in Chapter 2, indicating that at low pH, accessibility of the Ca-binding sites is limited.

4.3.2 The Mn Binding Variants

The Mn-binding site is comprised of three amino acids (Glu35, Glu39, and Asp179), and the two heme propionates, one as a direct ligand and the other via H-bonding to a water ligand (Figure 4.9) [376]. Additionally, the residue Arg177 forms an H-bond with Glu35, orienting the side chain for binding [360]. Residues Glu35 and Glu39 are on helix B, which contains the distal catalytic H46 residue. Residues Arg177 and Asp179 are on a loop that contains the catalytic proximal His173 between helices F and G [376].

Through these interactions and direct coordination at the propionates, binding of Mn to the enzyme most likely stabilizes the heme retarding loss of the cofactor. The E_a for Soret loss in the wtPcMnP in present study is about ~ 328 kJ·mol^{-1} in the absence of metal and increases to ~ 333 kJ·mol^{-1} in the presence of 1 mM Mn.

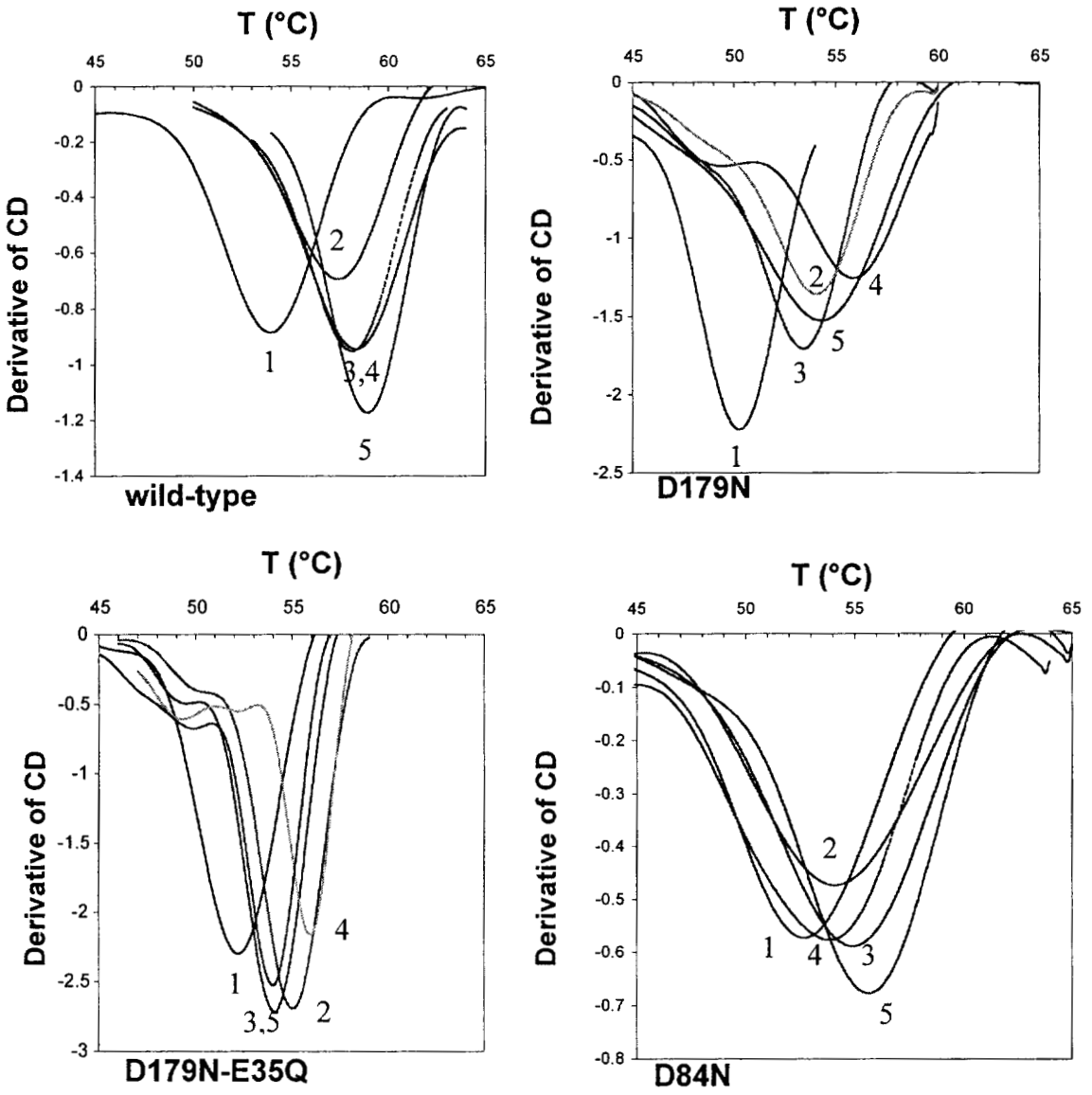

Figure 4.4 First derivative plots of the circular dichroism melting curves of various PcMnPs in the absence of exogenous metals (1), and the presence of 500 μM final concentration $CaCl_2$ (2), $MnSO_4$ (3), or $CdSO_4$ (4) or 250 μM each $MnSO_4$ + $CdSO_4$ (5). All solutions contained 10 μM enzyme in 4 mM succinate, pH 4.5, ionic strength adjusted to 0.1 M with K_2SO_4.

Addition of exogenous Mn to the wild-type enzyme delays loss of the Soret absorption, increasing the half-life approximately 6-fold, whereas no effect is observed in the Mn-binding variant, D179N (Table 4.4). Accordingly, atomic absorption analysis (Table 4.2) indicates that this variant does not bind Mn, consistent with kinetic data (Table 4.1).

The effect of Mn on preserving the more global, secondary structure of the enzyme is less clear. Melting curves for the D179N PcMnP variant are shown in Figure 4.5. Melting temperatures (T_m) were determined from the first derivative replots (Figure 4.4C and D). The addition of Mn^{2+} increases the melting temperature, measured by circular dichroism by $\sim 4°C$ in the wild-type enzyme. However, Mn also increased the T_m in the Mn-binding variants by $\sim 2°C$ (Table 4.4), similar to the effect of Ca. As the solutions were adjusted for ionic strength, this is most likely not a simple salt effect. The explanation for this phenomenon may lie at the C-terminus.

4.3.3 D84N and the Putative C-Terminal Binding Site

X-ray crystal structure analysis also indicates that, in addition to binding at the Mn-binding site, Cd^{2+} also binds at the C-terminus of MnP, coordinating to the terminal carboxyl moiety of Ala357 and to the residues Asp84 and, through a bridging water ligand, to Asn76 (Figure 4.6). The site is exposed to the solvent and could accommodate a Mn ion with a bound chelator such as oxalate or malonate, which are produced by the fungus and required for enzyme activity [see Chapter 6]. Although Mn is not observed to bind at this site in the crystal structures, potentiometric binding analysis indicates a second Mn-binding site, with a 12-fold lower affinity for Mn^{2+} at pH 4.5 may exist somewhere in the protein [260]. Therefore, it is possible that Mn binds weakly to this site under physiological conditions (pH 4.5), but not under the conditions for crystal formation (pH 6.5 in cacodylate buffer). This is in accordance with the potentiometric studies, which indicated that the affinity of the second site for Mn^{2+} decreased as the pH was increased from 4 to 6.5 [260]. Cd^{2+}, however, may exhibit a higher affinity for this site than Mn^{2+}, due to its ability to adopt a wider range of ligation geometries.

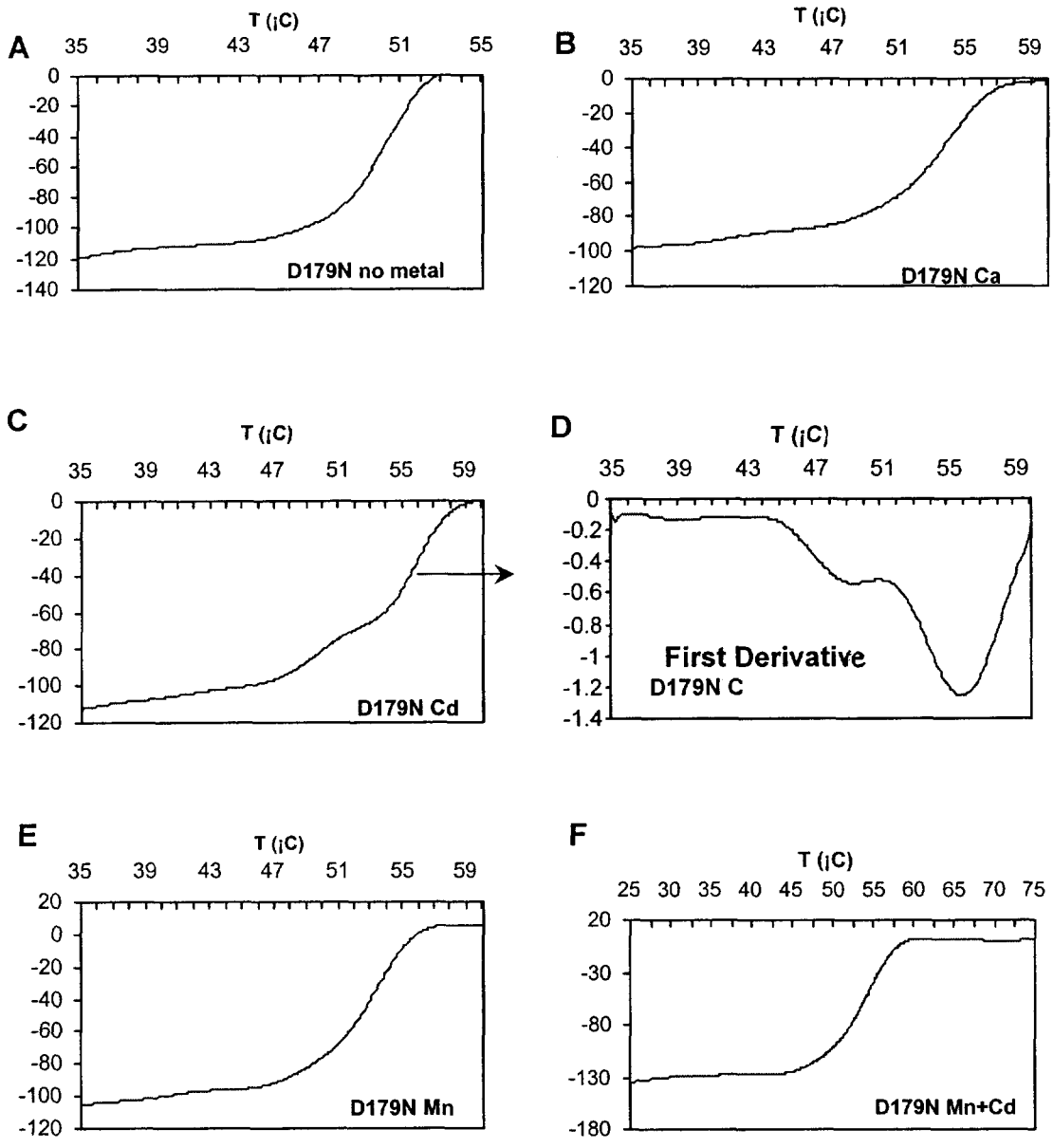

Figure 4.5 Circular dichroism melting curves of the Mn-binding variant D179N. Solutions contained 10 μM enzyme in 4 mM sodium succinate, pH 4.5. 500 μM (final concentration) $CaCl_2$, $MnSO_4$, $CdSO_4$ or 250 μM each $MnSO_4$ + $CdSO_4$ were added. Ionic strength was adjusted to 0.1 M with K_2SO_4.

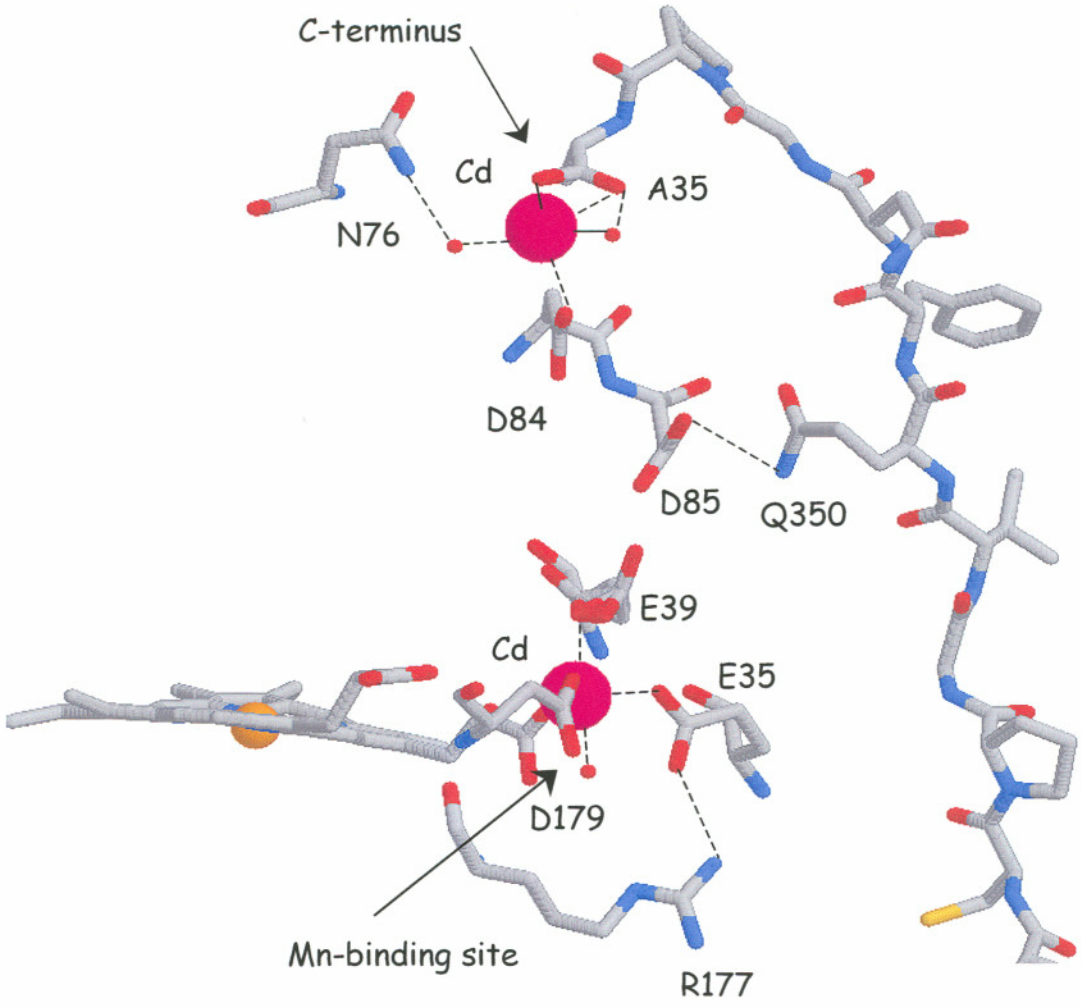

Figure 4.6 The Mn-binding site and C-terminus of cadmium bound wild-type Mn peroxidase from *P. chrysoporium*. Possible interaction between the putative C-terminal metal binding site and the Mn-binding site is illustrated through the residues D84, D85, and E39 [378].

Although atomic absorption analysis indicates that only one equivalent of Cd^{2+} binds per mole protein, partial occupation of both sites may also occur with this metal. Some interaction between this site and the Mn binding site is suggested by the synergistic effect of Cd^{2+} and Mn^{2+} binding to wild-type MnP.

To examine the possible role for this site in thermal stability, a D84N variant was examined. Analysis of the D84N variant supports a role for this residue in Mn-binding and thermal stability. The steady-state parameters for the D84N variant indicate a slight ($\sim$2.5-fold) increase in the K_m for Mn^{2+} compared to the wtPcMnP, although the other constants appear to be unchanged by the mutation (Table 4.1A). When wtPcMnP is incubated with both Mn and Cd a synergistic effect is observed. The thermal inactivation of the protein is dramatically decreased (Table 4.3), the melting temperature is further increased (though marginally), and one equivalent of each metal bound per mole protein are observed (Table 4.2). This synergistic effect is abolished in the D84N variant. The $t_{1/2}$ for inactivation in the presence of Mn and Cd together is only slightly higher than each metal alone, in contrast to the wild-type (Table 4.3), the melting temperature is not increased over either metal (Table 4.5), and upon incubation with both metals 1 equivalent of Cd binds but only 0.3 equivalents of Mn bind per mole protein. Finally, the kinetic parameters appear to indicate some slight effect on Mn binding (Table 4.1). Although the k_{cat} is similar to wild-type, the K_m is almost 3-fold higher in the D84N variant. This could indicate that the Mn-binding site is affected. However, the Mn binding ligands are still intact, such that once bound, Mn oxidation may occur at a normal rate, similar to variants at Arg177 [360].

Interaction between the putative C-terminal site and the Mn-binding site could occur via hydrogen bonding networks. Asp84 is adjacent to Asp85, which forms an H-bond to Gln350 on the C-terminal tail (Figure 4.6). Structural overlays of the Cd-bound MnP and the D179N variant indicate slight movement in the tail away from the body of the protein (0.5 to 1.0 Å) in the D179N structure, which lacks metal at the Mn-binding site [not shown]. Additionally, the Glu39 residue appears to adopt multiple conformations and may be protonated [378], possibly influenced by electrostatic interactions with Asp85 (Figure 4.6). It is possible, therefore, that

binding of metal to one site influences the geometry at the other site. Finally, although this second site may stabilize the protein by "tethering" the C-terminal tail, it apparently plays a lesser role in thermal stability than the Mn-binding site.

4.3.4 Mn Peroxidase from *Dichomitus squalens*

Dichomitus squalens belongs to a group of white-rot fungi that produce Mn peroxidase and laccase but do not appear to produce lignin peroxidase. These fungi are capable of mineralizing lignin, despite the lack of lignin peroxidase. Therefore, the Mn peroxidases and laccases produced by these fungi are of interest.

The amino acid sequences of the Mn peroxidases of *D. squalens* (DsMnP) and *P. chrysosporium* (PcMnP) are similar (~69% identical, 80% similar). As expected, the absorption spectrum of the recombinant DsMnP is very similar to spectra of the wild-type MnPs from *D. squalens* and *P. chrysosporium*, respectively [299, 423, data not shown]. Preliminary studies indicated that the MnP isozymes from *D. squalens* are kinetically similar to the MnP produced by *P. chrysosporium* [299]. The steady-state kinetic parameters, K_m, k_{cat} and $k_{cat} \cdot K_m^{-1}$, for rDsMnP, and several variant PcMnPs are compared to the kinetic parameters for wild-type PcMnP in Table 4.1. The K_m and k_{cat} values for rDsMnP are only slightly lower (<2-fold) than those of PcMnP and the catalytic efficiencies ($k_{cat} \cdot K_m^{-1}$) of the two enzymes are similar (Table 4.1A). The transient-state parameters for rDsMnP compound I formation and the reduction of rDsMnP compounds I and II by Mn^{2+} are not significantly different from those of PcMnP (Table 4.1B).

Also similar to PcMnP, rDsMnP is inhibited by Cd^{2+} and Sm^{3+} but not divalent metals such as Ca^{2+}, Mg^{2+}, or Zn^{2+} (Figure 4.7). Inhibition constants for Cd^{2+} and Sm^{3+} are ~10 μM and ~250 μM for the rDsMnP, similar to those for PcMnP [see Chapter 3].

Previous binding experiments with the wild-type DsMnP indicate that the native enzyme has a K_D for Mn ~30 μM [299], similar to that of PcMnP [425]. These data, along with the kinetically determined K_D for Mn^{2+} by compound II (~24 μM), indicate that the Mn-binding sites of PcMnP and DsMnP are very similar. Both

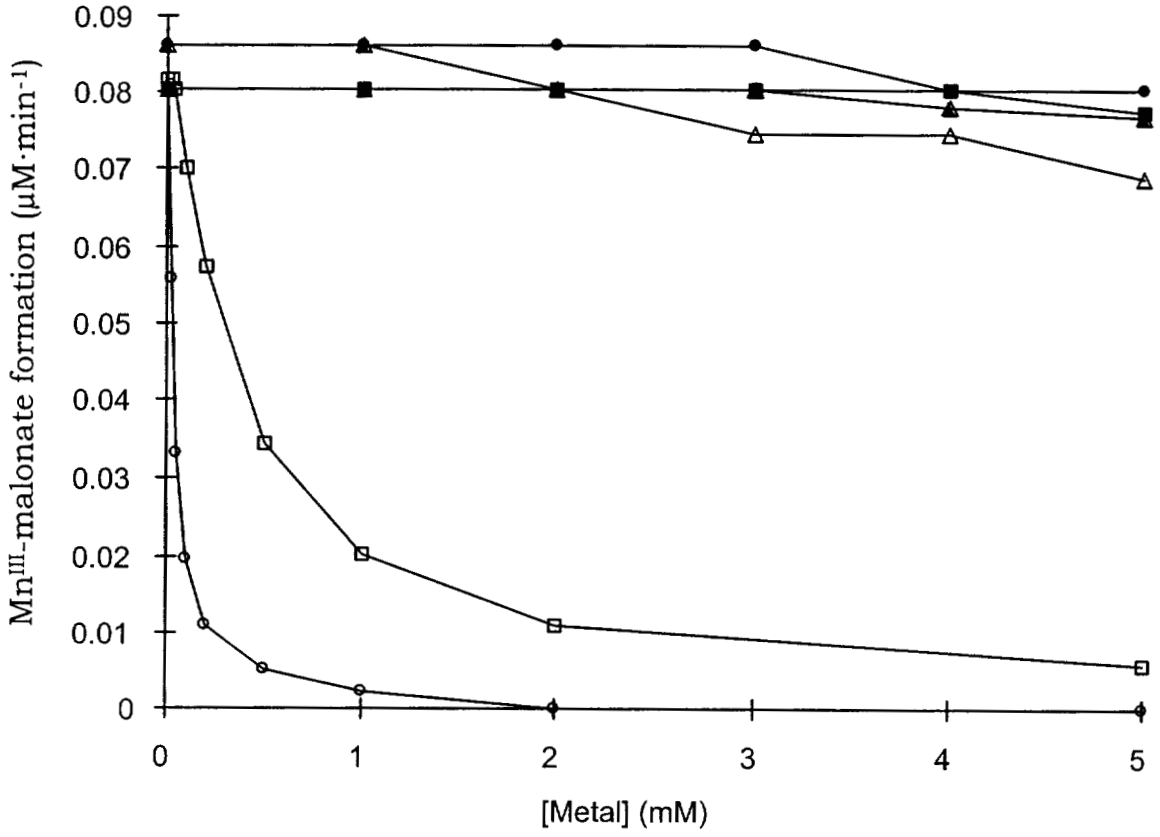

Figure 4.7 Inhibition of rDsMnP-catalyzed Mn^{3+}-malonate formation by various metals. $CaCl_2$ (Δ), $CdSO_4$ (○), $CoCl_2$ (•), $MgSO_4$ (■), $SmCl_3$ (□), or $ZnSO_4$ (▲). Reaction mixtures contained 0.5 $\mu g \cdot mL^{-1}$ enzyme with 500 μM $MnSO_4$ and 100 μM H_2O_2 in 50 mM malonate, pH 4.5.

sites bind Mn^{2+} with similar affinities, as indicated by the dissociation and inhibition constants, and in similar fashions, as evidenced by the catalytic constants which indicate similar ligand-induced reductions in the Mn redox potential, a phenomenon highly dependent on the coordination geometry and local environment of the metal binding site. Finally, both sites show similar specificities for other cations.

While the overall sequences and Mn-binding sites of the two proteins appear to be very similar, there must be subtle differences in the structures of these two proteins. The melting temperature of the rDsMnP may be nearly 50°C higher than that of PcMnP ($\sim$100 vs. $\sim$50°C). Upon heating to 95°C, rDsMnP retains substantial secondary structure (Figure 4.8). A melting point could not be obtained for this protein using the water bath. The protein only begins to lose secondary structure around 90°C. Typically, the transition occurs over a 10 to 15°C range, indicating that the melting point for this protein is mostly likely 95°C < T_m < 05°C.

The increase in stability is also evident in the residual activity analysis. The linear log plots for rDsMnP at 55°C and 65°C are shown in Figure 4.9. In the absence of exogenous metal, MnP from *Dichomitus* is significantly ($\sim$16-fold) more stable than PcMnP at 55°C (Table 4.3). The log plot for this sample indicates only one phase for inactivation, unlike all the other samples which indicate at least two phases, an initial slow phase and a secondary fast phase, similar to PcMnP (Figure 4.9B).

The stabilization of rDsMnP at 55°C appears to involve extension of the initial, reversible phase of inactivation. Whereas, this phase is not observed in the sample without exogenous metal added, it extends to $\sim$100 min in the sample with Cd^{2+}. Addition of Zn^{2+} or Mn^{2+} extends this phase to $\sim$200 min (Figure 4.9). Unlike PcMnP, addition of Cd^{2+} to DsMnP stabilizes the protein to a lesser extent than Mn^{2+} (Table 4.3). Surprisingly, addition of Zn^{2+} to rDsMnP extends the half-time 5-fold over the enzyme in the absence of metal at 55°C. No such stabilization is observed in PcMnP, indicating possible differences in the affinity of metal binding sites of the surface of these two proteins.

The thermal stability of rDsMnP was also analyzed in the presence of various metals at 65°C. This temperature was chosen because the half-lives are comparable

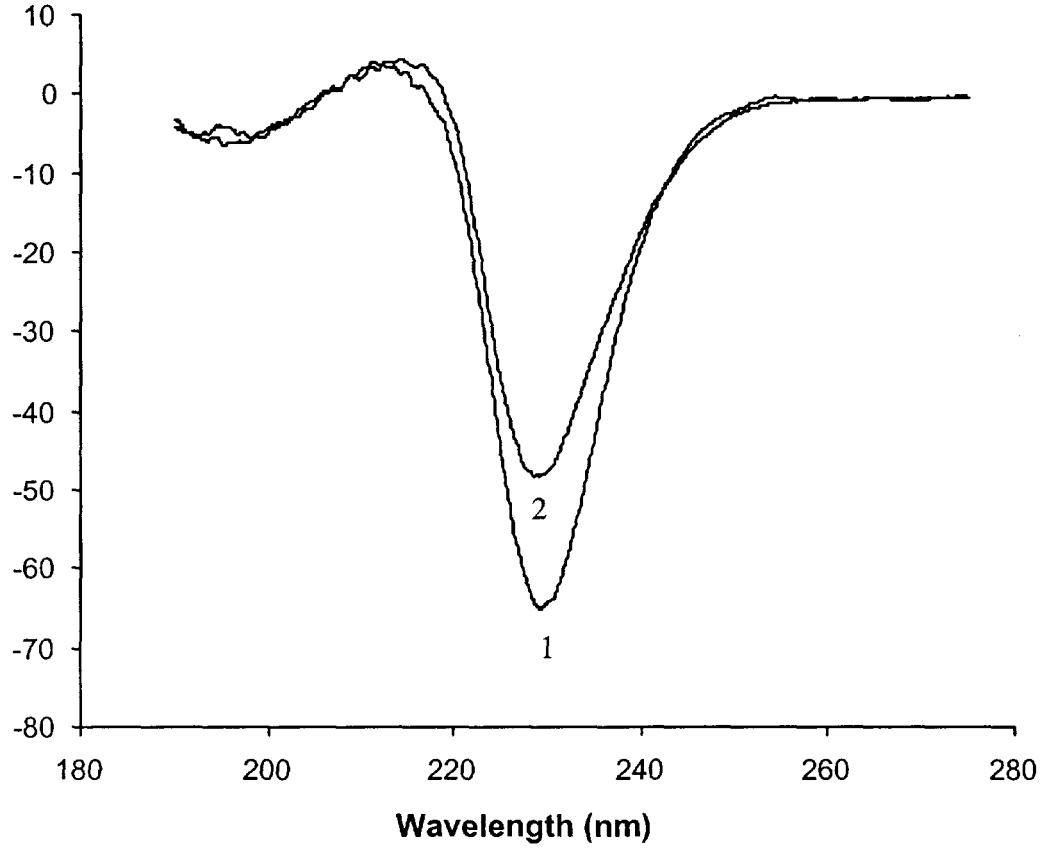

Figure 4.8 Circular dichroism spectra of rDsMnP before heating (spectrum 1) and after heating to 95°C at 50°C/h (spectrum 2). Solutions contained 10 μM chelex-treated enzyme in 4 mM sodium succinate, pH 4.5, ionic strength adjusted to 0.1 M K_2SO_4. No exogenous metal was added.

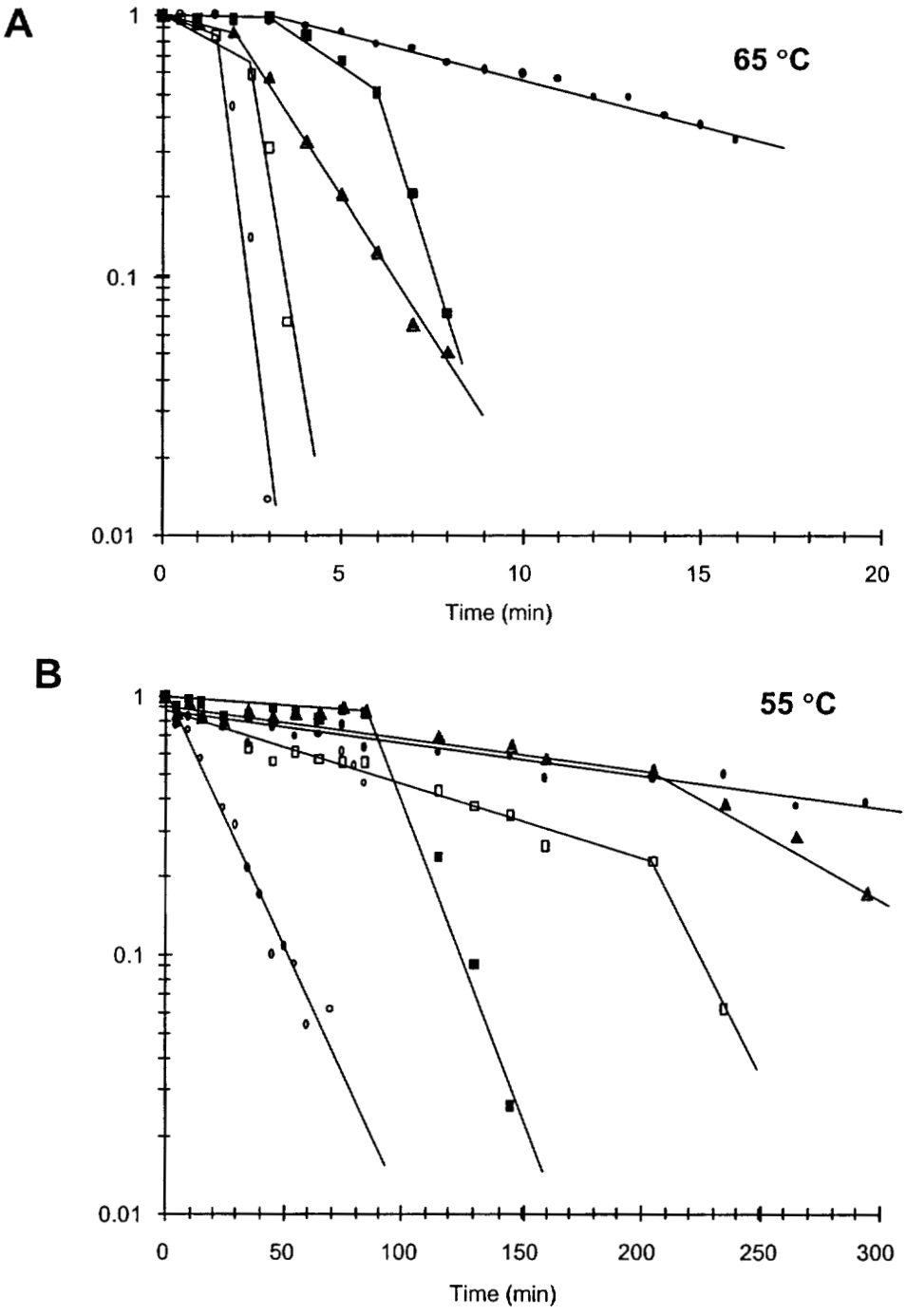

Figure 4.9 Thermal stability of rDsMnP at 65°C (**A**) and 55°C (**B**) in the absence of exogenous metal (○), or in the presence of 1 mM each $ZnCl_2$ (□), $MnSO_4$ (▲), $CdSO_4$ (■), or 0.5 mM $MnSO_4$ + $CdSO_4$ (•). Incubation mixtures contained 10 $\mu g \cdot mL^{-1}$ enzyme in 50 mM malonate, pH 4.5, plus the various metals. Reaction mixtures contained 50 μL incubation mixture in 50 mM malonate, pH 4.5, with 1 mM $MnSO_4$ and 100 μM H_2O_2.

to those of PcMnP at 55°C. Interestingly, the enzyme shows slightly different trends for the various metals at this temperature (Table 4.3). All curves show biphasic inactivation, except the Cd^{2+} sample which exhibits three distinct phases (Figure 4.9). The initial phase is extended from 2 min in the sample without exogenous metal to ~3 min in the samples containing Zn^{2+} and Mn^{2+} and 4 min in the Cd^{2+} and the Mn^{2+} + Cd^{2+} samples. The slope of the second phase varies considerably among the samples and appears to be responsible for the extension in half-lives at this temperature.

The reason for the remarkable difference in the stability of rDsMnP compared to PcMnP is not clear. The amino acid sequences share 80% homology and no differences, outside of the C-terminal regions, are immediately obvious. The stability of rDsMnP is similar to that of soybean peroxidase SBP (T_m ~95°C). Although no crystal structure is yet available for SBP, another plant enzyme, peanut peroxidase (PNP) has been found to contain an additional disulfide bond that anchors the distal calcium [345]. rDsMnP does not appear to contain additional disulfides [245]. The carbohydrate content of DsMnP is not known. The predicted protein mass is 45 kDa, whereas the mass determined by SDS-PAGE is ~48 kD [246]. Glycosylation enhances the thermal stability of PcMnP [284]. Therefore, the role of sugar moieties in providing additional stabilization cannot be ruled out.

The predicted C-terminus of the *mnp2* gene of *Dichomitus* contains several acidic and polar amino acids, which could serve as metal ligands [245] (Figure 4.1). Atomic absorption experiments indicate that the native rDsMnP may bind more than one equivalent of Mn, in contrast to PcMnP (Table 4.2). Similarly, the half-life of the enzyme is extended 10-fold for rDsMnP versus only 4-fold for PcMnP by exogenously added Mn^{2+} at 55°C (Table 4.3). In contrast, both native PcMnP and rDsMnP appear to bind one equivalent of Cd^{2+} and the half-lives of both enzymes are extended ~4-fold by the addition of exogenous Cd^{2+} at 55°C. Finally, whereas Zn^{2+} does not affect the half-life of PcMnP, Zn^{2+} extends the half-life of rDsMnP 5-fold, similar to the effect of Cd^{2+} on DsMnP. Cd^{2+} inhibits rDsMnP with a K_i similar to that of PcMnP. Zn^{2+} does not inhibit either enzyme and, therefore, most likely stabilizes rDsMnP through interaction at a site other than the Mn-binding site.

Whereas the combination of Mn^{2+} and Cd^{2+} extend the half-life of PcMP an additional 5-fold over either metal alone, the combination in rDsMnP does not extend the half-life at all over that for Mn^{2+} alone at 55°C. It is possible, therefore, that in PcMnP, Mn^{2+} and Cd^{2+} each bind preferentially to the Mn-binding site and the combination of both metals is required to fill the alternate metal binding site which conveys additional thermal stability to the enzyme. A mechanism where Cd^{2+} competes only for the Mn-binding site, Zn^{2+} occupies only an alternate site, and Mn^{2+} can occupy both sites can be envisioned.

4.4 CONCLUSIONS

The thermal denaturation of MnP at pH 4.5, the optimum pH, can be described at a two-step process as follows:

$$N \leftrightarrow I \rightarrow U \qquad \text{(Equation 4.2)}$$

where the native enzyme (N) is reversibly converted to the inactive bis-histidyl form (I) and irreversibly converted to the denatured enzyme (U). Irreversible denaturation occurs at around 54°C in the wild-type enzyme. The addition of exogenous metal to Mn peroxidase stabilizes the enzyme to environmental changes. At low pH, near the enzyme's optimum, exogenous Mn^{2+} provides greater protection from inactivation than Ca^{2+} and increases the melting temperature by $\sim$5°C. Whereas the Ca-binding sites apparently provide protection from thermal and alkaline inactivation, the Mn-binding site appears to function primarily in thermal stabilization of the protein, primarily by prolonging the initial, reversible inactivation stage. A putative C-terminal site may also stabilize the protein to thermal denaturation and cooperativity between this site and the Mn-binding site is postulated. A thermostable MnP homolog in *D. squalens* exhibits similar denaturation kinetic patterns, though at a melting temperature near 100°C. The structural basis for the remarkable stability of this enzyme remains unknown.

CHAPTER 5

THE ROLE OF Glu39 IN Mn^{2+} BINDING AND OXIDATION BY MANGANESE PEROXIDASE FROM *PHANEROCHAETE CHRYSOPORIUM*[*]

5.1 INTRODUCTION

White-rot fungi are uniquely adapted to degrade lignin, a phenylpropanoid cell wall polymer which provides rigidity, cell adhesion, and microbial resistance to vascular plants [111, 339]. The best-studied white-rot basidiomycete, *Phanerochaete chrysosporium*, preferentially degrades lignin under nutrient nitrogen limiting (idiophasic) conditions by secreting enzymes, including lignin and manganese peroxidases (LiP and MnP), and a hydrogen peroxide generating system [58a, 143, 159a, 222]. Though specific components of the lignin degrading machinery of various white-rot fungi vary, manganese peroxidases (MnPs) have been detected in virtually all lignin-degrading fungi so far studied [168, 182, 286, 295, 299].

P. chrysosporium produces a series of extracellular MnP isozymes under ligninolytic conditions [136, 221]. MnP isozyme 1 has been purified and studied extensively by a variety of biochemical and biophysical methods [135, 136, 143, 144, 426]. Spectroscopic, DNA sequence comparison, and X-ray crystallographic studies indicate that the heme environment of MnP is similar to that of other plant and fungal peroxidases [105, 139, 235, 301, 313, 345, 376]. Kinetic and spectroscopic characterization of the native and oxidized intermediates of MnP indicates that the

---

[*] Originally published in this or similar form in *Biochemistry* and used with permission of the American Chemical Society.

Youngs, H. L., Sollewijn Gelpke, M. D., Li, D., Sundaramoorthy, M., and Gold, M. H. (2001) The role of Glu39 in Mn^{II} binding and oxidation by manganese peroxidase from *Phanerochaete chrysosporium*. *Biochemistry* **40**, 2243–2250.

catalytic cycle is similar to that of other plant and fungal peroxidases [423, 426]. However, MnP is unique among peroxidases in utilizing Mn^{2+} as its primary reducing substrate [135, 426]. The peroxidatic cycle is as follows:

$$MnP + H_2O_2 \rightarrow MnPI\ (Fe^{IV}{=}O^{\bullet+}) + H_2O$$

$$MnPI + Mn^{2+} \rightarrow MnPII\ (Fe^{IV}{=}O) + Mn^{3+}$$

$$MnPII + Mn^{2+} + 2H^{+} \rightarrow MnP + H_2O + Mn^{3+}$$

where MnPI contains an oxoferryl porphyrin π cation radical (two-electron-oxidized) and MnPII contains an oxoferryl (one-electron-oxidized) heme. Enzyme-generated Mn^{3+} is stabilized by dicarboxylic organic acid chelators, such as oxalate [227, 231, 426]. The Mn^{3+}–chelator complex is stable enough to diffuse from the enzyme and oxidize terminal phenolic substrates, including lignin [403] and aromatic pollutants [198, 199, 406, 408]. Oxidation of non-phenolic lignin substructures by MnP has been proposed to occur via radical mediators [27, 427].

The Mn^{2+}-binding site of MnP isozyme 1 from *P. chrysosporium* was identified by X-ray crystallographic and initial site-directed mutagenesis studies [226, 237, 376, 377]. The MnP crystal structure indicates that enzyme-bound Mn^{2+} is hexacoordinate with two water ligands and four carboxylate ligands from heme propionate 6 and three amino acid residues: D179, E35, and E39 [376]. Several variant MnPs—D179N, E35Q, E39Q, and D179N–E39Q—were created by exchanging the amino acid carboxylate ligands for their respective amides via site-directed mutagenesis of the *mnp1* gene [226, 237]. The amino acid substitutions were chosen to maintain steric constraints within the site while abolishing Mn^{2+} ligation. Binding and oxidation of Mn^{2+} were greatly reduced in all the variant enzymes. In all other respects, including reactivity toward H_2O_2 and substrates with alternate binding sites, the variant enzymes were similar to the wild type, indicating that the mutations specifically affected Mn^{2+} binding and oxidation rather than the overall structure or function of the enzyme [226, 237]. This was confirmed by X-ray crystallographic analysis of the variants, which clearly showed disruption of the Mn binding site, while other structural features remained unchanged [377].

As a result of these combined studies, D179, E35, and E39 were identified as Mn^{2+} ligands. However, a recent mutagenesis study of these ligands has raised

doubts regarding the importance of E39 in Mn^{2+} binding and oxidation [436]. In that study, site-directed mutagenesis was used to shorten the alkyl side chains of the E35 and E39 ligands by "isochemical" substitution to produce E35D and E39D mutant *mnp* genes. A D179A variant was also made. The proteins were then heterologously expressed in *E. coli*, isolated from inclusion bodies, and reconstituted. The D179A and E35D variants exhibited characteristics similar to the previous single variant MnPs (D179N and E35Q), including increased K_m for Mn^{2+} and decreased k_{cat} values [436]. In striking contrast to previous E39Q variant [226], the E39D variant was claimed to exhibit wild-type characteristics including wild-type kinetics for Mn^{2+} binding and oxidation under both steady-state and transient-state conditions [436]. Those investigators concluded that E39 was "not critically important" to Mn^{2+} binding nor electron transfer from Mn^{2+} to the enzyme. In this chapter, the role of E39 in Mn^{2+} binding and oxidation is reexamined through computer modeling and steady-state and transient-state kinetic analysis of our own homologously expressed E39 variant as well as a new variant, E39A. The flexibility of the Mn^{2+} binding site in MnP is also probed by examining an isochemical triple mutant, D179E-E35D-E39D.

5.2 EXPERIMENTAL PROCEDURES

5.2.1 Organisms

P. chrysosporium wild-type strain OGC101, auxotropic strain OGC107-1 (Ade1), and prototrophic transformants were maintained as described previously [5]. *Escherichia coli* DH5α was used for subcloning plasmids.

5.2.2 Molecular Modeling

Structures were modeled using the Swiss PDB Viewer v3.6b3 (Glaxo-Wellcome). The crystal structure data for wild-type MnP were obtained from the Protein Data Bank file 1mnp [376]. As recommended by the software documentation, ligands and Mn were first manually translated/rotated to avoid steric interactions following introduction of mutation. The structures were then subjected to successive

energy minimization using the GROMOS96 protocol [409]. Structures were then rendered using the POV-Ray for Windows 3.1 g.watcom.win32 rendering engine (Persistence of Vision Development Team).

5.2.3 Construction of Transformation Plasmids

Site-directed mutations were introduced into the pGM1 plasmid [226], which contains 1.1 kb of the *gpd* promoter fused to the coding region of *P. chrysosporium mnp1* at the ATG translation initiation codon, by the PCR-based Quikchange (Stratagene) method. Forward and reverse primers (16–20 bp) containing altered codons were obtained to introduce the mutations for each amino acid. The GAG codon for E39 was changed to GAC (E39D) or GCG (E39A). The GAA codon for E35 was changed to GAC (E35D). The triple variant was constructed by successive rounds of the Quikchange protocol. The E39D construct was used to create an E39D-E35D double mutation. Subsequently, the GAC codon of D179 of this double variant was altered to GAG (D179E) to create the E39D-E35D-D179E triple variant. Following mutagenesis, the plasmids were isolated and sequenced in both directions to confirm the mutations and check for any other sequence alterations. Plasmids were double-digested, and the *Xba*I–*Eco*RI fragments, containing the *gpd* promoter and mutated *mnp1* genes, were subcloned into pOGI18 [5, 7], a *P. chrysosporium* transformation plasmid containing the *Schizophyllum commune ade5* aminoimidazole ribonucleotide synthetase gene as a selectable marker. The entire *mnp1* coding regions of the resulting plasmids were sequenced to again verify the mutations and to ensure no other sequence alterations occurred.

5.2.4 Transformation of *P. chrysosporium*

Protoplasts of the Ade$^-$ strain of OGC107-1 were transformed as described [5, 7, 9, 263], using 1 μg of *Eco*RI-linearized plasmid as the transforming DNA. Protoptrophic transformants were transferred to minimal medium slants to confirm adenine prototrophy and were subsequently assayed for MnP activity using the *o*-anisidine plate assay as described previously [263]. Transformants exhibiting the

highest activity on plates were purified by fruiting as described previously [8], and the progeny were rescreened for MnP activity by the plate assay. The purified transformants exhibiting the highest activity in large shaking cultures were selected for further study.

5.2.5 Production and Purification of Variant MnP Proteins

Selected transformants were maintained on MYV slants and grown in high carbon–high nitrogen (HCHN) liquid medium in stationary culture from conidial inocula as described previously [263]. These stationary cultures were homogenized and used as inocula for shaking cultures containing 1 L of liquid medium in 2-L flasks, and were grown for 3 days at 28°C. The extracellular medium was filtered and concentrated, and the mutant MnP proteins were purified by a combination of Phenyl Sepharose CL-6B hydrophobic interaction, Cibacron blue 3GA dye affinity, and MonoQ anionic exchange chromatographies as described previously [226, 263]. Purified variant enzyme had R_z values ≥ 4 and yields of ~ 2 mg $\cdot$ L^{-1}. The enzyme concentration was determined using $\epsilon_{406} = 129$ mM$^{-1} \cdot$ cm^{-1} [136]. Wild-type enzyme was produced as described previously [see Chapter 3].

5.2.6 Spectroscopic Procedures and Kinetic Analysis

Electronic absorption spectra and steady-state kinetic analyses were performed using a Shimadzu UV-260 spectrophotometer at room temperature. Steady-state Mn^{2+} oxidation was measured as the formation of Mn^{3+}-malonate, followed at 270 nm ($\epsilon_{270} = 11.6$ mM^{-1}) [426]. Apparent K_m and k_{cat} values for Mn^{2+} and H_2O_2 were calculated from Lineweaver-Burke plots. Reaction mixtures contained 0.5 μg $\cdot$ mL^{-1} enzyme, 50 mM malonate, pH 4.5, and various concentrations of $MnSO_4$ and H_2O_2, as indicated. Transient-state kinetic experiments were performed using an Applied PhotoPhysics SX.18MV sequential stopped-flow reaction analyzer at 25.0 $\pm$ 0.2°C as described [360]. Reductions of each intermediate by ferrocyanide were measured individually. Complete formation of enzyme intermediates was confirmed by diode array rapid scanning. All reactions contained 50 mM potassium malonate, pH 4.5, and the ionic strength of all solutions was adjusted to $\mu = 0.1$ M with K_2SO_4. The final

concentration of enzyme was 1 μM, and a minimum 10-fold excess of substrate was used in all reactions to ensure pseudo-first-order reaction kinetics. All kinetic traces displayed single-exponential character from which pseudo-first-order rate constants were calculated.

5.2.7 PCR of Genomic DNA

Mycelia from 3-day-old stationary cultures (HCHN) of the selected E39D transformant were flash-frozen in liquid nitrogen and ground by mortar and pestle. Genomic DNA was extracted as described previously [4, 139]. To ensure selective amplification of recombinant *mnp*, primers in both the *gpd* and *mnp* genes were selected. The 19-bp forward primer in the PCR reaction annealed to the *gpd* promoter, 75 bp 5′ of the *mnp* ATG [263]. The 24-bp reverse primer annealed to the first 13 bp of intron IV and 12 bp of exon III in the *mnp1* gene. The resulting fragment 685-bp fragment was purified using the QIAquick PCR purification kit (Qiagen) and sequenced directly.

5.2.8 Chemicals

All chemicals were reagent grade and obtained from Sigma/Aldrich. Solutions for kinetic analyses were prepared with HPLC-grade water.

5.3 RESULTS

5.3.1 Computer Modeling of Variant Enzymes

Prior to construction, the variant MnPs were modeled using the Swiss PDB-Viewer. Virtual mutations were introduced into the 2.06-Å crystal structure [376]. Figure 5.1A indicates the Mn^{2+}–ligand distances for the wild-type protein. Modeling of the E39D and the E35D-E39D-D179E variants showed various scenarios in repeated energy minimizations, indicating some variability in the software's ability to predict the most stable conformation. Modeling of the E39D variant indicated some conformations with bond lengths similar to the wild type but with altered Mn ligand geometry [data not shown]. If the wild-type Mn geometry was maintained, the

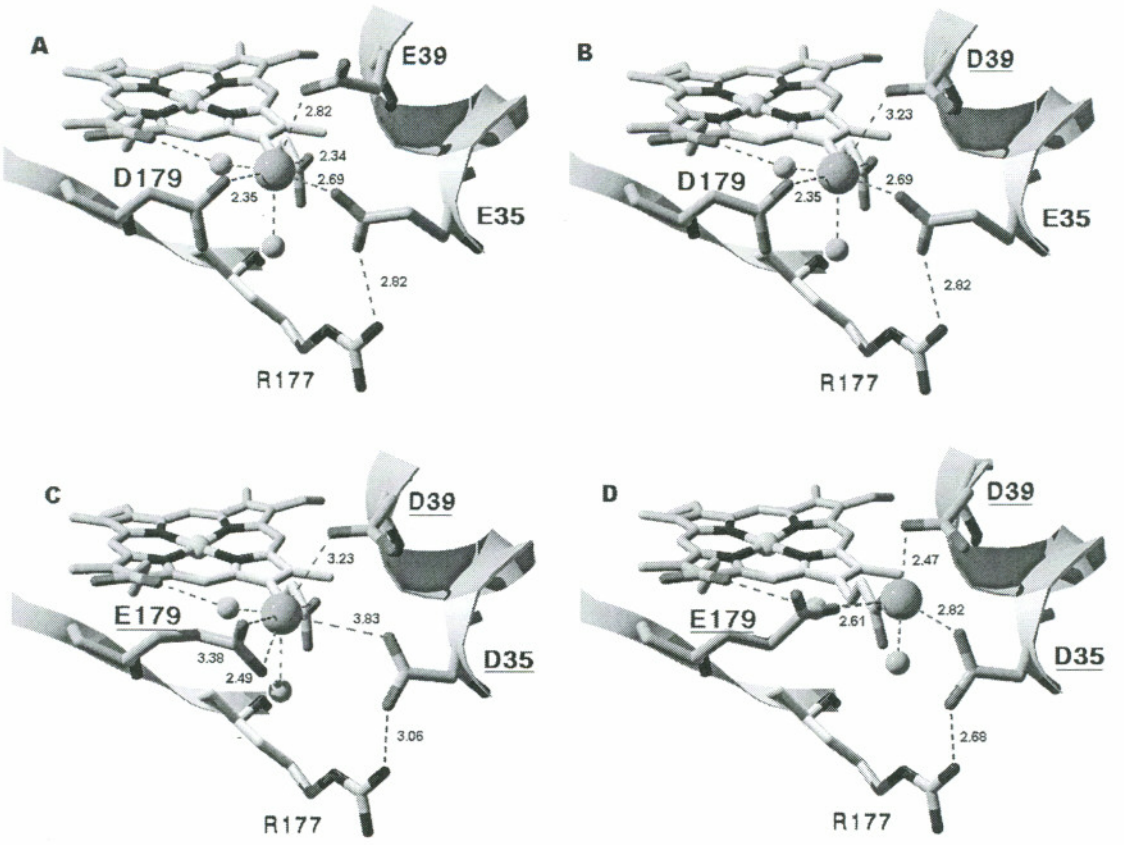

Figure 5.1 (**A**) Mn^{2+} binding site of wild-type manganese peroxidase isozyme 1 from *P. chrysosporium* from X-ray crystal structure data [376]. Mn^{2+} binding sites of the (**B**) E39D single variant and (**C, D**) DDE (E35D–E39D–D179E) triple variant could be modeled with either retention of the wild-type geometry (B, C) or optimization of ligand bond distances (D), but not both. Mutated residues are underlined. Mn–ligand distances are reported in angstroms. Structures were modeled using the Swiss PDB Viewer v3.6b3 and POV-Ray for Windows as described.

models showed an increase in the Mn–residue 39 bond length to 3.23 Å, indicating probable loss of this ligand from the Mn coordination sphere (Figure 5.1B). Similarly, modeling of the E35D-E39D-D179E triple variant with wild-type Mn geometry showed retention of the 179 ligand (with possible bidentate coordination) and loss of the residue 35 and residue 39 ligands (Figure 5.1C). Shorter bond lengths, suggesting retention of all the ligands, could be obtained for the triple variant, but only with an accompanying distortion of the Mn ligation geometry (Figure 5.1D). Modeling of the E35D variant showed a 0.8-Å incrase in the Mn–residue 35 bond distance [data now shown] from 2.6 Å for E35 to 3.4 Å for D35, suggesting that the D35 residue can no longer function effectively as a Mn ligand.

5.3.2 Expression and Purification of the Variant Enzymes

Prior to the fungal transformation, the entire coding regions of the mutant *mnp1* in the pAGM plasmids were sequenced. The only variations in the sequence versus the wild-type *mnp1* gene were the desired mutations. Transformation of the Ade^- strain (OGC107-1) with the *Eco*RI-linearized plasmids resulted in multiple (10–80) transformants. Typically, 20% of the transformants were positive for MnP activity by the *o*-anisidine plate assay, using 5 mM $MnSO_4$ [263]. For each mutant, three transformants exhibiting maximal activity on the plate assay were selected and purified by fruiting [5, 7, 8]. Colonies from single basidiospores were rescreened for MnP activity by the plate assay, and three purified isolates for each mutant were then grown in large HCHN shake cultures for 3 days at 28°C, when endogenous MnP is not expressed [263]. Extracellular medium from the transformants was tested for MnP activity [426], and the transformant exhibiting the highest activity was selected for further study. Enzymes were purified from extracellular medium by successive Phenyl Sepharose, Blue Agarose affinity, and MonoQ anion exchange chromatographies [226, 263]. The yields were comparable to those for previous variants and recombinant wild-type MnP ($\sim 2\ mg \cdot L^{-1}$) [226, 237, 263, 360]. The R_z values of the purified enzymes were >4.

5.3.3 Sequence Analysis of E39D Genomic DNA

Genomic DNA was isolated from 3-day-old stationary cultures of the E39D transformant grown in HCHN medium. PCR amplification of the introduced *gpd–mnp1* construct was performed using a forward primer in the *gpd* promoter and a reverse primer in intron IV and exon III of the *mnp1* coding region. The 685-bp amplified fragment encoded the first 118 amino acids of the MnP1 protein. The fragment was sequenced and the E39D mutation identified. The introduced mutation was the only alteration found in the E39D genomic fragment versus the wild-type *mnp1* gene.

5.3.4 Spectral Analyses

Electronic absorbance maxima of the native and oxidized intermediates for the wild-type and variant MnP proteins were compared [data not shown]. All of the spectra were stable for the duration of several successive scans (up to 30 s) and exhibited only slow auto-oxidation ($k < 1\ s^{-1}$) thereafter, indicating that the enzymes were kinetically active and stable. Spectral maxima for the variant enzymes and their respective intermediates closely matched those of wild-type MnP, indicating no significant alterations in the heme environments of the variant MnPs.

5.3.5 Steady-State Kinetic Analyses

Steady-state parameters for the wild-type and each of the variant enzymes (E39A, E39D, E35D, and DDE) are listed in Table 5.1. Constants for the E35D–E39D double variant were not calculated, since Mn oxidation by the enzyme was barely detectable [data not shown]. Table 5.1 also lists the redetermined values for D179N, E39Q, E35Q variants which were previously constructed [226, 237]. With the exception of the E39D variant, the changes in k_{cat} and K_m values for Mn^{2+} were consistent with previous reports [226, 237, 436].

The E39D variant showed markedly different kinetics from those previously reported for this variant (Table 5.1) [436]. Our variant showed a 50-fold decrease in k_{cat} to 6.5 s^{-1} compared with the wild-type rate of 300 s^{-1} [426] and in contrast to the previous report citing no change in the k_{cat} value associated with this mutation versus

Table 5.1

Steady-State Kinetic Parameters for Wild-Type and Mutant MnPs[a]

	k_{cat} (s^{-1})	K_m Mn^{II} (mM)	K_m H_2O_2 (μM)	k_{cat}/K_m Mn^{II} ($M^{-1}s^{-1}$)	k_{cat}/K_m H_2O_2 ($M^{-1}s^{-1}$)
wtMnP	300	0.060	40	5.0×10^6	7.5×10^6
E39D	6.5	1.3	6.0	5.0×10^3	1.1×10^6
E39D[b]	410	0.036	54	1.1×10^7	7.6×10^6
E39Q	3.5	0.8	3.2	4.4×10^3	1.1×10^6
E39A	0.77	1.9	0.69	4.1×10^2	1.1×10^6
E35D	3.3	2.5	0.43	1.3×10^3	7.7×10^6
E35Q	0.83	3.8	0.5	2.2×10^2	1.7×10^6
D179N	2.87	2.0	1.6	1.4×10^3	1.8×10^6
DDE[c]	1.3	2.5	0.6	5.2×10^2	2.2×10^6

[a] Reactions contained 0.5 μg/mL enzyme in 50 mM malonate (pH 4.5). The ionic strength was adjusted to μ = 0.1 M with K_2SO_4. Parameters for Mn^{2+} were determined using 0.1 M H_2O_2. Parameters for H_2O_2 were determined using 5 mM $MnSO_4$.

[b] From ref. *37*.

[c] DDE = the triple variant E35D–E39D–D179E.

the wild type [436]. The k_{cat} values for the majority of the single ligand variants (D179A, D179N, E39Q, and E35D) decreased 50–100-fold, while several mutants (E39A, E35Q, and DDE) showed 300–400-fold decreases in k_{cat}, in agreement with previous work [226, 237, 436].

Our E39D variant also showed a 20-fold increase in the K_m for Mn^{2+} to approximately 1 mM, in contrast to the previously reported K_m of 36 μM for this same variant [436]. Again, this 20-fold increase in K_m is consistent with the other single ligand variants, which all showed a 15–60-fold increase in the K_m for Mn^{2+}. The resulting catalytic efficiency for Mn^{2+} was decreased 10^3-fold for all of the variants except E39A, E35A, and DDE, for which the efficiency dropped 10^4-fold, again conflicting with the previous report citing no change in efficiency for the E39D variant [436]. None of the variants exhibited changes in the catalytic efficiency for H_2O_2, in agreement with the previous report for E35D and in contrast with previous reports for the E39Q, E35Q, and D179N variants [226, 237].

5.3.6 Formation of MnP Compound I

The rates of compound I formation for wild-type MnP and the E39D, E39A, E35D, and DDE variants were measured in 50 mM malonate at pH 4.5 by following the change in absorption of the enzyme at 397 nm, the isosbestic point between compound I and compound II. Kinetic traces, from which pseudo-first-order rate constants (k_{1obs}) were measured, displayed exponential character. Plots of k_{1obs} versus $[H_2O_2]$ were linear with zero ordinate intercepts, indicating irreversible second-order kinetics [data not shown]. Apparent second-order rate constants for the variant MnPs were similar to the wild type and previously reported values for other binding site variants [226, 237, 436] (Table 5.2).

5.3.7 Reduction of MnP Compound I

Kinetic parameters for the reduction of compound I are listed in Table 5.2. Single-electron reductions of compound I to compound II of the variant enzymes by K_4FeCN_6 and Mn^{2+} were examined in 50 mM malonate, pH 4.5, at 416 nm, the isosbestic point between compound II and native enzyme. The two-electron reduction

Table 5.2

Transient-State Kinetic Parameters:
Apparent Second-Order Rate Constants ($M^{-1}s^{-1}$)
for Formation and Reduction of Compound I[a]

Enzyme	Compound I formation	Compound I reduction		
	H_2O_2	Mn^{II}	Br^-	$K_4Fe(CN)_6$
wild type	$(4.8 \pm 0.1) \times 10^6$	$\sim 3 \times 10^7$	$(2.7 \pm 0.5) \times 10^3$	$(4.8 \pm 0.1) \times 10^5$
E39D	$(4.4 \pm 0.7) \times 10^6$	$(1.3 \pm 0.1) \times 10^6$	$(2.4 \pm 0.1) \times 10^3$	$(4.8 \pm 0.1) \times 10^5$
E35D	$(5.1 \pm 0.1) \times 10^6$	$(4.7 \pm 0.2) \times 10^5$	$(2.4 \pm 0.1) \times 10^3$	$(4.5 \pm 0.1) \times 10^5$
E39A	$(4.9 \pm 0.1) \times 10^6$	$(8.3 \pm 0.2) \times 10^4$	$(1.6 \pm 0.1) \times 10^3$	$(3.6 \pm 0.1) \times 10^5$
DDE[b]	$(5.0 \pm 0.1) \times 10^6$	$(9.0 \pm 0.2) \times 10^4$	$(2.1 \pm 0.3) \times 10^3$	$(4.0 \pm 0.2) \times 10^5$

[a] Reaction mixtures contained 1 μM enzyme and 50 mM malonate (pH 4.5), final concentrations. The ionic strength of all solutions was adjusted to μ = 0.1 M with K_2SO_4. Reactions were conducted under pseudo-first-order conditions, and substrate concentrations were varied as described in the text. Constants were determined from slopes of linear k_{obs} vs. [S] plots. Individual kinetic traces showed exponential character and were fitted to obtain k_{obs}.

[b] DDE = the triple variant E35D–E39D–D179E.

of compound I to native enzyme by Br^- was followed at 406 nm. All kinetic traces used to calculate pseudo-first-order rate constants (k_{2obs}) were exponential in character, and plots of k_{2obs} versus substrate concentration were linear (Figures 5.2 and 5.3). The second-order rate constants for reduction of the variant MnPs by K_4FeCN_6 and Br^- were similar to wild-type MnP. However, second-order rate constants for reduction by Mn^{2+} were significantly lower than wild-type MnP and varied considerably for the different variants. The rate constant for the E39D mutant was ~30-fold lower than that of wild-type MnP and that previously reported for this variant [436]. The rate constant for E35D was 100-fold lower than that of wild-type MnP and 10-fold lower than that previously reported for this variant [436]. The rate constants for both the E39A single variant and the E35D-E39D-D179E triple variant were 1000-fold lower than that of wild-type MnP.

5.3.8 Reduction of MnP Compound II

Reduction of compound II by K_4FeCN_6 (Table 5.3) and Mn^{2+} (Table 5.3) was measured in 50 mM malonate, pH 4.5, at 420 nm. Plots of k_{obs} versus Mn^{2+} concentration exhibited saturation kinetics (Figure 5.4) as have been previously observed for wild-type MnP [226] and the E35D and E39D variants [436]. Dissociation constants, K_D, and first-order rate constants, k_3, were determined as previously described [426] (Table 5.3). The K_D values increased 10–80-fold while the k_{cat} value decreased 40-fold for the E39D variant, 120-fold for E35D, and 1200-fold for E39A, compared with the wild type. The calculated apparent second-order rate constants decreased 10^3–10^4-fold compared with wild-type MnP. Values for the E35D variant are in agreement with those previously reported for this variant, whereas the values for the E39D variant are in sharp contrast to the previous report that this mutation does not affect Mn binding or the rate of compound II reduction by Mn^{2+} [436].

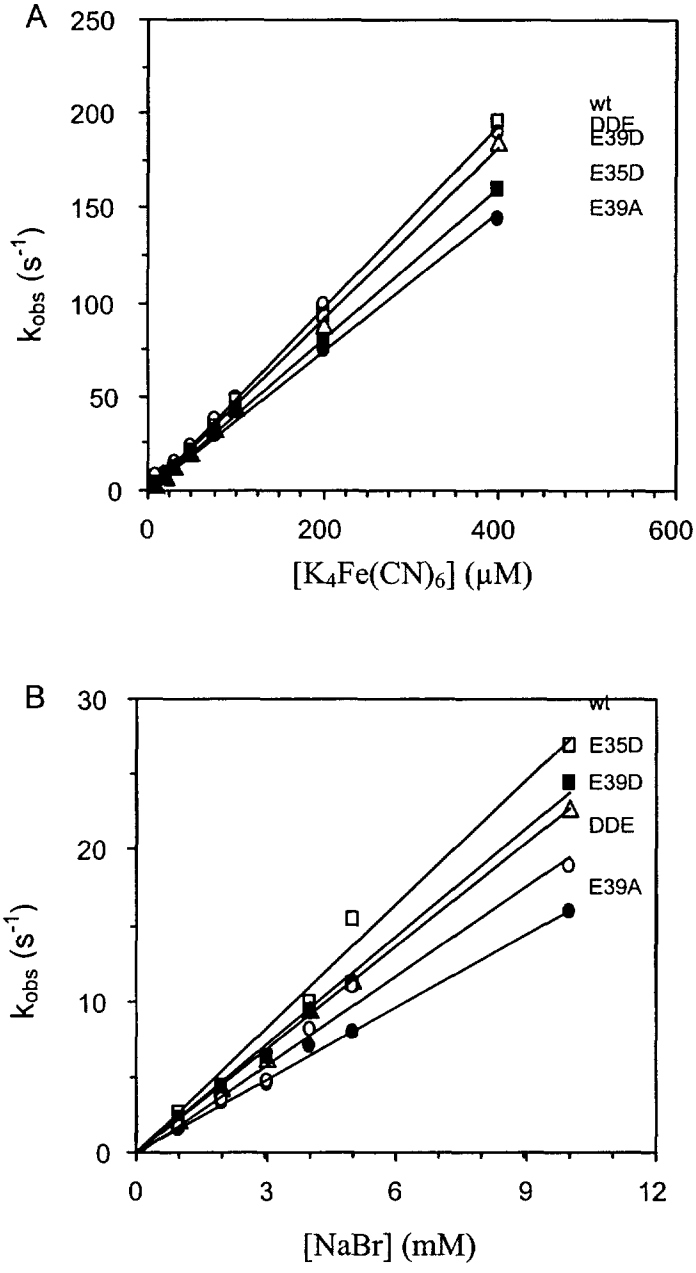

Figure 5.2 Kinetics of compound I reduction by ferrocyanide (**A**) and bromide (**B**). Wild-type (□), E39D (△), E35D (■), E39A (•), and E35D-E39D-D179E (○). Reaction mixtures contained a final concentration of 1 μM enzyme and 50 mM malonate (pH 4.5). All kinetic traces displayed single-exponential character and were fitted to obtain k_{obs} values.

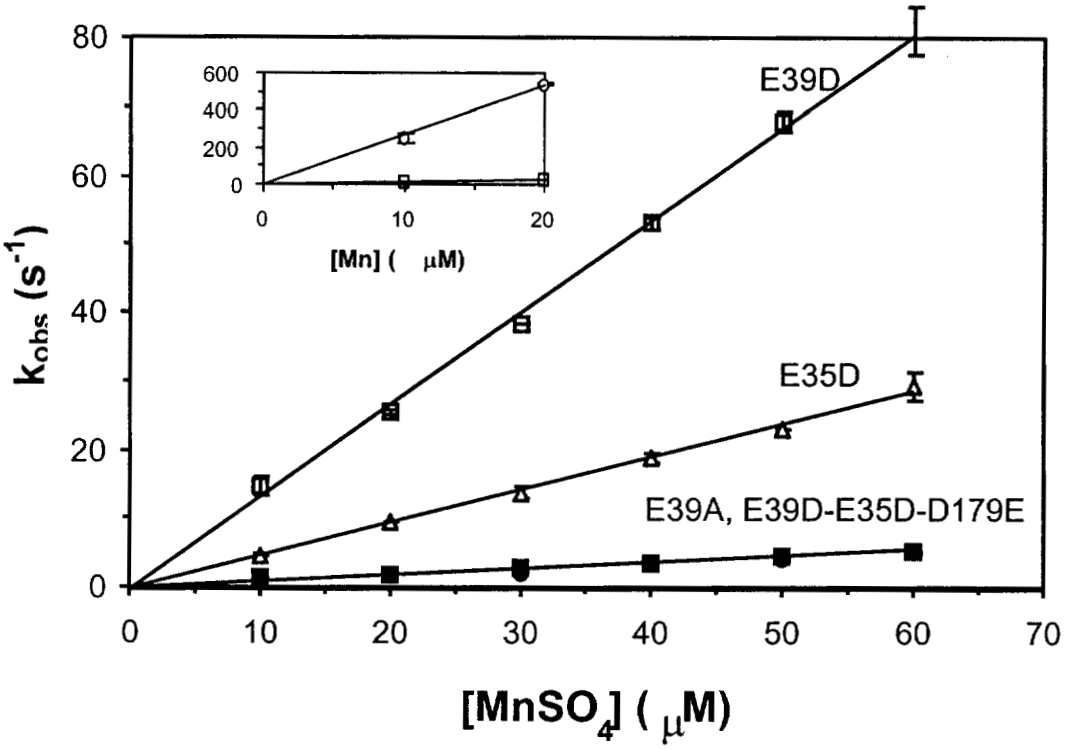

Figure 5.3 Kinetics of compound I reduction by Mn^{2+}. E39D (□), E35D (Δ), E39A (■), and DDE (E39D–E35D–D179E) (•). The wild type (○) and E39D (□) are shown in the insert for comparison; note the difference in scale. Reaction mixtures contained a final concentration of 1 μM enzyme and 50 mM malonate, pH 4.5. All kinetic traces displayed single-exponential character and were fitted to obtain k_{obs} values.

Table 5.3

Transient-State Kinetic Parameters for the Reduction of Compound II[a]

Enzyme	$K_4Fe(CN)_6$	Mn^{II}		
	k_{3app} ($M^{-1}s^{-1}$)	k_3 (s^{-1})	K_D (M)	k_{3app} ($M^{-1}s^{-1}$)
wild type	$(7.8 \pm 0.2) \times 10^3$	$(5.6 \pm 0.1) \times 10^2$	$(1.1 \pm 0.3) \times 10^{-4}$	5.2×10^6
E39D	$(6.4 \pm 0.5) \times 10^3$	$(1.4 \pm 0.1) \times 10^1$	$(1.1 \pm 0.1) \times 10^{-3}$	9.4×10^3
E35D	$(6.6 \pm 0.4) \times 10^3$	$(4.8 \pm 0.5) \times 10^0$	$(8.1 \pm 1.7) \times 10^{-3}$	5.9×10^2
E39A	$(6.5 \pm 0.2) \times 10^3$	$(4.5 \pm 0.5) \times 10^{-1}$	$(1.8 \pm 0.1) \times 10^{-3}$	2.4×10^2
DDE[b]	$(7.0 \pm 0.2) \times 10^3$	$(4.0 \pm 0.3) \times 10^{-1}$	$(2.3 \pm 0.4) \times 10^{-3}$	1.7×10^2

[a] Reaction mixtures contained 1 μM enzyme and 50 mM malonate (pH 4.5), final concentrations. The ionic strength of all solutions was adjusted to $\mu = 0.1$ M with K_2SO_4. Reactions were conducted under pseudo-first-order conditions, and substrate concentrations were varied as described in the text. Constants were determined as described [426]. Individual kinetic traces showed exponential character and were fitted to obtain k_{obs}.

[b] DDE = the triple variant E35D–E39D–D179E.

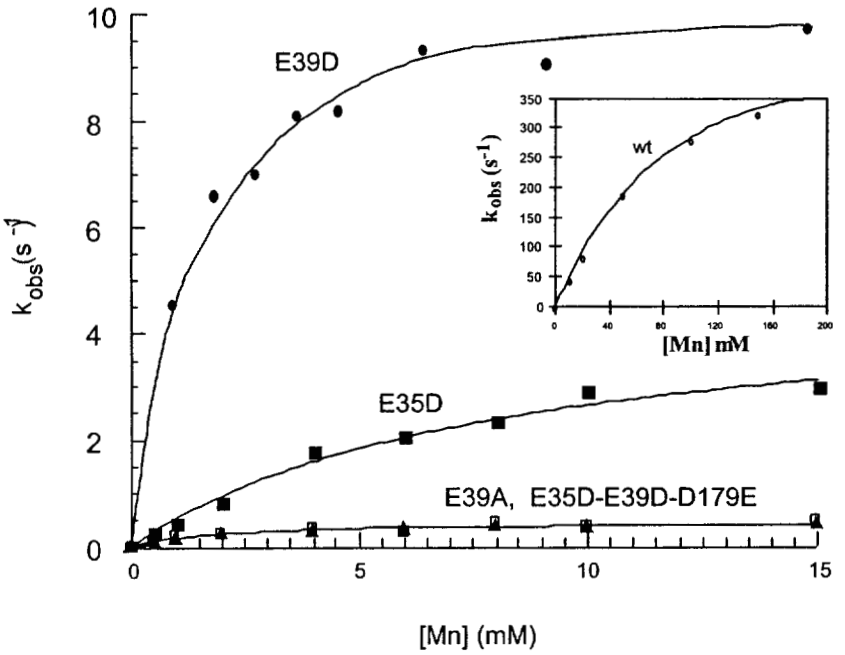

Figure 5.4 Kinetics of compound II reduction by Mn^{2+}. E39D (•), E35D (■), DDE (E35D-E39D-D179E) (□), and E39A (▲). The wild type (○) and E39D (•) are shown in the insert for comparison; note the difference in scale. Reactions contained a final concentration of 1 μM enzyme and 50 mM malonate, pH 4.5. All kinetic traces displayed exponential character and were fitted to obtain k_{obs} values.

5.4 DISCUSSION

MnP is unique among Mn-binding enzymes in its ability to bind and oxidize Mn^{2+} and efficiently release Mn^{3+}. This discriminatory binding is a critical aspect of MnP function. As a result of combined kinetic and crystallographic studies of these variants, the residues D179, E35, and E39 were identified as catalytically important Mn^{2+} ligands [226, 237, 376, 377]. In the first set of binding site mutants, the amino acid carboxylate ligands were exchanged for their respective amides via site-directed mutagenesis of the *mnp1* gene from *P. chyrsosporium* [226, 237]. Since amides are poor ligands for Mn, these variants were designed to maintain steric constraints in the enzyme while selectively interfering with Mn ligation.

E39 is conserved in all known MnP sequences [144] and previous kinetic analyses [226] and the X-ray crystral structures [376, 377] clearly indicate that E39 is, in fact, a ligand to the Mn. However, a more recent mutagenesis study using isochemical substitution of these ligands has raised doubts about the importance of E39 in Mn^{2+} binding and oxidation [436]. In that study, an E39D variant MnP was constructed which was claimed to exhibit wild-type reaction kinetics for Mn^{2+}. As a result, Whitwam and co-workers proposed that E39 was not a ligand to the Mn. There are two alternate explanations for the proposed wild-type kinetics of the E39D variant in that study [436]. The first is that the mutation was lost and the kinetics observed really are those of the wild-type enzyme. The second possibility concerns the isochemical nature of the substitution. In the E39D mutation, the functional carboxyl group is retained, although the side chain is shortened by one methylene group. It is possible that a shortened D39 residue could still ligate the Mn in a fashion similar to the original E39 residue, if there were some flexibility in the Mn binding site.

To further investigate this possibility, we first performed molecular modeling of the E39D and E35D variants. In the model, the Mn–ligand bond distances indicate that perhaps the mutated D35 residue is no longer capable of binding Mn, in agreement with the kinetic analysis of this mutant [436]. However, modeling of the E39D and E35D-E39D-D179E variants indicated possible flexibility in the binding

site, whereby the mutated residues might still function as a ligands, but only with an accompanying change in the Mn ligation geometry (Figure 5.1). If the ligation geometry of the variants was fixed into wild-type, near-octahedral conformation, the metal-ligand bond distances were increased by 0.5–0.8 Å, resulting in probable loss of the mutated ligands.

To evaluate the models, we constructed the E39D and E35D variant MnPs using our homologous expression system [263]. The results of our kinetic analysis of the E35D variant are very similar to those previously obtained (Tables 5.1–5.3) [436], which is significant since the variants were expressed in different systems. The previous E35D variant was heterologously expressed in *E. coli* and reconstituted with calcium and heme. The resulting enzyme was not glycosylated. In contrast, homologous expression in *P. chryosporium* results in a fully processed and secreted enzyme which is glycosylated and which does not require reconstitution. The similar kinetic results for both the E35D variant MnPs in this work and the previous study [436] indicate that differences in the expression systems did not affect the overall kinetic characteristics of these variants.

Our results for the E39D variant, however, are markedly different from those of the previous study [436]. Steady-state and transient-state analyses of our E39D variant MnP clearly indicate that the binding and oxidation of Mn^{2+} are significantly reduced by this substitution. Sequencing of genomic DNA from the transformed fungus containing the recombinant gene indicated that the E39D mutation was correct with no other sequence alterations present. We also constructed an E39A mutation, effectively removing the ligand from the binding site. As expected, kinetic analysis indicates that the E39A substitution decreases Mn binding and oxidation to a similar but slightly greater extent than the E39D substitution. Transient-state kinetics indicate similar changes (Tables 5.2 and 5.3). These results, combined with those for the previous E39Q variant, clearly indicate that E39 plays an important role in binding and oxidation of Mn^{2+}.

In addition to the single-site substitutions, we constructed an E35D-E39D-D179E isochemical triple variant. In this variant, two of the ligand side chains were shortened while the third was lengthened. Molecular modeling indicated that this

triple-substituted binding site might still be functional for Mn binding and oxidation if the Mn and associated water ligands were to move a few angstroms outward toward residues 35 and 39 (Figure 5.1D). Whereas the kinetics for Mn oxidation by the double variant (E35D–E39D) were barely measurable, the triple variant performed almost as well as the E39A single variant.

These combined results indicate that the Mn binding site may be relatively inflexible to changes in the geometry of the site. It appears that even isochemical substitutions greatly reduce both Mn binding and the rate of Mn oxidation. Although both the E39D and the isochemical triple variants are theoretically capable of Mn binding, both binding and electron transfer are in fact diminished. The kinetic data support the assertion that maintenance of the octahedral Mn ligation geometry predominates bond formation. The fact that the E39D variants perform slightly better than the E39A and E39Q variants and the E35D–E39D–D179E triple variant performs as well as the single variant indicates weak ligation in the altered sites. However, it is most likely energetically unfavorable for the Mn to adopt the altered geometry required for the substituted residues to act as good ligands. This is supported by crystal field theory in which tetragonally distortion of an octahedral complex is accompanied by electron spin pairing in the metal, which is energetically unfavorable for Mn [76].

Our results have interesting implications for attempts to engineer MnP-like Mn binding sites into other proteins. Recent studies with variants of cytochrome *c* peroxidase (CcP) engineered to contain an Mn binding site also indicate that precise geometry is required for efficient Mn binding and oxidation [438a, 439]. Similar to our results for MnP, and despite promising modeling of the CcP variants, the best Mn binding CcP performed only as well as any of the single ligand MnP variants [438a]. The preference of Mn ions for octahedral ligation and the preferential differences in the binding geometries of Mn^{2+} and Mn^{3+} for carboxyl oxygens may prove important to the mechanism of the Mn binding site in MnP. While Mn^{2+} can bind equally well in either the syn or anti orientation, Mn^{3+} prefers the anti orientation [72]. Therefore, the exact orientation of ligands within the Mn site might directly affect

binding of Mn^{2+}, modulate the redox transition from Mn^{2+} to Mn^{3+}, or affect release of Mn^{3+}.

In summary, mutation of the E39 residue in MnP decreases both Mn binding and oxidation as indicated by both steady-state and transient-state kinetics. The catalytic efficiency of the E39A (as shown herein) and E39Q [226] variants decreases $\sim 10^4$-fold, while that of the E39D variant decreases $\sim 10^3$-fold. These results clearly indicate that the E39 residue is a ligand to the Mn. We also investigated a E35D–E39D–D173E triple variant MnP which, despite favorable modeling studies, performed only as well as any of the single Mn ligand variants. The catalytic efficiency of the triple mutant was decreased 10^4-fold, which is, however, $\sim 10^2$-fold better than that reported for a double variant MnP [226]. These combined modeling and steady-state and transient-state kinetic studies indicate that precise geometry of the Mn ligands in the Mn binding site of MnP is essential for the efficient binding, oxidation, and release of Mn by this enzyme.

CHAPTER 6
UNDERSTANDING THE ROLE OF CHELATORS IN THE Mn PEROXIDASE REACTION CYCLE: A CLOSER LOOK AT Mn SPECIATION

6.1 INTRODUCTION

The role of chelators in the MnP reaction cycle has long been a subject of debate. Chelators are required for enzyme turnover [136, 227, 231, 233, 422, 423, 426]; however, the exact mechanism is not known. The evidence has been distilled into two conflicting theories illustrated in Figure 6.1. (1) MnP binds free, unchelated Mn^{2+}, oxidizes it and releases chelated Mn^{3+}, either by mediated release (ligand exchange) or via a transient chelate–Mn^{3+}–MnP complex [22, 426]. (2) MnP only binds and oxidizes chelated Mn^{2+} and then releases the Mn^{3+}–chelate product [227, 231].

Support for the role of chelator in release of Mn^{3+} from the enzyme is overwhelming. Chelator is required for turnover and stimulates rate of reduction rate by Mn^{2+} even in the transient-state [22, 227, 231, 426]. However, whether this occurs by an equilibrium-driven process such as ligand exchange or by formation of an actual ternary complex is not discernable from the data. The only evidence for such a complex is from the ^{1}H-NMR data using lanthanides [22]; however, the assertion by Banci and co-workers, that lanthanides mimic Mn^{3+}, is questionable. Lanthanides can accommodate many more ligands in a much looser geometric arrangement than Mn^{3+} [76]. There is no need for ternary complex formation to account for the stimulation of activity by chelator.

Based on stability constants, nearly all of the Mn^{3+} in solution at physiological concentrations is chelated by compounds such as oxalate at pH 4.5 [349]. Only

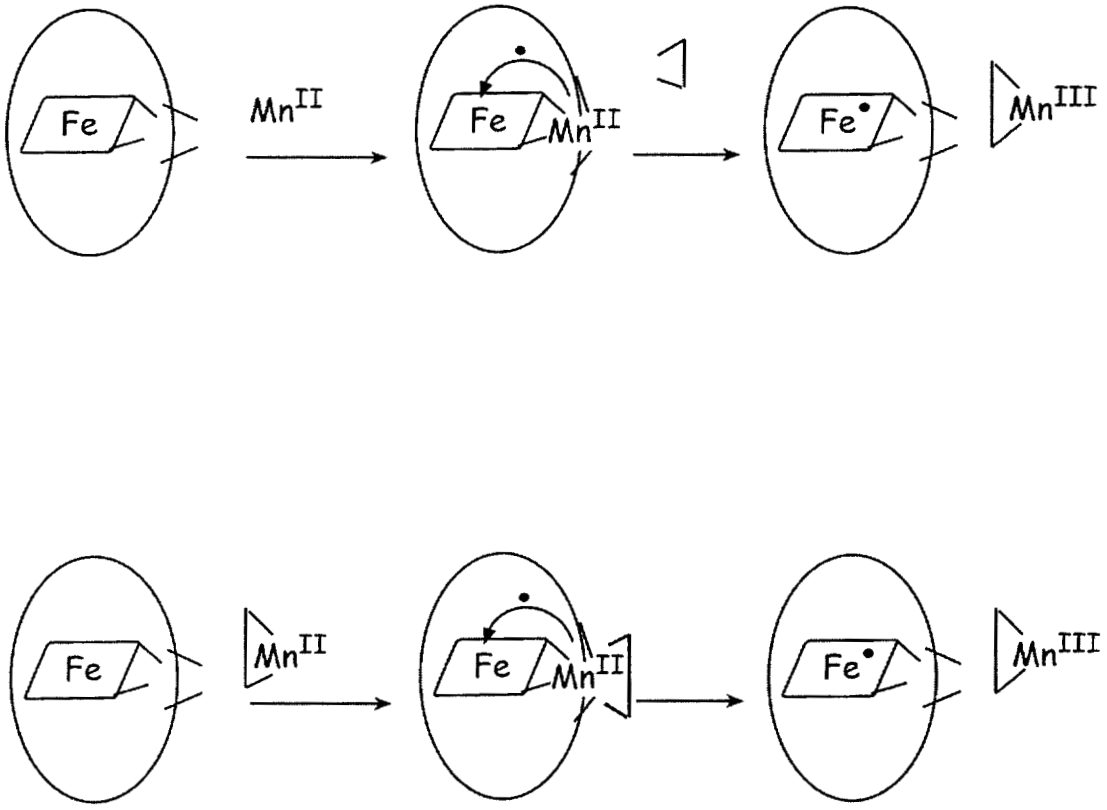

Figure 6.1 Two theories on the role of chelators in the reaction cycle of manganese peroxidase. (**Top**) Free (aquo) Mn^{2+} binds to the enzyme, with chelator effecting release of Mn^{3+} [22, 245]. (**Bottom**) A 1:1 chelator:Mn^{2+} complex binds to the enzyme, is oxidized, and released [227, 231].

competition between the chelator and the enzyme would alter this condition. Given the geometric constraints in the enzyme active site, the dramatic reduction in the size of the Mn^{3+} ion (0.7 Å) versus the Mn^{2+} ion (0.91 Å) [76], and the 10^6-fold increase in stability constants for Mn^{3+}-chelate complexes over Mn^{2+} complexes [349], an equilibrium-driven process is likely.

The question as to whether free Mn^{2+} or Mn^{2+}-chelate complex binds the enzyme and is subsequently oxidized is much more controversial. The requirement for chelator in the reduction of compound II by Mn^{2+} has been interpreted to indicate formation of a complex. The observed kinetics change as the concentration of chelator is increased. For example, a shift from first to second-order is observed, in the case of oxalate [227]. However, these changes can be correlated to the first, equilibrium model. At higher concentrations of chelator, inhibition by chelation of the substrate, Mn^{2+} should cause changes in the compound II kinetics similar to those of competitive substrate inhibition by Cd^{2+} presented in Chapter 3. It seems that the entire weight of the argument for a complex rests squarely on speciation data, suggesting that the stimulation of activity is due to the presence of a 1:1 Mn^{2+}-chelator complex that is oxidized, binds chelator, and dissociates in a 1:2 Mn^{3+}-chelator complex [231]. Kuan and co-workers correlate the observed rate of compound II reduction by Mn^{2+} with the 1:1 Mn^{2+} chelator complex (Figure 6.2A). However, no additional evidence for the formation of a ternary complex has been found by X-ray crystallography [376], ^{1}H-NMR [22], or isotope labeling studies [personal observation, unpublished]. Upon re-evaluating the method by which the graph in Figure 6.2A was generated, there were flaws in the calculation.

6.2 MATHEMATICAL TREATMENT

The equations used were corrected as follows:

$$[Mn]_{total} = [Mn] + K_1[Mn][C] + K_1K_2[Mn][C]^2 \ldots + K_1 \ldots K_n[Mn][C]^n \qquad \text{(Equation 6.1)}$$

$$\alpha Mn = \frac{[Mn]}{[Mn]_{total}} = \frac{1}{1 + K_1[C] + K_1K_2[C]^2 + K_1 \ldots K_n[C]^n} \qquad \text{(Equation 6.2)}$$

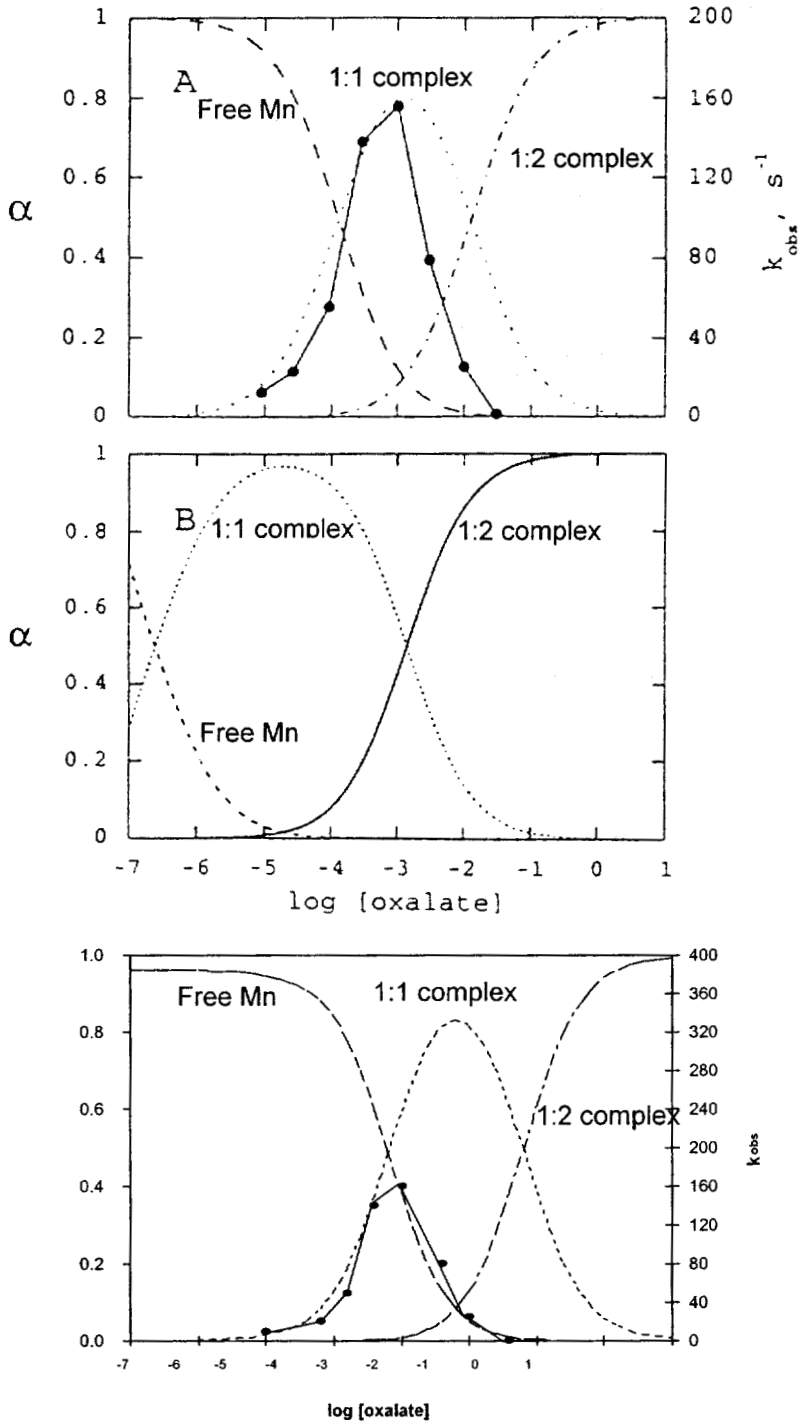

Figure 6.2 Mn speciation in 10 mM succinate, pH 4.5, and various concentrations of oxalate. From Kuan et al. [231]* (**A,B**). Calculated using the MacμQL program (**C**).

* Originally published as Figure 5 in: Kuan, I. C., Johnson, K. A., and Tien, M. (1993) Kinetic analysis of manganese peroxidase. The reaction with manganese complexes. *J. Biol. Chem.* **268,** 20064–20070. Used with permission of Academic Press.

$$\alpha Mn(C) = \frac{[MnC]}{[Mn]_{total}} = \frac{K_1[C]}{1 + K_1[C] + K_1K_2[C]^2 + K_1 \ldots K_n[C]^n} \quad \text{(Equation 6.3)}$$

$$\alpha Mn = \frac{[MnC_n]}{[Mn]_{total}} = \frac{K_1 \ldots K_n[C]^n}{1 + K_1[C] + K_1K_2[C]^2 + K_1 \ldots K_n[C]^n} \quad \text{(Equation 6.4)}$$

with stability constants for Mn^{2+}-oxalate: $K_1 = 7.9 \times 10^3\ M^{-1}$, $K_2 = 7.9 \times 10\ M^{-1}$ and Mn^{3+}-oxalate: $K_1 = 9.5 \times 10^9\ M^{-1}$, $K_2 = 3.9 \times 10^6\ M^{-1}$, and $K_3 = 7 \times 10^2\ M^{-1}$.

6.3 RESULTS AND DISCUSSION

The experiment to measure compound II reduction was performed in 10 mM succinate, pH 4.5, with 20 μM Mn^{2+} (assumed to be $MnSO_4$) and various amounts of oxalate [231]. However, when the authors calculate the Mn speciation, they used the total concentration of oxalate added to denote [C] in Equations 6.1–6.4. This is incorrect as C represents the deprotonated chelator (C^{-2}), which must be calculated from the pKa values. Also, the effect of the 10 mM succinate (the pKa values and stability constants for Mn^{2+} complex formation) and the protons associated with adjusting the solution to pH 4.5 must be included in the calculation. The enzyme and its K_D should also be included, but in this case did not influence the outcome of the graph [data not shown]. Figure 6.1C shows the speciation ratios calculated iteratively using all the values in the MacμQL program for Macintosh (Beat Müller, Limnological Research Center EAWAG/ETH, CH-6047 Kastanienbaum). When the kinetic data from Figure 6.1A [231] is replotted on this new speciation graph, it no longer aligns with the appearance of the 1:1 complex (stimulation) and disappearance of the 1:1 complex/appearance of the 1:2 complex (inhibition). Instead, stimulation occurs while there is still free Mn^{2+} in solution. The second half of the curve (inhibition) coincides with the *appearance* of the 1:1 complex, suggesting that it is free Mn^{2+} that binds the protein and that complexation of Mn^{2+} by higher concentrations of chelator inhibits the reaction.

Kuan and co-workers were careful not to actually plot the kinetic data on the Mn^{3+} speciation graph. Rather, they align the two graphs and allow the reader to draw the conclusion that activity corresponds with the disappearance of the 1:2 Mn^{3+}-chelator and appearance of a 1:3 Mn^{3+}-chelator complex. In fact this graph makes little sense in the context of the experiment. The speciation graph was calculated using 20 μM Mn^{3+} as the total Mn concentration, as was the case for Mn^{2+}. However, the experiment was conducted under transient-state conditions and the rate measure is a single turnover. At the start of the experiment there is 20 μM Mn^{2+} in solution, binding to chelator. The substrate solution is then mixed with 1 μM enzyme already in the compound II state. There is no Mn^{3+} until the reaction begins. The experiment is conducted in the transient-state such that only a single transition from MnPII to native enzyme is measured. Thus, even when the Mn^{3+} is generated, the maximum concentration of Mn^{3+} equals the concentration of compound II (1 μM). Furthermore, the Mn^{3+} is bound to the enzyme and must then compete for chelator in a solution with a $\sim$19 μM Mn^{2+}. The difference in stability constants ensures that Mn^{3+} will replace the Mn^{2+} in the chelator complexes, if it can escape the enzyme. The ratio calculation is practically meaningless. In essence all of the Mn^{3+} generated is bound, either to enzyme or to chelator and chelator can facilitate release by simple equilibrium.

6.4 CONCLUSIONS

Together the evidence suggests that no ternary complex between MnP, Mn and chelator is ever formed. Rather, all of the kinetic and biophysical data can be explained by equilibrium phenomena. At low levels, the Mn^{3+}-chelator complex and free Mn^{2+} dominate the speciation profiles. Activity is stimulated because Mn^{2+} is the enzyme substrate and formation of the Mn^{3+}-chelator complex removes Mn^{3+} from the active site, facilitating turnover. In contrast, high levels of chelator inhibit activity by sequestering free Mn^{2+}, competing with the enzyme.

CHAPTER 7
FINAL COMMENTS AND FUTURE DIRECTIONS

7.1 IMPROVING STRUCTURAL STABILITY IN Mn PEROXIDASE

7.1.1 Recent Reports on the Alkaline Transition in Other Peroxidases

Concomitant with the publication of Chapter 2, a study of alkaline inactivation in lignin peroxidase (LiP), employing IR-MCD and EPR spectroscopy, also showed formation of a bis-histidyl heme at high pH [128]. In that study, isotope labeling indicated that both calcium ions are lost from LiP during alkaline inactivation [128], lending support to our speculation that the same phenomenon occurs in MnP [Chapter 2].

Analysis of a F221M variant of horseradish peroxidase (HRP-C) was reported recently [184]. Phe221 is equivalent to F190 in MnP. Several plant peroxidases from *Arabidopsis thaliana* are reported to contain a Met at this position [297]. Like MnP, HRP-C undergoes alkaline inactivation with a heme–iron transition from high spin to low spin. However, the transition in HRP-C occurs at much higher pH ($\sim$ 10–12) and apparently involves formation of a hydroxyl, rather than a bis(histidyl), heme [351]. Like peanut peroxidase (PNP), HRP contains a disulfide bridge anchoring the distal calcium [125, 345]. This additional reinforcement, not present in the class II peroxidases, most likely prevents coordination of the distal histidine, even at high pH. However, exactly as the other MnP variants discussed in this work, the F221M variant of HRP-C undergoes the alkaline transition at $\sim$2 pH units lower than the transition in wild type MnP [225]. ^{1}H-NMR and resonance Raman studies of the transition in the HRP-C variant indicate a lengthening of the Fe-imidazole bond and exposure of the proximal His to solvent [184], suggesting a role for this proximal residue in maintaining integrity of the heme environment.

7.1.2 Reinforcing the Distal Calcium

To date, six extracellular plant and fungal peroxidases have been studied by X-ray crystallography. Three class II fungal peroxidases have been studied: lignin peroxidase (LiP) [105, 304, 309], manganese peroxidase (MnP) [376], and *Coprinus cinereus/Arthromyces ramosus* peroxidase (CiP/ArP) [235, 302]. Three class III plant peroxidases have been studied: peanut peroxidase (PNP) [345], horseradish peroxidase (HRP) [125], and the major peroxidase from barley grain (BP1) [173]. All six enzymes contain two structural Ca-binding sites, one in each of the domains distal and proximal to the heme. The structures indicate a major difference in the two classes of enzymes involving the architecture of the distal calcium binding sites. In all the enzymes, the distal calcium sites are formed primarily by a single loop at the end of helix B, which contains the catalytic distal histidine. However, the class III enzymes contain a disulfide linkage closing the loop (Figure 7.1). For example, in PNP the loop begins after the distal His41 at residue 43 and extends to residue 50, with the disulfide between Cys44 and Cys49 [345]. The loop in BP1 is slightly longer, from residues 50–59, just after the distal His49 with the disulfide linkage between Cys51 and Cys59 [173]. Interestingly, while BP1 shows an unusual pH dependency, reflecting a unique alternate H-bonding network in the distal domain, both PNP and BP1 are extremely thermostable (T_m > 90 °C). In contrast, MnP is considerably less thermostable (T_m ~ 54 °C) and contains a longer distal calcium loop, from Ala48 to Ala63, lacking the stabilizing disulfide (Figure 7.1).

Disruption of the distal Ca-binding site in these enzymes affects the positioning of the catalytic distal histidine and influences the activity of the enzymes. In LiP and MnP, loss of calcium at high temperature or pH has been correlated with coordination of the distal His to the heme iron, inactivating the enzyme [128, 225, 381, Chapter 2]. An opposing phenomenon occurs in BP1, although with a similar end result. At neutral to high pH, a sodium ion replaces the distal calcium in BP1, causing rearrangement of the Ca^{2+}-binding loop and H-bond network. Rather than allowing movement of the distal His closer to the heme, as in the fungal enzymes, the disruption in BP1 causes the distal His to move away from the heme iron [173]. The displaced His can no longer participate in peroxide cleavage, resulting in an inactive,

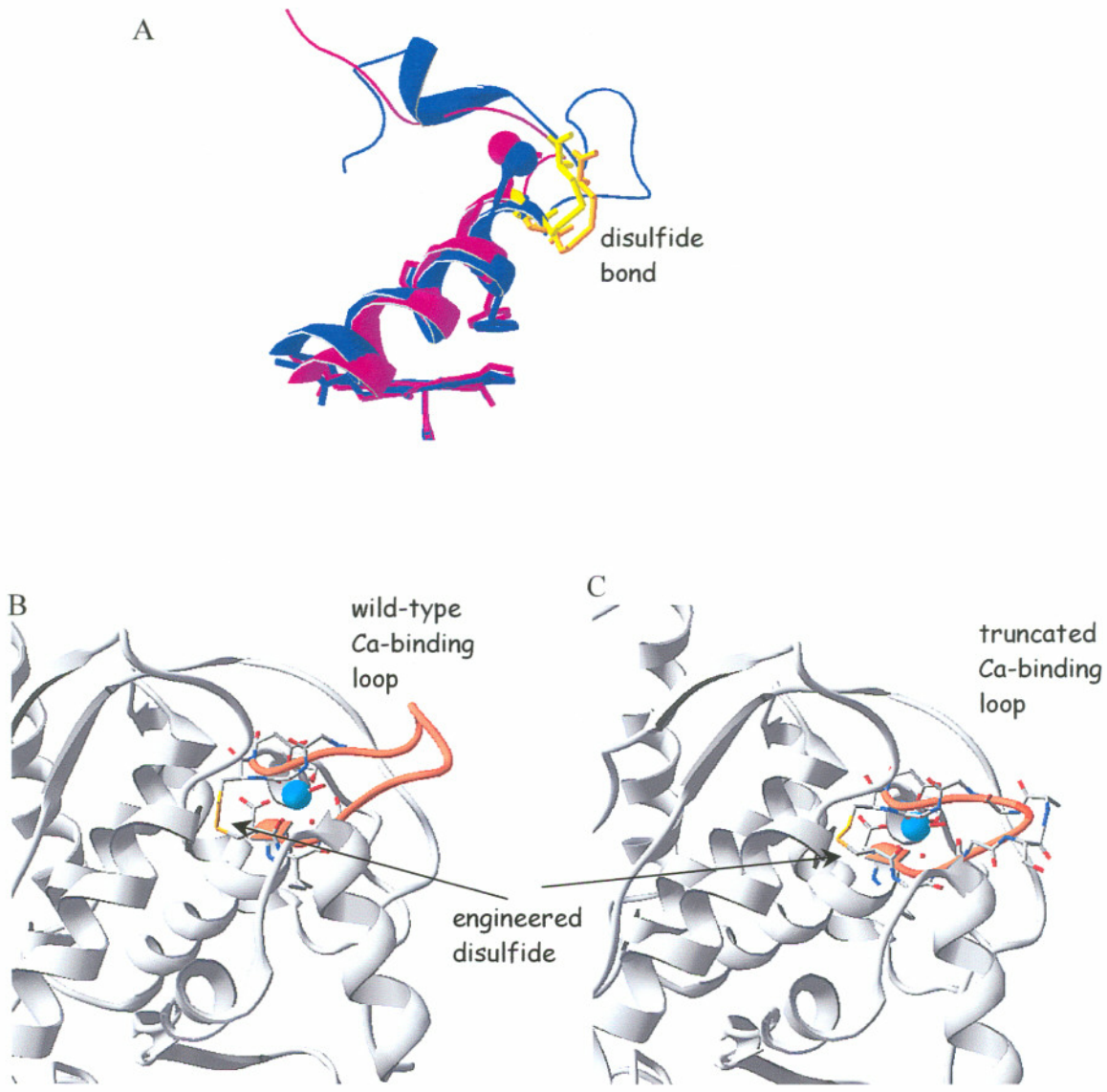

Figure 7.1 Modeling of an A48C-A63C disulfide in the distal Ca-binding site of Mn peroxidase with wild-type Ca-binding loop (**A**) and a truncation involving deletion of residues 53–58 (**B**). Created using the crystal structure coordinates [376] in the Swiss PDB Viewer.

although stable, enzyme conformation. The enzyme activity is restored following lowering of the pH and addition of exogenous Ca^{2+} to the protein [173].

A stabilizing disulfide near the distal Ca-binding site, similar to those in the plant peroxidases, was recently engineered into recombinant MnP [319]. Figure 7.1 shows an overlay of the distal Ca-binding sites of PNP and the A48C–A63C double mutant. Unfortunately, the variant MnP protein was heterologously expressed in *Escherichia coli*, a process in which the protein is not glycosylated and must be isolated from inclusion bodies and reconstituted with heme and calcium [437]. Although the recombinant enzyme produced by this expression system appears to exhibit normal kinetics, it is much less thermostable than the wild-type enzyme, presumably due to the lack of glycosylation [284, 437]. Although the additional disulfide at the distal Ca-binding site did improve the recombinant MnP thermal stability, the engineered enzyme was still only as stable as the wild-type enzyme [319]. Engineering the disulfide in a construct that could be used for homologous expression in *Phanerochaete chrysosporium* would allow production of glycosylated protein, which would presumably be more stable to heat and high pH than the wild type. In addition, truncating the long surface loop near the Ca-binding site by eliminating residues 53–38 may increase stability (Figure 7.1).

7.1.3 Tethering the C-Terminus and Extended Proximal Loops in Mn Peroxidase

MnP from *P. chrysosporium* contains two extended loops that are not conserved in other class II peroxidases: an extended C-terminus and a loop in the proximal domain (Figure 7.2) [376]. The C-terminus extends around the protein, up past the Mn-binding site, and curving around to terminate in the distal domain at a putative metal binding site [376, Chapters 3 and 4]. In addition to the putative C-terminal metal binding site, the extended C-terminal region of MnP contains a fifth disulfide linkage that is found only in other MnPs and not in any of the other class II peroxidases [140, 144]. This linkage causes a kink in the C-terminal peptide (Figure 7.2), which has been hypothesized to push the C-terminal peptide away from interfering with the Mn-binding site [376]. One conserved residue in this C-terminal loop, His340, appears to H-bond Arg177, which in turn interacts with the Mn-ligand

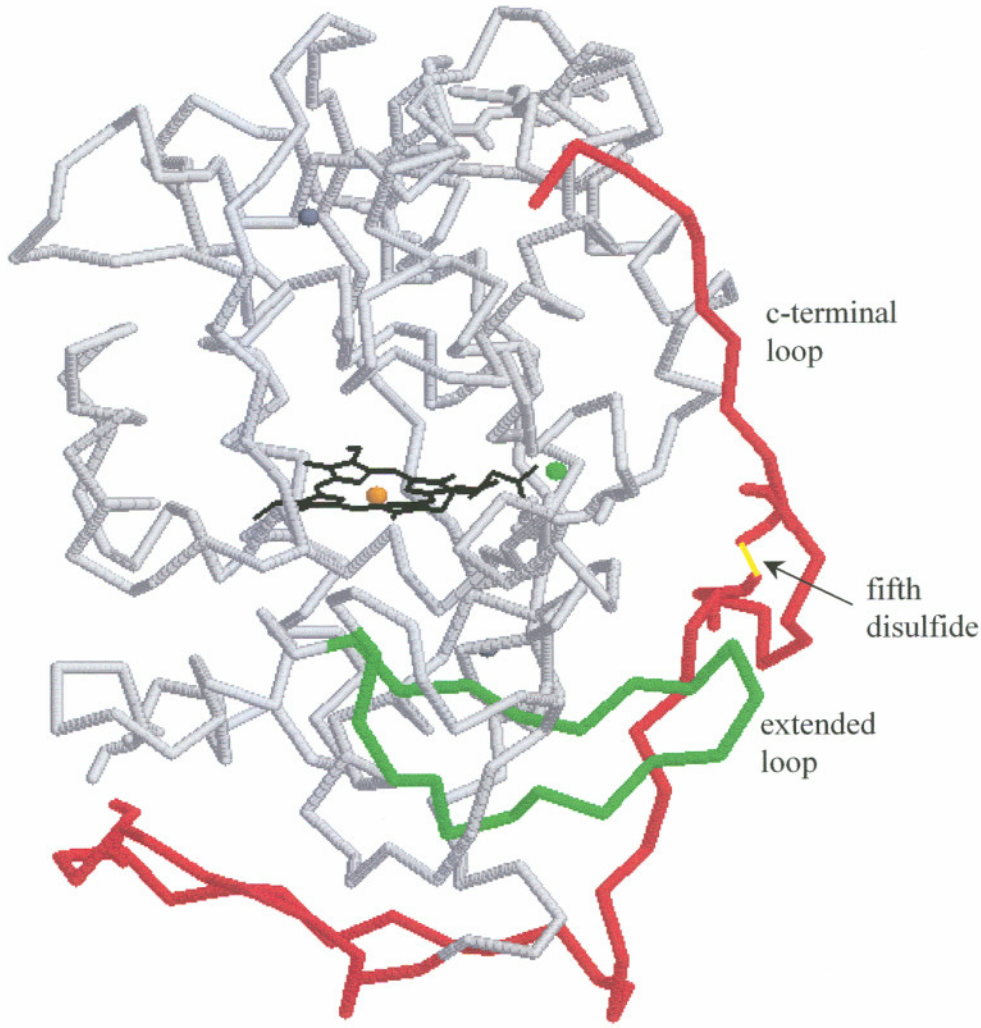

Figure 7.2 X-ray crystal structure of MnP indicating the unconserved C-terminal peptide (red) and extended proximal loop (green) [376].

Glu35 (Figure 7.3) [360, 376]. The extended proximal loop contains one residue, Ser232, that appears to H-bond to the backbone carbonyl of His340, providing a point of interaction between the two loops and, indirectly, with the Mn-binding site. The actual roles of the C-terminal peptide, the fifth disulfide and that of His340 in MnP catalysis (influence on the Mn-binding site environment) and/or stability have not yet been tested.

A common adaptation of thermostable enzymes is the stabilization or fixation of surface loops [12]. Thus, engineering additional salt bridges or disulfide bonds to stabilize the C-terminus and/or the proximal loop may further stabilize the protein. A possible H-bond occurs between Asp85 (adjacent to Asp84 in the putative C-terminal metal binding site) and Gln352 on the C-terminal peptide (Figure 7.3). The distance between the two sites is 3.97 to 4.26 $\pm$ 0.5 Å in the MnP crystal structures in the absence and presence of Cd^{2+}, respectively [376, 378]. A salt bridge with a distance of $\sim$2.27 Å can be modeled by constructing a virtual D85E–Q352K double mutant in the existing space between the C-terminal peptide and the body of the protein without movement of C-terminus (Figure 7.3). The variant should exhibit increased stability; however, other effects, including changes in the kinetics of Mn^{2+} binding and interference in protein folding, are possible.

7.2 DIRECTED EVOLUTION OF LIGNIN AND Mn PEROXIDASES

White-rot fungi can oxidize recalcitrant aromatic compounds including natural lignin and toxic aromatic pollutants, including chlorinated phenolic compounds, dioxins, dyes and munitions waste [158, 159, 320, 321, 375, 406–408]. Application of ligninolytic enzymes to biomaterial processing, bioremediation, and detoxification of industrial byproducts is promising. The two extracellular peroxidases produced by these fungi, MnP and LiP, can oxidize a wide variety of terminal substrates, including complex polymers, via highly redox active mediator molecules. Chelated Mn^{3+} is generated by MnP [135, 426]; whereas the veratryl alcohol cation radical (VA•+) is generated by LiP [132, 157, 166, 215].

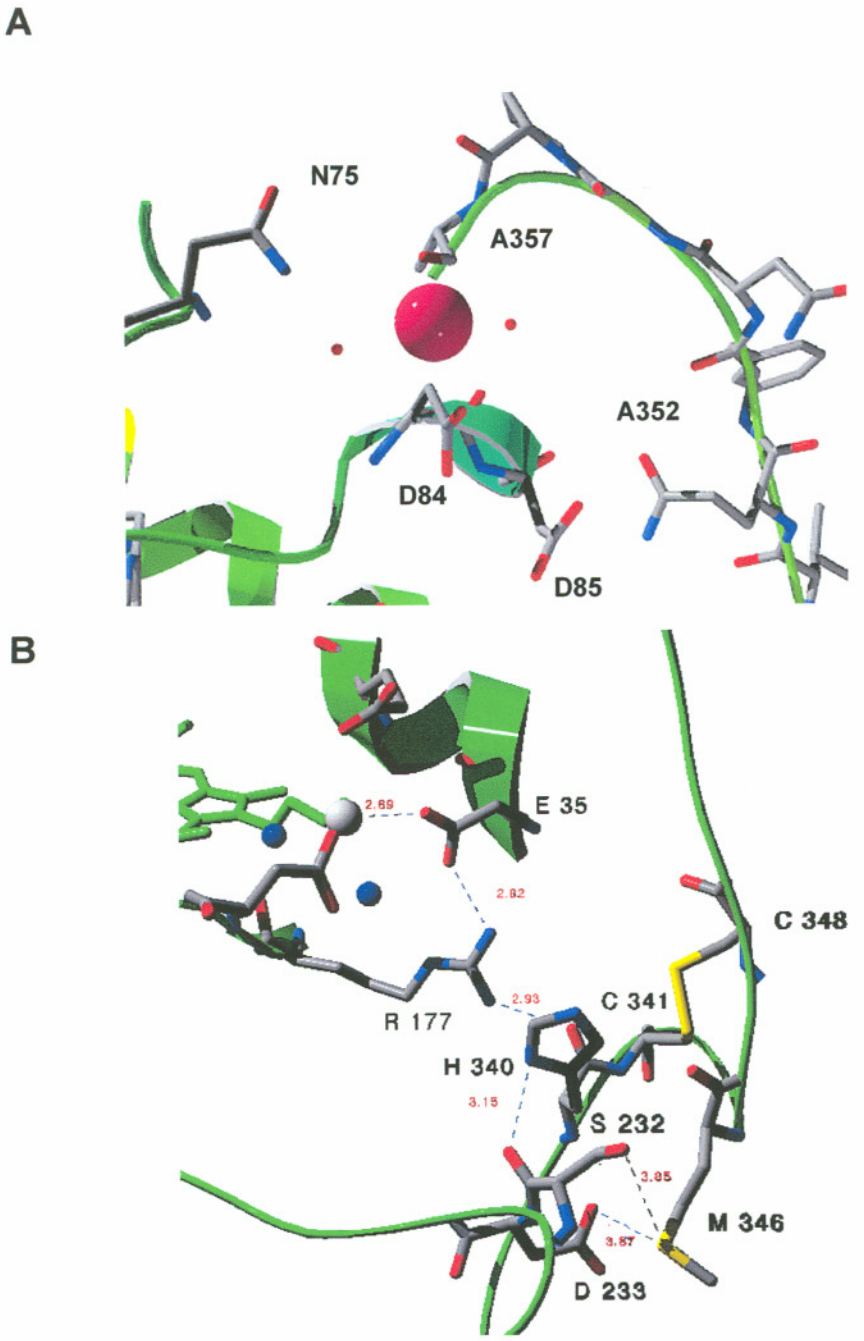

Figure 7.3 The X-ray crystal structure of Mn peroxidase indicating the C-terminus with Cd bound and showing the H-bond between Q352 and D85 (**A**). Structure of the Mn-bound Mn peroxidase indicating interactions between the C-terminal and extended proximal loops (**B**).

Unlike other related peroxidases, such as HRP and CiP, which oxidize a wide variety of small compounds, MnP and LiP possess highly specific binding sites for the substrates, Mn^{2+} and veratryl alcohol (VA), respectively, and are the only peroxidases that efficiently oxidize these substrates.

Directed or *in vitro* evolution is an interesting and effective method to alter or extend the functionality of enzymes. Genes are subjected to repeated cycles of change and selection. Methods of change include mutagenesis (e.g., error prone PCR [61, 272]) or generation of chimeric libraries (e.g., DNA shuffling [370, 371] or random priming PCR techniques such as staggered extension processing (StEP) [347, 447]). So far, four proteins have been subjected to directed molecular evolution by error prone PCR to improve their peroxidase activity: CcP [188], HRP [274], CiP/ArP [68], and the oxygen binding protein, myglobin [420]. Two enzymes, yeast CcP and horse heart myglobin, were heterologously expressed and underwent selection in an *E. coli* system [188, 420]; whereas the other two, HRP and CiP/ArP, were heterologously expressed and underwent selection in *S. cerevisiae* [68, 274]. In all cases, the process was extremely successful, although individual results varied according to the selection schema. The peroxidase activity of myoglobin was increased 25-fold [420]. The thermal stability of CiP was increased 110-fold and the oxidative stability 2.8-fold [68]. The thermal stability of HRP was increased 3-fold and showed increased activity towards small organic substrates [274]. Finally, the specificity of CcP toward guaiacol was increased 1000-fold [188].

Extensive mutational analyses of MnPs are difficult. Expression of the enzyme in *E. coli*, results in insoluble inclusion bodies that require reconstitution of the calciums and heme. Expression of MnP in other eukaryotic systems such as baculovirus [294] and *Aspergillus oryzae* [372] has not been overly successful. The fungus *P. chrysosporium* can be used to homologously express a recombinant version of its own MnP [263] or to heterologously express MnPs from other species [246]. The system yields useful amounts of glycosylated protein with proper insertion of metal ions and heme, but is cumbersome and time consuming. The fungus grows slowly, is difficult to transform efficiently, and can grow as a heterodikaryon requiring fruiting and purification to prevent genetic recombination [5, 7, 9].

The expression of MnP in yeasts, such as *S. cerevisiae* or *Pichia pastoris*, would allow directed evolution studies. As with other systems, error-prone PCR could be used to develop more stable MnPs or to increase the substrate range. Compared to other class II peroxidases such as LiP and *Pleurotus eryngii* peroxidase, MnP is uniquely poor at oxidizing small aromatic molecules in the absence of Mn, most likely due to an atypically acidic δ-meso edge environment [62]. While each of the ten or so amino acids surrounding the proposed aromatic substrate entry site could be manipulated by site-directed mutagenesis, directed evolution seems a much more efficient approach. DNA shuffling techniques could also be employed. Peroxidases are a large group of proteins, have a highly conserved core structure, and are expressed as multiple isozymes in most organisms. This group of enzymes possesses an inherent wide range of evolutionary possibilities. For example, 14 isozymes of HRP alone have been identified: 3 acidic isozymes (A1A3), 5 neutral isozymes (B1–B3, C1–C2), and 6 basic isozymes (E1–E6) [100]. Some of these isozymes have pI values over 12! There are more than 30 gene sequences just for Mn peroxidases from various fungi in the NCBI database. It seems the possibilities are limited mainly by the implementation of desired selection schema.

LITERATURE CITED

1. **Abelskov, A. K., A. T. Smith, C. B. Rasmussen, H. B. Dunford, and K. Welinder.** 1997. pH dependence and structural interpretation of the reactions of *Coprinus cinereus* peroxidase with hydrogen peroxide, ferulic acid, and 2,2′-azinobis(3-ethylbenzthiazoline-6-sulfonic) acid. Biochemistry **36:**9453–9463.

2. **Aitken, M. D. and R. L. Irvine.** 1989. Stability testing of ligninase and Mn-peroxidase from *Phanerochaete chrysosporium.* Biotechnol. Bioengin. **34:**1251–1260.

3. **Aitken, M. D. and R. L. Irvine.** 1990. Characterization of reactions catalyzed by manganese peroxidase from *Phanerochaete chrysosporium.* Arch. Biochem. Biophys. **276:**405–414.

4. **Alic, M., L. Akileswaran, and M. H. Gold.** 1997. Characterization of the gene encoding manganese peroxidase isozyme 3 from *Phanerochaete chrysosporium.* Biochim. Biophys. Acta **1338:**1–7.

5. **Alic, M., E. K. Clark, J. R. Kornegay, and M. H. Gold.** 1990. Transformation of *Phanerochaete chrysosporium* and *Neurospora crassa* with adenine biosynthetic genes from *Schizophyllum commune.* Curr. Genet. **17:**305–311.

6. **Alic, M. and M. H. Gold.** 1985. Genetic recombination in the lignin-degrading basidiomycete *Phanerochaete chrysosporium.* Appl. Environ. Microbiol. **50:**27–30.

7. **Alic, M., J. R. Kornegay, D. Pribnow, and M. H. Gold.** 1989. Transformation by complementation of an adenine auxotroph of the lignin-degrading basidiomycete *Phanerochaete chrysosporium.* Appl. Environ. Microbiol. **55:**406–411.

8. **Alic, M., C. Letzring, and M. H. Gold.** 1987. Mating system and basidiospore formation in the lignin-degrading basidiomycete *Phanerochaete chrysosporium.* Appl. Environ. Microbiol. **53:**1464–1469.

9. **Alic, M., M. B. Mayfield, L. Akileswaran, and M. H. Gold.** 1991. Homologous transformation of the lignin-degrading basidiomycete *Phanerochaete chrysosporium*. Curr. Genet. **19:**491–494.

10. **Ambert-Balay, K., M. Dougherty, and M. Tien.** 2000. Reactivity of manganese peroxidase: site-directed mutagenesis of residues in proximity to the porphyrin ring. Arch. Biochem. Biophys. **382:**89–94.

11. **Andrawis, A., E. A. Pease, I. Kuan, E. Holzbaur, and M. Tien.** 1989. Characterization of two lignin peroxidase clones from *Phanerochaete chrysosporium*. Biochem. Biophys. Res. Commun. **162:**673–680.

12. **Arnold, F. H., P. L. Wintrode, K. Miyazaki, and A. Gershenson.** 2001. How enzymes adapt: lessons from directed evolution. Trends Biochem. Sci. **26:**100–106.

13. **Artolozaga, M. J., E. Kubatova, J. Volc, and H. M. Kalisz.** 1997. Pyranose 2-oxidase from *Phanerochaete chrysosporium*—further biochemical characterization. Appl. Microbiol. Biotechnol. **47:**508–514.

14. **Asada, Y., Y. Kimura, M. Kuwahara, A. Tsukamoto, K. Koide, and A. Oka.** 1988. Cloning and sequencing of a ligninase gene from a lignin-degrading basidiomycete, *Phanerochaete chrysosporium*. Appl. Microbiol. Biotechnol. **29:**469–473.

15. **Asada, Y., A. Watanabe, T. Irie, T. Nakayama, and M. Kuwahara.** 1995. Structures of genomic and complementary DNAs coding for *Pleurotus ostreatus* manganese (II) peroxidase. Biochim. Biophys. Acta **1251:**205–209.

16. **Attalla, R. H. and U. P. Agrawal.** 1985. Raman microprobe evidence for lignin orientation in the cell walls of native woody tissues. Science **227:**636–638.

17. **Baghorn, E. S.** 1964. Evolution of cambium in geologic time. *In* The Formation of Wood in Forest Trees (Zimmerman, M. H., Ed.). Academic Press, New York. pp. 3–17.

18. **Baldrian, P., J. Gabriel, and F. Nerud.** 1996. Effect of cadmium on the ligninolytic activity of *Stereum hirsutum* and *Phanerochaete chrysosporium*. Fol. Microbiol. **41:**363–367.

19. **Baldrian, P., F. Nerud., F. Zadrazil, C. in der Wiesche, and J. Gabriel.** 1998. Effect of cadmium on the biodegradative ability of *Pleurotos ostreatus*. *In* Sixth International Mycological Congress IMC6, Jerusalem. Kenes, Inc., Tel Aviv. p. 107.

20. **Banci, L., I. Bertini, T. Bini, M. Tien, and P. Turano.** 1993. Binding of horseradish, lignin, and manganese peroxidases to their respective substrates. Biochemistry **32:**5825–5831.

21. **Banci, L., I. Bertini, C. Capannoli, R. Del Conte, and M. Tien.** 1999. Spectroscopic characterization of active mutants of manganese peroxidase: mutations on the proximal side affect calcium binding of the distal side. Biochemistry **38:**9617–9625.

22. **Banci, L., I. Bertini, L. Dal Pozzo, R. Del Conte, and M. Tien.** 1998. Monitoring the role of oxalate in manganese peroxidase. Biochemistry **37:**9009–9015.

23. **Banci, L., I. Bertini, I. C. Kuan, M. Tien, P. Turano, and A. J. Vila.** 1993. NMR investigation of isotopically labeled cyanide derivatives of lignin peroxidase and manganese peroxidase. Biochemistry **32:**13483–13489.

24. **Banci, L., I. Bertini, E. A. Pease, M. Tien, and P. Turano.** 1992. ^{1}H NMR investigation of manganese peroxidase from *Phanerochaete chrysosporium*. A comparison with other peroxidases. Biochemistry **31:**10009–10017.

25. **Banci, L., I. Bertinini, P. Turano, M. Tien, and T. K. Kirk.** 1991. Proton NMR investigation into the basis for the relatively high redox potential of lignin peroxidase. Proc. Natl. Acad. Sci. U.S.A. **88:**6956–6960.

26. **Banci, L., S. Ciofi-Baffoni, and M. Tien.** 1999. Lignin and Mn peroxidase-catalyzed oxidation of phenolic lignin oligomers. Biochemistry **38:**3205–3210.

27. **Bao, W., Y. Fukushima, K. A. Jensen, Jr., M. A. Moen, and K. E. Hammel.** 1994. Oxidative degradation of non-phenolic lignin during lipid peroxidation by fungal manganese peroxidase. FEBS Lett. **354:**297–300.

28. **Barceloux, D. G.** 1999. Manganese. J. Toxicol.-Clin. Toxicol. **37:**293–307.

29. **Bar-Lev, S. S. and T. K. Kirk.** 1981. Effects of molecular oxygen on lignin degradation by *Phanerochaete chrysosporium*. Biochem. Biophys. Res. Commun. **99:**373–378.

30. **Barr, D. P., M. M. Shah, T. A. Grover, and S. D. Aust.** 1992. Production of hydroxyl radical by lignin peroxidase from *Phanerochaete chrysosporium*. Arch. Biochem. Biophys. **298:**480–485.

31. **BenHamman, O., T. deLaRubia, and J. Martinez.** 1997. Effect of carbon and nitrogen limitation on lignin peroxidase and manganese peroxidase production by *Phanerochaete flavido-alba*. J. Appl. Microbiol. **83:**751–757.

32. **Bietti, M., E. Baciocchi, and S. Steenken.** 1998. Lifetime, reduction potential and base-induced fragmentation of the veratryl alcohol radical cation in aqueous solution. Pulse radiolysis studies on a ligninase "mediator." J. Phys. Chem. A **102:**7337–7342.

33. **Bisaria, V. S. and T. K. Ghose.** 1981. Biodegradation of cellulosic materials: substrates, microorganisms, enzymes and products. Enzyme Microb. Technol. **3:**90–104.

34. **Blanchette, R. A.** 1984. Screening wood decayed by white-rot fungi for preferential lignin degradation. Appl. Environ. Microbiol. **48:**647–653.

35. **Blanchette, R. A.** 1984. Manganese accumulation in wood decayed by white rot fungi. Phytopathology **74:**725–730.

36. **Blanchette, R. A.** 1991. Delignification by wood-decay fungi. Annu. Rev. Phytopathol. **29:**381–398.

37. **Blanchette, R. A. and C. G. Shaw.** 1978. Associations among bacteria, yeasts and basidiomycetes during wood decay. Phytopathology **68:**684–690.

38. **Blanchette, R. A., J. B. Sutherland, and D. L. Crawford.** 1981. Actinomycetes in discolored wood of living silver maple. Can. J. Bot. **59:**1–7.

39. **Blumberg, W. E., J. Peisach, B. A. Wittenberg, and J. B. Wittenberg.** 1968. The electronic structure of protoheme proteins. I. An electron study of horseradish peroxidase and its derivatives. J. Biol. Chem. **243:**1854–1862.

40. **Bockle, B., M. J. Martinez, F. Guillen, and A. T. Martinez.** 1999. Mechanism of peroxidase inactivation in liquid cultures of the ligninolytic fungus *Pleurotus pulmonarius*. Appl. Environ. Microbiol. **65:**923–928.

41. **Boe, J. F., P. Goulas, and J. L. Seris.** 1993. Effect of organic acids on reactions catalyzed by manganese peroxidase from *Phanerochaete chrysosporium*. Biocatalysis **7:**297–308.

42. **Bogan, B. W. and R. T. Lamar.** 1996. Polycyclic aromatic hydrocarbon-degrading capabilities of *Phanerochaete laevis* HHB-1625 and its extracellular ligninolytic enzymes. Appl. Environ. Microbiol. **62:**1597–1603.

43. **Bogumil, R., R. Kappl, J. Huettermann, and H. Witzel.** 1997. Electron paramagnetic resonance of D-xylose isomerase: evidence for metal ion movement induced by binding of cyclic substrates and inhibitors. Biochemistry **36:**2345–2352.

44. **Bonagura, C. A., M. Sundaramoorthy, H. S. Pappa, W. R. Patterson, and T. L. Poulos.** 1996. An engineered cation site in cytochrome *c* peroxidase alters the reactivity of the redox active tryptophan. Biochemistry **35:**6107–6115.

45. **Bonnarme, P. and T. W. Jeffries.** 1990. Mn(II) regulation of lignin peroxidases and manganese-dependent peroxidases from lignin-degrading white rot fungi. Appl. Environ. Microbiol. **56:**210–217.

46. **Bonnen, A., L. Anton, and A. B. Orth.** 1994. Lignin-degrading enzymes of the commercial button mushroom, *Agaricus bisporus*. Appl. Environ. Microbiol. **60:**960–965.

47. **Boudet, A. M., C. Lapierre, and J. Grima-Pettenati.** 1995. Biochemistry and molecular biology of lignification. New Phytol. **129:**203–236.

48. **Brock, B. J., S. Rieble, and M. H. Gold.** 1995. Purification and characterization of a 1,4-benzoquinone-reductase from the basidiomycete *Phanerochaete chrysosporium*. Appl. Environ. Microbiol. **61:**3076–3081.

49. **Brown, J. A., M. Alic, and M. H. Gold.** 1991. Manganese peroxidase gene transcription in *Phanerochaete chrysosporium*: activation by manganese. J. Bacteriol. **173:**4101–4106.

50. **Brown, J. A., J. K. Glenn, and M. H. Gold.** 1990. Manganese regulates expression of manganese peroxidase by *Phanerochaete chrysosporium*. J. Bacteriol. **172:**3125–3130.

51. **Brumer, H., P. F. G. Sims, and M. L. Sinnott.** 1999. Lignocellulose degradation by *Phanerochaete chrysosporium*: purification and characterization of the main α-galactosidase. Biochem. J. **339:**43–53.

52. **Burdsall, H. H., Jr.** 1981. The taxonomy of *Sporotrichum pruinosum* and *Sporotrichum pulverentum*/*Phanerochaete chrysosporium*. Mycologia **73:**675–680.

53. **Burdsall, H. H., Jr. and W. E. Eslyn.** 1974. A new *Phanerochaete* with a *chrysosporium* imperfect state. Mycotaxon **1:**123–133.

54. **Burlat, V., K. Ambert, K. Ruel, and J.-P. Joseleau.** 1997. Relationship between the nature of lignin and the morphology of degradation performed by white-rot fungi. Plant Physiol. Biochem. **35:**645–654.

55. **Burlat, V., M. Kwon, L. B. Davin, and N. G. Lewis.** 2001. Dirigent proteins and dirigent sites in lignifying tissues. Phytochemistry **57:**883–897.

56. **Buswell, J. A., Y. Cai, and S.-T. Chang.** 1995. Effect of nutrient nitrogen and manganese on manganese peroxidase and laccase production by *Lentinula (Lentinus) edodes*. FEMS Microbiol. Lett. **128:**81–88.

57. **Buswell, J., Y. Cai, S. Chang, J. Peberdy, S. Fu, and H. Yu.** 1996. Lignocellulytic enzyme profiles of edible mushroom fungi. World J. Microbiol. Biotechnol. **12:**537–542.

58. **Buswell, J. A. and K.-E. L. Eriksson.** 1979. Intracellular quinone reduction in *Sporotrichum pulverulentum* by a NAD(P)H:quinone oxidoreductase. FEBS Lett. **108:**229–232.

58a. **Buswell, J. A. and E. Odier.** 1987. Lignin biodegradation. CRC Crit. Rev. Biotechnol. **6:**1–60.

59. **Butcher, J. A. and T. Nilsson.** 1982. Influence of variable lignin content amongst hardwoods on soft-rot susceptibility and performance of CCA perservatives. International Research Group on Wood Preservation Doc. No. IRG/WP/1151.

60. **Cai, D. and M. Tien.** 1993. Lignin-degrading peroxidases of *Phanerochaete chrysosporium*. J. Biotechnol. **30:**79–90.

61. **Caldwell, R. C. and G. F. Joyce.** 1994. Mutagenic PCR. PCR Methods Appl. **2:**28–33.

62. **Camarero, S., S. Sarkar, F. J. Ruiz-Duenas, M. J. Martinez, and A. T. Martinez.** 1999. Description of a versatile peroxidase involved in the natural degradation of lignin that has both manganese peroxidase and lignin peroxidase substrate interaction sites. J. Biol. Chem. **274:**10324–10330.

63. **Camarero, S. B., M. Bockle, M. J. Martinez, and A. T. Martinez.** 1996. Manganese-mediated lignin degradation by *Pleurotus pulmonarius*. Appl. Environ. Microbiol. **62:**1070–1072.

64. **Cameron, M. D., S. Timofeevski, and S. D. Aust.** 2000. Enzymology of *Phanerochate chrysosporium* with respect to the degradation of recalcitrant compounds and xenobiotics. Appl. Microbiol. Biotechnol. **54:**751–758.

65. **Candeias, L. P. and P. J. Harvey.** 1995. Lifetime and reactivity of the veratryl alcohol radical cation. Implications for lignin peroxidase catalysis. J. Biol. Chem. **270:**16745–16748.

66. **Caramelo, L., M. J. Martinez, and A. T. Martinez.** 1999. A search for ligninolytic peroxidases in the fungus *Pleurotus eryngii* involving α-keto-γ-

thiomethylbutyric acid and lignin model dimers. Appl. Environ. Microbiol. **65:**916–922.

67. **Cheek, J., D. Mandelman, T. L. Poulos, and J. H. Dawson.** 1999. A study of the K^+-site mutant of ascorbate peroxidase: mutations of protein residues on the proximal side of the heme cause changes in iron ligation on the distal side. J. Biol. Inorg. Chem. **4:**64–72.

68. **Cherry, J. R., M. H. Lamsa, P. Schneider, J. Vind, A. Svendsen, A. Jones, and A. H. Pedersen.** 1999. Directed evolution of a fungal peroxidase. Nat. Biotechnol. **17:**379–384.

69. **Choi, S. and T. G. Spiro.** 1983. Out-of-plane deformation modes in the resonance Raman spectra of metalloporphyrins and heme proteins. J. Am. Chem. Soc. **105:**3683–3692.

70. **Choi, S., T. G. Spiro, K. C. Langry, K. M. Smith, D. L. Budd, and G. N. LaMar.** 1982. Structural correlations and vinyl influences in resonance Raman spectra of protoheme complexes and proteins. J. Am. Chem. Soc. **104:**4345–4351.

71. **Choinowski, T., W. Blodig, K. H. Winterhalter, and K. Piontek.** 1999. The crystal structure of lignin peroxidase at 1.70 Å resolution reveals a hydroxy group on the C-β of tryptophan 171: a novel radical site formed during the redox cycle. J. Mol. Biol. **286:**809–827.

72. **Christianson, D. W.** 1997. Structural chemistry and biology of manganese metalloenzymes. Prog. Biophys. Mol. Biol. **67:**217–252.

73. **Chung, N. and S. D. Aust.** 1995. Veratryl alcohol-mediated indirect oxidation of phenol by lignin peroxidase. Arch. Biochem. Biophys. **316:**733–737.

74. **Copa-Patino, J.-L. and P. Broda.** 1994. A *Phanerochaete chrysosporium* β-D-xylosidase with specificity for (1-3)-β-D-glucan linkages. Carbohyd. Res. **253:**265–275.

75. **Copa-Patino, J.-L., Y. B. Kim, and P. Broda.** 1993. Production and initial characerization of the xylan-degrading system of *Phanerochaete chrysosporium*. Appl. Microbiol. Biotechnol. **40:**69–76.

76. **Cotton, F. A. and G. Wilkinson.** 1980. Advanced Inorganic Chemistry: A Comprehensive Text, 4th Ed. Wiley Interscience, New York.

77. **Cowling, E. B. and W. Merrill.** 1966. Nitrogen in wood and its role in wood deterioration. Can. J. Bot. **44:**1539–1554.

78. **Crawford, D. L. and J. B. Sutherland.** 1980. Isolation and characterization of lignocellulose-decomposing actinomycetes. *In* Lignin Biodegradation: Microbiology, Chemistry and Applications, Vol. II (Kirk, T. K., T. Higuchi, and H.-M. Chang, Eds.). CRC Press, Boca Raton, FL. pp. 95–101.

79. **Crawford, R. L.** 1981. Lignin Biodegradation and Transformation. Wiley, New York.

80. **Crawford, R. L., D. L. Crawford, and G. J. Dizikes.** 1981. Catabolism of a lignin substructure model compound dehydrovanillin by a lignin-degrading *Streptomyces*. Arch. Microbiol. **41:**1112–1116.

81. **Cromack, K. J., P. Sollins, R. L. Todd, R. Fogel, A. W. Todd, W. M. Fender, M. E. Crossley, and D. A. J. Crossley.** 1977. The role of oxalic acid and bicarbonate in calcium cycling by fungi and bacteria: some possible implications for soil animals. Ecol. Bull. **25:**246–252.

82. **Crowley, J. D., D. A. Traynor, and D. C. Weatherburn.** 2000. Enzymes and proteins containing manganese: an overview. *In* Manganese and Its Role in Biological Processes (Sigel A. and H. Sigel, Eds.). Marcel Dekker, New York. pp. 211–278.

83. **Cui, F. and D. Dolphin.** 1991. Veratryl alcohol as a mediator in lignin model compound biodegradation. Holzforschung **45:**31–35.

84. **Daniel, G., T. Nilsson, and B. Pettersson.** 1989. Intra- and extracellular localization of lignin peroxidase during the degradation of solid wood and wood fragments by *Phanerochaete chrysosporium* by using transmission electron microscopy and immuno-gold labeling. Appl. Environ. Microbiol. **55:**871–881.

85. **Daniel, G., B. Pettersson, T. Nilsson, and J. Volc.** 1990. Use of immunogold cytochemistry to detect Mn^{II}-dependent and lignin peroxidases in wood degraded by the white rot fungi *Phanerochaete chyrsosporium* and *Lentinula edodes*. Can. J. Bot. **68:**920–933.

86. **Daniel, G., J. Volc, and E. Kubatova.** 1994. Pyranose oxidase, a major source of H_2O_2 during wood degradation by *Phanerochaete chrysosporium, Trametes versicolor,* and *Oudemansiella mucida*. Appl. Environ. Microbiol. **60:**2524–2532.

87. **Daniel, G., J. Volc, E. Kubatova, and T. Nilsson.** 1992. Ultrastructural and immunocytochemical studies on the H_2O_2-producing enzyme pyranose oxidase in *Phanerochaete chrysosporium* grown under liquid culture conditions. Appl. Environ. Microbiol. **58:**3667–3676.

88. **D' Annibale, A., C. Crestini, E. Di Mattia, and G. Giovannozzi Sermanni.** 1996. Veratryl alcohol oxidation by manganese-dependent peroxidase from *Lentinus edodes*. J. Biotechnol. **48:**231–239.

89. **Dass, S. B., C. G. Dosoretz, C. A. Reddy, and H. E. Grethlein.** 1995. Extracellular proteases produced by the wood-degrading fungus *Phanerochaete chrysosporium* under ligninolytic and non-ligninolytic conditions. Arch. Microbiol. **163:**254–258.

90. **Datta, A.** 1992. Purification and characterization of a novel protease from solid substrate cultures of *Phanerochaete chrysosporium*. J. Biol. Chem. **267:**728–736.

91. **Datta, A., A. Bettermann, and T. K. Kirk.** 1991. Identification of a specific manganese peroxidase among ligninolytic enzymes secreted by *Phanerochaete chrysosporium* during wood decay. Appl. Environ. Microbiol. **57:**1453–1460.

92. **Davin, L. B., H. B. Wang, A. L. Crowell, D. L. Bedgar, D. M. Martin, S. Sarkanen, and N. G. Lewis.** 1997. Stereoselective bimolecular phenoxy radical coupling by an auxiliary (dirigent) protein without an active center. Science **275:**362–366.

93. **Demmer, H., I. Hinz, H. Keller-Rudex, K. Koeber, H. Kottelwesch, and D. Schneider.** 1980. Complexes and salts of carboxylic acids and their derivatives. *In* Coordination Compounds of Manganese, 8th Ed., Vol. 56 (Schleitzer-Rust, E., Ed.). Springer-Verlag, New York. pp. 1–196.

94. **DePillis, G. D., H. Wariishi, M. H. Gold, and P. R. Ortiz de Montellano.** 1990. Inactivation of lignin peroxidase by phenylhydrazine and sodium azide. Arch. Biochem. Biophys. **280:**217–223.

95. **Dix, N. J. and J. Webster.** 1995. Fungal Ecology. Chapman and Hall, London, U.K.

96. **Doerge, D., A. Taurog, and M. Dorris.** 1994. Evidence for a radical mechanism in peroxidase catalyzed coupling. II. Single turnover experiments with horseradish peroxidase. Arch. Biochem. Biophys. **315:**90–99.

97. **Donaldson, L.** 2001. Lignification and lignin topochemistry: an ultrastructural view. Phytochemistry **57:**859–873.

98. **D' Souza, T. M., K. Boominathan, and C. A. Reddy.** 1996. Isolation of laccase gene-specific sequences from white-rot and brown-rot fungi by PCR. Appl. Environ. Microbiol. **62:**3739–3744.

99. **Ducros, V., A. M. Brzozowski, K. S. Wilson, S. H. Brown, P. Ostergaard, P. Schneider, D. S. Yaver, A. H. Pedersen, and G. J. Davies.** 1998. Crystal structure of the type-2 Cu depleted laccase from *Coprinus cinereus* at 2.2 Å resolution. Nat. Struct. Biol. **5:**310–316.

100. **Dunford, H. B.** 1999. Heme Peroxidases. Wiley-VCH, New York.

101. **Dunford, H. B. and J. S. Stillman.** 1976. On the function and mechanism of action of peroxidase. Coord. Chem. Rev. **19:**187–251.

102. **Dutton, M. V. and C. S. Evans.** 1996. Oxalate production by fungi: it's role in pathogenicity and ecology in the soil environment. Can. J. Microbiol. **42:**881–895.

103. **Dutton, M. V., C. S. Evans, P. T. Atkey, and D. A. Wood.** 1992. Oxalate production in Basidiomycetes, including the white-rot species *Coriolus versicolor* and *Phanerochaete chrysosporium*. Appl. Microbiol. Biotechnol. **39:**5–10.

104. **Dzedzyulya, E. I. and E. G. Becker.** 2000. Mn-peroxidase from *Bjerkandera adusta* 90–41. Purification and substrate specificity. Biochemistry (Moscow) **65:**707–712.

105. **Edwards, S. L., R. Raag, H. Wariishi, M. H. Gold, and T. L. Poulos.** 1993. Crystal structure of lignin peroxidase. Proc. Natl. Acad. Sci. U.S.A. **90:**750–754.

106. **Eggert, C., U. Temp, J. F. D. Dean, and K. E. L. Erksson.** 1996. A fungal metabolite mediates degradation of non-phenolic lignin structures and synthetic lignin by laccase. FEBS Lett. **391:**144–148.

107. **Eggert, C., U. Temp, and K. E. Eriksson.** 1996. The ligninolytic system of the white rot fungus *Pycnoporus cinnabarinus*: purification and characterization of the laccase. Appl. Environ. Microbiol. **62:**1151–1158.

108. **Elisashvili, V. I., T. S. Khardziani, N. D. Tsiklauri, and E. T. Kachlishvili.** 1999. Cellulase and xylanase activities in higher basidiomycetes. Biochemistry (Moscow) **64:**718–722.

109. **Enoki, A., G. Goldsby, K. Krisnangkura, and M. H. Gold.** 1981. Degradation of the lignin model compounds 4-ethoxy-3-methoxyphenylglycol

β-guaiacyl and vanillic acid ethers by *Phanerochaete chrysosporium*. FEMS Microbiol. Lett. **10:**373–377.

110. **Eriksson, K.-E., R. A. Blanchette, and P. Ander.** 1990. Biodegradation of lignin. *In* Microbial and Enzymatic Degradation of Wood and Wood Components (Timell, T. E., Ed.). Springer-Verlag KG, Berlin. pp. 225–333.

111. **Eriksson, K.-E. L., R. A. Blanchette, and P. Ander.** 1990. Morphological aspects of wood degradation by fungi and bacteria. *In* Microbial and Enzymatic Degradation of Wood and Wood Components (Timell, T. E., Ed.). Springer-Verlag, Berlin. pp. 1–72.

112. **Evans, C. S.** 1985. Laccase activity in lignin degradation by *Coriolus versicolor* in vivo and in vitro studies. FEMS Microbiol. Lett. **27:**339–343.

113. **Fahraeus, G. and H. Ljunggren.** 1961. Monophenolase and polyphenolase activity of fungal laccase. Biochim. Biophys. Acta **54:**192–194.

114. **Faison, B. D. and T. K. Kirk.** 1983. Relationship between lignin degradation and production of reduced oxygen species by *Phanerochaete chrysosporium*. Appl. Environ. Microbiol. **46:**1140–1145.

115. **Farmer, V. C., M. E. K. Henderson, and J. D. Russell.** 1960. Aromatic-alcohol-oxidase activity in the growth medium of *Polystictus versicolor*. Biochem. J. **74:**257–262.

116. **Fee, J. A. and B. G. Malmstrom.** 1968. The redox potential of fungal laccase. Biochim. Biophys. Acta **153:**299–302.

117. **Fengel, D. and G. Wegener.** 1984. Wood: Chemistry, Ultrastructure, Reactions. Walter de Gruyter, Berlin, New York.

118. **Ferrer, J. C., P. Turano, L. Banci, I. Bertinin, I. K. Morris, K. M. Smith, M. Smith, and G. M. Mauk.** 1994. Active site coordination chemistry of the cytochrome *c* peroxidase Asp235Ala variant: spectroscopic and functional characterization. Biochemistry **33:**7819–7829.

119. **Finzel, B. C., T. L. Poulos, and J. Kraut.** 1984. Crystal structure of yeast cytochrome *c* peroxidase refined at 1.7-Å resolution. J. Biol. Chem. **259:**13027–13036.

120. **Forrester, I. T., A. C. Grabski, R. R. Burgess, and G. F. Leatham.** 1988. Manganese, Mn-dependent peroxidases, and the biodegradation of lignin. Biochem. Biophys. Res. Commun. **157:**992–999.

121. **Frausto da Silva, J. R. R. and R. J. P. Williams.** 1991. The Biological Chemistry of the Elements: The Inorganic Chemistry of Life. Oxford University Press, New York.

122. **Fry, S. C.** 1986. Cross-linking of matrix polymers in the growing cell walls of angiosperms. Annu. Rev. Plant Physiol. Plant Mol. Biol. **37:**165–186.

123. **Fu, S. Y., H.-S. Yu, and J. A. Buswell.** 1997. Effect of nutrient nitrogen and manganese on manganese peroxidase and laccase production by *Pleurotus sajor-caju*. FEMS Microbiol. Lett. **147:**133–137.

124. **Fujii, H., M. G. Finnegan, T. Miki, B. R. Crouse, K. Kakinuma, and M. K. Johnson.** 1995. Spectroscopic identification of the heme axial ligation of cytochrome b_{558} in the NADPH oxidase of porcine neutrophils. FEBS Lett. **377:**345–348.

125. **Gajhede, M., D. J. Schuller, A. Henriksen, A. T. Smith, and T. L. Poulos.** 1997. Crystal structure of horseradish peroxidase C at 2.15 angstrom resolution. Nat. Struct. Biol. **4:**1032–1038.

126. **Galliano, H., G. Gas, J. L. Seris, and A. M. Boudet.** 1991. Lignin degradation by *Rigidoporus lignosus* involves synergistic action of two oxidizing enzymes: Mn peroxidase and laccase. Enzyme Microb. Technol. **13:**478–482.

127. **Gang, D. R., M. A. Costa, M. Fujita, A. T. Dinkova Kostova, H. B. Wang, V. Burlat, W. Martin, S. Sarkanen, L. B. Davin, and N. G. Lewis.** 1999. Regiochemical control of monolignol radical coupling: a new paradigm for lignin and lignan biosynthesis. Chem. Biol. **6:**143–151.

128. **George, S. J., M. Kvaratskhelia, M. J. Dilworth, and R. N. F. Thorneley.** 1999. Reversible alkaline inactivation of lignin peroxidase involves the release of both the distal and proximal site calcium ions and bishistidine co-ordination of the haem. Biochem. J. **344:**237–244.

129. **Gettemy, J. M., B. Ma, R. Alic, and M. H. Gold.** 1998. Reverse transcription PCR analysis of the regulation of the manganese peroxidase gene family. Appl. Environ. Microbiol. **64:**569–574.

130. **Giardina, P., V. Aurilia, R. Cannio, L. Marzullo, A. Amoresano, R. Siciliano, P. Pucci, and G. Sannia.** 1996. The gene, protein and glycan structures of laccase from *Pleurotus ostreatus*. Eur. J. Biochem. **235:**508–515.

131. **Giffhorn, F.** 2000. Fungal pyranose oxidase: occurence, properties and biotechnical applications in carbohydrate chemistry. Appl. Microbiol. Biotechnol. **54:**727–740.

132. **Gilardi, G., P. J. Harvey, A. E. Cass, and J. M. Palmer.** 1990. Radical intermediates in veratryl alcohol oxidation by ligninase. NMR evidence. Biochim. Biophys. Acta **1041:**129–132.

133. **Gilbertson, R. L.** 1980. Wood-rotting fungi of North America. Mycologia **72:**1–49.

134. **Gilbertson, R. L.** 1981. North American wood-rotting fungi that cause brown rots. Mycotaxon **12:**372–416.

135. **Glenn, J. K., L. Akileswaran, and M. H. Gold.** 1986. Mn(II) oxidation is the principal function of the extracellular Mn-peroxidase from *Phanerochaete chrysosporium*. Arch. Biochem. Biophys. **251:**688–696.

136. **Glenn, J. K. and M. H. Gold.** 1985. Purification and characterization of an extracellular Mn^{II}-dependent peroxidase from the lignin-degrading basidiomycete, *Phanerochaete chrysosporium*. Arch. Biochem. Biophys. **242:**329–341.

137. **Glenn, J. K., M. A. Morgan, M. B. Mayfield, M. Kuwahara, and M. H. Gold.** 1983. An extracellular H_2O_2-requiring enzyme preparation involved in lignin biodegradation by the white rot basidiomycete *Phanerochaete chrysosporium*. Biochem. Biophys. Res. Commun. **114:**1077–1083.

138. **Godfrey, B. J., L. Akileswaran, and M. H. Gold.** 1994. A reporter gene construct for studying the regulation of manganese peroxidase gene expression. Appl. Environ. Microbiol. **60:**1353–1358.

139. **Godfrey, B. J., M. B. Mayfield, J. A. Brown, and M. H. Gold.** 1990. Characterization of a gene encoding a manganese peroxidase from *Phanerochaete chrysosporium*. Gene **93:**119–124.

140. **Gold, M. H. and M. Alic.** 1993. Molecular biology of the lignin-degrading basidiomycete *Phanerochaete chrysosporium*. Microbiol. Rev. **57:**605–622.

141. **Gold, M. H. and T. M. Cheng.** 1979. Conditions for fruit body formation in the white rot basidiomycete *Phanerochaete chrysosporium*. Arch. Microbiol. **121:**37–41.

142. **Gold, M. H., M. Kuwahara, A. A. Chiu, and J. K. Glenn.** 1984. Purification and characterization of an extracellular H_2O_2-requiring

diarylpropane oxygenase from the white rot basidiomycete, *Phanerochaete chrysosporium*. Arch. Biochem. Biophys. **234:**353–362.

143. **Gold, M. H., H. Wariishi, and K. Valli.** 1989. Extracellular peroxidases involved in lignin degradation by the white rot basidiomycete *Phanerochaete chrysosporium*. ACS Symp. Ser. **389:**127–140.

144. **Gold, M. H., H. L. Youngs, and M. D. Sollewijn Gelpke.** 2000. Manganese peroxidase. *In* Manganese and Its Role in Biological Processes (Sigel, A. and H. Sigel, Eds.). Marcel Dekker, New York. pp. 559–586.

145. **Golovleva, L. A., A. A. Leontievsky, O. V. Maltseva, and N. M. Myasoedova.** 1993. Ligninolytic enzymes of the fungus *Panus tigrinus* 8/18: biosynthesis, purification and properties. J. Biotechnol. **30:**71–77.

146. **Goodell, B., J. Jellison, J. Liu, G. Daniel, A. Paszczynski, F. Fekete, S. Krishnamurthy, L. Jun, and G. Xu.** 1997. Low molecular weight chelators and phenolic compounds isolated from wood decay fungi and their role in the fungal biodegradation of wood. J. Biotechnol. **53:**133–162.

147. **Goodin, D. B. and D. E. McRee.** 1993. The Asp-His-Fe triad of cytochrome *c* peroxidase controls the reduction potential, electronic structure, and coupling of the tryptophan free radical to the heme. Biochemistry **32:**3313–3324.

148. **Goodwin, D. C., S. D. Aust, and T. A. Grover.** 1995. Evidence for veratryl alcohol as a redox mediator in lignin peroxidase-catalyzed oxidation. Biochemistry **34:**5060–5065.

149. **Grabski, A. C., J. K. Rasmussen, P. L. Coleman, and R. R. Burgess.** 1996. Immobilization of manganese peroxidase from *Lentinula edodes* on alkylaminated Emphaze AB 1 polymer for generation of Mn^{3+} as an oxidizing agent. Appl. Biochem. Biotechnol. **60:**1–17.

150. **Greaves, H.** 1969. Micromorphology of the bacterial attack on wood. Wood Sci. Technol. **3:**150–166.

151. **Greaves, H.** 1970. The effect of some wood-inhabiting bacteria on the permeability characteristics and microscopic features of *Eucalyptus regnans* sapwoods and *Pinus radiata* heartwood. Holzforschung **24:**6–14.

152. **Grisebach, H.** 1981. Lignins. *In* The Biochemistry of Plants, Vol. 7 (Conn, E. E.. Ed.). Academic Press, New York. pp. 457–478.

153. **Guillen, F., A. T. Martinez, and M. J. Martinez.** 1992. Substrate specificity and properties of the aryl-alcohol oxidase from the ligninolytic fungus *Pleurotus eryngii*. Eur. J. Biochem. **209:**603–611.

154. **Gutheil, W. G., M. E. Stefanova, and R. A. Nicholas.** 2000. Fluorescent coupled enzyme assays for D-alanine: application to penicillin-binding protein and vancomycin activity assays. Anal. Biochem. **287:**196–202.

155. **Ha, H.-C., Y. Honda, T. Watanabe, and M. Kuwahara.** 2001. Production of manganese peroxidase by pellet culture of the lignin-degrading basidiomycete, *Pleurotus ostreatus*. Appl. Microbiol. Biotechnol. **55:**704–711.

156. **Haemmerli, S. D., M. S. Leisola, D. Sanglard, and A. Fiechter.** 1986. Oxidation of benzo(a)pyrene by extracellular ligninases of *Phanerochaete chrysosporium*. Veratryl alcohol and stability of ligninase. J. Biol. Chem. **261:**6900–6903.

157. **Haemmerli, S. D., H. E. Schoemaker, H. W. H. Schmidt, and M. S. A. Leisola.** 1987. Oxidation of veratryl alcohol by the lignin peroxidase of *Phanerochaete chrysosporium*: involvement of activated oxygen. FEBS Lett. **220:**149–154.

158. **Hammel, K. E.** 1989. Organopollutant degradation by ligninolytic fungi. Enzyme Microb. Technol. **11:**776–777.

159. **Hammel, K. E., W. Z. Gai, B. Green, and M. A. Moen.** 1992. Oxidative degradation of phenanthrene by the ligninolytic fungus *Phanerochaete chrysosporium*. Appl. Environ. Microbiol. **58:**1832–1838.

159a. **Hammel, K. E., K. A. Jensen, Jr., M. D. Mozuch, L. L. Landucci, M. Tien, and E. A. Pease.** 1993. Ligninolysis by a purified lignin peroxidase. J. Biol. Chem. **268:**12274–12281.

160. **Hammel, K. E., B. Kalyanaraman, and T. K. Kirk.** 1986. Substrate free radicals are intermediates in ligninase catalysis. Proc. Natl. Acad. Sci. U.S.A. **83:**3708–3712.

161. **Hammel, K. E., M. D. Mozuch, K. A. Jensen, Jr., and P. J. Kersten.** 1994. H_2O_2 recycling during oxidation of the arylglycerol β-aryl ether lignin structure by lignin peroxidase and glyoxal oxidase. Biochemistry **33:**13349–13354.

162. **Hammel, K. E., P. J. Tardone, M. A. Moen, and L. A. Price.** 1989. Biomimetic oxidation of nonphenolic lignin models by Mn^{III}: new observations

on the oxidizability of guaiacyl and syringyl substructures. Arch. Biochem. Biophys. **270:**404–409.

163. **Harkin, J. M. and J. R. Obst.** 1973. Lignification in trees: indication of exclusive peroxidase participation. Science **180:**296–298.

164. **Harris, R. Z., H. Wariishi, M. H. Gold, and P. R. Ortiz de Montellano.** 1991. The catalytic site of manganese peroxidase. Regiospecific addition of sodium azide and alkylhydrazines to the heme group. J. Biol. Chem. **266:**8751–8758.

165. **Harvey, P. J. and J. M. Palmer.** 1990. Oxidation of phenolic compounds by ligninase. J. Biotechnol. **13:**169–179.

166. **Harvey, P. J., H. E. Schoemaker, and J. M. Palmer.** 1986. Veratryl alcohol as a mediator and the role of radical cations in lignin biodegradation by *Phanerochaete chrysosporium.* FEBS Lett. **195:**242–246.

167. **Harvey, P. J., H. E. Schoemaker, and J. M. Palmer.** 1987. Mechanisms of lignin catalysis. *In* Lignin Enzymic and Microbial Degradation (Odier, E., Ed.), INRA, Paris, pp. 125–130. (International Symposium, April 23–24, 1987, Paris)

168. **Hatakka, A.** 1994. Lignin-modifying enzymes from selected white-rot fungi: production and role in lignin degradation. FEMS Microbiol. Rev. **13:**125–135.

169. **Heinecke, J. W., W. Li, G. A. Francis, and J. A. Goldstein.** 1993. Tyrosyl radical generated by myeloperoxidase catalyzes the oxidative cross-linking of proteins. J. Clin. Invest. **91:**2866–2872.

170. **Heinfling, A., M. J. Martinez, A. T. Martinez, M. Bergbauer, and U. Szewzyk.** 1998. Purification and characterization of peroxidases form the dye-decolorizing fungus *Bjerkandera adusta.* FEMS Microbiol. Lett. **165:**45–50.

171. **Heinfling, A., F. J. Ruiz-Duenas, M. J. Martinez, M. Bergbauer, U. Szewzyk, and A. T. Martinez.** 1998. A study on reducing substrates of manganese-oxidizing peroxidases from *Pleurotus eryngii* and *Bjerkandera adusta.* FEBS Lett **428:**141–146.

172. **Henriksen, A., D. J. Schuller, K. Meno, K. G. Welinder, A. T. Smith, and M. Gajhede.** 1998. Structural interactions between horseradish peroxidase C and the substrate benzhydroxamic acid determined by X-ray crystallography. Biochemistry **37:**8054–8060.

173. **Henriksen, A., K. G. Welinder, and M. Gajhede.** 1998. Structure of barley grain peroxidase refined at 1.9-Å resolution—a plant peroxidase reversibly inactivated at neutral pH. J. Biol. Chem. **273:**2241–2248.

174. **Henriksson, G., A. Nutt, H. Henriksson, B. Pettersson, J. Stahlberg, G. Johansson, and G. Pettersson.** 1999. Endoglucanase 28 (Cel12A), a new *Phanerochaete chrysosporium* cellulase. Eur. J. Biochem. **259:**88–95.

175. **Hering, T. F.** 1982. Decomposing activity of basidiomycetes in forest litter., *In* Decomposer Basidiomycetes: Their Biology and Ecology (Frankland, J. C., J. N. Hedger, and M. J. Swift, Eds.). Cambridge University Press, Cambridge, New York. pp. 212–225.

176. **Higuchi, T.** 1985. Biosynthesis of lignin. *In* Biosynthesis and Biodegradation of Wood Components (Higuchi, T., Ed.). Academic Press, Orlando. pp. 141–160.

177. **Higuchi, T.** 1989. Mechanisms of lignin degradation by lignin peroxidase and laccase of white-rot fungi. *In* Plant Cell Wall Polymers: Biogenesis and Biodegradation (Lewis, N. G. and M. G. Paice, Eds.). ACS Symp. Ser. 399, American Chemical Society, Washington, DC. pp. 482–502.

178. **Higuchi, T.** 1990. Lignin biochemistry: biosynthesis and biodegradation. Wood Sci. Technol. **24:**23–63.

179. **Higuchi, T.** 1993. Biodegradation mechanism of lignin by white-rot basidiomycetes. J. Biotechnol. **30:**1–8.

180. **Hirofumi, H., M. Eiji, K. Yoshihiro, and F. Masao.** 2000. The 4-oxalomesaconate hydratase gene, involved in the protocatechuate 4,5-cleavage pathway, is essential to vanillate and syringate degradation in *Sphingomonas paucimobilis* SYK-6. J. Bacteriol. **184:**6950–6957.

181. **Holzbaur, E. L. F. and M. Tien.** 1988. Structure and regulation of a lignin peroxidase gene from *Phanerochaete chrysosporium*. Biochem. Biophys. Res. Commun. **55:**626–633.

182. **Homolka, L., F. Nerud, O. Kofronová, E. Novotná, and V. Machurová.** 1994. Degradation of wood by the basidiomycete *Coriolopsis occidentalis*. Fol. Microbiol. (Praha) **39:**37–43.

183. **Howes, B. D., J. N. Rodriguez-Lopez, A. T. Smith, and G. Smulevich.** 1997. Mutation of distal residues of horseradish peroxidase: influence on substrate binding and cavity properties. Biochemistry **36:**1532–1543.

184. **Howes, B. D., N. C. Veitch, A. T. Smith, C. G. White, and G. Smulevich.** 2001. Haem-linked interactions in horseradish peroxidase revealed by spectroscopic anlysis of the Phe221Met mutant. Biochem. J. **353:**181–191.

185. **Hudson, H. J.** 1980. Fungal Saprophytism, 2nd Ed. Edward Arnold, London.

186. **Hurst, H. M. and N. A. Burges.** 1967. Lignin and humic acids. *In* Soil Biochemistry (McLaren, A. D. and G. H. Peterson, Eds.). Marcel Dekker, New York. pp. 260–286.

187. **Hurst, J. K., T. M. Loehr, J. T. Curnutte, and H. Rosen.** 1991. Resonance Raman and electron paramagnetic resonance structural investigations of neutrophil cytochrome b_{558}. J. Biol. Chem. **226:**1627–1634.

188. **Iffland, A., P. Tafelmeyer, C. Saudan, and K. Johnsson.** 2000. Directed molecular evolution of cytochrome *c* peroxidase. Biochemistry **39:**10790–10798.

189. **Irie, T., Y. Honda, Y. Matsuyama, T. Watanabe, and M. Kuwahara.** 1999. *Pleurotus ostreatus* manganese peroxidase gene sequence. GenBank Accession No. AB016519.

190. **Irie, T., Y. Honda, T. Watanabe, and M. Kuwahara.** 2001. Homologous expression of recombinant manganese peroxidase genes in ligninolytic fungus *Pleurotus ostreatus*. Appl. Microbiol. Biotechnol. **55:**566–570.

191. **Ishihara, H. and T. Oki.** 1964. The oxidative decomposition of lignin. I. The enzymatic degradation of softwood lignin and related aromatic compounds by peroxidase. J. Jpn. Wood Res. Soc. **10:**207–212.

192. **Jensen, K. A., W. Bao, S. Kawai, E. Srebotnik, and K. Hammel.** 1996. Manganese-dependent cleavage of nonphenolic lignin structures by *Ceriporiopsis subvermispora* in the absence of lignin peroxidase. Appl. Environ. Microbiol. **62:**3679–3686.

193. **Jiao, K., W. Sun, S. Zhang, and G. Sun.** 2000. Application of *p*-phenylendiamine as an electrochemical substrate in peroxidase-mediated voltammetric enzyme immunoassay. Anal. Chim. Acta **413:**71–78.

194. **Johansson, T. and P. O. Nyman.** 1996. A cluster of genes encoding major isozymes of lignin peroxidase and manganese peroxidase from the white-rot fungus *Trametes versicolor*. Gene **170:**31–38.

195. **Johansson, T., K. G. Welinder, and P. O. Nyman.** 1993. Isozymes of lignin peroxidase and manganese peroxidase from the white-rot basidiomycete

Trametes versicolor. II. Partial sequences, peptide maps, and amino acid and carbohydrate compositions. Arch. Biochem. Biophys. **300:**57–62.

196. **Johnson, F., G. H. Loew, and P. Du.** 1994. Homology models of two isozymes of manganese peroxidase: prediction of a Mn^{II} binding site. Proteins **20:**312–319.

197. **Jonsson, L., H. G. Becker, and P. O. Nyman.** 1994. A novel type of peroxidase gene from the white-rot fungus *Trametes versicolor*. Biochim. Biophys. Acta **1207:**255–259.

198. **Joshi, D. K. and M. H. Gold.** 1993. Degradation of 2,4,5-trichlorophenol by the lignin-degrading basidiomycete *Phanerochaete chrysosporium*. Appl. Environ. Microbiol. **59:**1779–1785.

199. **Joshi, D. K. and M. H. Gold.** 1994. Oxidation of dibenzo-*p*-dioxin by lignin peroxidase from the basidiomycete *Phanerochaete chrysosporium*. Biochemistry **33:**10969–10976.

200. **Kapich, A., M. Hofrichter, T. Vares, and A. Hatakka.** 1999. Coupling of manganese peroxidase-mediated lipid peroxidation with destruction of non-phenolic lignin model compounds and ^{14}C-lignins. Biochem. Biophys. Res. Commun. **259:**212–219.

201. **Katsuragi, H., K. Takahashi, H. Suzuki, and M. Maeda.** 2000. Chemiluminescent measurement of peroxidase activity and its application using lucigenin CT-complex. Luminescence **15:**1–7.

202. **Kawai, S., T. Umezawa, and T. Higuchi.** 1988. Degradation mechanisms of phenolic β-1 lignin substructure model compounds by laccase of *Coriolus versicolor*. Arch. Biochem. Biophys. **262:**99–110.

203. **Kawai, S., T. Umezawa, M. Shimada, T. Higuchi, K. Koide, T. Nishida, N. Morohoshi, and T. Haraguchi.** 1987. C_α and C_β cleavage of phenolic β-1-lignin substructure model compound by laccase of *Coriolus versicolor*. Mokuzai Gakkaishi **33:**792–797.

204. **Kawai, Y., J. Sugiura, and Y. Kita.** 1996. *Coriolus hirsutus* manganese peroxidase gene sequence. GenBank Accession No. E12284.

205. **Keilin, D., and E. F. Hartree.** 1951. Purification of horseradish peroxidase and comparison of its properties with those of catalase and methaemoglobin. Biochem. J. **49:**88–97.

206. **Keilin, D., and T. Mann.** 1937. On cytochrome, a respiratory pigment common to animals, yeast and higher plants. Proc. R. Soc. London B **122**:119–133.

207. **Kerr, A. J. and D. A. I. Goring.** 1975. The ultrastructural arrangement of the wood cell wall. Cellul. Chem. Technol. **9**:563–573.

208. **Kersten, P. J. and D. Cullen.** 1993. Cloning and characterization of cDNA encoding glyoxal oxidase, a H_2O_2-producing enzyme from the lignin-degrading basidiomycete *Phanerochaete chrysosporium*. Proc. Natl. Acad. Sci. U.S.A. **90**:7411–7413.

209. **Kersten, P. J., B. Kalyanaraman, K. E. Hammel, B. Reinhammar, and T. K. Kirk.** 1990. Comparison of lignin peroxidase, horseradish peroxidase and laccase in the oxidation of methoxybenzenes. Biochem. J. **268**:475–480.

210. **Kersten, P. J. and T. K. Kirk.** 1987. Involvement of a new enzyme, glyoxal oxidase, in extracellular H_2O_2 production by *Phanerochaete chrysosporium*. J. Bacteriol. **169**:2195–2205.

211. **Kersten, P. J., C. Witek, A. vanden Wymelenberg, and D. Cullen.** 1995. *Phanerochaete chrysosporium* glyoxal oxidase is encoded by two allelic variants: structure, genomic organization, and heterologous expression of *glx1* and *glx2*. J. Bacteriol. **177**:6106–6110.

212. **Keyser, P., T. K. Kirk, and J. G. Zeikus.** 1978. Ligninolytic enzyme system of *Phanerohaete chrysosporium*: synthesized in the absence of lignin in response to nitrogen starvation. J. Bacteriol. **135**:790–797.

213. **Khindaria, A., D. P. Barr, and S. D. Aust.** 1995. Lignin peroxidases can also oxidize manganese. Biochemistry **34**:7773–7779.

214. **Khindaria, A., T. A. Grover, and S. D. Aust.** 1994. Oxalate-dependent reductive activity of manganese peroxidase from *Phanerochaete chrysosporium*. Arch. Biochem. Biophys. **314**:301–306.

215. **Khindaria, A., T. A. Grover, and S. D. Aust.** 1995. Evidence for formation of the veratryl alcohol cation radical by lignin peroxidase. Biochemistry **34**:6020–6025.

216. **Khindaria, A., I. Yamazaki, and S. D. Aust.** 1995. Veratryl alcohol oxidation by lignin peroxidase. Biochemistry **34**:16860–16869.

217. **Khindaria, A., I. Yamazaki, and S. D. Aust.** 1996. Stabilization of the veratryl alcohol cation radical by lignin peroxidase. Biochemistry **35:**6418–6424.

218. **Kimura, Y., Y. Asada, T. Oka, and M. Kuwahara.** 1991. Molecular analysis of a *Bjerkandera adusta* lignin peroxidase gene. Appl. Microbiol. Biotechnol. **35:**510–514.

219. **Kirk, T. K.** 1971. Effect of microorganisms on lignin. Annu. Rev. Phytopathol. **9:**185–210.

220. **Kirk, T. K. and E. Adler.** 1970. Methoxyl-deficient structural elements in lignin of sweetgum decayed by a brown-rot fungus. Acta Chem. Scand. **24:**3379–3390.

221. **Kirk, T. K., S. Croan, M. Tien, K. E. Murtagh, and R. L. Farrell.** 1986. Production of multiple ligninases by *Phanerochaete chrysosporium*: effect of selected growth conditions and use of a mutant strain. Enzyme Microb. Technol. **8:**27–32.

222. **Kirk, T. K. and R. L. Farrell.** 1987. Enzymatic "combustion": the microbial degradation of lignin. Annu. Rev. Microbiol. **41:**465–505.

223. **Kirk, T. K. and A. Kelman.** 1965. Lignin degradation as related to the phenoloxidases of selected wood-decaying basidiomycetes. Phytopathology **55:**739–745.

224. **Kirk, T. K., E. Schultz, W. J. Connors, L. F. Lorenz, and J. G. Zeikus.** 1978. Influence of culture parameters on lignin metabolism by *Phanerochaete chrysosporium*. Arch. Microbiol. **177:**277–285.

225. **Kishi, K., D. P. Hildebrand, M. Kusters-van Someren, J. Gettemy, A. G. Mauk, and M. H. Gold.** 1997. Site-directed mutations at phenylalanine-190 of manganese peroxidase: effects on stability, function, and coordination. Biochemistry **36:**4268–4277.

226. **Kishi, K., M. Kusters-van Someren, M. B. Mayfield, J. Sun, T. M. Loehr, and M. H. Gold.** 1996. Characterization of manganese(II) binding site mutants of manganese peroxidase. Biochemistry **35:**8986–8994.

227. **Kishi, K., H. Wariishi, L. Marquez, H. B. Dunford, and M. H. Gold.** 1994. Mechanism of manganese peroxidase compound II reduction: effect of organic acid chelators and pH. Biochemistry **33:**8694–8701.

228. **Koduri, R. S. and M. Tien.** 1994. Kinetic analysis of lignin peroxidase: explanation for the mediation phenomenon by veratryl alcohol. Biochemistry **33:**4225–4230.

229. **Kofujita, H., Y. Asada, and M. Kuwahara.** 1991. Alkyl-aryl cleavage of phenolic β-O-4 lignin substructure model compound by Mn^{II}-peroxidase isolated from *Pleurotus ostreatus*. Mokuzai Gakkaishi **37:**555–561.

230. **Kofujita, H., T. Ohta, Y. Asada, and M. Kuwahara.** 1991. Purification and characterization of laccase from *Lentinus edodes*. Mokuzai Gakkaishi **37:**562–569.

231. **Kuan, I. C., K. A. Johnson, and M. Tien.** 1993. Kinetic analysis of manganese peroxidase. The reaction with manganese complexes. J. Biol. Chem. **268:**20064–20070.

232. **Kuan, I. C. and M. Tien.** 1993. Glyoxylate-supported reactions catalyzed by Mn peroxidase of *Phanerochaete chrysosporium*: activity in the absence of added hydrogen peroxide. Arch. Biochem. Biophys. **302:**447–454.

233. **Kuan, I. C. and M. Tien.** 1993. Stimulation of Mn peroxidase activity: a possible role for oxalate in lignin biodegradation. Proc. Natl. Acad. Sci. U.S.A. **90:**1242–1246.

234. **Kunichika, N., O. Toshihiko, and K. Shinichi.** 1997. Non-heme hydroquinone peroxidase from *Azobacter beijerinckii* HM121. J. Ferment. Bioeng. **84:**14–21.

235. **Kunishima, N., K. Fukuyama, H. Matsubara, H. Hatanaka, Y. Shibano, and T. Amachi.** 1994. Crystal structure of the fungal peroxidase from *Arthromyces ramosus* at 1.9 Å resolution. Structural comparisons with the lignin and cytochrome *c* peroxidases. J. Mol. Biol. **235:**331–344.

236. **Kurek, B., B. Monties, and E. Odier.** 1990. Influence of the physical state of lignin on its degradability by the lignin peroxidase of *Phanerochaete chrysosporium*. Enzyme Microb. Technol. **12:**771–777.

237. **Kusters-van Someren, M., K. Kishi, T. Lundell, and M. H. Gold.** 1995. The manganese binding site of manganese peroxidase: characterization of an Asp179Asn site-directed mutant protein. Biochemistry **34:**10620–10627.

238. **Kuwahara, M., J. K. Glenn, M. A. Morgan, and M. H. Gold.** 1984. Separation and characterization of two extracellular H_2O_2-dependant oxidases from the ligninolytic cultures of *Phanerochaete chrysosporium*. FEBS Lett. **169:**247–250.

239. **Laddaga, R. A., R. Bessen, and S. Silver.** 1985. Cadmium-resistant mutant of *Bacillus subtilis* 168 with reduced cadmium transport. J. Bacteriol. **162:**1106–1110.

240. **Lang, E., F. Nerud, and F. Zadrazil.** 1998. Production of ligninolytic enzymes by *Pleurotus* sp. and *Dichomitus squalens* in soil and lignocellulose substrate as influenced by soil microorganisms. FEMS Microbiol. Lett. **167:**239–244.

241. **Larsen, M. J., M. F. Jurgensen, and A. E. Harvey.** 1982. N_2 fixation in brown-rotted soil wood in an intermountain cedar-hemlock ecosystem. Forest Sci. **28:**292–296.

242. **Lee, S.-Y., H.-D. Shin, and K.-J. Kim.** 1994. Correlative production of Mn-peroxidase and glucose oxidase depending on the culture condition of *Schizopora paradoxa*. Korean J. Mycol. **22:**325–331.

243. **Lewis, N. G. and E. Yamamoto.** 1990. Lignin: occurence, biogenesis and biodegradation. Annu. Rev. Plant Physiol. Plant Mol. Biol. **41:**455–496.

244. **Li, D., M. Alic, and M. H. Gold.** 1994. Nitrogen regulation of lignin peroxidase gene transcription. Appl. Environ. Microbiol. **60:**3447–3449.

245. **Li, D., N. Li, B. Ma, M. B. Mayfield, and M. H. Gold.** 1999. Characterization of genes encoding two manganese peroxidases from the lignin-degrading fungus *Dichomitus squalens*. Biochim. Biophys. Acta **1434:**356–364.

246. **Li, D., H. L. Youngs, and M. H. Gold.** 2001. Heterologous expression of a thermostable manganese peroxidase from *Dichomitus squalens* in *Phanerochaete chrysosporium*. Arch. Biochem. Biophys. **385:**348–356.

247. **Li, D. Y., J. Eberspacher, B. Wagner, J. Kuntzer, and F. Lingens.** 1991. Degradation of 2,4,6-trichlorophenol by *Azotobacter* sp. strain GP1. Appl. Environ. Microbiol. **57:**1920–1928.

248. **Limongi, P., M. Kjalke, J. Vind, J. W. Tams, T. Johansson, and K. G. Welinder.** 1995. Disulfide bonds and glycosylation in fungal peroxidases. Eur. J. Biochem. **227:**270–276.

249. **Lippard, S. J. and J. M. Berg.** 1994. Principles of Bioinorganic Chemistry. University Science Books, Mill Valley, CA.

250. **Lohmann, R. D. and D. Beyersmann.** 1993. Cadmium and zinc mediated changes of the Ca^{2+}-dependent endonuclease in apoptosis. Biochem. Biophys. Res. Commun. **190:**1097–1103.

251. **Lundell, T., H. Schoemaker, A. Hatakka, and G. Brunow.** 1993. New mechanism of the C_α–C_β cleavage in non-phenolic arylglycerol β-aryl ether lignin substructures catalyzed by lignin peroxidase. Holzforschung **47:**219–224.

252. **Lundquist, K. and P. Kristersson.** 1985. Exhaustive laccase-catalysed oxidation of a lignin model compound (vanillyl glycol) produces methanol and polymeric quinoid products. Biochem. J. **229:**277–279.

253. **Ma, B., M. B. Mayfield, and M. H. Gold.** 2001. The green fluorescent protein functions as a reporter of gene expression in *Phanerochaete chrysosporium*. Appl. Environ. Microbiol. **67:**948–955.

254. **Maeda, Y., S. Kajiwara, and K. Ohtaguchi.** 2001. Manganese peroxidase gene of the perennial mushroom *Elfvingia applanta*: cloning and evaluation of its relationship with lignin degradation. Biotechnol. Lett. **23:**103–109.

255. **Magliozzo, R. M. and J. A. Marcinkeviciene.** 1997. The role of Mn^{II} peroxidase activity of mycobacterial catalase-peroxidase in activation of the antibiotic isoniazid. J. Biol. Chem. **272:**8867–8870.

256. **Maranon, M. J. R. and R. B. Van Huystee.** 1994. Plant peroxidases: interaction between their prosthetic groups. Phytochemistry **37:**1217–1225.

257. **Marcinowski, S. and H. Grisenbach.** 1978. Enzymology of lignification. Cell-wall-bound β-glucosidase for coniferin from spruce (*Picea abies*) seedlings. Eur. J. Biochem. **87:**37–44.

258. **Martinez, M. J., F. J. Ruiz Duenas, F. Guillen, and A. T. Martinez.** 1996. Purification and catalytic properties of two manganese-peroxidase isoenzymes from *Pleurotus eryngii*. Eur. J. Biochem. **237:**424–432.

259. **Mata, G. and J.-M. Savoie.** 1998. Extracellular enzyme activities in six *Lentinula edodes* strains during cultivation in wheat straw. World J. Microbiol. Biotechnol. **14:**513–519.

260. **Mauk, M. R., K. Kishi, M. H. Gold, and A. G. Mauk.** 1998. pH-linked binding of Mn^{II} to manganese peroxidase. Biochemistry **37:**6767–6771.

261. **Mauro, J. M., L. A. Fishel, J. T. Hazzard, T. E. Meyer, G. Tollin, M. A. Cusanovich, and J. Kraut.** 1988. Tryptophan-191—phenylalanine, a

proximal-side mutation in yeast cytochrome *c* peroxidase that strongly affects the kinetics of ferrocytochrome *c* oxidation. Biochemistry **27:**6243–6256.

262. **Mayfield, M. B., B. J. Godfrey, and M. H. Gold.** 1994. Characterization of the *mnp2* gene encoding manganese peroxidase isozyme 2 from the basidiomycete *Phanerochaete chrysosporium*. Gene **142:**231–235.

263. **Mayfield, M. B., K. Kishi, M. Alic, and M. H. Gold.** 1994. Homologous expression of recombinant manganese peroxidase in *Phanerochaete chrysosporium*. Appl. Environ. Microbiol. **60:**4303–4309.

264. **McEldoon, J. P. and J. S. Dordick.** 1991. Thiol and Mn^{2+}-mediated oxidation of veratryl alcohol by horseradish peroxidase. J. Biol. Chem. **266:**14288–14293.

265. **McFee, W. W. and E. L. Stone.** 1966. The persistence of decaying wood in the humus layers of nothern forests. Proc. Soil Sci. Soc. Am. **30:**513–516.

266. **Menyhard, D. K. and G. Naray-Szabo.** 1999. Electrostatic effect on electron transfer at the active site of heme peroxidases: a comparative molecular orbital study on cytochrome *c* peroxidase and ascorbate peroxidase. J. Phys. Chem. B **103:**227–233.

267. **Messerschmidt, A. and R. Huber.** 1990. The blue oxidases, ascorbate oxidase, laccase and ceruloplasmin. Modeling and structural relationships. Eur. J. Biochem. **187:**341–352.

268. **Mester, T. and J. A. Field.** 1998. Characterization of a novel manganese peroxidase-lignin peroxidase hybrid isozyme produced by *Bjerkandera* species strain BOS55 in the absence of manganese. J. Biol. Chem. **273:**15412–15417.

269. **Millis, C. D., D. Y. Cai, M. T. Stankovich, and M. Tien.** 1989. Oxidation-reduction potentials and ionization states of extracellular peroxidases from the lignin-degrading fungus *Phanerochaete chrysosporium*. Biochemistry **28:**8484–8489.

270. **Mino, Y., H. Wariishi, N. J. Blackburn, T. M. Loehr, and M. H. Gold.** 1988. Spectral characterization of manganese peroxidase, an extracellular heme enzyme from the lignin-degrading basidiomycete, *Phanerochaete chrysosporium*. J. Biol. Chem. **263:**7029–7036.

271. **Miura, M., T. Deguchi, C. Yanagi, J. Suzuki, Y. Kitaoka, and M. Kakezawa.** 1997. The indicative culture parameters of manganese peroxidase production by white rot fungus IZU-154. J. Ferment. Bioeng. **84:**414–420.

272. **Miyazaki, K. and F. H. Arnold.** 1999. Exploring nonnatural evolutionary pathways by saturation mutagenesis: rapid improvement of protein function. J. Mol. Evol. **49:**716–720.

273. **Monties, B.** 1989. Lignins. *In* Methods in Plant Biochemistry, Vol. 1 (Dey, P. M. and J. B. Harborne, Eds.). Academic Press, New York. pp. 113–157.

274. **Morawski, B., S. Quan, and F. H. Arnold.** 2001. Functional expression and stabilization of horseradish peroxidase by directed evolution in *Saccharomyces cerevisiae*. Biotechnol. Bioeng. **76:**99–107.

275. **Morgan, J. J.** 2000. Manganese in natural waters and Earth's crust: it's availability to organisms. *In* Manganese and Its Role in Biological Processes (Sigel, A. and H. Sigel, Eds.). Marcel Dekker, New York. pp. 1–34.

276. **Morishima, I., S. Ogawa, T. Inubushi, T. Yonezawa, and T. Iizuka.** 1977. Nuclear magnetic resonance studies of hemoproteins. Acid-alkaline transition, ligand binding characteristics, and structure of the heme environments in horseradish peroxidase. Biochemistry **16:**5109–5115.

277. **Muheim, A., R. Waldner, D. Sanglard, J. Reiser, H. E. Schoemaker, and M. S. Leisola.** 1991. Purification and properties of an aryl-alcohol dehydrogenase from the white-rot fungus *Phanerochaete chrysosporium*. Eur. J. Biochem. **195:**369–375.

278. **Musha, Y. and D. A. I. Goring.** 1975. Distribution of syringyl and guaiacyl moieties in hardwoods as indicated by ultraviolet microscopy. Wood Sci. Technol. **9:**45–58.

279. **Neish, A. C.** 1965. Comarins, phenylpropanes, and lignin. *In* Plant Biochemistry (Bonner, J. and J. E. Varner, Eds.). Academic Press, New York. pp. 581–617.

280. **Nelson, D. P. and L. A. Kiesow.** 1972. Enthalpy of decomposition of hydrogen peroxide by catalase at 25°C (with molar extinction coefficients of H_2O_2 solutions in the UV). Anal. Biochem. **49:**474–478.

281. **Neri, F., C. Indiani, K. G. Welinder, and G. Smulevich.** 1998. Mutation of the distal arginine in *Coprinus cinereus* peroxidase—structural implications. Eur. J. Biochem. **251:**830–838.

282. **Nerud, F., Z. Zouchova, and Z. Misurcova.** 1991. Ligninolytic properties of different white-rot fungi. Biotechnol. Lett. **13:**657–660.

283. **Nie, G. and S. D. Aust.** 1997. Effect of calcium on the reversible thermal inactivation of lignin peroxidase. Arch. Biochem. Biophys. **337:**225–231.

284. **Nie, G., N. S. Reading, and S. D. Aust.** 1999. Relative stability of recombinant versus native peroxidases from *Phanerochaete chyrosporium.* Arch. Biochem. Biophys. **365:**328–334.

285. **Novotny, C., P. Erbanova, T. Cajthaml, N. Rothschild, C. Dososretz, and V. Sasek.** 2000. *Irpex lacteus*, a white rot fungus applicable to water and soil bioremediation. Appl. Microbiol. Biotechnol. **54:**850–853.

286. **Orth, A. B., D. J. Royse, and M. Tien.** 1993. Ubiquity of lignin-degrading peroxidases among various wood-degrading fungi. Appl. Environ. Microbiol. **59:**4017–4023.

287. **Ortiz de Montellano, P. R.** 1992. Catalytic sites of hemoprotein peroxidases. Annu. Rev. Pharmacol. Toxicol. **32:**89–107.

288. **Oxenrider, K. A. and P. J. Kennelly.** 1993. A protein-serine phosphatase from the halophilic archaeon *Haloferax volcanii*. Biochem. Biophys. Res. Commun. **194:**1330–1335.

289. **Ozols-Kalnin, V. G., A. G. Kokorevich, and J. Gravitis.** 1986. Estimation of the fractal and chemical dimensions of bulk and end-wise polymers. Chim. Drev. **5:**108–109.

290. **Palmer, G.** 1985. The electron paramagnetic resonance of metalloproteins. Biochem. Soc. Trans. **13:**548–560.

291. **Paszczynski, A., V. B. Huynh, and R. Crawford.** 1986. Comparison of ligninase-I and peroxidase-M2 from the white-rot fungus *Phanerochaete chrysosporium*. Arch. Biochem. Biophys. **244:**750–765.

292. **Patterson, W. R., T. L. Poulos, and D. B. Goodin.** 1995. Identification of a porphyrin π cation radical in ascorbate peroxidase compound I. Biochemistry **34:**4342–4345.

293. **Pease, E. A., A. Andrawis, and M. Tien.** 1989. Manganese-dependent peroxidase from *Phanerochaete chrysosporium*: primary structure deduced from cDNA sequence. J. Biol. Chem. **264:**13531–13535.

294. **Pease, E. A., S. D. Aust, and M. Tien.** 1991. Heterologous expression of active manganese peroxidase from *Phanerochaete chrysosporium* using the baculovirus expression system. Biochem. Biophys. Res. Commun. **179:**897–903.

295. **Pelaez, F., M. J. Martinez, and A. T. Martinez.** 1995. Screening of 68 species of basidiomycetes for enzyme involved in lignin degradation. Mycol. Res. **99:**37–42.

296. **Pember, S. O., B. L. Heyl, J. Kinkade, J. M., and J. D. Lambeth.** 1984. Cytochrome b_{558} from (bovine) granulocytes. J. Biol. Chem. **259:**10590–10595.

297. **Penel, S., N. Capelli, J. Flach, S. Overny, M. Tognoli, C. Penel, and H. Greppin.** 1996. The peroxidase gene family of *Arabidopsis thaliana*. Presented at the Arabidopsis Conference, Geneva (Obinger, C., U. Burner, R. Ebermann, C. Penel, Eds.). pp. 179–183.

298. **Périé, F. H., V. J. B. Reddy, N. J. Blackburn, and M. H. Gold.** 1998. Purification and characterization of laccases from the white-rot basidiomycete *Dichomitus squalens*. Arch. Biochem. Biophys. **353:**349–355.

299. **Périé, F. H., D. Sheng, and M. H. Gold.** 1996. Purification and characterization of two manganese peroxidase isozymes from the white-rot basidiomycete *Dichomitus squalens*. Biochim. Biophys. Acta **1297:**139–148.

300. **Perry, R. and S. Silver.** 1982. Cadmium and manganese transport in *Staphylococcus aureus* membrane vesicles. J. Bacteriol. **150:**973–976.

301. **Petersen, J. F., A. Kadziola, and S. Larsen.** 1994. Three-dimensional structure of a recombinant peroxidase from *Coprinus cinereus* at 2.6 Å resolution. FEBS Lett. **339:**291–296.

302. **Petersen, J. F., J. W. Tams, J. Vind, A. Svensson, H. Dalboge, K. G. Welinder, and S. Larsen.** 1993. Crystallization and X-ray diffraction analysis of recombinant *Coprinus cinereus* peroxidase. J. Mol. Biol. **232:**989–991.

303. **Petersen, M. and A. W. Alfermann.** 2001. The production of cytotoxic lignans by plant cell cultures. Appl. Microbiol. Biotechnol. **55:**135–142.

304. **Piontek, K., T. Glumoff, and K. Winterhalter.** 1993. Low pH crystal structure of glycosylated lignin peroxidase from *Phanerochaete chrysosporium* at 2.5 Å resolution. FEBS Lett. **315:**119–124.

305. **Pointing, S. B., J. A. Buswell, E. B. G. Jones, and L. L. P. Vrijmoed.** 1999. Extracellular cellulolytic enzyme profiles of five lignicolous mangrove fungi. Mycol. Res. **103:**696–700.

306. **Polle, A., and K. Chakrabarti.** 1994. Effects of manganese deficiency on soluble apoplastic peroxidase activities and lignin content in needles of Norway spruce (*Picea abies*). Tree Physiol. **14:**1191–1200.

307. **Polle, A., T. Otter, and H. Sandermann Jr.** 1997. Biochemistry and physiology of lignin synthesis. *In* Trees—Contributions to Modern Tree Physiology (Rennenberg, H., W. Eschrich, and H. Ziegler (ed.). Backhuys Publishers, Leiden. pp. 455–475.

308. **Popp, J. L. and T. K. Kirk.** 1991. Oxidation of methoxybenzenes by manganese peroxidase and by Mn^{3+}. Arch. Biochem. Biophys. **288:**145–148.

309. **Poulos, T. L., S. L. Edwards, H. Wariishi, and M. H. Gold.** 1993. Crystallographic refinement of lignin peroxidase at 2 Å. J. Biol. Chem. **268:**4429–4440.

310. **Poulos, T. L., and B. C. Finzel.** 1984. Heme enzyme structure and function. Peptide Protein Rev. **4:**115–171.

311. **Poulos, T. L. and J. Kraut.** 1980. The stereochemistry of peroxidase catalysis. J. Biol. Chem. **255:**8199–8205.

312. **Poulos, T. L., W. R. Patterson, and M. Sundaramoorthy.** 1995. The crystal structure of ascorbate and manganese peroxidases: the role of non-haem metal in the catalytic mechanism. Biochem. Soc. Trans. **23:**228–232.

313. **Pribnow, D., M. B. Mayfield, V. J. Nipper, J. A. Brown, and M. H. Gold.** 1989. Characterization of a cDNA encoding a manganese peroxidase, from the lignin-degrading basidiomycete *Phanerochaete chrysosporium.* J. Biol. Chem. **264:**5036–5040.

314. **Radotic, K., J. Simic-Krstic, M. Jeremic, and M. Trifunovic.** 1994. A study of lignin formation at the molecular level by scanning tunneling microscopy. Biophys. J. **66:**1763–1767.

315. **Radotic, K., M. Tasic, M. Jeremic, Z. Budimilija, J. Simic-Krstic, A. Polzovic, and Z. Bozovic.** 2000. Fractal analysis of STM images of lignin polymer obtained by *in vitro* synthesis. Gen. Physiol. Biophys. **19:**171–180.

316. **Raghukumar, C., D. Chandramohan, F. C. Michel, and C. A. Reddy.** 1996. Degradation of lignin and decolorization of paper mill bleach plant effluent (BPE) by marine fungi. Biotechnol. Lett. **18:**105–106.

317. **Rayner, A. D. M. and L. Boddy.** 1988. Fungal Decomposition of Wood: Its Biology and Ecology. Wiley, Chichester, New York.

318. **Reading, N. S. and S. D. Aust.** 1998. Effect of modified hemes on the spectral properties and activity of manganese peroxidase. Arch. Biochem. Biophys. **359:**291–296.

319. **Reading, N. S. and S. D. Aust.** 2000. Engineering a disulfide bond in recombinant manganese peroxidase results in increased thermostability. Biotechnol. Prog. **16:**326–333.

320. **Reddy, G. V. B. and M. H. Gold.** 1999. Degradation of pentachlorophenol by *Phanerochaete chrysosporium*: intermediates and reactions involved. Microbiology **146:**405–413.

321. **Reddy, G. V. B., M. D. Sollewijn Gelpke, and M. H. Gold.** 1998. Degradation of 2,4,6-trichlorophenol by *Phanerochaete chrysosporium*: involvement of reductive dechlorination. J. Bacteriol. **180:**5159–5164.

322. **Reed, G. H. and R. R. Poyner.** 2000. Mn^{2+} as a probe of divalent metal ion binding and function in enzymes and other proteins. *In* Manganese and Its Role in Biological Processes (Sigel, A. and H. Sigel, Eds.). Marcel Dekker, New York. pp. 183–207.

323. **Reinhammer, B.** 1984. Laccase. *In* Copper Proteins and Copper Enzymes, vol. 3. R. Lontie (ed.), CRC Press, Boca Raton. p. 1–36.

324. **Renganathan, V. and M. H. Gold.** 1986. Spectral characterization of the oxidized states of lignin peroxidase, an extracellular heme enzyme from the white-rot basidiomycete *Phanerochaete chrysosporium*. Biochemistry **25:**1626–1631.

325. **Rieble, S., D. K. Joshi, and M. H. Gold.** 1994. Purification and characterization of a 1,2,4-trihydroxybenzene 1,2-dioxygenase from the basidiomycete *Phanerochaete chrysosporium*. J. Bacteriol. **176:**4838–4844.

326. **Ritch, T. G., Jr. and M. H. Gold.** 1992. Characterization of a highly expressed lignin peroxidase-encoding gene from the basidiomycete *Phanerochaete chrysosporium*. Gene **118:**73–80.

327. **Roberts, J. B., B. M. Hoffman, R. Rutter, and L. P. Hager.** 1981. Electron-nuclear double resonance of horseradish peroxidase compound I: Detection of the porphyrin π-cation radical. J. Biol. Chem. **256:**2118–2121.

328. **Rodriguez, S., M. A. Longo, C. Cameselle, and A. Sanroman.** 1999. Production of manganese peroxidase and laccase in laboratory-scale bioreactors by *Phanerochaete chrysosporium*. Bioprocess Eng. **20:**531–535.

329. **Rodriguez-Maranon, M. J., M. J. Stillman, and R. B. van Huystee.** 1993. Co-dependency of calcium and porphyrin for an integrated molecular structure of peanut peroxidase: a circular dichroism analysis. Biochem. Biophys. Res. Commun. **194:**326–332.

330. **Roy, B. P., M. G. Paice, F. S. Archibald, S. K. Misra, and L. E. Misiak.** 1994. Creation of metal-complexing agents, reduction of manganese dioxide, and promotion of manganese peroxidase-mediated Mn(III) production by cellobiose:quinone oxidoreductase from *Trametes versicolor*. J. Biol. Chem. **269:**19745–19750.

331. **Ruel, K., V. Burlat, and J. P. Joseleau.** 1999. Relationship between ultrastructural topochemistry of lignin and wood properties. IAWA J. **20:**203–211.

332. **Ruel, K. and J.-P. Joselau.** 1991. Involvement of an extracellular glucan sheath during degradation of *Populus* wood by *Phanerochaete chrysosporium*. Appl. Environ. Microbiol. **57:**374–384.

333. **Ruiz-Duenas, F. J., M. J. Martinez, and A. T. Martinez.** 1999. Molecular characterization of a novel peroxidase isolated from the ligninolytic fungus *Pleurotus eryngii*. Mol. Microbiol. **31:**223–235.

334. **Ruiz-Dueñas, F. J., M. J. Martínez, and A. T. Martínez.** 1999. Heterologous expression of *Pleurotus eryngii* peroxidase confirms its ability to oxidize Mn^{2+} and different aromatic substrates. Appl. Environ. Microbiol. **65:**4705–4707.

335. **Saloheimo, M., V. Barajas, M.-L. Niku-Paavola, and J. K. C. Knowles.** 1989. A lignin peroxidase-encoding cDNA from the white-rot fungus *Phlebia radiata*: characterization and expression in *Trichoderma reesei*. Gene **85:**343–351.

336. **Saloheimo, M. and M. L. Niku Paavola.** 1991. Heterologous production of a ligninolytic enzyme: expression of the *Phlebia radiata* laccase gene in *Trichoderma reesei*. Biotechnology **9:**987–990.

337. **Saloheimo, M., M. L. Niku Paavola, and J. K. C. Knowles.** 1991. Isolation and structural analysis of the laccase gene from the lignin-degrading fungus *Phlebia radiata*. J. Gen. Microbiol. **137:**1537–1544.

338. **Santucci, R., C. Bongiovanni, S. Marini, R. Del Conte, M. Tien, L. Banci, and M. Coletta.** 2000. Redox equilibria of manganese peroxidase from *Phanerochaete chrysosporium*: functional role of residues on the proximal side of the haem pocket. Biochem. J. **349:**85–90.

339. **Sarkanen, K. V. and C. H. Ludwig.** 1971. Lignins: Occurrence, Formation, Structure and Reactions. Wiley-Interscience, New York.

340. **Saterlee, J. D., J. E. Erman, J. M. Mauro, and J. Kraut.** 1990. Comparative proton NMR analysis of wild-type cytochrome *c* peroxidase from yeast, the recombinant enzyme from *Escherichia coli*, and an Asp-235–Asn-235 mutant. Biochemistry **29:**8797–8804.

341. **Scheel, T., M. Hofer, S. Ludwig, and U. Holker.** 2000. Differential expression of manganese peroxidase and laccase in white-rot fungi in the presence of manganese or aromatic compounds. Appl. Microbiol. Biotechnol. **54:**686–691.

342. **Schneegass, I., M. Hofrichter, K. Scheibner, and W. Fritsche.** 1997. Purification of the main manganese peroxidase isoenzyme MnP2 from the white-rot fungus *Nematoloma frowardii* b19. Appl. Microbiol. Biotechnol. **48:**602–605.

343. **Schoemaker, H. E. and M. S. A. Leisola.** 1990. Degradation of lignin by *Phanerochaete chrysosporium.* J. Biotechnol. **13:**101–109.

344. **Schoemaker, H. E., T. K. Lundell, A. I. Hatakka, and K. Piontek.** 1994. The oxidation of veratryl alchol, dimeric lignin models and lignin by lignin peroxidase: the redox cycle revisted. FEMS Microbiol. Rev. **13:**321–332.

345. **Schuller, D. J., N. Ban, R. B. Huystee, A. McPherson, and T. L. Poulos.** 1996. The crystal structure of peanut peroxidase. Structure **4:**311–321.

346. **Sethuraman, A., D. E. Akin, and K.-E. L. Eriksson.** 1999. Production of ligninolytic enzymes and synthetic lignin mineralization by the bird's nest fungus *Cyathus stercoreus*. Appl. Microbiol. Biotechnol. **52:**689–697.

347. **Shao, Z., H. Zhao, L. Giver, and F. H. Arnold.** 1998. Random-priming in vitro recombination: an effective tool for directed evolution. Nucleic Acids Res. **26:**681–683.

348. **Shiono, H., H. Nohta, C. Utsuyama, and M. Hiramatsu.** 2000. New method for adding reagents: an application of caged molecules to analytical chemistry. Anal. Chim. Acta **405:**17–21.

349. **Sillen, L. G. and A. E. Martell.** 1964. Stability Constants of Metal-Ion Complexes. Section II: Organic Ligands, Special Publication No. 17, 2nd Ed. The Chemical Society, Burlington House, London.

350. **Sims, P. F. G., M. S. Soares Felipe, Q. Wang, M. E. Gent, C. A. M. Tempelaars, and P. Broda.** 1994. Differential expression of multiple exo-cellobiohydrolase I-like genes in the lignin-degrading fungus *Phanerochaete chrysosporium*. Mol. Microbiol. **12:**209–216.

351. **Sitter, A. J., J. R. Shifflett, and J. Terner.** 1988. Resonance Raman spectroscopic evidence for heme iron-hydroxide ligation in peroxidase alkaline forms. J. Biol. Chem. **263:**13032–13038.

352. **Sivaraja, M., D. B. Goodin, M. Smith, and B. M. Hoffman.** 1989. Identification by ENDOR of Trp191 as the free-radical site in cytochrome *c* peroxidase compound ES. Science **245:**738–740.

353. **Smiley, C. J., J. Ray, and L. M. Huggins.** 1975. Preservation of Miocene fossils in unoxidized lake deposits, Clarkia, Idaho. J. Paleontol. **51:**885–901.

354. **Smith, A. T., S. A. Sanders, R. N. Thorneley, J. F. Burke, and R. R. Bray.** 1992. Characterisation of a haem active-site mutant of horseradish peroxidase, Phe41-Val, with altered reactivity towards hydrogen peroxide and reducing substrates. Eur. J. Biochem. **207:**507–519.

355. **Smith, D. W. and R. J. Williams.** 1968. Analysis of the visible spectra of some sperm whale ferrimyoglobin derivatives. Biochem. J. **110:**297–301.

356. **Smulevich, G., J. M. Mauro, L. A. Fishel, A. M. English, J. Kraut, and T. G. Spiro.** 1988. Heme pocket interactions in cytochrome *c* peroxidase studied by site-directed mutagenesis and resonance Raman spectroscopy. Biochemistry **27:**5477–5485.

357. **Smulevich, G., M. A. Miller, J. Kraut, and T. G. Spiro.** 1991. Conformational change and histidine control of heme chemistry in cytochrome *c* peroxidase: resonance Raman evidence from Leu-52 and Gly-181 mutants of cytochrome *c* peroxidase. Biochemistry **30:**9546–9558.

358. **Smulevich, G., F. Neri, M. P. Marzocchi, and K. G. Welinder.** 1996. Versatility of heme coordination demonstrated in a fungal peroxidase. Absorption and resonance Raman studies of *Coprinus cinereus* peroxidase and the Asp245→Asn mutant at various pH values. Biochemistry **35:**10576–10585.

359. **Sollewijn Gelpke, M. D., M. Mayfield-Gambill, G. P. L. Cereghino, and M. H. Gold.** 1999. Homologous expression of recombinant lignin peroxidase in *Phanerochaete chrysosporium*. Appl. Environ. Microbiol. **65:**1670–1674.

360. **Sollewijn Gelpke, M. D., P. Moënne-Loccoz, and M. H. Gold.** 1999. Arginine 177 is involved in Mn^{II} binding by manganese peroxidase. Biochemistry **38:**11482–11489.

361. **Sollewijn Gelpke, M. D., D. Sheng, and M. H. Gold.** 2000. Mn^{II} is not a productive substrate for wild-type or recombinant lignin peroxidase isozyme H2. Arch. Biochem. Biophys. **381:**16–24.

362. **Sollewijn Gelpke, M. D., H. L. Youngs, and M. H. Gold.** 2000. Role of arginine 177 in the Mn^{II} binding site of manganese peroxidase: studies with R177D, R177E, R177N and R177Q mutants. Eur. J. Biochem. **267:**7038–7045.

363. **Soo, K. Y. and P. Singh Adya.** 2000. Micromorphological characteristics of wood biodegradation in wet environments: a review. IAWA J. **21:**135–155.

364. **Spaulding, L. D., C. C. Chang, N.-T. Yu, and R. H. Felton.** 1975. Resonance Raman spectra of metallooctaethylporphyrin. A structural probe of metal displacement. J. Am. Chem. Soc. **97:**2517–2525.

365. **Spiro, T. G.** 1988. Resonance Raman spectroscopy of metalloporphyrins. *In* Biological Applications of Raman Spectroscopy: Resonance Raman Spectra of Heme and Metalloproteins, Vol. 3 (Spiro, T. G., Ed.). Wiley, New York. pp. 1–38.

366. **Srebotnik, E., K. A. Jensen, Jr., and K. E. Hammel.** 1994. Fungal degradation of recalcitrant nonphenolic lignin structures without lignin peroxidase. Proc. Natl. Acad. Sci U.S.A. **91:**12794–12797.

367. **Srebotnik, E., K. Messner, and R. Foisner.** 1988. Penetrability of white-rot degraded pine wood by the lignin peroxidase of *Phanerochaete chrysosporium.* Appl. Environ. Microbiol. **54:**2608–2614.

368. **Srebotnik, E., K. Messner, R. Foisner, and B. Petterson.** 1988. Ultrastructural localization of ligninase of *Phanerochaete chrysosporium* by immunogold labeling. Curr. Microbiol. **16:**221–227.

369. **Steffan, K. T., M. Hofrichter, and A. Hatakka.** 2000. Mineralisation of ^{14}C-labelled synthetic lignin and ligninolytic enzyme activities of litter-decomposing basidiomycetous fungi. Appl. Microbiol. Biotechnol. **54:**819–825.

370. **Stemmer, W. P. C.** 1991. DNA shuffling by random fragmentation and reassembly: in vitro recombination for molecular evolution. Proc. Natl. Acad. Sci. U.S.A. **91:**10747–10751.

371. **Stemmer, W. P. C.** 1994. Rapid evolution of a protein by intro DNA shuffling. Nature **370:**389–391.

372. **Stewart, P., R. E. Whitwam, P. J. Kersten, D. Cullen, and M. Tien.** 1996. Efficient expression of a *Phanerochaete chrysosporium* manganese peroxidase gene in *Aspergillus oryzae.* Appl. Environ. Microbiol. **62:**860–864.

373. **Strittmatter, P. and S. F. Velick.** 1956. The isolation and properties of microsomal cytochrome. J. Biol. Chem. **221:**253–264.

374. **Stubblefield, S. P., T. N. Taylor, and C. B. Beck.** 1985. Studies of Paleozoic fungi. IV. Wood decaying fungi in *Callixylon newberryi* from the Upper Devonian. Am. J. Bot. **72:**1765–1774.

375. **Sublette, K. L., E. V. Ganapathy, and S. Schwartz.** 1992. Degradation of munition wastes by *Phanerochaete chrysosporium.* Appl. Biochem. Biotechnol. **34/35:**709–723.

376. **Sundaramoorthy, M., K. Kishi, M. H. Gold, and T. L. Poulos.** 1994. The crystal structure of manganese peroxidase from *Phanerochaete chrysosporium* at 2.06-Å resolution. J. Biol. Chem. **269:**32759–32767.

377. **Sundaramoorthy, M., K. Kishi, M. H. Gold, and T. L. Poulos.** 1997. Crystal structures of substrate binding site mutants of manganese peroxidase. J. Biol. Chem. **272:**17574–17580.

377a. **Sundaramoorthy, M., J. Terner, and T. L. Poulos.** 1998. Stereochemistry of the chloroperoxidase active site: crystallographic and molecular modeling studies. Chem. Biol. **5:**461–473.

378. **Sundaramoorthy, M., H. L. Youngs, M. H. Gold, and T. Poulos.** 2002. High resolution crystal structures of manganese peroxidase complexed with substrates and inhibitors. In preparation.

379. **Sutherland, G. and S. D. Aust.** 1996. The effects of calcium on the thermal stability and activity of manganese peroxidase. Arch. Biochem. Biophys. **332:**128–134.

380. **Sutherland, G. and S. Aust.** 1997. Thermodynamics of binding of the distal calcium to manganese peroxidase. Biochemistry **36:**8567–8573.

381. **Sutherland, G., L. Zapanta, M. Tien, and S. Aust.** 1997. Role of calcium in maintaining the heme environment of manganese peroxidase. Biochemistry **36:**3654–3662.

382. **Sutherland, G. R., A. Khindaria, and S. D. Aust.** 1996. The effect of veratryl alcohol on manganese oxidation by lignin peroxidase. Arch. Biochem. Biophys. **327:**20–26.

383. **Swift, M. J.** 1977. The role of fungi and animals in the immobilisation and release of nutrient elements from decomposing branch-wood. *In* Soil Organisms as Components of Ecosystems (Lohm, U. and T. Persson, Eds.). Swedish Natural Sciences Research Council, Stockholm. pp. 193–202.

384. **Takio, K., K. Titani, L. H. Ericsson, and T. Yonetani.** 1980. Primary structure of yeast cytochrome *c* peroxidase. II. The complete amino acid sequence. Arch. Biochem. Biophys. **203:**615–629.

385. **Tams, J. W. and K. G. Welinder.** 1998. Glycosylation and thermodynamic verus kinetic stability of horseradish peroxidase. FEBS Lett. **421:**234–236.

386. **Tamura, M., T. Asakura, and T. Yonetani.** 1972. Heme-modification studies of horseradish peroxidase. Biochim. Biophys. Acta **268:**292–304.

387. **Tanaka, M., K. Ishimori, and I. Morishima.** 1998. Structural roles of the highly conserved Glu residue in the heme distal site of peroxidases. Biochemistry **37:**2629–2638.

388. **Taylor, J. G., T. P. Owen, Jr., L. T. Koonce, and C. H. Haigler.** 1992. Dispersed lignin in tracheary elements treated with cellulose synthesis inhibitors provides evidence that molecules of the secondary cell wall mediate wall patterning. Plant J. **2:**959–970.

389. **Tello, M., G. Corsini, L. F. Larrondo, L. Salas, S. Lobos, and R. Vicuna.** 2000. Characterization of three new manganese peroxidase genes from the ligninolytic basidiomycte *Ceriporiopsis subvermispora*. Biochim. Biophys. Acta **149:**137–144.

390. **Terazawa, M. and M. Miyake.** 1984. Phenolic compounds in living tissue of woods. II. Seasonal variations of phenolic glucosides in the cambial sap of woods. Mokuzai Gakkaishi **30:**329–334.

391. **Teroaka, J. and T. Kitagawa.** 1981. Structural implications of the heme-linked ionization of horseradish peroxidase in the Fe-histidine stretching Raman line. J. Biol. Chem. **256:**3969–3977.

392. **Tham, L., S. Matsuhashi, and T. Kume.** 1998. Responses of *Ganoderma lucidum* to heavy metals. *In* Sixth International Mycological Congress IMC6, Jerusalem, Kenes, Inc., Tel Aviv, p. 107.

393. **Theorell, H.** 1942. Crystalline peroxidase. Enzymologia **10:**250–252.

394. **Thurston, C. F.** 1994. The structure and function of fungal laccases. Microbiology **140:**19–26.

395. **Tien, M. and T. K. Kirk.** 1983. Lignin-degrading enzyme from the hymenomycete *Phanerochaete chrysosporium* Burds. Science **221:**661–663.

396. **Tien, M., and T. K. Kirk.** 1984. Lignin-degrading enzyme from *Phanerochaete chrysosporium*: purification, characterization, and catalytic properties of a unique H_2O_2-requiring oxygenase. Proc. Natl. Acad. Sci. U.S.A. **81:**2280–2284.

397. **Tien, M., T. K. Kirk, C. Bull, and J. A. Fee.** 1986. Steady-state and transient-state kinetic studies on the oxidation of 3,4-dimethoxybenzyl alcohol catalyzed by the ligninase of *Phanerochaete chrysosporium* Burds. J. Biol. Chem. **261:**1687–1693.

398. **Timofeevski, S. and S. D. Aust.** 1997. Effects of Mn^{2+} and oxalate on the catalytic activity of manganese peroxidase. Biochem. Biophys. Res. Commun. **239:**645–649.

399. **Tonon, F. and E. Odier.** 1988. Influence of veratryl alcohol and hydrogen peroxide on ligninase activity and ligninase production by *Phanerochaete chrysosporium*. Appl. Environ. Microbiol. **54:**466–472.

400. **Toon, S. P., M. Ghirardi, P. Mohanty, and M. Seibert.** 1995. Cadmium inhibition of O-2 evolution and electron transport in isolated photosystem II membranes. Plant Physiol. **108:**89.

401. **Trevors, J., G. Stratton, and G. Gadd.** 1986. Cadmium transport, resistance, and toxicity in bacteria, algae, and fungi. Can. J. Microbiol. **32:**447–464.

402. **Tsai, T. C., J. Hart, R. T. Jiang, K. Bruzik, and M. D. Tsai.** 1985. Phospholipids chiral at phosphorus. Use of chiral thiophosphatidylcholine to study the metal-binding properties of bee venom phospholipase A2. Biochemistry **24:**3180–3188.

403. **Tuor, U., H. Wariishi, H. E. Schoemaker, and M. H. Gold.** 1992. Oxidation of phenolic arylglycerol β-aryl ether lignin model compounds by manganese peroxidase from *Phanerochaete chrysosporium*: oxidative cleavage of an α-carbonyl model compound. Biochemistry **31:**4986–4995.

404. **Ulmer, D., M. Leisola, J. Puhakka, and A. Fiechter.** 1983. *Phanerochaete chrysosporium*: growth pattern and lignin degradation. Eur. J. Appl. Microbiol. Biotechnol. **18:**153–157.

405. **Urzua, U., L. Fernando Larrondo, S. Lobos, J. Larrain, and R. Vicuna.** 1995. Oxidation reactions catalyzed by manganese peroxidase isoenzymes from *Ceriporiopsis subvermispora*. FEBS Lett. **371:**132–136.

406. **Valli, K., B. J. Brock, D. K. Joshi, and M. H. Gold.** 1992. Degradation of 2,4-dinitrotoluene by the lignin-degrading fungus *Phanerochaete chrysosporium*. Appl. Environ. Microbiol. **58:**221–228.

407. **Valli, K., and M. H. Gold.** 1991. Degradation of 2,4-dichlorophenol by the lignin-degrading fungus *Phanerochaete chrysosporium*. J. Bacteriol. **173:**345–352.

408. **Valli, K., H. Wariishi, and M. H. Gold.** 1992. Degradation of 2,7-dichlorodibenzo-*p*-dioxin by the lignin-degrading basidiomycete *Phanerochaete chrysosporium*. J. Bacteriol. **174:**2131–2137.

409. **van Gunsteren, W. F.** 1990. Computer simulation of molecular dynamics: methodology, applications and perspectives in chemistry. Angew. Chem., Int. Ed. Engl. **29:**992–1023.

410. **van Huystee, R. B., and M. T. McManus.** 1998. Glycans of higher plant peroxidases: recent observations and future speculations. Glycoconjugate J. **15:**101–106.

411. **Vares, T., and A. Hatakka.** 1997. Lignin-degrading activity and ligninolytic enzymes of different white-rot fungi: effects of manganese and malonate. Can. J. Bot. **75:**61–71.

412. **Vares, T., T. K. Lundell, and A. I. Hatakka.** 1992. Novel heme-containing enzyme possibly involved in lignin degradation by the white-rot fungus *Junghuhnia separabilima*. FEMS Microbiol. Lett. **99:**53–58.

413. **Veitch, N. C.** 1993. NMR studies of the substrate binding site in plant and fungal peroxidases. Plant Peroxidases: Biochemistry and Physiology. III International Symposium 1993 Proceedings (Welinder, K. G., S. K. Rasmussen, C. Penel, H. Greppin, Eds.). University of Geneva, Geneva. pp. 57–64.

414. **Vickery, L., T. Nozawa, and K. Sauer.** 1976. Mangnetic circular-dichroism studies of myoglobin complexes—correlations with heme spin state and axial ligation. J. Am. Chem. Soc. **98:**343–350.

415. **Vitello, L. B., J. E. Erman, M. A. Miller, J. M. Mauro, and J. Kraut.** 1992. Effect of Asp-235→Asn substitution on the absorption spectrum and hydrogen peroxide reactivity of cytochrome *c* peroxidase. Biochemistry **31:**11524–11535.

416. **Vitello, L. B., J. E. Erman, M. A. Miller, J. Wang, and J. Kraut.** 1993. Effect of arginine-48 replacement on the reaction between cytochrome *c* peroxidase and hydrogen peroxide. Biochemistry **32:**9807–9818.

417. **Volc, J., N. P. Denisova, F. Nerud, and V. Musilek.** 1985. Glucose-2-oxidase activity in mycelial cultures of basidiomycetes. Fol. Microbiol. **30:**141–147.

418. **Vyas, B. R. and H. P. Molitoris.** 1995. Involvement of an extracellular H_2O_2-dependent ligninolytic activity of the white rot fungus *Pleurotus ostreatus* in the decolorization of Remazol brilliant blue R. Appl. Environ. Microbiol. **61:**3919–3927.

419. **Walther, I., M. Kaelin, J. Reiser, F. Suter, B. Fritsche, and M. Saloheimo.** 1988. Molecular analysis of a *Phanerochaete chrysosporium* lignin peroxidase gene. Gene **70:**127–137.

420. **Wan, L., M. B. Twitchett, L. D. Eltis, A. G. Mauk, and M. Smith.** 1998. In vitro evolution of horse heart myoglobin to increase peroxidase activity. Proc. Natl. Acad. Sci. U.S.A. **95:**12825–12831.

421. **Wang, J. M., M. Mauro, S. L. Edwards, S. J. Oatley, L. A. Fishel, V. A. Ashford, N. H. Xuong, and J. Kraut.** 1990. X-ray structures of recombinant yeast cytochrome *c* peroxidase and three heme-cleft mutants prepared by site-directed mutagenesis. Biochemistry **29:**7160–7173.

422. **Wariishi, H., L. Akileswaran, and M. H. Gold.** 1988. Manganese peroxidase from the basidiomycete *Phanerochaete chrysosporium*: spectral characterization of the oxidized states and the catalytic cycle. Biochemistry **27:**5365–5370.

423. **Wariishi, H., H. B. Dunford, I. D. MacDonald, and M. H. Gold.** 1989. Manganese peroxidase from the lignin-degrading basidiomycete *Phanerochaete chrysosporium*: transient state kinetics and reaction mechanism. J. Biol. Chem. **264:**3335–3340.

424. **Wariishi, H., K. Valli, and M. H. Gold.** 1989. Oxidative cleavage of a phenolic diarylpropane lignin model dimer by manganese peroxidase from *Phanerochaete chrysosporium*. Biochemistry **28:**6017–6023.

425. **Wariishi, H., K. Valli, and M. H. Gold.** 1991. In vitro depolymerization of lignin by manganese peroxidase of *Phanerochaete chrysosporium.* Biochem. Biophys. Res. Commun. **17:**269–275.

426. **Wariishi, H., K. Valli, and M. H. Gold.** 1992. Manganese(II) oxidation by manganese peroxidase from the basidiomycete *Phanerochaete chrysosporium.* Kinetic mechanism and role of chelators. J. Biol. Chem. **267:**23688–23695.

427. **Wariishi, H., K. Valli, V. Renganathan, and M. H. Gold.** 1989. Thiol-mediated oxidation of nonphenolic lignin model compounds by manganese peroxidase of *Phanerochaete chrysosporium.* J. Biol. Chem. **264:**14185–14191.

428. **Welinder, K. G.** 1975. Covalent structure of the glycoprotein horseradish peroxidase (E.C. 1.11.1.7). FEBS Lett. **72:**19–23.

429. **Welinder, K. G.** 1991. The plant peroxidase superfamily. *In* Biochemical, Molecular, and Physiological Aspects of Plant Peroxidases (Penel, C., H. Greppin, Th. Gaspar, and J. Lobarzewski, Eds.). University of Geneva, Geneva. pp. 3–14.

430. **Welinder, K. G.** 1992. Superfamily of plant, fungal and bacterial peroxidases. Curr. Opin. Struct. Biol. **2:**388–393.

431. **Welinder, K. G., B. Bjornholm, and H. B. Dunford.** 1995. Functions of electrostatic potentials and conserved distal and proximal His-Asp H-bonding networks in haem peroxidases. Biochem. Soc. Trans. **23:**257–262.

432. **Welinder, K. G., and M. Gajhede.** 1993. Structure and evolution of peroxidases. Plant Peroxidases: Biochemistry and Physiology. III International Symposium 1993 Proceedings (Welinder, K. G., S. K. Rasmussen, C. Penel, and H. Greppin, Eds.). University of Geneva, Geneva. pp. 35–42.

433. **Welinder, K. G., J. M. Mauro, and L. Norskov-Lauritsen.** 1992. Structure of plant and fungal peroxidases. Biochem. Soc. Trans. **20:**337–340.

434. **Whittaker, M. M., P. J. Kersten, N. Nakamura, J. Sanders-Loehr, E. S. Schweizer, and J. W. Whittaker.** 1996. Glyoxal oxidase from *Phanerochaete chrysosporium* is a new radical-copper oxidase. J. Biol. Chem. **271:**681–687.

435. **Whitwam, R. and M. Tien.** 1996. Heterologous expression and reconstitution of fungal Mn peroxidase. Arch. Biochem. Biophys. **333:**439–446.

436. **Whitwam, R. E., K. R. Brown, M. Musick, M. J. Natan, and M. Tien.** 1997. Mutagenesis of the Mn^{2+}-binding site of manganese peroxidase affects

oxidation of Mn^{2+} by both compound I and compound II. Biochemistry **36:**9766–9773.

437. **Whitwam, R. E., I. G. Gazarian, and M. Tien.** 1995. Expression of fungal Mn peroxidase in *E. coli* and refolding to yield active enzyme. Biochem. Biophys. Res. Commun. **216:**1013–1017.

438. **Whitwam, R. E., R. S. Koduri, M. Natan, and M. Tien.** 1999. Role of axial ligands in the reactivity of Mn peroxidase from *Phanerochaete chrysosporium*. Biochemistry **38:**9608–9616.

438a. **Wilcox, S. K., C. D. Putnam, M. Sastry, J. Blankenship, W. J. Chazin, D. E. McRee, and D. B. Goodin.** 1998. Rational design of a functional metalloenzyme: introduction of a site for manganese binding and oxidation into a heme peroxidase. Biochemistry **37:**16853–16862.

439. **Yeung, B. K., X. Wang, J. A. Sigman, P. A. Petillo, and Y. Lu.** 1997. Construction and characterization of a manganese-binding site in cytochrome *c* peroxidase: towards a novel manganese peroxidase. J. Chem. Biol. **4:**215–221.

440. **Youn, H.-D., Y. C. Hah, and S.-O. Kang.** 1995. Role of laccase in lignin degradation by white-rot fungi. FEMS Microbiol. Lett. **132:**183–188.

441. **Young, H. E. and V. P. Guinn.** 1966. Chemical elements in complete mature trees of seven species in Maine. TAPPI J. **49:**190–197.

442. **Youngs, H. L., M. Sundaramoorthy, and M. H. Gold.** 2000. Effects of cadmium on manganese peroxidase: competitive inhibition of Mn^{II} oxidation and thermal stabilization of the enzyme. Eur. J. Biochem. **267:**1761–1769.

443. **Yu, B. Z., O. G. Berg, and M. K. Jain.** 1993. The divalent cation is obligatory for the binding of ligands to the catalytic site of secreted phospholipase A2. Biochemistry **32:**6485–6492.

444. **Zainal, A. A.** 1976. The soft rot fungi: the effect of lignin. Mater Org. **3:**121–127.

445. **Zapanta, L. S. and M. Tien.** 1997. The roles of veratryl alcohol and oxalate in fungal lignin degradation. J. Biotechnol. **53:**93–102.

446. **Zhang, Y., C. Reddy, and A. Rasooly.** 1991. Cloning of several lignin peroxidase (LIP)-encoding genes: sequence analysis of the LIP6 gene from the white-rot basidiomycete, *Phanerochaete chrysosporium*. Gene **97:**191–198.

447. **Zhao, H., L. Giver, Z. Shao, J. A. Affholter, and F. H. Arnold.** 1998. Molecular evolution by staggered extension process (STEP) in vitro recombination. Nature Biotechnol. **16:**258–261.

448. **Ziegenhagen, D. and M. Hofrichter.** 2000. A simple and rapid method to gain high amounts of manganese peroxidase with immobilized mycelium of the agaric white-rot fungus *Clitocybula dusenii*. Appl. Microbiol. Biotechnol. **53:**553–557.

449. **Zou, P. and H. Schrempf.** 2000. The heme-independent manganese-peroxidase activity depends on the presence of the C-terminal domain within the *Streptomyces reticuli* catalase-peroxidase CpeB. Eur. J. Biochem. **267:**2840–2849.

APPENDIX I

Transient-state Inhibition constants for compound I.

$$E + S \xrightarrow{k_1} P$$

$$+$$

$$I \qquad K_I = \frac{[E][I]}{[EI]} \quad \text{and} \quad \frac{-d[E]_{tot}}{dt} = [E][S]k_1 = k_{obs}[E]_{tot}$$

$$\Updownarrow K_I$$

$$EI$$

$$[E]_{tot} = [E] + [EI] = [E] + \frac{[E][I]}{K_I} = [E]\left(1 + \frac{[I]}{K_I}\right)$$

$$k_{obs}[E]_{tot} = k_{obs}[E]\left(1 + \frac{[I]}{K_I}\right) = k_1[S][E] \quad \therefore \; k_{obs} = k_1[S]\left(1 + \frac{[I]}{K_I}\right) \text{ and as I}\rightarrow 0 \; k_{obs} = k_1[S]$$

Transient-state Inhibition constants for compound II.

$$E + S \underset{}{\overset{K_1}{\Leftrightarrow}} ES \xrightarrow{k_2} P$$

$$+$$

$$I \qquad K_1 = \frac{[E][S]}{[ES]} \quad \text{or} \quad [E] = \frac{[ES]K_1}{[S]} \quad \text{and} \quad K_I = \frac{[E][I]}{[EI]} \quad \text{or} \quad [EI] = \frac{[E][I]}{K_I}$$

$$\Updownarrow K_I$$

$$EI$$

$$(1)\; [E]_{tot} = [E] + [ES] + [EI] = [E] + \frac{[E][S]}{K_1} + \frac{[E][I]}{K_I} = \frac{k_1[ES]}{[S]}\left(1 + \frac{[S]}{K_1} + \frac{[I]}{K_I}\right)$$

(Assumption 1: Pseudo first order conditions. [S]>>[E] $\therefore \; \frac{-d[S]}{dt} = 0$)

(Assumption 2: Because hyperbolic curve, there is buildup of ES and k_2 is rate limiting)

$$(2)\; \frac{-d[E]_{tot}}{dt} = k_{obs}[E]_{tot} = k_2[ES]$$

$$\text{from (1):} \quad [ES] = [E]_{tot}\left(\frac{[S]}{K_1}\right)\left(\frac{1}{1 + \frac{[S]}{K_1} + \frac{[I]}{K_I}}\right) = [E]_{tot}\left(\frac{[S]}{K_1 + [S] + \frac{K_1[I]}{K_I}}\right)$$

$$\text{from (2):} \quad k_{obs} = \frac{k_2[ES]}{[E]_{tot}} = \left(\frac{k_2[S]}{K_1 + [S] + \frac{K_1[I]}{K_I}}\right) \text{ such that as [I]}\rightarrow 0 \ldots \; k_{obs} = \left(\frac{k_2[S]}{K_1 + [S]}\right)$$

BIOGRAPHICAL SKETCH

Heather Lynne Youngs was born on August 8, 1967 in Coral Gables, Florida. She studied chemical engineering at the University of Michigan from 1985 to 1986, and biochemistry at Michigan State University from 1989 to 1991 where she worked as a research assistant studying the nesting behavior of solitary leaf-cutter bees and was awarded a Michigan Competitive Scholarship. Ms. Youngs then attended Michigan Technological University from 1992 to 1994, where she studied the biochemistry of red algal cell wall polysaccharides. She received a grant from Sigma Xi in 1993 to study carbohydrate biosynthesis in the red algae. In 1994, Ms. Youngs was awarded the MTU Student Award and received a B.S. in Biological Sciences *cum laude* in 1996. She entered graduate school at Purdue University, studying plant physiology from 1995 to 1996, and continued her graduate education at the Oregon Graduate Institute of Science & Technology (OGI), studying biochemistry and molecular biology from 1997 to 2001. During that time, Ms. Youngs served as an adjunct faculty member at the University of Portland, teaching laboratory techniques in inorganic chemistry in 1999. She also taught a course in Bioethics at OGI in 2000 and was awarded the Outstanding Student Award in 2001.